Familial Glucocorticoid Deficiency:

New Genes and Mechanisms

Julia C. Kowalczyk

Thesis submitted for the degree of Doctor of Philosophy

(PhD)

Centre for Endocrinology,

William Harvey Research Institute,

Queen Mary, University of London

Abstract

Mutations in the melanocortin 2 receptor (*MC2R*) and its accessory protein (*MRAP*), in the ACTH signalling pathway, and the antioxidant genes nicotinamide nucleotide transhydrogenase (*NNT*) and thioredoxin reductase 2 (*TXNRD2*) have been associated with familial glucocorticoid deficiency (FGD). Using a tandem affinity purification and mass spectrometry approach to identify interacting partners of MC2R and MRAP failed to identify putative candidate genes for further FGD cases. However in a male patient a homozygous mutation in another antioxidant gene, glutathione peroxidase 1 (*GPX1*), was identified. *In vitro* studies showed H295R cells with knockdown of *GPX1* had 50% less basal GPX activity and were less viable than wild-type when exposed to oxidative stress. Adrenals from *Gpx1*$^{-/-}$ mice showed no gross morphological changes and corticosterone levels were not significantly different from their wild-type counterparts (in contrast to the *Nnt* mutants). Sequencing of >100 FGD patients did not reveal any other *GPX1* mutations. This equivocal data lead to the hypothesis that there could be a second gene defect present in this proband contributing to his disease.

Whole exome sequencing revealed a homozygous loss-of-function mutation in peroxiredoxin 3 *PRDX3* (p.Q67X) in this patient, that was also present in his unaffected brother. *In vitro* studies revealed both single and double knockdown of the two genes in H295R cells reduced cell viability, but redox homeostasis and cortisol production were unaffected.

GPXs and PRDXs work simultaneously to reduce H_2O_2, preventing cellular damage. My data suggest that loss of *PRDX3* alone is insufficient to cause adrenal failure and further that mutation in *GPX1*, either alone or in combination with *PRDX3* mutation, may tip the redox balance to cause FGD.

Acknowledgements

I would like to thank:

The Medical Research Council and Barts and the London Charity, for funding this project.

My supervisor Lou Metherell for her support and encouragement throughout my PhD, for helping to open up new opportunities and challenges that have helped me to develop as a person and scientist. I will always appreciate the time she has invested in me.

Eirini Meimaridou, whose training and support has lasted throughout the course of my PhD, for which I am very grateful. I am particularly grateful for her guidance and assistance on the tandem affinity purification technique.

My second supervisor Adrian Clark, whose wise words are always worthwhile.

My many mentors in the lab for sharing their expertise and encouragement including Sadani Cooray, Li Chan, Tatiana Novoselova, Irina Bogdarina and Claire Hutchison, who are all inspirational scientists.

My colleagues in Endocrinology who have made the lab an enjoyable place to work and have become wonderful friends.

Rathi Prasad, whose enthusiasm is contagious, making solving the mystery of science, all that bit more exciting.

My fantastic friends, who have provided me with much needed encouragement, and never fail to make me laugh.

Finally, my parents and my sister Anna and brother Stefan, who have continued to support me not only through the PhD, but through my life, and are always telling me I can do it.

Statement of originality

I confirm that the work presented in this thesis is my own.

Contents

List of Figures

List of Tables

Abbreviations

µM	micromolar
3β-HSD	3β-hydroxysteroid dehydrogenases
5'DI	5' deiodinase
ABC	ATP binding cassette
ABCD1	Adrenoleukodystrophy protein
ACAT	Acyl-coenzymes-A-cholesterol-acyl-transferase
ACE	Angiotensin converting enzyme
ACTH	Adrenocorticotropic hormone
AD	Addison's disease
AI	Adrenal insufficiency
AMN	Adrenomyeloneuropathy
AngII	Angiotensin II
ANT	Adenine nucleotide transporter
Asn	Asparagine
ATP	Adenosine triphosphate
AVP	Vasopressin
BMA	Body mass index
bp	Base pair
BSA	Bovine serum albumin
CAH	Congenital adrenal hyperplasia
cAMP	Cyclic adenosine monophosphate
cDNA	Complementary deoxyribonucleic acid
CHO	Chinese hamster ovary cells
CHO	Chinese hamster ovary cells
CNS	Central nervous system
Co-IP	Co-immunoprecipitation
CREB	cAMP element binding protein
CRF	Corticotropin-releasing factor
CYP11A1	p450 side chain cleavage enzyme
CYP11B1	11β-hydroxylase

CYP11B2	aldosterone synthase
CYS	Cysteine
DAPI	4’,6-diamidino-2-phenylindole
dATP	2’-deoxyadenosine 5’-triphosphate
dCTP	2’-deoxycytidine 5’-triphosphate
dGTP	2’-deoxyguanosine 5’-triphosphate
DMEM	Dulbecco’s Modified Eagle Medium
DMSO	Dimethyl sulphoxide
DNA	Deoxyribonucleic acid
DNase	Deoxyribonuclease
dNTP	Deoxyribonucleotide triphosphate
dTTP	2’-deoxythymidine 5’-triphosphate
E.coli	*Escherichia coli*
EDTA	Ethylenediaminetetraacetic acid
ELISA	Enzyme-linked immunosorbent assay
ER	Endoplasmic reticulum
FAI	Free androgen index
FBS	Foetal bovine serum
FDXR	Ferredoxin reductase
FGD	Familial Glucocorticoid Deficiency
FHC1	Ferritin heavy chain protein
GAPDH	Glyceraldehyde-3-phosphate dehydrogenase
GDP	Guanosine diphosphate
GFP	Green fluorescent protein
Gln	Glutamine
GPCR	G protein-coupled receptor
GPX	Glutathione peroxidase
GR	Glutathione reductase
GTP	Guanosine triphosphate
h	Hours
H295R	Human Adrenal carcinoma cells
H_2O_2	Hydrogen peroxide

HA	Hemagglutinin epitope tag
HDL	High-density lipoproteins
HEK293	Human Embryonic Kidney 293T cells
HEK293T	Human Embryonic Kidney cells
HPA	Hypothalamic-pituitary-adrenal
HRP	Horse radish peroxidase
HSL	Hormone sensitive lipase
IDH_2	Isocitrate dehydrogenase
IMAGe	Intrauterine growth restriction, metaphyseal dysplasia, adrenal hypoplasia congenita, and genital anomalies syndrome
IRMA	Immunoradiometric assay
kb	Kilobase pairs
KD	Knock down
kDa	Kilodaltons
KO	knockout
LAL	Liposomal acid lipase
LB	Luria-Bertani
LCAH	Lipoid congenital adrenal hyperplasia
LDL	Low-density lipoprotein
m	Mouse
M	Molar
MC2R	Melanocortin-2-receptor
MCM4	Mini Chromosome Maintenance protein 4
MCRs	Melanocortin receptors
MEF2	Myocyte enhancer factor-2
mM	Millimolar
M-MLV RT	Moloney Murine Leukaemia Virus Reverse Transcriptase
MRAP	Melanocortin 2 receptor accessory protein
mRNA	Messenger ribonucleic acid
MS	Mass Spectrometry
MSH	Melanocyte stimulating hormone
MW	Molecular weight
NADPH	Nicotinamide adenine dinucleotide phosphate

NNT	Nicotinamide nucleotide transhydrogenase
NOX	NADPH oxidase subtypes
NPC	nuclear pore complex
NS	Not significant
OD	Optical density
ORF	Open reading Frame
PAP7	PKA regulatory subunit RIα-associated protein 7
PBS	Phosphate buffered saline
PBS-Tw	PBS-Tween
PC	prohormone convertase
PCR	Polymerase chain reaction
PKA	Protein kinase A
PNGase F	N-Glycosidase F
POMC	Proopiomelanocortin
PRAX-1	TSPO-associated protein-1
PRDX	Peroxiredoxin
PVN	Paraventricular nucleus
R2C	Rat testicular leydig tumour cells
RAAS	renin-angiotensin-aldosterone system
RAMPs	Receptor activity-modifying proteins
REEPS	Receptor expression-enhancing proteins
RH1	Rhodopsin 1
RIA	Radio immunoassay
RNA	Ribonucleic acid
RNase	Ribonuclease
ROS	Reactive oxygen species
rpm	Rotations per minute
RT-PCR	Reverse Transcription-polymerase chain reaction
SD	Standard deviation of the mean
SDS-PAGE	Sodium dodecyl sulphate polyacrylamide gel electrophoresis
Se	Selenium
Sec	Selenocysteine

SECIS	Selenocysteine insertion element
SREBP	Sterol regulatory element binding protein
StAR	Steroidogenic acute regulatory protein
TAE	Tris-acetate-ethylenediaminetetraacetic acid
TAP	Tandem affinity purification
TCA	Tricarboxylic acid/citric acid cycle
TMD	Transmembrane domain
Tris	Tris(hydroxymethyl)aminomethane
Trp	Tryptophan
TSPO	Translocator protein
TXN	Thioredoxin
TXNRD	Thioredoxin reductase
UTR	Untranslated region
VDAC1	Voltage-dependent anion channel
VLCFA	Very long chain fatty acids
WES	Whole exome sequencing
WT	Wild-type
X-ALD	X-linked adrenoleukodystrophy
Y2H	Yeast-2-hybrid
ZF	Zona fasciculata
ZG	Zona glomerulosa
ZR	Zona reticularis

Chapter 1: Introduction

1.1 Hypothalamic-Pituitary-Adrenal Axis

The Hypothalamic-Pituitary-Adrenal (HPA) axis is a major endocrine system that mediates the stress response. The main structural components are the paraventricular nucleus (PVN) of the hypothalamus, the anterior lobe of the pituitary, and the adrenal cortex (Fig. 1.1). The stress response involves endocrine, neuronal and immune systems in order in evoke behavioural and physiological changes to cope with the external environmental or internal homeostatic sources of stress.

Stress stimuli are conveyed to the hypophysiotropic neurons in the PVN which express and secrete corticotropin-releasing factor (CRF) (Sawchenko and Swanson, 1985). These neurons project to hypophysial portal vessels that access the anterior pituitary gland. CRF secreted into hypophysial portal vessels, activates the CRH receptor on anterior pituitary corticotroph cells leading to corticotrophin release (ACTH) into peripheral circulation. CRF is the principle regulator of ACTH release, however vasopressin (AVP) is an additional regulator that is released from parvocellular neurons of the PVN into portal vessels, and acts via V_{1b} receptors on anterior pituitary corticotrophs to potentiate ACTH release (Smith and Vale, 2006). ACTH is synthesised from its precursor proopiomelanocortin (POMC), in addition to α-, β- and γ-Melanocyte-stimulating hormones (MSHs).

Once released into circulation ACTH acts on melanocortin 2 receptors (MC2R) in the adrenal cortex to induce the production of glucocorticoids, the effectors of the HPA axis. MC2R is a class A G Protein-coupled receptor (GPCR), that when activated, induces adenylyl cyclase activity which generates cyclic adenosine monophosphate (cAMP), leading to an increase in Protein Kinase A (PKA) activity.

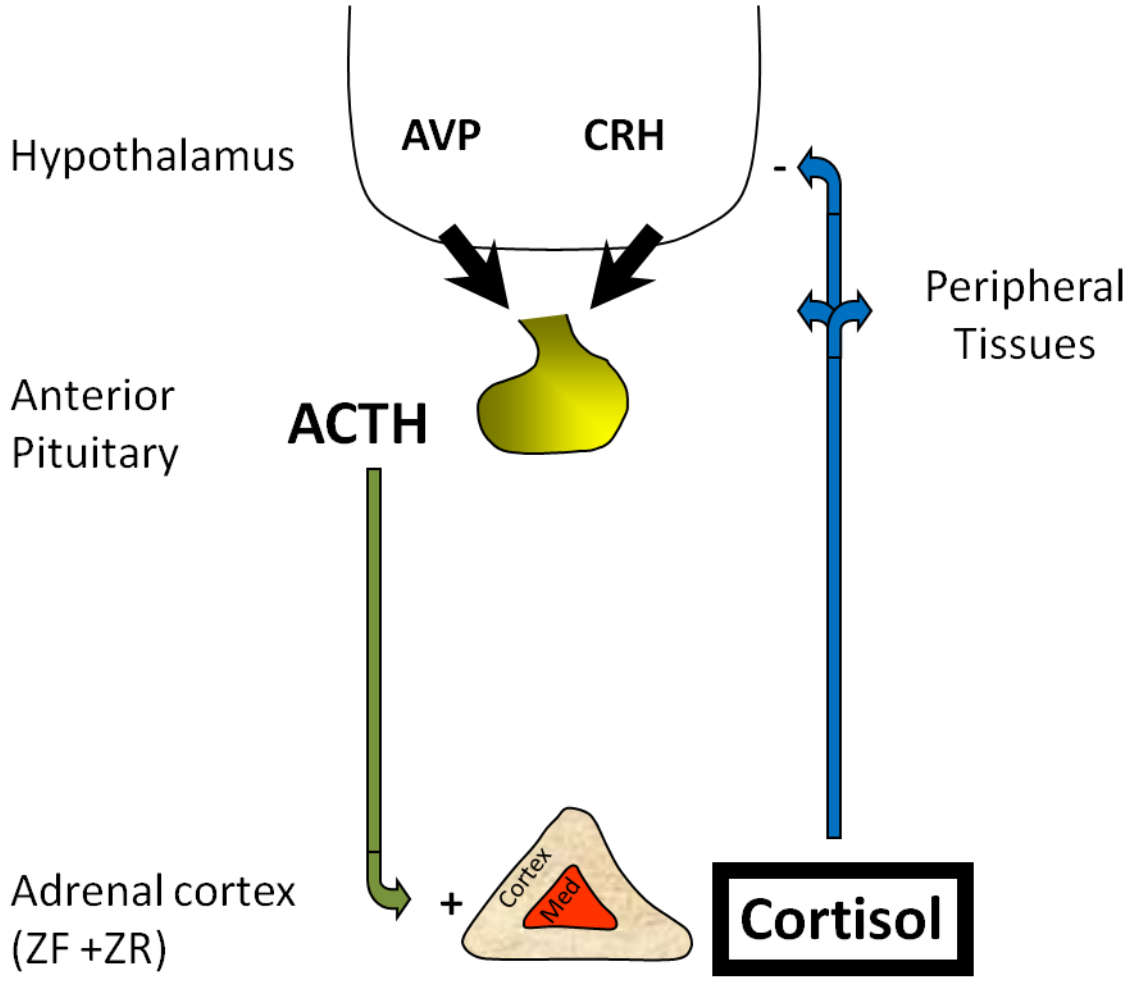

Figure 1. 1: The HPA axis

Hypophysiotropic neurons of the hypothalamus secreting CRF extend to the anterior pituitary and act on CRF receptors to stimulate ACTH synthesis and release into the circulation. Simultaneously parvocellular neurons secreting AVP also extend to the anterior pituitary and potentiate ACTH release. Circulating ACTH acts on MC2R receptors in the ZF and ZR of the adrenal cortex to activate cortisol synthesis. Cortisol acts on peripheral tissues and negatively feeds back to the hypothalamus and pituitary to prevent further ACTH release.

ACTH induced cAMP/PKA activity increases glucocorticoid production through various mechanisms. Firstly cAMP/PKA increases the availability of free cholesterol, the first

substrate in steroidogenesis, by stimulating the uptake of low-density lipoproteins (LDL) via LDL receptor-mediated endocytosis, and stimulating hormone sensitive lipase (HSL) whilst inhibiting acyl-coenzymes-A-cholesterol-acyl-transferase (ACAT), leading to the de-esterification of cholesterol stored in lipid droplets (section 1.2.2, Fig. 1.3) (Miller, 2013).

In the acute phase of ACTH stimulation, PKA increases transcription of steroidogenic acute regulatory protein (StAR) (Stocco *et al.*, 2005) and phosphorylates existing StAR at Ser195, doubling its activity (Arakane *et al.*, 1997). StAR mediates the transport of cholesterol from the outer to the inner mitochondrial membrane where the first step of steroidogenesis takes place. In the later stages of ACTH stimulation, cAMP activates cAMP element binding protein (CREB) which increases the transcription of steroidogenic genes (Chan *et al.*, 2011).

The major glucocorticoid in humans is cortisol, and in rodents corticosterone. When released into circulation, glucocorticoids act on ubiquitously expressed glucocorticoid receptors in the CNS and peripheral tissues. The receptors are intracellular and exist as homodimers in complexes with a number of heat shock proteins. Activation of the glucocorticoid receptor by its ligand results in a conformational change, which in turn leads to translocation of the receptor to the nucleus, where it binds and activates the transcription of target genes which contain specific glucocorticoid response elements in the promoter regions (Smith and Vale, 2006). This results in a number of metabolic, cardiovascular and immune changes (Smith and Vale, 2006).

As well as in response to stress stimuli, ACTH release follows a diurnal circadian rhythm, with maximum concentration seen early in the morning descending to minimum concentration at midnight (Weitzman *et al.*, 1971). The effects of glucocorticoids are therefore either permissive (basal), or stimulating (stress induced) (Dallman et al., 1989; De Kloet et al., 1998; Ratka et al., 1989). The permissive actions of glucocorticoids are mediated through the mineralocorticoid receptor, which binds glucocorticoids with a higher affinity than that of the glucocorticoid receptor and is selectively expressed in a tissue dependent manner within the brain (Reul and de Kloet, 1985, 1986). During stress when concentration of glucocorticoids is higher, the mineralocorticoid receptor becomes fully

saturated and glucocorticoids bind the glucocorticoid receptor (Reul and de Kloet, 1985; Smith and Vale, 2006). Overall, glucocorticoids act to increase blood glucose concentration through gluconeogenesis and metabolism of carbohydrates, proteins and lipids, and to dampen inflammatory and immune responses.

The duration and intensity of the stress response is regulated by several different mechanisms. In a typical negative feedback loop, glucocorticoids inhibit the HPA axis at both the hypothalamic and pituitary level. Hence, when a high concentration of circulating glucocorticoids is present, ACTH release is inhibited, and when plasma glucocorticoid concentration is low, ACTH release increases. Glucocorticoid receptors are ubiquitously expressed but particularly abundant in the PVN, where glucocorticoids negatively regulate expression of HPA specific genes, decreasing CRF release (Smith and Vale, 2006). In pituitary corticotrophs, glucocorticoids cause transcriptional repression of the POMC gene, reducing synthesis of ACTH (Sapolsky et al., 2000). There is also evidence to suggest that the HPA axis is regulated by CRF binding proteins. Recombinant CRF binding protein (CRF-BP) diminishes CRF-induced ACTH release from cultured anterior pituitary cells (Westphal and Seasholtz, 2006).

1.2 The Adrenal Gland

1.2.1 Adrenal Morphology

The adrenal glands lie on top of the kidneys and are each composed of two separate glands: the outer cortex and inner medulla (Ayres *et al.*, 1960) (Fig. 1.2.1). The medulla secretes catecholamines in response to the sympathetic nervous system under conditions of stress (Hillarp and Nilson, 1954). Unlike the medulla, the adrenal cortex is essential for life. Its primary role is to secrete steroids, which are synthesised in three morphologically distinct zones: mineralocorticoids such as aldosterone in the zona glomerulosa (ZG), glucocorticoids such as cortisol (corticosterone in rodents) in the zona fasciculata (ZF) and in humans and higher primates, adrenal androgens in the zona reticularis (ZR) (Ayres *et al.*, 1960; Giroud *et*

al., 1956). Arnold *et al.* first described the three major zones in 1866. Each zone can be easily distinguished on conventional staining by cell size and morphology, particularly between the ZG and ZF. In rats, a fracture plane exists between the ZG and ZF making mechanical separation of the zones easy, suggesting discontinuity between the zones (Miller and Auchus, 2011; Vinson, 2003).

The zones can also be distinguished by the spatially specific expression of steroidogenic cytochrome p450 (CYP) enzymes involved in the final steps of steroid synthesis. In rodents and humans, *CYP11B2* encoding aldosterone synthase (Curnow *et al.*, 1991) is selectively expressed in the ZG, preventing aldosterone production from the other zones, and *CYP11B1* encoding 11β-hydroxylase, is selectively expressed in the ZF (and the ZR in humans and higher primates) where it catalyses the final step of cortisol or corticosterone production (Domalik *et al.*, 1991; Nishimoto *et al.*, 2010; Ogishima *et al.*, 1992). In rats specifically, the outer region of the ZF contains functionally undifferentiated cells which express neither enzyme, referred to as the 'undifferentiated zone' (not shown) (Mitani et al., 1994). Unlike rodents which produce corticosterone, the major glucocorticoid in humans is cortisol, due to the expression of *CYP17A1* in the ZF and ZR, which catalyses the 17α-hydroxylation and 17, 20 lyase reactions and is not expressed in rodents (Sasano *et al.*, 1989).

Finally the zones are functionally responsive to different stimuli. Whereas *CYP11B2* expression and aldosterone production increases in the ZG following stimulation by potassium or angiotensin II, *CYP11B1* expression and cortisol/corticosterone synthesis are increased by ACTH stimulation.

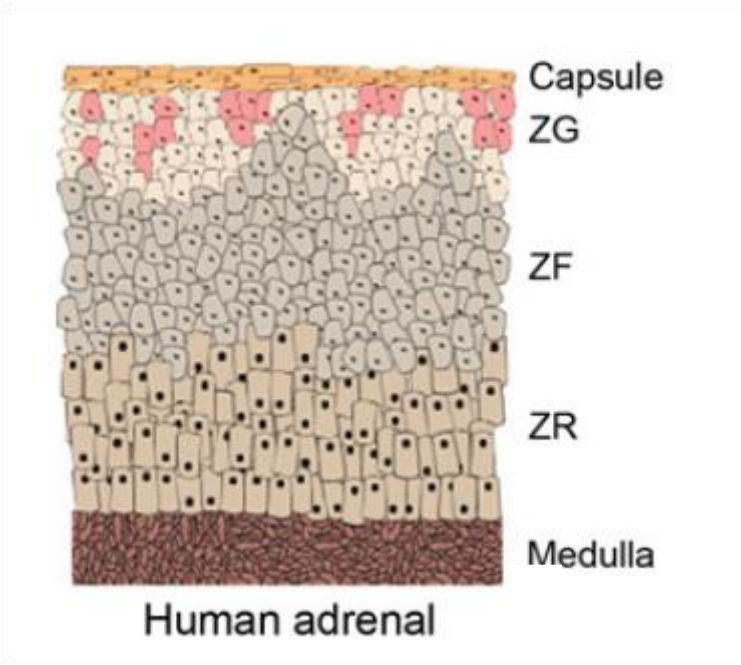

Figure 1. 2: The human adrenal gland

Illustration showing the adrenal gland and individual zones of the adrenal cortex. (Yates et al., 2013)

1.2.2 Adrenal Steroidogenesis

Adrenal steroidogenesis depends on the delivery of cholesterol to mitochondria and its catalysis by type 2 3β-hydroxysteroid dehydrogenases (3β-HSD) and p450 cytochrome (CYP) steroidogenic enzymes. The human adrenal cortex produces mineralocorticoids, glucocorticoids and adrenal androgens in the ZG, ZF and ZR respectively, the products being dependent on the zone-specific expression profile of steroidogenic enzymes, and the stimulus.

The initial substrate cholesterol is obtained from three sources: *de novo* synthesis from acetate, high-density lipoproteins (HDLs) internalised from circulation by scavenger receptor B1, or LDLs internalised by LDL receptor-mediated endocytosis. Humans source the majority of cholesterol from LDL proteins, whereas rodents use HDL (Miller, 2013).

Once internalised, LDL containing endosomes fuse with lysosomes where the LDL is degraded to cholesterol ester. The cholesterol ester is de-esterified to its 'free' form by liposomal acid lipase (LAL), then released from the endosome, in part by the binding to cholesterol transport proteins Niemann Pick type C proteins 1 and 2. Free cholesterol is targeted to the mitochondria for steroidogenesis, and excess cholesterol is converted back to its ester form by ACAT for storage in lipid droplets. Cholesterol is released from storage by HSL (Fig 1.3).

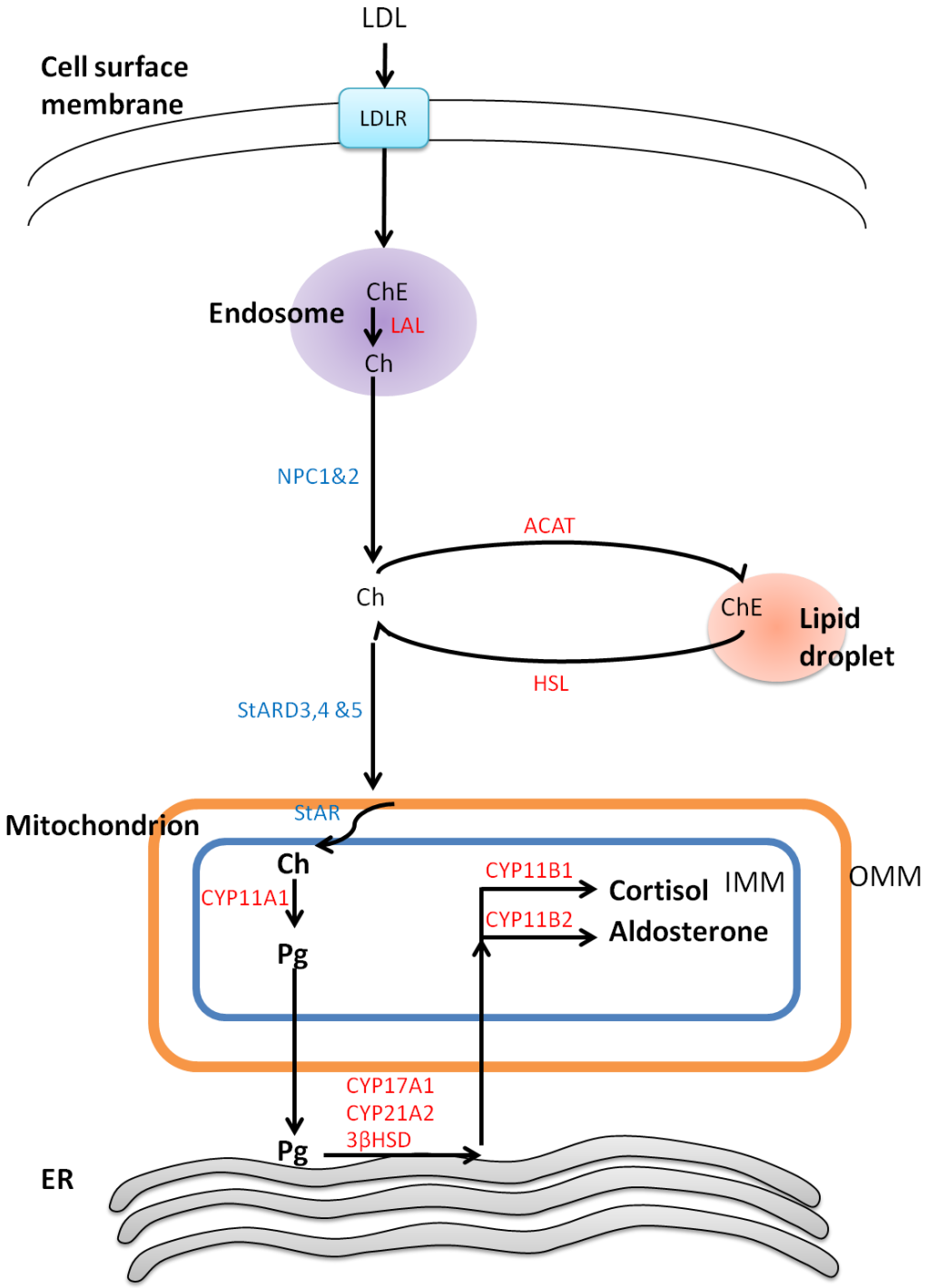

Figure 1. 3: Cholesterol transfer.

Cholesterol is sourced predominantly from low-density lipoproteins (LDL) in humans that are internalised from the circulation by receptor-mediated endocytosis via the LDL receptor. LDL undergoes proteolysis in the endosome to cholesterol ester (ChE), and is de-esterified to free cholesterol (Ch) by liposomal acid lipase (LAL). Niemann Pick type C proteins 1 and 2 (NPC1&2) are involved in the exit of Ch from the endosome. Free Ch is either targeted to mitochondria by STARD enzymes or stored in lipid droplets. Re-esterification is the domain of acyl-coenzymes-A-cholesterol-acyl-transferase, whereas

hormone sensitive neutral lipase (HSL) de-esterifies. Ch is transferred from the outer (OMM) to the inner mitochondrial membrane (IMM) where it is converted to pregnenolone (Pg). Pregnenolone is translocated to the ER and processed by CYP21A2 and 3β-HSD enzymes but the final steps of steroidogenesis occur back in the mitochondria, where the differential expression of *CYP* enzymes determines the steroid produced. (Androgens not shown)

Although the exact mechanism is unclear, the most recent literature suggests cholesterol is targeted to the mitochondria by members of the START-domain (StAR-D) family of proteins, which bind cholesterol and are activated by sterol regulatory element binding protein (SREBP) transcription factors. StarD3, 4 and 5, bind cholesterol and facilitate its non-vesicular transport through the cytoplasm to the outer mitochondrial membrane (Miller, 2013; Rodriguez-Agudo *et al.*, 2008), where StAR and StarD6 mediate transfer to the inner mitochondrial membrane (Bose *et al.*, 2008).

StAR is a 37kDa protein, with an N-terminal mitochondrial leader sequence that is cleaved to a 30kDa form following entry into the mitochondria. Although both 37kDa and 30kDa forms are active *in vitro*, the activity of StAR is proportional to the time spent on the OMM (Arakane *et al.*, 1996; Bose *et al.*, 2002).

To accept one molecule of cholesterol, StAR must undergo a pH dependent conformational change as the binding pocket is blocked by hydrogen bonds. It does this through binding with charged phospholipid molecules in the OMM (Baker *et al.*, 2005; Bose *et al.*, 1999)

On the outer mitochondrial membrane, StAR forms part of a 140-200kDa major complex that contributes to cholesterol internalisation, including translocator protein (TSPO), voltage-dependent anion channel (VDAC1), adenine nucleotide transporter (ANT), diazepam-binding inhibitor (acyl-coA-binding domain 1 ACBD1), TSPO-associated protein-1 (PRAX-1) and PKA regulatory subunit RIα-associated protein 7 (PAP7) (Miller, 2013). The most explored protein is TSPO, a 5 transmembrane domain protein that binds cholesterol and functions as a cholesterol channel (Hauet *et al.*, 2005; Joseph-Liauzun *et al.*, 1998; Korkhov *et al.*, 2010; Liu *et al.*, 2006). Knockdown (KD) of this gene in rat testicular leydig tumour (R2C) cells reduces cholesterol transport and steroidogenesis (Papadopoulos *et al.*, 1997).

Once cholesterol has been transferred to the inner mitochondrial membrane, it is converted into steroids through sequential catalysis by enzymes belonging to two families; the cytochrome p450 (CYP) hydroxylases and the 3βHSDs.

As illustrated in figure 1.4, three major pathways of steroidogenesis exist in the adrenal cortex producing mineralcorticoids, glucocorticoids and adrenal androgens in the ZG, ZF and ZR respectively. The different end products of each zone are the result of selective expression of steroidogenic enzymes and associated factors.

The first and only rate-limiting step, common to all three zones, involves the conversion of hydrophobic cholesterol to hydrophilic 21-carbon pregnenolone by side chain cleavage enzyme (CYP11A1) encoded by *CYP11A1*. Pregnenolone is then translocated to the endoplasmic reticulum for further catalysis by CYP17A1, 3βHSD and CYP21A2.

In the ZG, *CYP17A1* is not expressed, hence pregnenolone undergoes sequential activities of 3βHSD and CYP21A2 to produce progesterone and 11-deoxycorticosterone. 11-deoxycorticosterone is transferred to the mitochondrion for the final step in steroid synthesis, where CYP11B2 catalyses the 11β-hydroxylation, 18-hydroxylation and 18-methyl oxidation to aldosterone. Expression of *CYP11B2* is restricted to the ZG preventing aldosterone production in the other zones, and absence of *CYP17A1* expression prevents cortisol or androgen synthesis.

In the ZF, pregnenolone undergoes 17α-hydroxylation by CYP17A1 prior to 3βHSD and CYP21A2 catalysis, producing 11-deoxycortisol instead of deoxycorticosterone, thereby allowing for cortisol production rather than corticosterone. 11-deoxycortisol is translocated back to the mitochondrion where it undergoes 11β-hydroxylation by CYP11B1 to form cortisol.

Similar to the ZF, the ZR expresses *CYP17A1* which catalyses the 17α-hydroxylation of pregnenolone. Unlike the ZF, the ZR has high levels of cytochrome b_5, which enables CYP17A1a to catalyse a further 17, 20 lyase reaction. High expression of cytochrome b_5 coupled with low expression of *CYP21A2* and *CYP11B1* in the ZR favours androgen

production and diminishes cortisol production. The 17, 20 lyase activity of CYP17A1 converts 17-hydroxypregnenolone to dehydroepiandrosterone (DHEA), the major adrenal androgen. A small fraction of DHEA is converted to androsteonedione, and a subset of this is converted to testosterone by 17βHSD5, however this pathway is unfavoured as the expression of *HSD3B1* (encoding 3βHSD) is low in the ZR whereas the expression of *CYP17A1* is high (Miller and Auchus, 2011).

Differences in adrenal steroidogenesis are evident between species, for example, rodents do not express *CYP17A1*, hence the major glucocorticoid is corticosterone, and androgens are not produced.

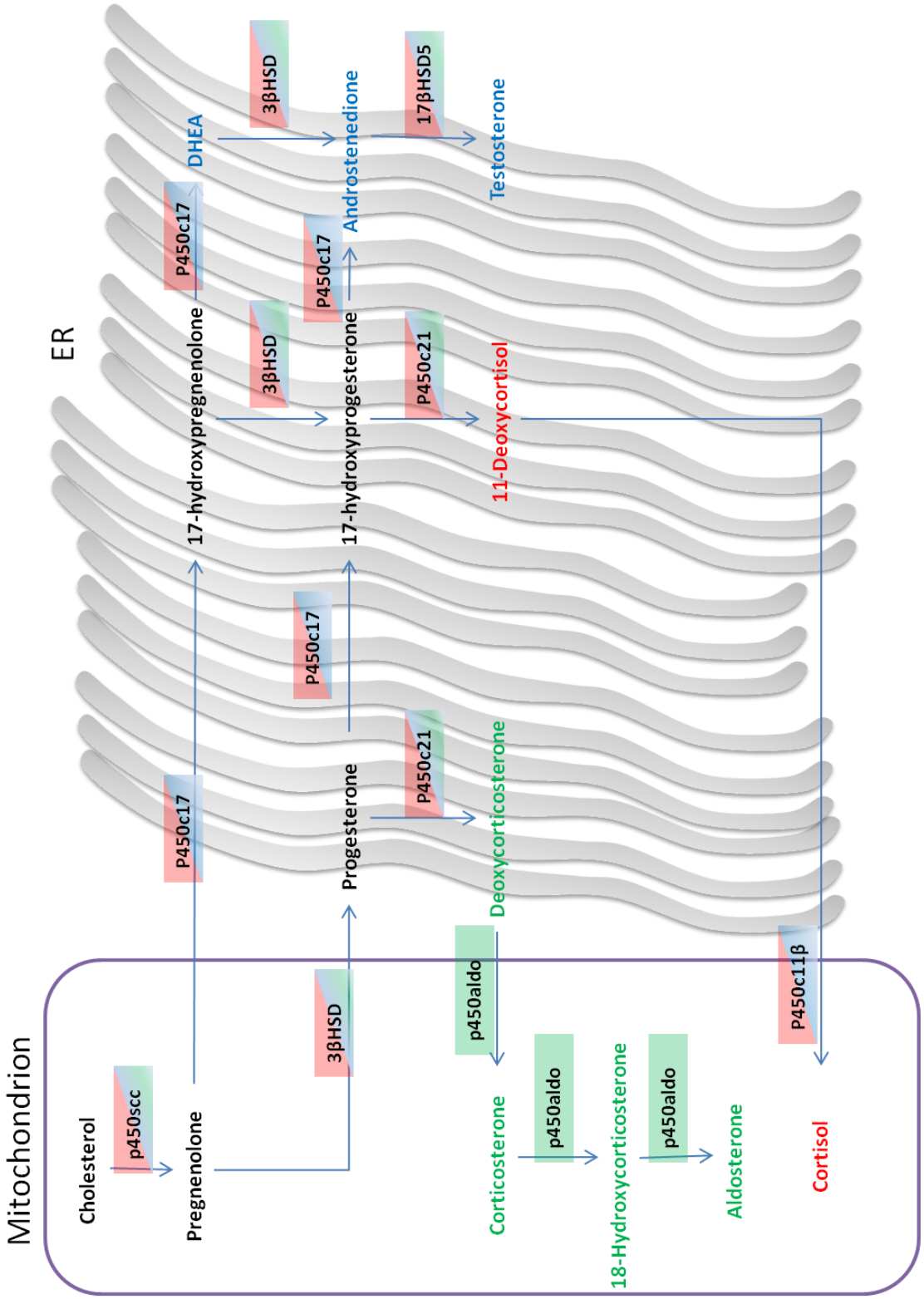

Figure 1. 4: Human adrenal steroidogenesis.

Summary of enzymatic reactions that lead to the synthesis of adrenal steroids. *Green text* depicts steroids synthesised in the ZG, *red* the ZF and *blue* the ZR. Expression of

steroidogenic enzymes is zone dependent: green boxes depict the ZG, red the ZF and blue the ZR.

The steroidogenic CYP enzymes require co-factors for their activity. Mitochondrial type 1 CYP enzymes receive electrons from nicotinamide adenine dinucleotide phosphate (NADPH), which is supplied by ferredoxin, which in turn is reduced by ferredoxin reductase (Miller, 2005). Type 2 CYP enzymes that reside in the endoplasmic reticulum (ER) receive electrons from 2-flavin P450 oxidoreductase (Miller, 2005).

The initiation of steroidogenesis is triggered by several different stimuli resulting in appropriate steroid synthesis. ACTH is the only regulator of glucocorticoid synthesis, and forms part of the hypothalamic-pituitary-axis. ACTH and potassium can stimulate the synthesis of aldosterone, however aldosterone production is primarily governed by angiotensin II (AngII) via the renin-angiotensin-aldosterone system (RAAS) (Yates et al., 2013).

Briefly, the RAAS plays an important role in inducing vasoconstriction when sodium levels fall or hemorrhage occurs (Collier et al., 1973; Scornik and Paladini, 1964). Renin is a proteolytic enzyme that is synthesised in the kidney and is stimulated by a number of factors including the sympathetic nervous system, catecholamines, decreased renal perfusion pressure and reduced sodium delivery to the distal tubule (Johnson and Davis, 1973; Tobian et al., 1959; Yates et al., 2013). On stimulation, renin is released into circulation and cleaves angiotensinogen to angiotensin I (Miller, 1981). Subsequently, angiotensin I is hydrolysed to AngII by angiotensin-converting enzyme (ACE) on pulmonary and renal endothelium, inducing vasoconstriction of arteriolar smooth muscle (Oparil et al., 1970). In addition, AngII stimulates the release of catecholamines and aldosterone into circulation.

AngII stimulates aldosterone production in the ZG by activating the AT1 G-protein coupled receptor, stimulating inositol 1,4,5-triphosphate (ins(1,4,5)P3) and 1,2,-diacylglycerol (DAG) signalling, associated with an influx of calcium to the cytoplasm and increased protein kinase

C activity. These events ultimately lead to aldosterone production, thought to be due to activation of trascription factors that target *CYP11B2*.

The exact mechanism governing androgen production in the adrenal is not clear.

1.3 Adrenal Insufficiency

Adrenal insufficiency was originally described by Thomas Addison in 1855, who recognised a syndrome of hyperpigmentation and wasting due to adrenal failure. The condition is found in multiple disorders, and presents with relatively unspecific symptoms which can delay diagnosis (Arlt and Allolio, 2003).

Acute adrenal insufficiency usually presents with severe hypotension or hypovolaemic shock with abdominal pain, nausea and fever and, in children, hypoglycaemic seizures (Arlt and Allolio, 2003). Patients with chronic adrenal insufficiency usually present with fatigue, lack of energy and muscle strength and irritability (Arlt and Allolio, 2003).

There are two main types of adrenal insufficiency (AI): primary AI, caused by damage to the adrenal gland and secondary AI, caused by interference at the pituitary level or hypothalamic level (Reddy, 2011).

Patients with primary adrenal insufficiency are deficient in glucocorticoids. Mineralocorticoid and adrenal androgen deficiency varies between conditions. Symptoms associated with glucocorticoid deficiency include weight loss, anorexia (or failure to thrive in children), nausea and muscle/joint pain (Arlt and Allolio, 2003). The most obvious clinical feature is hyperpigmentation, which is absent from secondary adrenal insufficiency (Reddy, 2011). Low levels of cortisol decrease negative feedback to the hypothalamus leading to high levels of ACTH, which activate MC1R receptors involved in pigmentation. Cortisol deficiency also causes a decrease in cardiac output and vascular tone which is exacerbated by mineralocorticoid deficiency (Reddy, 2011). This is because the permissive actions of cortisol are mediated through the mineralocorticoid receptor,

Mineralocorticoid deficiency causes dehydration and hypovolaemia leading to low blood pressure and postural hypotension (Arlt and Allolio, 2003). Some patients also have hyponatraemia, hyperkalaemia and salt craving (Kong and Jeffcoate, 1994; Nerup, 1974). DHEA deficiency in women causes loss of axillary and pubic hair, dry skin and loss of libido (Arlt and Allolio, 2003).

Patients with secondary AI have symptoms of cortisol deficiency with no symptoms of mineralocorticoid deficiency such as salt wasting or hyperkalaemia (Reddy, 2011). The causes of secondary AI affect ACTH secretion from the pituitary, hence mineralocorticoid function is not impaired (Reddy, 2011). Secondary AI can be grouped into isolated ACTH deficiency or combined pituitary hormone deficiency (pan-hypopituitarism). Isolated ACTH deficiency is most frequently caused by iatrogenic AI, the most common form of AI, where chronic glucocorticoid therapy suppresses the HPA axis. Other causes of isolated ACTH deficiency include autoimmune hypophysitis and defects in the pro-opiomelanocortin (POMC) cleavage enzyme which yields ACTH (Nussey *et al.*, 1993). Combined pituitary hormone deficiency is caused by tumours of the pituitary, surgery or radiotherapy, infectious diseases and mutations in genes encoding pituitary transcription factors such as *HESX1*, *SOX3* and *TPIT* (Kelberman et al., 2009).

The most common form of primary adrenal insufficiency in developing countries accounting for 80-90% patients is autoimmune adrenalitis (Addison's), either isolated or as part of an autoimmune polyendocrine syndrome (APS) (Betterle *et al.*, 2002; Neufeld *et al.*, 1981). APS type 1 (APS1) is characterised by adrenal insufficiency, hypoparathyroidism and chronic mucocutaneous candidiasis and develops in childhood to early adulthood (Ahonen *et al.*, 1990; Betterle *et al.*, 2002). Some cases also have childhood alopecia, chronic active hepatitis, malabsorption and the autoimmune diseases found in APS type 2. APS type 2, the most common form typically affecting middle-aged females, consists of adrenal insufficiency

and autoimmune thyroid disease, and in some cases the addition of other autoimmune disorders such as diabetes mellitus (Arlt and Allolio, 2003).

Other causes of primary adrenal insufficiency include tuberculous adrenalitis, which is a common cause in developing countries (Soule, 1999). Adrenal insufficiency can also occur through haemorrhage or adrenal infiltration, however this is rare (Arlt and Allolio, 2003).

A number of genetic disorders are associated with primary adrenal insufficiency. Mutations in the *ABCD1* gene encoding for peroxisomal adrenoleukodystrophy protein cause X-linked adrenoleukodystrophy, characterised by neurological impairment in addition to adrenal insufficiency (Moser, 1997). Mutations in *ABCD1* lead to a build-up of very long fatty acids and the demyelination of white matter (Moser, 1997). The disease has two forms: either rapid progression developing in early childhood or slow progression developing in early adulthood (Arlt and Allolio, 2003).

Congenital adrenal hyperplasia (CAH) is a group of monogenetic disorders, caused by mutations in the genes encoding the steroidogenic CYP enzymes and their co-factors (Krone et al., 2007; Miller, 1991; White and Speiser, 2000). The most common form is 21-hydroxylase deficiency which presents at in the neonatal period.

Although most conditions of primary adrenal insufficiency comprise combined glucocorticoid and mineralocorticoid deficiency, some genetic disorders result in glucocorticoid deficiency alone. These include ACTH insensitivity syndromes familial glucocorticoid deficiency type 1-4, which presents between neonatal and early childhood periods and triple A syndrome, which presents in the first two decades of life (Clark and Weber, 1998).

A number of conditions of primary adrenal insufficiency have been associated with a pathogenesis involving oxidative stress. These include Triple A syndrome, X-linked adrenoleukodystrophy and more recently, familial glucocorticoid deficiency. It is becoming

increasing clear that oxidative stress is a disease mechanism for some forms of adrenal insufficiency, and that the adrenal cortex is particularly sensitive to oxidative pressure.

1.4 Familial Glucocorticoid Deficiency

Familial glucocorticoid deficiency (OMIM 202200) (FGD) is a rare, autosomal recessive disorder characterised by isolated glucocorticoid deficiency and resistance of the adrenal cortex to ACTH (Clark and Weber, 1998). The syndrome was first described by Shepard *et al.* (1959) as 'Familial Addison's disease', based on post-mortem analysis and clinical study of two sisters. Both were described to have hyperpigmentation, weakness and convulsions. Clinical study showed glucocorticoid deficiency with normal aldosterone levels, and selective damage to the ZF and ZR in the adrenal cortex. In the 1970's, further reports of patients with isolated glucocorticoid deficiency surfaced prompting the search for genetic causes (Spark and Etzkorn, 1977; Thistlethwaite *et al.*, 1975; Thistlethwaite *et al.*, 1974). If untreated, the disease can be fatal due to severe hypoglycaemia (Clark and Weber, 1998).

1.4.1 FGD aetiology

Following Shepard and colleague's discovery a number of FGD cases were reported and the search for potential causes began. After the cloning of the ACTH Receptor (melanocortin receptor; MC2R), Clark *et al.* found the first mutation and went on to show that 25% of FGD cohorts had mutations in *MC2R* (Clark *et al.*, 1993; Huebner *et al.*, 1999). In 2005, a further 20% cases were found to have mutations in the Melanocortin Receptor Accessory Protein (*MRAP*) (Metherell et al., 2005). In 2009, a few patients were shown to have mutations in *STAR* (Baker *et al.*, 2006; Metherell *et al.*, 2009). In 2011, a few patients within the genetically isolated Irish traveller community were found to have mutations in Mini Chromosome Maintenance protein 4 (*MCM4*) (Hughes *et al.*, 2012). Most recently, 10% cases were found to have mutations in nicotinamide nucleotide transhydrogenase

(*NNT)*(Meimaridou *et al.*, 2012b). Approximately 40% of cases remain with unknown aetiology.

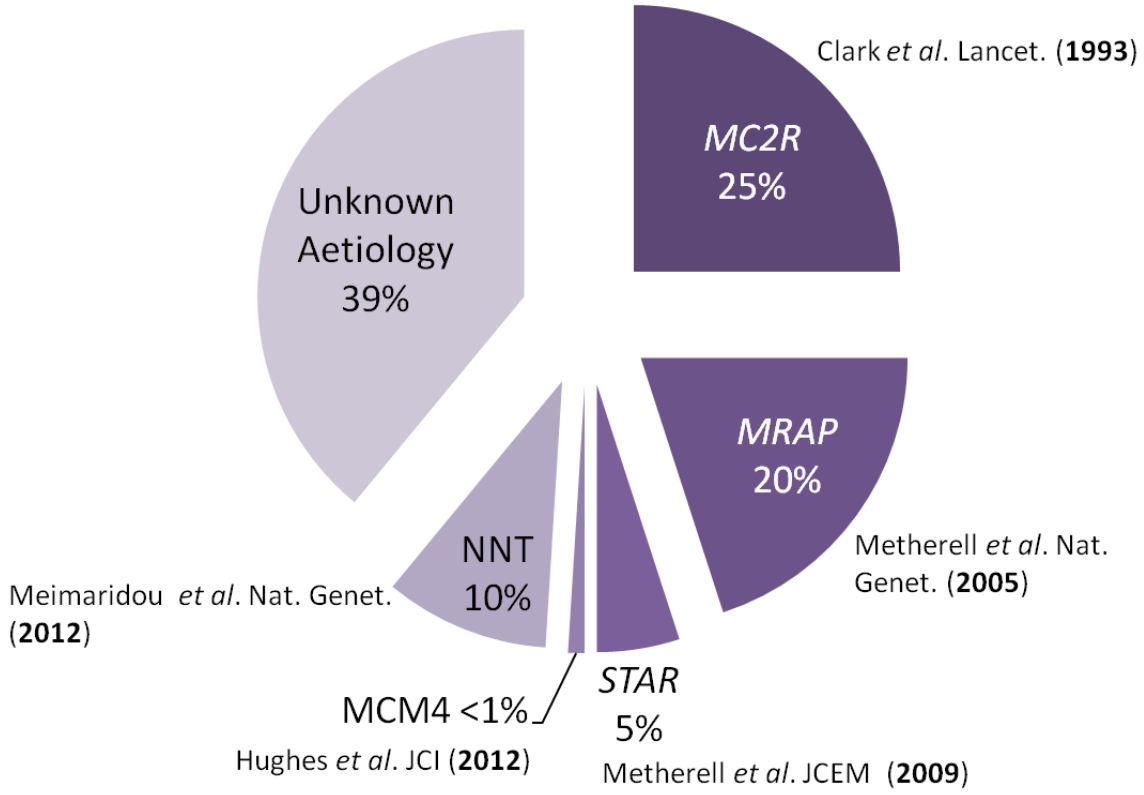

Figure 1. 5: FGD aetiology. Pie chart showing known causes of FGD.

1.4.2 Clinical features of FGD

Patients with FGD can present within the neonatal period, infancy or early childhood, depending on the severity of their condition. All symptoms are characteristic of hypocortisolaemia and elevated ACTH levels (Chan *et al.*, 2008).

Patients who present in the neonatal period tend to have severe hypoglycaemia, which often improves after more frequent feeding. These patients tend to have excessive skin pigmentation, and are sometimes jaundiced. Patients that are not diagnosed in the neonatal period tend to present over the next few years of life with recurrent hypoglycaemic episodes

and/or convulsions, skin pigmentation or poor recovery from infective episodes (Chan *et al.*, 2008).

If left untreated, recurrent hypoglycaemic episodes may incur long-term neurological damage ranging from learning difficulties to spastic quadriplegia (Chan *et al.*, 2008; Modan-Moses *et al.*, 2006), but coupled with frequent infection can ultimately result in death. Correct diagnosis early in life is therefore crucial to prevent the pathological sequelae, however diagnosis can be missed, for example during acute illness (Habeb *et al.*, 2013) or mistaken for Addison's disease because of subtle derangements of the renin-angiotensin axis.

FGD is confirmed biochemically by low plasma cortisol levels, with elevated ACTH levels but normal levels of aldosterone, renin and electrolytes. ACTH levels, measured by RIA or IRMA, are often above 1000pg/ml, normal range <50 and <80pg/ml respectively (Chan *et al.*, 2008; Clark and Weber, 1998). Cortisol levels are usually extremely low and sometimes undetectable. Further testing may include an ACTH stimulation test (Synacthen=1-24 ACTH), in which a normal response is a peak plasma cortisol level of over 550nmol/l.

FGD is commonly mistaken for Addison's disease (AD) (ICD10 E27.1), in which patients have deficiencies of both glucocorticoids and mineralocorticoids. Mineralocorticoid levels can indeed be low at presentation which can lead to the misdiagnosis as Addison's (Clark *et al.*, 2001; Clark and Weber, 1998). The low mineralocorticoids are often due to the child being ill or in shock, and should be checked after the child is stabilised to determine whether they are truly mineralocorticoid deficient.

One study suggested this phenotype might manifest in patients with particularly severe mutations in *MC2R* (Lin *et al.*, 2007), in particular frameshift mutations whereby receptor function is completely ablated, whereas the majority of *MC2R* mutations are missense and leave some degree of receptor function (Chung *et al.*, 2008). However, a review of patients with such *MC2R* mutations showed no clinically significant mineralocorticoid deficiency (Chan *et al.*, 2009a). Furthermore one report that investigated a cohort of autoantibody–

negative Addison's patients for mutations in genes known to cause FGD, showed that FGD is not underdiagnosed in the AD population (Dias *et al.*, 2010).

The absence of mineralocorticoid deficiency distinguishes FGD from other conditions of primary adrenal insufficiency many of which have additional features (Chan *et al.*, 2008). These additional features and the relevant tests are listed in table 1.1.

Symptoms	Associated condition	Investigations
Progressive neurological manifestations	X-adrenoleukodystrophy, triple-A syndrome	-Very-long-chain fatty acid measurement -Sequencing of *AAAS* and *ABCD1* genes
Ambiguous genitalia	Congenital adrenal hyperplasia	17-hydroxyprogesterone, monitoring of blood pressure
Hypogonadism, delayed puberty	Adrenal hypoplasia congenita	Sequencing of *DAX1* and *SF1* genes
Alacrima/achalasia	Triple A syndrome	Schirmer test of tear production together with a barium swallow
Dysmorphic features, skeletal abnormalities	Intrauterine growth restriction, metaphyseal dysplasia, adrenal hypoplasia congenita, and genital anomalies (IMAGe) syndrome	-Ultrasound of renal tract -X-ray (skeletal survey) -Sequencing of *CDKN1C* gene
Other autoimmune deficiencies	Polyglandular autoimmune syndromes	Adrenal antibodies

Table 1. 1: Clinical features absent from FGD.

FGD can be distinguished from other forms of adrenal insufficiency by the absence of the listed symptoms. These symptoms are associated with other conditions and should be investigated using the tests listed. (Table based on Chan *et al.* (2008))

Imaging of adrenals by MRI or CT scan can also distinguish FGD from other conditions of primary adrenal insufficiency, as FGD patients have relative small adrenal glands, whereas conditions such as adrenal tuberculosis and CAH have enlarged adrenals due to calcification and cholesterol build up respectively (Chan *et al.*, 2008; Clark and Weber, 1998). Post mortem histological analyses of adrenals from affected individuals with FGD have disorganised glomerulosa cells and absent fasciculata and/or reticularis cells (Clark and Weber, 1998). The disorganisation of the ZG in these patients may explain the subtle changes in mineralocorticoids sometimes seen in FGD patients. Subtle changes to aldosterone levels might be expected given that MC2R is expressed throughout the developing and adult adrenal cortex, including the ZG, and reports suggest ACTH stimulation can increase aldosterone synthesis (Arvat *et al.*, 2000; Davidai *et al.*, 1984; Reincke *et al.*, 1998; Spark and Etzkorn, 1977; Xia and Wikberg, 1996). However, aldosterone synthesis is primarily governed by the RAAS system, which would presumably prevent significant changes to aldosterone production.

A common phenotypic feature of FGD is hyperpigmentation, which either presents at birth or develops at a later stage. Hyperpigmentation is caused by elevated levels of ACTH over-stimulating MC1R receptors, which are responsible for the production of eumelanin pigment. Genetic variants in the *MC1R* gene are found in 80% individuals with red hair and pale skin (Valverde *et al.*, 1995). In an interesting case report, one patient with FGD was reported to have an *MC2R* mutation but no hyperpigmentation (Turan *et al.*, 2012). Sequencing of the *MC1R* gene in this patient revealed a homozygous inactivating mutation previously associated with red hair and fair skin, explaining the discrepancy (Turan *et al.*, 2012).

Another feature observed in FGD patients is the absence of adrenarche, the production of adrenal androgens during puberty, through the action of ACTH on MC2R receptors expressed in the ZR (Weber *et al.*, 1997). Patients with FGD have delayed or sparse pubic hair development due to low adrenal androgen levels, but breast development and ovarian development are normal as are regular menses in women, as the hypothalamic-pituitary-gonadal axis is not affected (Chan *et al.*, 2008; Ishii *et al.*, 2000).

FGD is easily treated with glucocorticoid replacement therapy in the form of oral hydrocortisone and long-term prognosis is good (Metherell *et al.*, 2006). Doses are usually 10–12 mg/m^2/day in children and 20–30 mg/day in adults (Chan *et al.*, 2008).

1.4.3 Melanocortin Receptor family

The first genetic cause of FGD was only identified following the cloning of the melanocortin receptors in 1992 by Mountjoy and colleagues (Cone *et al.*, 1993; Mountjoy *et al.*, 1992).

The Melanocortin receptors (MCR) are a subfamily of class A GPCRs and are characterised by their short coding sequences and absence of certain commonly conserved GPCR motifs. The receptors have typical GPCR topology with 7 α-helix transmembrane domains (TMD), three intracellular and three extracellular loops (Cooray and Clark, 2011), and are distinguished by short N- and C-terminal ends. MCR activity is mediated by adenylyl cyclase which induces cAMP signalling (Cooray and Clark, 2011).

The melanocortin receptors respond to ligands synthesized from the 231 amino-acid pro-opiomelanocortin precursor peptide (POMC), which is synthesised in the pituitary following CRF receptor activation from CRF secreting hypothalamic neurons. The enzyme is cleaved into a number of different products depending on tissue specific expression of prohormone convertase (PC) enzymes (Fig. 1.6).

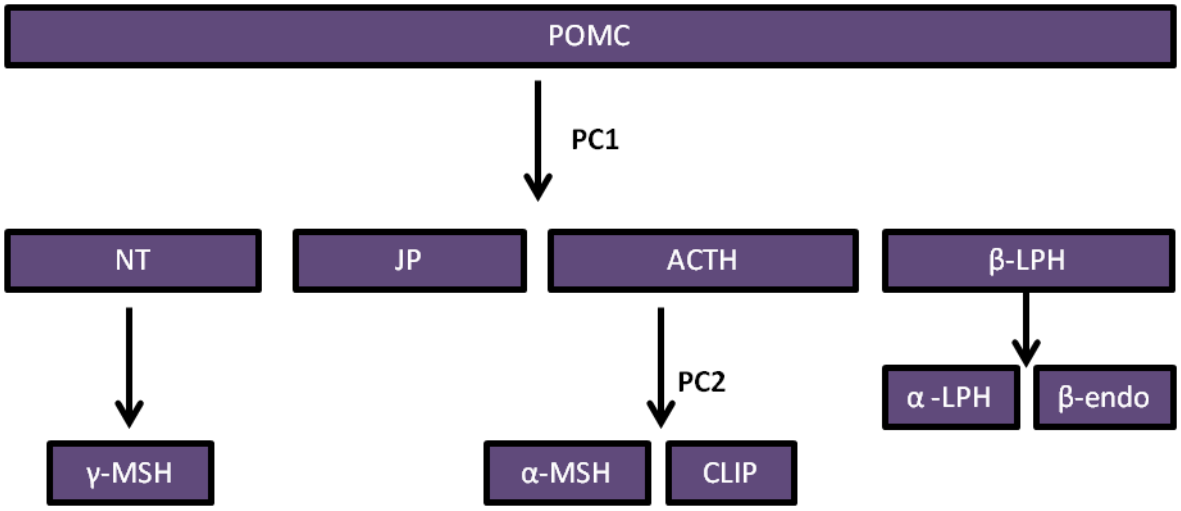

Figure 1. 6: POMC cleavage.

POMC is cleaved by prohormone convertases 1 and 2 (PC1 and PC2) in the pituitary gland to yield N-terminal peptide (NT), melanocyte stimulating hormone (MSH), corticotrophin-like intermediate peptide (CLIP), joining peptide (JP), adrenocorticotrophin (ACTH), Lipotrophin (LPH) and β-endorphin (β-endo) Adapted from (Raffin-Sanson *et al.*, 2003) and (Metherell *et al.*, 2006).

In corticotroph cells PC1 expression leads to cleavage of POMC into ACTH as well as other peptides. In melanotroph cells, these derivatives are further cleaved to peptides including α-, β- and γ-melanocyte stimulating hormone (MSH) (Raffin-Sanson *et al.*, 2003).

The ligand specificity for the melanocortin receptors is outlined in table 1.2. It is interesting to note, that whereas MC1,3,4,5R respond to multiple POMC derivatives, MC2R responds only to ACTH (Cone *et al.*, 1993).

Receptor	Ligand Specificity
MC1R	α-MSH> ACTH> γ-MSH
MC2R	ACTH
MC3R	γ-MSH >ACTH >α-MSH
MC4R	α-MSH> ACTH> γ-MSH
MC5R	α-MSH> ACTH> γ-MSH

Table 1. 2: Melanocortin receptors have varying ligand specificity.

MC1R, MC3R, MC4R and MC5R are all responsive to α-MSH, γ-MSH and ACTH. MC2R has one ligand which is ACTH (Metherell *et al.*, 2006).

The melanocortin receptors have a broad range of functions which are all important physiological processes. MC1R controls skin pigmentation (Valverde *et al.*, 1995), MC2R is vital for HPA axis regulation of steroidogenesis**,** MC3R and MC4R are involved in appetite regulation and energy homeostasis (Butler *et al.*, 2000; Chen *et al.*, 2000; Marsh *et al.*, 1999) and MC5R is thought to be involved in exocrine function (Chagnon *et al.*, 1997; Labbé *et al.*, 1994; Ogawa *et al.*, 2004).

1.4.4 Melanocortin 2 Receptor

The *MC2R* gene is located to chromosome 18p11.2 and is expressed as a 297 amino acid protein, making it the smallest member of the melanocortin receptor family. It is unique amongst the melanocortin receptors in that it responds only to one ligand, ACTH, and is often referred to as the ACTH receptor.

Like the other MCRs, MC2R has typical GPCR topology, as detailed above. The extracellular N-terminus is involved in membrane transport, as substitution of this segment for the corresponding MC4R segment reduces cell surface expression (Fridmanis *et al.*, 2010). The transmembrane domains (TM) contain binding sites for ACTH. Specifically, TM2, 3 and 6 contain binding sites analogous to other MCRs, but TM4, 5 and 7 contain unique binding sites for ACTH which determines the receptors selectivity for ACTH as a ligand (Chen *et al.*, 2007; Fridmanis *et al.*, 2010). TM3 and 4 were also reported to be involved in intracellular retention (Fridmanis *et al.*, 2010). Hirsch *et al* reported that loss of the C-terminus can impair cell surface expression and cAMP response.

1.4.5 MC2R life cycle

When activated, MC2R associates with heterotrimeric G proteins and catalyses the exchange of GDP for GTP on the alpha subunit ($G\alpha_s$), which results in the dissociation of the alpha unit from the beta and gamma (Clark et al., 2003; Ritter and Hall, 2009). The alpha unit binds to and activates adenylyl cyclase which generates cAMP, leading to an increase in Protein Kinase A (PKA) activity. PKA increases the transcription of steroidogenic genes and increases cholesterol import (Chan *et al.*, 2011). ACTH stimulation also upregulates the transcription of *MC2R*, increasing the amount of MC2R at the cell surface and prolonging signalling, hence the receptor is positively regulated by its ligand (Hofland *et al.*, 2012).

Following ACTH stimulation, desensitisation of the receptor occurs at a fast pace, with 60% of MC2R desensitised within 30 minutes (Baig et al., 2001; Clark et al., 2003). Baig *et al.* (2001) showed that PKA mediates desensitisation as the PKA inhibitor H89, used at concentrations specific to PKA, resulted in a complete loss of desensitisation for 30 to 60 minutes after a second ACTH stimulation. Site directed mutagenesis of a PKA phosphorylation site in MC2R (serine 208) resulted in a loss of desensitisation compared to wildtype MC2R when expressed in mouse Y6 adrenocortical cells.

Following desensitisation, MC2R is internalised by the clathrin dependent mechanism. Baig *et al.* (2002) showed that internalisation of MC2R in Y1 cells is halted when cells are treated with concanavalin A or hypertonic sucrose, which inhibit clathrin-mediated endocytosis. Clark and colleagues also confirmed that MC2R is not internalised through the caveolae mechanism because inhibitors filipin and nystatin had no effect on internalisation. Kilianova *et al* (2006) also confirmed these results using immunofluorescence on M3 cells, showing that β-arrestin-2-GFP colocalises with myc-hMC2R in endocytic compartments following incubation with ACTH. hMC2R did not colocalise with caveolin-1 with or without ACTH incubation (Kilianova *et al.*, 2006).

1.4.6 *MC2R* expression

MC2R is predominantly expressed in the adrenal cortex where it mediates cAMP signalling leading to steroidogenesis. It is expressed in all three zones, however ACTH acts predominantly on the ZF (Mountjoy *et al.*, 1992). Gorrigan *et al.* showed through *in situ* hybridisation that in the rat adrenal, *MC2R* expression is high in the ZF, following a gradient reduction towards the medulla. The highest expression was seen in the inner undifferentiated zone of adrenal cortex, a region between the ZG and ZF which is deficient of *CYP11B1* expression, and is thought to contain stem cells involved in adrenal cell differentiation and maintenance (Mitani *et al.*, 2003; Wright and Voncina, 1977).

Outside of the adrenal, MC2R is expressed at low levels in the skin, lymphocytes, and adipose tissue (Andersen *et al.*, 2005; Boston, 1999; Mountjoy *et al.*, 1992; Slominski *et al.*, 1996). Though the role of MC2R in these tissues is not completely understood, in adipocytes, MC2R as well as MC5R, have been shown to be involved in lipolytic actions of ACTH and α-MSH (Boston, 1999). Furthermore, studies have reported the involvement of MC2R and MC5R signalling in the inhibition of leptin production, a satiety hormone (Maffei *et al.*, 1995; Norman *et al.*, 2003; Zhang *et al.*, 1994). The expression of *MC2R* in the undifferentiated zone of the adrenal cortex suggests a role for ACTH in zonal development

(Gorrigan *et al.*, 2011). It is important to note that port-mortem analysis of adrenals taken from patients with FGD show a disorganised ZG with loss of the ZF and ZR (Clark and Weber, 1998).

During development, MC2R is widely expressed, with particularly high expression in the adrenal gland. High expression is also seen in the developing lung, where the production of glucocorticoids modulates maturation (Simard *et al.*, 2010), and in the testes, where it regulates steroidogenesis (O'Shaughnessy *et al.*, 2003).

1.4.7 *Mc2r*$^{-/-}$ knockout mice

The *Mc2r*$^{-/-}$ mouse was characterised in 2007 by Chida and colleagues (Chida *et al.*, 2007). In some regards, it shares a similar phenotype to that of FGD patients with elevated ACTH levels, almost undetectable glucocorticoid levels and loss of ZF with relative preservation of ZG. Unlike FGD patients, there was no increase in longitudinal growth and the mice had aldosterone deficiency similarly to *Pomc*$^{-/-}$ mice. Furthermore, *Mc2r*$^{-/-}$ mice showed low expression of *CYP11B2*. This might suggest that ACTH has a more prominent role in the ZG function and development in mice compared to that in humans (Coll *et al.*, 2006; Karpac *et al.*, 2005). It also shows that the mouse model does not fully recapitulate the human condition.

1.4.8 Familial Glucocorticoid Deficiency (FGD) 1 : mutations in *MC2R*

Early reports predicted that the cause of FGD may be defects in the ACTH receptor MC2R. It wasn't until the receptor was cloned, that Clark and colleagues (1993) identified the first inactivating *MC2R* mutation in a patient with FGD, which was a homozygous base change causing amino acid substitution p.S74I. Since then, more than 40 pathogenic mutations have been reported, and mutations in *MC2R* are found in 25% of the FGD cohort (Fig 1.7) (Clark *et al.*, 2009; Clark *et al.*, 2005). The other 75% of patients remained with unknown aetiology,

showing FGD is a genetically heterogeneous condition (Weber and Clark, 1994). Mutations in *MC2R* are classed as FGD type 1 (FGD1).

The majority of *MC2R* mutations are missense mutations that render the receptor incapable of trafficking to the cell surface; however some are trafficking competent and affect ligand binding (Chung *et al.*, 2008). The pathogenetic mechanism underlying FGD therefore lies in the inability for ACTH to promote downstream cAMP signalling (Chung *et al.*, 2008). For this reason, FGD is sometimes referred to as 'the hereditary unresponsiveness or resistance to ACTH' (Clark *et al.*, 2009).

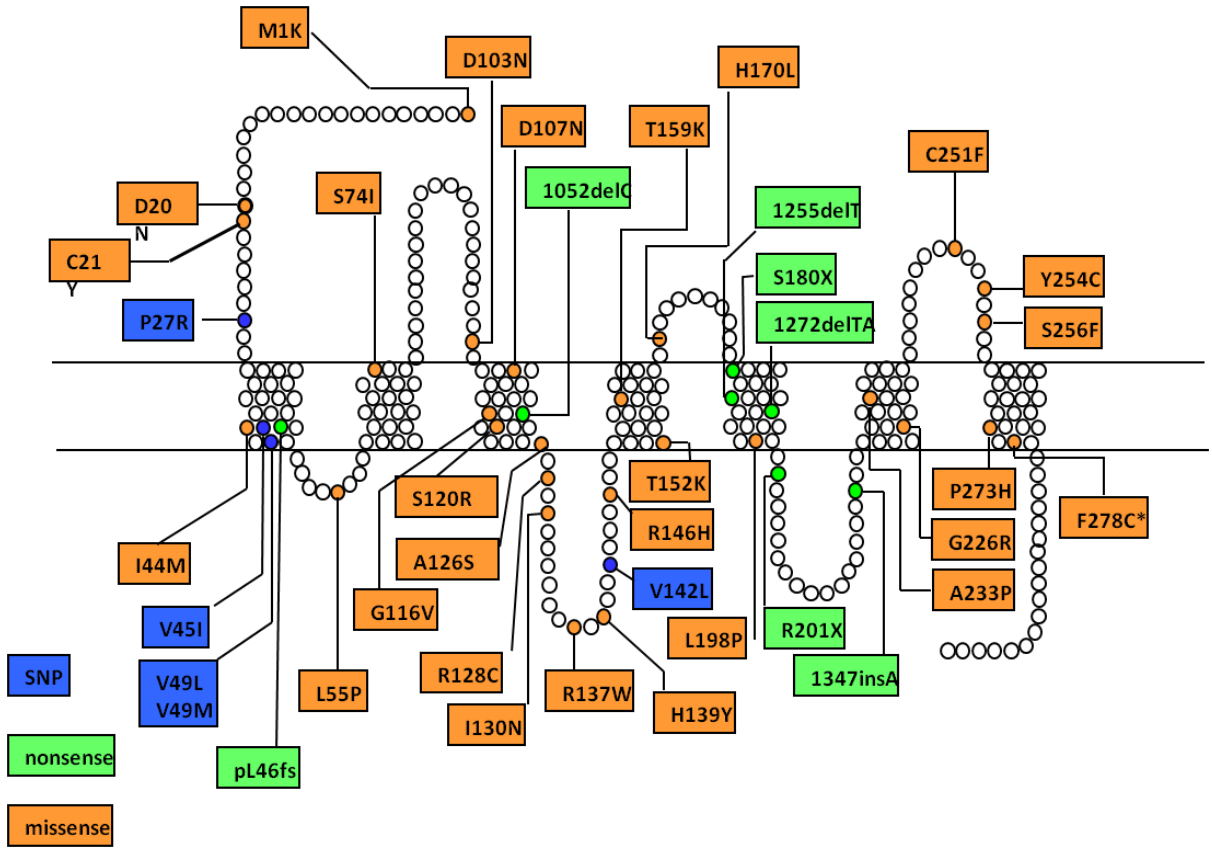

Figure 1. 7. *MC2R* mutations

The majority of MC2R mutations are missense mutations, affecting trafficking of the receptor to the cell surface. (Chung *et al.*, 2008) *Blue*, single nucleotide polymorphism (SNP); *Green*, nonsense mutation; *Orange* missense mutation.

Homozygous nonsense mutations in *MC2R* are rare which suggests the mutations might present a different phenotype than FGD, or that such mutations lead to reduced survival during foetal development (Clark *et al.*, 2009). However, nonsense mutations have been reported and suggested to cause a more severe phenotype including derangements to the RAAS axis (Lin *et al.*, 2007). A second study clinically reviewed a separate group of FGD patients with nonsense *MC2R* mutations and discounted these findings showing the derangements were mild and not associated with clinically significant mineralocorticoid deficiency that would require long-term mineralocorticoid replacement (Chan *et al.*, 2009a)**.**

Gain-of-function *MC2R* mutations are even rarer. One patient has been reported with such a mutation resulting in cyclical Cushing's syndrome (Swords *et al.*, 2002). Another patient with the same gain-in-function mutation also had a loss-in-function *MC2R* mutation. Because the loss-of-function mutation rendered the receptor trafficking-incompetent, the gain-of-function was void, and the patient presented with FGD (Chan et al., 2009a).

Generally the genotype-phenotype correlation of FGD1 patients is poor and one genotype may show highly variable levels of ACTH resistance and cortisol production in different individuals (Elias *et al.*, 1999). However, a specific clinical feature of FGD type 1 is tall stature, the mechanism for which is not fully understood. With the growth hormone-insulin-like growth factor (IGF-1) axis unchanged (Elias *et al.*, 2000), it has been suggested that tall stature is due to excessive ACTH acting on melanocortin receptors expressed in bone, increasing intracellular free $Ca2^{+}$ in resting chondrocytes causing chondrocyte terminal differentiation (Elias *et al.*, 2000; Evans *et al.*, 2004; Imamine *et al.*, 2005). Increased growth rate can be attenuated in patients following hydrocortisone treatment (Chan *et al.*, 2008; Clark and Weber, 1998).

1.4.9 Expression of *MC2R* in heterogeneous cells lines

Studies attempting to characterise MC2R have been hindered by the apparent inability to functionally express MC2R at the cell surface in heterologous cell lines. MC2R is retained in

the ER when expressed in heterologous cells, and a functional receptor that is ACTH responsive is only attainable in cell lines that endogenously express MC2R such as adrenocortical cells. Functional expression of *MC2R* was possible in Y6 and OS3 cell lines (Schimmer *et al.*, 1995), which lack endogenous MC2R, but possess all the other machinery necessary for the expression of a functional MC2R. This enabled researchers to characterise a number of *MC2R* mutations associated with FGD, without interference of endogenous receptors (Elias *et al.*, 1999). Y6 and OS3 cell lines are derived from the mouse Y1 adrenal cell line, and hence, it was suggested that an adrenal specific factor, was necessary for cell surface expression of MC2R (Noon *et al.*, 2002).

1.4.10 Discovery of melanocortin receptor 2 accessory protein (MRAP)

Given that 75% FGD cases had unknown aetiology, the theory that an adrenal specific factor was required for MC2R cell surface expression, suggested a potential candidate gene for FGD. In search of this gene, Metherell *et al.* (2005) carried out a whole genome scan by single nucleotide polymorphism (SNP) array in one consanguineous family. Homozygosity mapping revealed a locus on chromosome 21q22.1. Analysing the tissue distribution of genes in this region identified one gene, *C21orf61* that was expressed in the adrenal but not brain or liver. Further analysis of the tissue distribution by RT-PCR showed it was highly expressed in the adrenal cortex, with lower expression levels in the brain, thyroid, ovary, testis and breast. Sequencing the index patient revealed a homozygous splice site mutation, and screening probands from over 100 patients identified 26 affected individuals with mutations, accounting for 20% of the FGD cohort.

The gene identified encoded a small protein named ‘fat-associated low-molecular weight protein’ (FALP), originally described by Xu *et al.* (2002) as a protein that was upregulated on differentiation of mouse 3T3-L1 cells into adipocytes; however the function was mainly unknown. It was hypothesised that this protein was the adrenal specific factor required to traffic MC2R to the cell surface.

Functional analysis of the gene resulted in its renaming to *M*elanocortin 2 *R*eceptor *A*ccessory *P*rotein *(MRAP)*. MRAP was shown to co-immunoprecipitate with MC2R indicating the two formed a complex. When expressed in heterologous chinese hamster ovary (CHO) cells, epitope-tagged mouse MRAP localised to the ER and plasma membrane. Expression of epitope-tagged mouse MC2R alone, showed localisation to the ER. However, co-expression of MRAP with MC2R in these cells led to a proportion of the MC2R pool shifting localisation to the plasma membrane, co-localising with MRAP. These immunocytological studies have been confirmed using human MRAP (Sebag and Hinkle, 2007; Webb *et al.*, 2009). Furthermore, co-transfection of MRAP with MC2R in heterologous SK-N-SH cells led to ACTH-responsiveness, which was absent when MC2R was transfected alone.

Other studies have since shown endogenous MRAP and MC2R in mouse Y1 cells co-localise at the cell surface, and produce a cAMP response when stimulated with ACTH, which is significantly reduced following knockdown of *MRAP* with small interfering RNA (siRNA) (Cooray *et al.*, 2008). The cAMP response can be rescued following transfection of siRNA resistant human MRAP. Analysing cell lysates by immunoblotting for MC2R showed that MC2R migrates as different species depending on the cotransfection of MRAP. The authors suggest that MRAP may promote some post-translational modifications to increase trafficking of MC2R (Sebag and Hinkle, 2007). Interestingly, glycosylation of MC2R promotes cell surface expression (Roy *et al.*, 2010).

MRAP follows a similar expression pattern to *MC2R* in the foetal and adult adrenal cortex, with highest expression in the undifferentiated zone, and high expression also observed in the ZF (Gorrigan *et al.*, 2011). The mRNA expression, like *MC2R*, is upregulated by ACTH in a pulsatile manner, suggesting the expression of steroidogenic enzymes depends on the level of MC2R at the cell surface (Hofland *et al.*, 2012; Spiga *et al.*, 2011; Xing *et al.*, 2010).

1.4.11 MRAP structure and topology

Human *MRAP* is a 6 exon gene localised to chromosome 21q22.1. Alternative splicing of the gene yields two MRAP isoforms: *MRAPα,* encoded by exons 3 to 5, and *MRAPβ*, encoded by exons 3, 4 and 6, expressed as 172 and 102 amino acid proteins respectively (Fig. 1.8). Studies into the expression of *MRAP* in the adrenal gland, have not observed mRNA transcripts that include the first two exons (Webb and Clark, 2010). MRAP is a single TMD protein with a highly conserved N-terminus and TMD and divergent C-terminus which is evident between α and β isoforms (Webb and Clark, 2010).

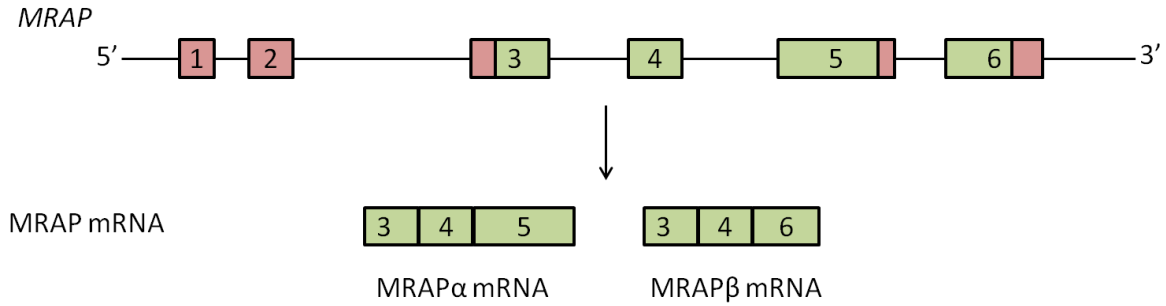

Figure 1. 8: *MRAP* splicing.

Alternative splicing of the *MRAP* leads to two isoforms of the gene: MRAPα (encoded by exons 3-5) and MRAPβ (encoded by exons 3, 4 and 6) respectively. In addition, *MRAP* has a homologue gene called *MRAP2* which has 39% sequence identity (not shown).

Generally, *MRAP* is not particularly conserved amongst species; human and mouse *MRAP* share 63% homology with sequence variation occurring at the C-terminus. An ortholog of MRAPα is detectable in zebrafish, but there is no ortholog in Fugu or Tetraodon (Klovins *et al.*, 2004), indicating MRAP may not have been needed for MC2R cell surface expression in these species, or that *MRAP2*, a homologous gene to *MRAP*, took on this role. There is also no expression data to suggest the MRAPβ isoform is expressed outside of primates (Webb and Clark, 2010).

Western blot analysis of endogenous mouse MRAP (mMRAP) revealed a 32kDa band, much heavier than its predicted weight of 14.1kDa. In two separate studies investigating both endogenous and epitope-tagged MRAP, immunoprecipitation and mass spectrometry confirmed that MRAP is able to form a SDS-resistant homodimer (Cooray *et al.*, 2008; Sebag and Hinkle, 2007). Moreover, prediction tools suggested MRAP orientated with its N-terminus extracellular to the plasma membrane. However, immunofluorescent staining of non-permeabilised Y1 cells endogenously expressing *Mrap* with both N- and C-terminal mMRAP antibodies detected both termini at the cell surface, suggesting dual topology (Sebag and Hinkle, 2007). Further investigation by Sebag and Hinkle (2007) using coimmunoprecipitation and glycosylation analysis showed that mMRAP exists as an antiparallel homodimer, a unique dual topology previously undocumented for single TMD proteins (Sebag and Hinkle, 2007).

The proteomic domains involved in MRAP function have been explored in multiple studies. After it was confirmed that MRAP and MC2R formed a complex (Cooray *et al.*, 2008; Metherell *et al.*, 2005; Sebag and Hinkle, 2007), Webb *et al.* (2009) used a number of *MRAP* truncation constructs to investigate the functional domains of human MRAP, and showed using co-immunoprecipitation that a region between residues 36 and 61, corresponding to the TMD, was required for interaction with MC2R. In agreement, Sebag and Hinkle (2007) also showed, using mMRAP, that substituting the TMD with the corresponding region of RAMP3, an accessory protein to the odorant receptors, prevented MC2R trafficking. mMRAP was however able to form a homodimer indicating this region was not required for dimerisation of mMRAP.

Sebag and Hinkle (2007) used biomolecular fluorescence complementation to show mMRAP could form an antiparallel homodimer at the ER and plasma membrane, and that parallel homodimers were not apparent. Deleting residues 31-37 of the N-terminus, proximal to the TMD forced mMRAP into a N_{exo}/C_{cyto} topology suggesting the region was needed for antiparallel topology. Deletion of this positively charged region also prevented dimerisation. Interestingly, inserting this region into RAMP3, which has single N_{exo}/C_{cyto} topology, forced

RAMP3 into dual topology, as detected by ELISA. MC2R was retained at the ER when the dimerisation domain was deleted showing mMRAP needs to be a dimer to traffic MC2R.

The N-terminus of MRAP has been shown to have different roles in human and mice. In humans, deletion of the N-terminus, specifically between residues 9-24, a tyrosine rich region, prevents MC2R trafficking to the cell surface (Fig. 1.9) (Webb *et al.*, 2009). However, deletion of the N-terminus of mMRAP does not affect trafficking. It does however abolish ACTH responsiveness, suggesting that mMRAP has two roles in MC2R function: trafficking and signalling. Narrowing this region, mutation of residues 18-21 within the N-terminus, the LDYI motif, resulted in no measurable ACTH response. Sebag *et al* went on to show that these residues are involved in MC2R binding of ACTH.

The unconserved C-terminus of MRAP is not essential to its function, as its deletion does not prevent MC2R function. The C-terminus has been suggested to have a regulatory role in MC2R function, based on observations made in several studies. The length of the C-terminus seems to be a key factor, for example cell surface expression and ACTH responsiveness of MC2R in transfected 293/FRT cells were higher in cells co-expressing the shorter 102aa MRAPβ than 172aa MRAPα, and more MRAPβ was localised to the plasma membrane than MRAPα (Roy *et al.*, 2007). Similarly, deletion of the C-terminus of human MRAP increases cell surface expression of MC2R (Webb *et al.*, 2009). For mouse Mrap, deletion of the C-terminus did not affect cell surface expression. It did however, attenuate ACTH responsiveness but did not completely abolish the cAMP response (Sebag and Hinkle, 2007).

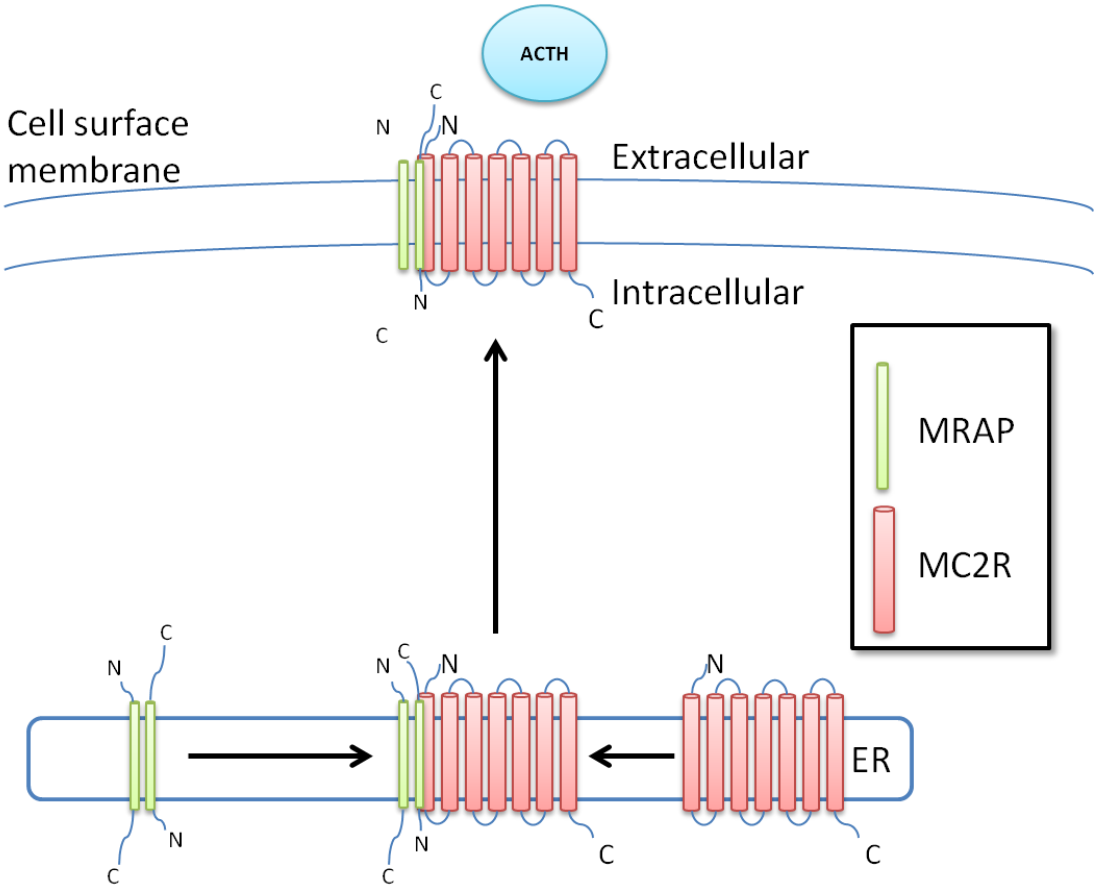

Figure 1. 9: MC2R trafficking by MRAP

Illustration showing MC2R cell surface expression is facilitated by MRAP. The MRAP antiparallel homodimer binds to MC2R in the ER through its TMD, and transports the receptor to the cell surface where it is able to respond to ACTH. It is essential that MRAP forms an antiparallel homodimer to be capable of transporting MC2R. For human MRAP, trafficking is also dependent on the N-terminus whereas the C-terminal region has a regulatory role, its length influencing the percentage of MC2R at the cell surface. In mice, the N-terminus is essential for ACTH responsiveness and the C-terminus regulates the intensity of the response. ER; Endoplasmic reticulum (Based on Webb *et al.* 2009).

1.4.12 MRAP2

A homologue of MRAP named MRAP2 exists which was identified shortly after the discovery of MRAP (Chan *et al.*, 2009b; Metherell *et al.*, 2005). MRAP2 shares 39% sequence identity with MRAP at the N-terminus, and is expressed as a 205aa single transmembrane domain protein.

Compared to *MRAP* which has a broad expression pattern, in humans *MRAP2* is expressed exclusively in the adrenal and brain, particularly the hypothalamus (Chan *et al.*, 2009b). This differs in lower vertebrates such as zebrafish where *MRAP2* is more ubiquitous (Agulleiro *et al.*, 2010). The conservation of *MRAP2* is higher than *MRAP* in vertebrates, suggesting *MRAP2* is the ancestral gene (Webb and Clark, 2010). *MRAP2* expression is relatively low in the adult adrenal compared to *MRAP*, but high in the foetal adrenal suggesting a role in adrenal development (Gorrigan *et al.*, 2011).

MRAP2 has been functionally characterised and shown to have similar function to MRAP. It is expressed at the plasma membrane and endoplasmic reticulum (ER), mirroring the subcellular localisation of MRAP, and is capable of forming homodimers as well as heterodimers with MRAP, both of which are thought to be anti-parallel (Chan *et al.*, 2009b; Sebag and Hinkle, 2009b, 2010). It is also capable of trafficking MC2R to the cell surface in heterologous cells to the same degree as MRAP, and enables the receptor to respond to ACTH.

There are however, differences between the proteins. Firstly, deglycosylation of MRAP2 abolishes the ability for MC2R to respond to ACTH, indicating the separate roles of MRAP2 in trafficking and signalling are dependent on glycosylation whereas glycosylation does not affect the functioning of MRAP.

Secondly, the MC2R-MRAP2 complex requires 1000X ACTH concentration to elicit the same cAMP response as MC2R-MRAP following ACTH stimulation (Gorrigan *et al.*, 2011). These levels are supraphysiological, indicating the MC2R-MRAP2 complex has low affinity

for ACTH binding (Gorrigan *et al.*, 2011; Sebag and Hinkle, 2009b). Interestingly, MRAP2 does not have the LDYI domain of MRAP, shown to be involved in ACTH binding and response (Sebag and Hinkle, 2009). Insertion of this motif into MRAP2 increases the ACTH response of MC2R to levels that are seen with MRAP.

The role of MRAP2 in the adrenal is not fully understood. It has been suggested that MRAP2 negatively regulates MC2R function, by competing with MRAP for binding of the receptor (Sebag and Hinkle, 2010). In this study, changing the ratio of MRAP/MRAP2 in cells cotransfected with MC2R shifted the cAMP dose response curve further right when MRAP2 concentration was increased. However, this phenomenon has not been observed in other studies, which suggest addition of MRAP2 has an additive effect to MRAP/MC2R complex cAMP generation (Agulleiro *et al.*, 2010) or no effect at all (Gorrigan *et al.*, 2011).

1.4.13 MRAP and MRAP2 extra adrenal functions

The tissue expression profiles of *MRAP* and *MRAP2* are broader than that of *MC2R*, suggesting the proteins have additional non-adrenal functions independent of MC2R (Metherell *et al.*, 2005). Indeed, MRAP and MRAP2 have been demonstrated to interact with all 5 MCRs by co-immunoprecipitation (Chan *et al.*, 2009b). Apart from MC2R, which requires an accessory protein, the other members of the melanocortin receptor family are capable of cell surface expression in heterologous cell lines.

In keeping with this, co-transfection of MC1R with human MRAP or MRAP2, does not affect cell surface expression or responsiveness of the receptor (Chan *et al.*, 2009b; Sebag and Hinkle, 2010). Similarly, MC3R cell surface expression is not affected by co-transfection of MRAP or MRAP2, however one study found MC3R signalling was reduced in presence of MRAP2 (Chan *et al.*, 2009b), supporting the dual functions of MRAPs (Novoselova *et al.*, 2013).

In contrast to these receptors, MC5R cell surface expression and signalling have been found to be negatively regulated by MRAP and MRAP2 (Chan et al., 2009b; Sebag and Hinkle, 2009a, 2010). The effect of the MRAPs on MC4R is not clear, as there are mixed reports of no effect and negative regulation of the receptor MRAP2 (Chan et al., 2009b; Sebag and Hinkle, 2009a, 2010). It is of value to note that these studies used different techniques to measure receptor responsiveness.

The significance of these interactions is relatively unexplored. *MC3R* is expressed in the arcuate nucleus and ventromedial nucleus of the hypothalamus, and is involved in energy metabolism. *MC3R* mutations are also associated with obesity (Feng *et al.*, 2005). *MC4R* is expressed in the PVN of the hypothalamus and nuclear accumbens and is involved in appetite regulation. Consequently, knockout mice are obese and mutations in *MC4R* cause obesity in early childhood (Lee *et al.*, 2008; Vaisse *et al.*, 1998; Yeo *et al.*, 1998). MC4R in part mediates the stress response, however bar one case there are no reports of *MRAP* mutations causing obesity (Rumie *et al.*, 2007). On the other hand, *MRAP2* is highly expressed in the hypothalamus, and fittingly, a recent study has reported that *Mrap2*$^{-/-}$ mice are obese (Asai *et al.*, 2013). Given that no *MRAP2* mutations are associated with derangements to the HPA axis, the above studies suggest MRAP2 has a role independent of adult adrenal function. In support of this notion, whereas *MC2R* and *MRAP* are transcriptionally upregulated by ACTH, *MRAP2* is unaffected (Hofland *et al.*, 2012) and to date, there are no mutations in *MRAP2* associated with adrenal insufficiency.

1.4.14 Familial Glucocorticoid Deficiency (FGD) type 2: *MRAP* mutations

Mutations in *MRAP* account for 20% of the FGD cohort. Since the initial discovery of MRAP, further mutations have been described by other groups (Akın *et al.*, 2010; Jain *et al.*, 2011; Modan-Moses *et al.*, 2006; Rumie *et al.*, 2007). The majority of these mutations are nonsense or splice site mutations, therefore extremely deleterious to protein function and hence, patients with FGD2 typically present earlier with a more severe phenotype compared

to FGD1 patients, who typically have missense mutations (Chung *et al.*, 2010; Chung *et al.*, 2008). Despite earlier presentation, baseline levels of cortisol and ACTH do not differ between FGD1 and 2 patients (Chung *et al.*, 2010).

Two missense mutations in *MRAP* have been described, which give rise to a milder phenotype with later onset (Hughes *et al.*, 2010). Most *MRAP* mutations, excluding these two missense mutations, result in truncation of the transmembrane domain, which is involved in MC2R interaction, and therefore trafficking to the cell surface (Meimaridou *et al.*, 2012a). As a result, MC2R is retained at the ER.

1.4.15 Familial Glucocorticoid Deficiency (FGD) type 3/Non-classical LCAH: Mutations in *STAR*

A genome-wide linkage study using microsatellite markers previously linked a locus on chromosome 8 (8q12-1-21-2) to FGD in 3 families with unknown aetiology (Génin *et al.*, 2002; Metherell *et al.*, 2009). With no obvious candidate gene, SNP array genotyping of 1 of the 3 families was carried out in order to narrow the region, however the region was in fact expanded, revealing *STAR* as a putative candidate gene for FGD. Mutations in *STAR* are a known cause of lipoid congenital adrenal hyperplasia (LCAH), a disease characterised by severe adrenal and gonadal insufficiency. However, mutations retaining a certain degree of functionality of the gene present a milder phenotype with late onset, classed as non-classical LCAH (OMIM #201710). In some cases where salt loss is minimal, the phenotype is indistinguishable from FGD, and therefore also classed as FGD3 (OMIM %609197 GCCCD3).

Classical LCAH is characterised by very low levels of steroids including cortisol and aldosterone, with elevated basal levels of plasma ACTH and renin. Patients have grossly enlarged adrenals due to the build-up of cholesterol in lipid droplets, and are hyperpigmented because of excess ACTH (Miller, 1997). Presentation usually occurs a few months into life, with no salt loss crisis at birth because aldosterone is synthesised at low levels in the foetal

adrenal (Miller, 2013). Because of the absence of testosterone production during gestation, androgenisation does not occur in 46XY karyotypes leading to female external genitalia, but female internal reproductive organs do not develop because sertoli cells function normally expressing anti-mullerian hormone (Miller, 2013). 46XX individuals might have normal puberty with breast development and cyclic vaginal bleeding due to the low levels of oestrogen that is synthesised through a StAR-independent mechanism, but have hypergonadotropic hypogonadism leading to anovulatory cycles and build-up of cholesterol causing damage to the ovaries (Bose *et al.,* 1997; Fujieda *et al.,* 1997).

The development of LCAH has been described in a '2-hit model', where the diminished activity of StAR leads to steroid deficiency evoking increased ACTH and gonadotropin levels to compensate, which increases cholesterol uptake and synthesis. Cholesterol build-up leads to mitochondrial damage which further incurs damage to the steroidogenic capacity of the cell (Bose *et al.,* 1996; Miller, 1995).

Over 40 mutations in *STAR* have been described that are most frequently in the C-terminal regions between exons 5 and 7 (Miller and Auchus, 2011). Most mutations result in a complete loss of function, however the patients described by Metherell *et al.* (2009) to have isolated glucocorticoid deficiency had mutations p.R188C and p.R192C, which retain 20% StAR activity (Baker *et al.,* 2006). The absence of mineralocorticoid deficiency may have resulted from the low production rate of aldosterone compared to cortisol, hence the ZG would remain relatively undamaged. The patients had normal pubertal development corresponding to their genetic karyotype and 46XX individuals had normal menstrual cycles. There were however additional features compared to classical FGD, for example some patients had hypospadias and affected individuals exhibited varying degrees of fertility (Metherell *et al.,* 2009).

A similar phenomenon is seen with mutations in the *CYP11A1* gene. Mutations in *CYP11A1* that ablate all CYP11A1 activity cause a phenotype clinically indistinguishable from LCAH (Miller, 2013). However, mild mutations in this gene cause milder phenotype, similarly to mild mutations in *STAR* (Parajes et al., 2011). Although *STAR* mutation leads to a more

enlarged adrenal than *CYP11A1* deficiency, which can be diagnostic, the only dependable method of distinguishing between *CYP11A1* and *STAR* mutations is genetic sequencing (Gucev *et al.*, 2013).

1.4.16 *MCM4* mutations in the Irish traveller population

FGD is common amongst the Irish traveller community, a highly consanguineous genetically isolated population. Patients have a variant form of FGD with additional phenotypic characteristics including short stature, increased chromosomal breakage and natural killer (NK) cell deficiency. In addition the cortisol deficiency is mild compared to other forms of FGD**.** In 2012, after ruling out all known causes of FGD, Hughes *et al.* (2012) carried out SNP array and microsatellite genotyping of 7 individuals from 3 families in order to unveil the genetic cause of these pathologies. SNP array genotyping identified three regions of homozygosity shared by 5 of the affected patients on chromosome 4 and 8. Exome capture and resequencing of these regions in one affected patient identified a homozygous splice site mutation c.71-1insG in mini-chromosome maintenance-deficient protein 4 (*MCM4*), which segregated with the disease.

In a parallel study, another group used similar methodology to assess a separate group of 10 affected children with the same phenotype of NK cell deficiency, DNA breakage and FGD, and likewise identified *MCM4* as a candidate gene (Casey et al., 2012).

MCM4 is a DNA helicase, part of the MCM2-7 complex involved in DNA replication. The single nucleotide change prior to exon 2 shifted the consensus splice site upstream, resulting in the insertion of a base into the coding region and a frameshift, leading to a downstream premature stop codon and predicting a severely truncated protein. Immunoblotting lysates from control and patient lymphocytes with MCM4 antibody showed that MCM4 migrated as 2 main species in control cells, but the heavier species representing full length MCM4 was absent from affected patients. The smaller species of MCM4 corresponded to the size of the

protein produced by translation from the third in-frame methionine. The smaller isoform was not detected with an N-terminal antibody, consistent with the N-terminus being absent.

In addition to these findings, immunohistological analysis of adrenals from *MCM4* mutant mice showed abnormal morphology, with atypical spindle-shaped non-steroidogenic cells.

Given that *Mcm4*$^{-/-}$ mice are embryonic lethal, Hughes *et al.* (2012) concluded that the relatively mild phenotype of these patients was due to the remaining translation of the smaller isoform of *MCM4* rescuing patients from a lethal phenotype. The shorter isoform maintains the highly conserved C-terminal domains required for MCM4 function, but lacks the relatively poorly conserved N-terminus involved in protein kinase regulation of cell cycle progression (Sheu and Stillman, 2010). *MCM4* mutations in the Irish traveller population account for 1% of the FGD cohort. (Hughes *et al.*, 2012)

1.4.17 FGD4: Mutations in *NNT*

In a search for further causes of FGD, Metherell *et al.* carried out SNP array genotyping using the GeneChip Human Mapping 10K array Xba142 (Affymetrix) in nine probands with unknown aetiology. Linkage to a locus on chromosome 5 was identified in three consanguineous families (Meimaridou *et al.*, 2012a). Targeted exome sequencing of the proband from one kindred identified a homozygous mutation, p.V533A, in nicotinamide nucleotide transhydrogenase (*NNT*) which was heterozygous in the parents and absent in controls. Homozygous novel variants were also discovered in the other two probands with chromosome 5 linkage.

Sequencing a further 100 FGD patients of unknown aetiology revealed a total of 23 homozygous or compound heterozygous mutations in 16 kindreds, accounting for 10% of the FGD cohort (Fig. 1.10). The mutations spanned the 22 exons of *NNT*, and ranged from missense and nonsense mutations, to splice site mutations and even abolition of the initial methionine (Fig. 1.10).

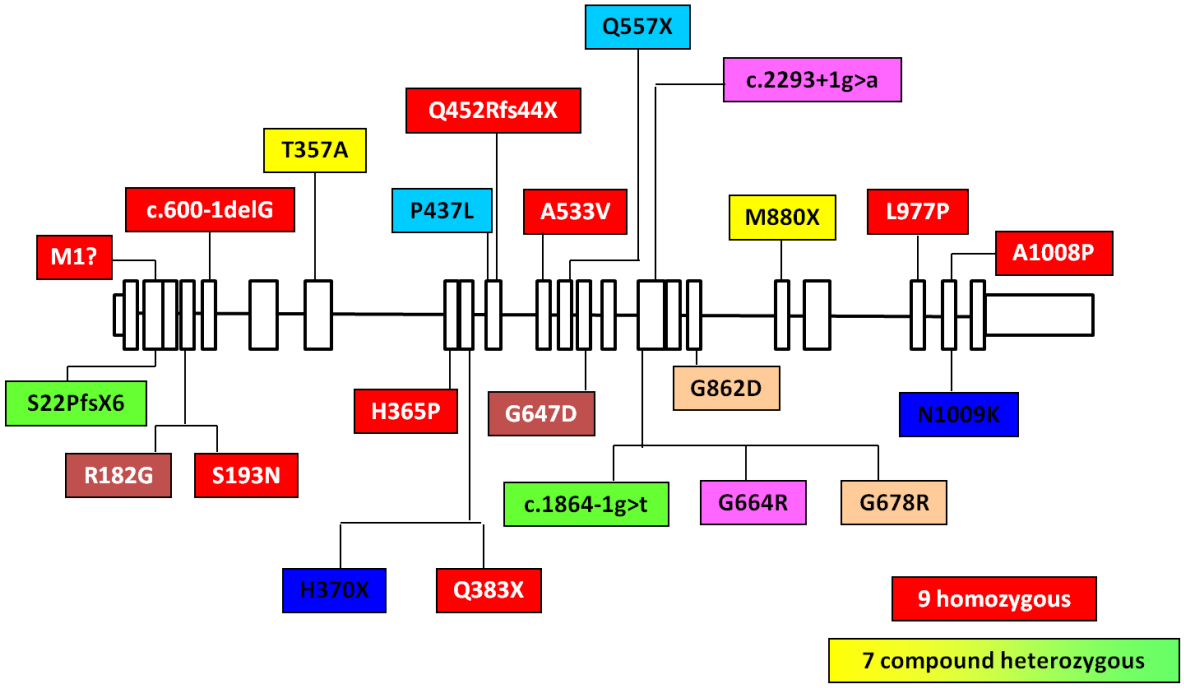

Figure 1. 10: Mutations in *NNT*.

Illustration showing gene structure of *NNT* and mutations described to date. NNT exons are represented by black boxes, with homozygous mutations in white lettering and compound heterozygous mutations in black lettering. Mutations are presented at the protein level or cDNA level (denoted by 'c.'). To date, a total of 23 mutations in 16 families have been described.

NNT is a highly conserved proton translocating dehydrogenase localised to the inner mitochondrial membrane, where it catalyses the interconversion of $NADP^+$ and NAPDH by the reversible reaction NADH + $NADP^+$ <--> NADPH + NAD^+. Under normal physiological conditions and an electrochemical gradient favouring NADPH production, NNT supplies the mitochondria with high concentrations of NAPDH, which is required for the glutathione and thioredoxin systems (Fig. 1.11).

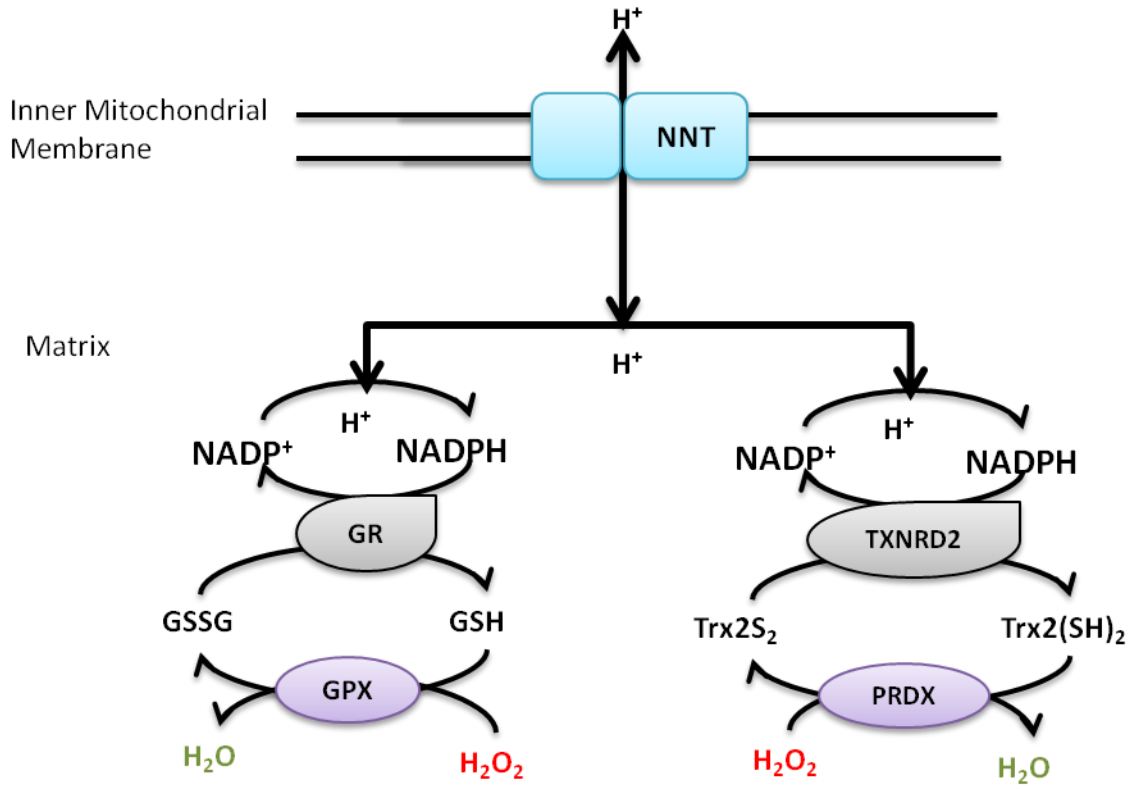

Figure 1. 11: NNT is a mitochondrial dehydrogenase.

NNT supplies glutathione and thioredoxin systems with NADPH which reduces GR and TXNRD2, which in turn reduce GPX and PRDX respectively. *NNT*, nicotinamide nucleotide transhydrogenase; *GR*, glutathione reductase; *TXNRD2*, thioredoxin reductase 2; *Trx2* thioredoxin 2; *GPX*, glutathione peroxidase (1 or 4); *PRDX*, peroxiredoxin (3 or 5).

NADPH is utilised by glutathione reductase to regenerate reduced glutathione (GSSG) from glutathione (GSH) (Rydström, 2006). Glutathione is a potent antioxidant that can reduce disulphides, but it also acts as a cosubstrate in reduction of toxic hydrogen peroxide by the glutathione peroxidases, as described in section 1.7.4. NADPH is also required by thioredoxin reductase 2, the mitochondrial enzyme that reduces thioredoxin, which acts as cosubstrate for peroxiredoxin 3 and 5 which also reduce hydrogen peroxide. Finally NADPH is used by the ferredoxin reductase electron donor system to supply ferredoxin and in turn

mitochondrial steroidogenic CYP enzymes. It therefore clear that mutations in *NNT* have the potential to impair mitochondrial function through several mechanisms.

Previous studies have illustrated the antioxidant role of NNT, for example *Caenorhabditis elegans* lacking *nnt-1,* are more susceptible to oxidative stress because of a lower GSH/GSSG ratio (Arkblad *et al.,* 2005). Furthermore, human phaeochromocytoma (PC12) cells with knockdown of *NNT* exhibited lower cellular NADPH and GSH levels (relative to GSSG) and increased H_2O_2 levels (Yin *et al.,* 2012b).

Investigation into the disease mechanism revealed that *NNT* is widely expressed in humans with high expression in the adrenal, heart, kidney, thyroid and adipose tissues, in agreement with previous studies in mice/rats (Dezso *et al.,* 2008; Meimaridou *et al.*, 2012b; Su *et al.*, 2002; Walker *et al.,* 2004). Knockdown of *NNT* in human adrenocortical carcinoma (H295R) cells increased levels of reactive oxygen species (ROS) and markers of apoptosis, and lowered the GSH/GSSG ratio, indicating an impaired redox potential (Meimaridou *et al.*, 2012b). A sub-strain of C57BL6/J mice carrying a spontaneous 5 exon deletion in *Nnt* had slightly disorganised cells within the ZF with higher levels of apoptosis, and lower basal and stimulated corticosterone levels (Meimaridou *et al.,* 2012b). These mice have previously been demonstrated to have impaired insulin secretion and glucose intolerance due to increased oxidative stress in pancreatic β-cells (Toye *et al.,* 2005).

The above data indicated a novel disease mechanism for FGD, associated with increased levels of oxidative stress.

1.5 Triple A syndrome

Triple A syndrome (OMIM#231550) was initially discovered by Allgrove *et al.* (1978) who reported two pairs of siblings with a combination of adrenal insufficiency, achalasia of the cardia and alacrima (Clark and Weber, 1998). These three features characterise the disorder, as well as the progression of highly variable neurological defects in 60% of cases (Clark and

Weber, 1998). The phenotype of Triple A syndrome is highly variable even within one family, with a low correlation of genotype to phenotype (Prpic *et al.*, 2003). Patients often present with only one or two of these symptoms, the rest developing over time, and therefore should be suspected on the presence of any symptom (Metherell *et al.*, 2006)**.** The earliest symptom to present is usually alacrima, followed by achalasia, which can be easily overlooked on diagnosis (Clark and Weber, 1998). These usually precede adrenal insufficiency which develops at a later stage, suggesting progressive destruction of the gland (Clark and Weber, 1998; Huebner *et al.*, 1999). Hypoglycaemia and hyperpigmentation usually manifest in the first decade of life (Clark and Weber, 1998). Biochemically, 90% patients have isolated glucocorticoid deficiency, but 10% also develop mineralocorticoid deficiency most likely due to destruction of the adrenal cortex (Metherell *et al.*, 2006). Post mortem analysis of patient adrenals revealed atrophy of the ZF. Apart from glucocorticoid replacement, there is currently no treatment for the disease other than symptom relief.

Following linkage of the disease to chromosome 12q13 (Weber *et al.*, 1996), it was demonstrated the 90% of patients with Triple A syndrome possess mutations in the *AAAS* gene (Clark and Weber, 1998). *AAAS* encodes a 60kDa WD-repeat protein which forms part of the nuclear pore complex (NPC), called *al*acrima-*a*chalasia-a*d*renal *i*nsufficiency *n*eurological disorder (ALADIN).

ALADIN is widely expressed with particularly high expression in the adrenal cortex and brain (Cho *et al.*, 2009; Huebner *et al.*, 2002; Metherell *et al.*, 2006; Storr *et al.*, 2005). It is localised to the cytoplasmic side of the NPC, and *AAAS* mutations usually result in incorrect subcellular localisation of the protein, but do not affect the structure of the NPC, indicating targeting of ALADIN to the NPC is key to its function (Cronshaw and Matunis, 2003; Krumbholz *et al.*, 2006)**.**

The exact function of ALADIN at the NPC is not known. Over the past decade, the pathogenesis of Triple A syndrome has been explored and found to be associated with oxidative stress, which may reflect the progressive nature of the disease. Using a bacterial-2-hybrid assay Storr *et al.* showed that ALADIN interacted with ferritin heavy chain protein

(FTH1), which has a DNA-protective role in the nucleus (Storr *et al.*, 2009). FTH1 was not detected in nuclear fractions taken from patient fibroblasts, nor by confocal microscopy when transfected alone in these cells. Only on cotransfection with *AAAS* was FTH1 detected at the nucleus, suggesting ALADIN has a role in nuclear translocation of FTH1. Apoptosis in neuronal cells induced by hydrogen peroxide was reduced by transfection of *AAAS* and/or *FTH1*, suggesting nuclear import of FTH1 by ALADIN is crucial to the DNA-protective role of FTH1, preventing oxidative stress at/in the nucleus.

Other studies have also implicated oxidative stress in the pathogenesis of triple A syndrome. Patient fibroblasts have increased susceptibility to oxidative stress and have higher basal levels of ROS (Hirano *et al.*, 2006; Kind *et al.*, 2010; Kiriyama *et al.*, 2008). Fibroblast cell survival is reduced following depletion of antioxidant glutathione with L-buthionine-(S,R)-sulfoximine (BSO) compared to wildtype cells (Hirano *et al.*, 2006). These cells fail to import DNA repair protein aprataxin (APTX) and DNA ligase I. Transfection of these latter two proteins into patient fibroblasts attenuated the toxic effects of BSO, suggesting these effects were the consequence of failed nuclear import of antioxidant proteins (Hirano *et al.*, 2006).

Despite the above insights into ALADIN function, the disease mechanism for Triple A remains to be understood. Using patient fibroblast models does not consider the tissue specific nature of the disease. Unfortunately, the *Aaas*$^{-/-}$ mouse model does not recapitulate the human phenotype, showing no histological abnormalities compared to wildtype, and only mild neurological disturbances (Huebner *et al.*, 2006).

Taking this into consideration, Prasad *et al.* (2013) generated a human *in vitro* model with shRNA knockdown of *AAAS* in human adrenocortical and neuronal cells to better understand the disease mechanisms underlying Triple A syndrome. Cell viability was significantly reduced in *AAAS* knockdown cells compared to wildtype, which could be rescued with the antioxidant N-acetylcysteine. Cell viability in neuronal cells was not affected by *AAAS* knockdown, but *AAAS* knockdown did increase the sensitivity of these cells to induced oxidative stress. Both adrenal and neuronal *AAAS* deficient cell lines had a reduced

GSH/GSSG ratio indicating cellular toxicity. Crucially, in adrenal cells *AAAS* knockdown lowered cortisol production, due to reduced transcription of *STAR* and protein expression of steroidogenic enzyme CYP11B1, which catalyses the final step of cortisol production. The reduction in cortisol could be partly rescued by treatment of cells with N-acetylcysteine. These data give further evidence that oxidative stress is involved in the pathogenesis of Triple A which subsequently impairs steroidogenesis, but further investigations are required to fully understand the function of ALADIN.

1.6 X-Linked Adrenoleukodystrophy

X-linked adrenoleukodystrophy (X-ALD) (OMIM #300100) is a rare genetic disorder characterised by the build-up of very long chain fatty acids (VLCFA) leading to progressive demyelination in the central nervous system, axonopathy in the spinal cord, and adrenal insufficiency (Galea *et al.*, 2012). There are two phenotypes of the disorder: adrenomyeloneuropathy (AMN), and cerebral demyelinating X-ALD (cerebral-ALD) (Kemp *et al.*, 2012).

AMN is the most common form of X-ALD, and is characterised by peripheral neuropathy and non-inflammatory distal axonopathy in the spinal cord leading to progressive spastic paraplegia (Galea *et al.*, 2012; Kemp *et al.*, 2012). This form of the disease has late onset, manifesting between the ages of 20 to 30 in the hemizygous males and (Chaudhry *et al.*, 1996) and between 50 to 60 years in 65% of heterozygous females (Kemp *et al.*, 2012). In males, 20%, cases with AMN develop cerebral demyelination that becomes inflammatory (van Geel *et al.*, 2001)**.**

The celebral-ALD form of X-ALD has a more severe prognosis. It presents earlier in life, in childhood or adolescence, and is characterised by rapidly progressive inflammatory demyelination in the central nervous system leading to severe neurological and cognitive

disabilities (Kemp *et al.*, 2012). Within two to five years after symptoms appear, the patient reaches a vegetative state which is terminal (Kemp *et al.*, 2012).

Another defining feature of X-ALD is adrenal insufficiency, which can present before any neuropathological symptoms (Kemp *et al.*, 2012). Adrenal insufficiency occurs in two thirds of AMN cases, and 1% of heterozygous females. In addition to adrenal insufficiency, adult males sometimes develop testicular insufficiency (Kemp *et al.*, 2012).

X-ALD is caused by mutations in the *ABCD1* gene on Xq28, which encodes ATP binding cassette (ABC) transporter, adrenoleukodystrophy protein (ALDP/ABCD1). ALDP is a subclass D, membrane-bound ABC transporter that catalyses the transport of metabolites, such as VLCFAs, into the peroxisome in exchange for ATP, where they undergo β-oxidation. Absence of this protein leads to the build-up of VLCFAs and reduced β-oxidation of VLCFAs in the peroxisome (Kemp and Wanders, 2010).

In humans *ABCD1* is ubiquitously expressed with particularly high expression in the pituitary and adrenal glands, testis, liver, kidney, digestive tract, heart, skeletal muscle and skin (Höftberger *et al.*, 2007). Within the adrenal cortex, *ABCD1* is expressed in the ZF and ZR, where cortisol is produced (Höftberger *et al.*, 2007)**.**

The disease mechanism for X-ALD is not completely understood, but is thought to be due to the build-up of VLCFAs. The accumulation of VLCFAs is the earliest biochemical abnormality observed in tissues taken from X-ALD patients (Theda *et al.*, 1992). Children with cerebral-ALD, have higher accumulations of VLCFAs in white matter than AMN, indicating the severity of the condition is proportional to the accumulation of VLCFAs (Asheuer *et al.*, 2005).

The *Abcd1*$^{-/-}$ mouse model displays elevated levels of VLCFA particularly in the nervous system and adrenal gland early in life, but no signs of cerebral demyelination until 6 months

(Forss-Petter *et al.*, 1997; Kobayashi *et al.*, 1997; Lu *et al.*, 1997). From 16 months the mice develop axonopathy leading to neuronal damage and locomotor alterations by 20-22 months of age (Pujol et al., 2004; Pujol et al., 2002). The mouse model therefore recapitulates the human disease progression of AMN (Galea *et al.*, 2012; Pujol *et al.*, 2002)**,** however, mice do not develop hypocortisolism (Lu *et al.*, 2007).

The consequences of VLCFA accumulation have been explored to better understand the pathogenesis of X-ALD. Evidence from both human and mouse models suggest that oxidative stress plays a crucial role in disease development. Post mortem analysis of X-ALD brains show higher levels of markers of oxidative stress, such as increased nitrotyrosylated proteins, NOS2, lipid peroxides within neuropathological inflammatory lesions of cerebral-ALD, as well as up-regulation of the mitochondrial antioxidant *SOD2* (Powers *et al.*, 2005). Human X-ALD fibroblasts with VLCFA excess have increased levels of ROS, reduced GSH and reduced mitochondrial membrane potential (Fourcade *et al.*, 2008; Fourcade *et al.*, 2010). *Abcd1*$^{-/-}$ mice have elevated levels of MnSOD which is induced by oxidative stress in the cerebellum, liver, kidney and adrenal cortex (Powers *et al.*, 2005).

Although the precise mechanism is not clear, it is thought that accumulation of VLCFAs causes oxidative stress by impairing energy balance and inducing inflammation, which cumulatively and synergistically lead to oligodendrite and axonal death.

Evidence suggests a certain degree of cross-talk between peroxisomes and mitochondria, so ROS generated in peroxisomes can disrupt mitochondrial redox status and cause mitochondrial fragmentation (Ivashchenko *et al.*, 2011). Oxidative stress impairs the activity not only of mitochondrial antioxidant enzymes, exacerbating the oxidative damage, but also enzymes involved in glycolysis and the TCA cycle, as observed in the spinal cord of *Abcd1*$^{-/-}$ mice (Galino *et al.*, 2011). Mice consequently have diminished ATP and NADH levels coupled with reduced GSH levels in spinal cords (Galino *et al.*, 2011)**.** Diminished ATP production is highly damaging to axonal function, which requires high levels of energy, and

hence may lead to degeneration (Ferrer, 2009; Galea *et al.*, 2012). Mitochondria may also undergo oxidative damage directly from VLCFAs, as *Abcd1*$^{-/-}$ mice have enlarged mitochondria in the spinal cord due to lipid accumulation.

1.7 Overview of Antioxidant mechanisms in Oxidative stress

1.7.1 Reactive Oxygen Species

Reactive oxygen species (ROS) are molecules or free radicals with one unpaired electron that are highly reactive and cause oxidative damage to DNA, lipids and proteins when levels are not maintained at a steady-state. Indeed, a basal level of ROS is required for some signalling cascades, for example H_2O_2 acts as a secondary messenger in growth factor signalling (Rhee *et al.*, 2012). However, if ROS exceeds normal levels, cells undergo 'oxidative stress', in which vulnerable proteins undergo structural alterations that alter their function, DNA undergoes fragmentation, and lipid peroxidation destabilises membranes, ultimately inducing cell death. Hence, cells have an army of antioxidant defence proteins that ensure ROS levels are appropriately maintained.

Different forms of ROS exist, which include the superoxide anion (O^{-}_2), hydrogen peroxide (H_2O_2), hydroxyl radical ($HO^{\bullet}$), peroxyl radical ($RO^{\bullet}2$), alkosyl radical ($RO^{\bullet}$), hydroperoxyl radical ($HO^{\bullet}_2$), hypochlorous acid (HOCl), hypobromous acid (HOBr), and singlet oxygen (O_2) (Galea *et al.*, 2012). Superoxide anion is the predominant form of ROS and a precursor to most other ROS (Galea *et al.*, 2012).

1.7.2 Sources of ROS

ROS is generated from multiple sources including uncoupled nitric oxide synthase, NADPH oxidase subtypes (NOX), which generate superoxide, and H_2O_2 is also produced directly by xanthine oxidase and NOX4 (Lubos *et al.*, 2011). The main source of cellular ROS comes from mitochondria, the energy houses of our cells. As a result, many disorders associated

with oxidative stress are also associated with mitochondrial dysfunction, including neurodegenerative disorders (Barnham *et al.*, 2004), diabetes (Kaneto *et al.*, 2005), cardiovascular diseases (Sheeran *et al.*, 2010) and aging (Mattson and Magnus, 2006; Navarro and Boveris, 2007)**.** Sources of mitochondrial ROS include complexes I and III of the electron transport chain that leak electrons which can be transferred to molecular oxygen forming the superoxide anion (Galea *et al.*, 2012), and in steroidogenic cells, the steroidogenic CYP enzyme donor system is inefficiently coupled leading to electron leakage and superoxide production (Lubos *et al.*, 2011)**.**

1.7.3 Antioxidant defence

Humans have evolved multiple antioxidant systems to counteract ROS production. The primary line of defence is the superoxide dismutase (SOD) enzymes, which convert superoxide anions to H_2O_2. There are 3 forms of this enzyme which are localised to different cellular compartments: cytosolic copper-zinc SOD (CuZn-SOD; encoded by *SOD1*), extracellular SOD (*SOD3*), and mitochondrial manganese SOD (MnSOD). The mitochondrial MnSOD (encoded by *SOD2*) is most critical for survival, and depletion can lead to neonatal lethality (Galea *et al.*, 2012). *SOD2* is transcriptionally upregulated by oxidative stress.

The production of H_2O_2 by SOD is simply an intermediate step, as hydrogen peroxide can also be detrimental. Unlike superoxide, H_2O_2 can diffuse across lipid membranes and it has a longer half-life than superoxide (Lubos *et al.*, 2011). It can also react with Fe^{2+} to form the hydroxyl radical ($HO^{\bullet}$), which is highly damaging to cells (Lubos *et al.*, 2011).

The reduction of H_2O_2 to water is catalysed by three enzyme families: the glutathione peroxidases (GPXs), peroxiredoxins (PRDXs) and catalase (CAT). The GPX and PRDX families share a thioredoxin fold, but differ in their catalytic mechanisms and electron donors. Both families have multiple isoforms that vary in tissue specific expression patterns and cellular compartment. The majority of these isozymes are cytosolic but GPX1, GPX4,

PRDX3 and PRDX5 also reside in mitochondria. However, PRDX3 is the only thiol peroxidase to be specifically localised to mitochondria. GPX1 and PRDX5 also reside in peroxisomal compartments to complement catalase activity, and GPX3 and PRDX4 are secretory proteins. Although relatively little is known about GPX7 and 8, these enzymes have been demonstrated to be ER bound (Brigelius-Flohé and Maiorino, 2013).

There are 8 glutathione peroxidases (GPXs) that depend on glutathione as a co-factor, 5 of which are selenium-containing proteins with a selenocysteine residue at the active site, enabling extremely high reactivity with H_2O_2. Six peroxiredoxins exist that use a redox active cysteine at the active site, ultimately resulting in a lower rate constant than GPXs. However, in comparison to GPXs, PRDXs have a higher affinity for H_2O_2 (K_m <20μM) , and are highly abundant enzymes accounting for 1% of soluble protein (Chae *et al.*, 1999; Rhee *et al.*, 2001; Wood *et al.*, 2003b). PRDXs are therefore efficient in reducing low levels of H_2O_2. PRDXs use thioredoxins as electron donors, which are the either type 1 cytosolic, type 2 mitochondrial or type 3 testes specific isoforms (Hanschmann *et al.*, 2013).

Catalase is specifically localised to peroxisomes in mammals where it removes H_2O_2 produced during α-oxidation of fatty acids (Rhee *et al.*, 2005b). Catalase acts as a dismutase converting two H_2O_2 molecules to one H_2O and one O_2 molecule, hence the requirement of two H_2O_2 molecules at the active site means catalase requires a high H_2O_2 concentration to be active and therefore has a low affinity for H_2O_2 (Rhee *et al.*, 2005b). Once active, catalase achieves high rates of reaction, and is therefore considered to have an important role when H_2O_2 levels are high. The different catalytic mechanisms and tissue/compartment specific expression of these enzymes provide beneficial antioxidant defence in different circumstances.

1.7.4 Mitochondrial mechanisms of antioxidant defence

Mitochondria have a stringent antioxidant defence system that is coupled to the TCA cycle, regulating the ROS output from energy metabolism. Antioxidant enzymes of mitochondria

rely principally on NADPH as an electron donor, which is generated by $NADP^+$-dependent isocitrate dehydrogenase (IDH_2) during oxidative phosphorylation, malate dehydrogenase during the TCA cycle or nicotinamide nucleotide transhydrogenase (NNT) (Yin *et al.*, 2012a). NNT accounts for approximately 50% of the mitochondrial NADPH pool under physiological conditions (Rydström, 2006).

NADPH sits at the top of an electron donor chain involving glutathione and thioredoxin 2 dependent antioxidant systems (Fig. 1.12). NADPH reduces glutathione reductase, an enzyme that subsequently reduces protein thiol glutathione. As previously mentioned, reduced glutathione (GSH) is a highly abundant non-enzymatic antioxidant present both in mitochondria and the cytosol, present in millimolar concentrations (up to 10mM) (Chakravarthi *et al.*, 2006). It directly reduces ROS and other targets such as vitamin C, the second most abundant non-enzymatic antioxidant in most species (Sies *et al.*, 1992). A lower ratio of reduced to oxidised glutathione is associated with reduced cell viability (Deneke and Fanburg, 1989). Hence, glutathione acts as a redox buffer for the cell, maintaining a reducing environment. Glutathione also acts as a co-factor for antioxidant glutathione peroxidases, glutathione transferases, sulfiredoxins as well as peroxiredoxins (Marí *et al.*, 2009; Rhee and Woo, 2011; Yin *et al.*, 2012a). The main mitochondrial glutathione peroxidases are GPX1, which is also cytosolic and ubiquitously expressed, and mitochondrial specific GPX4, which is predominantly expressed in the testes.

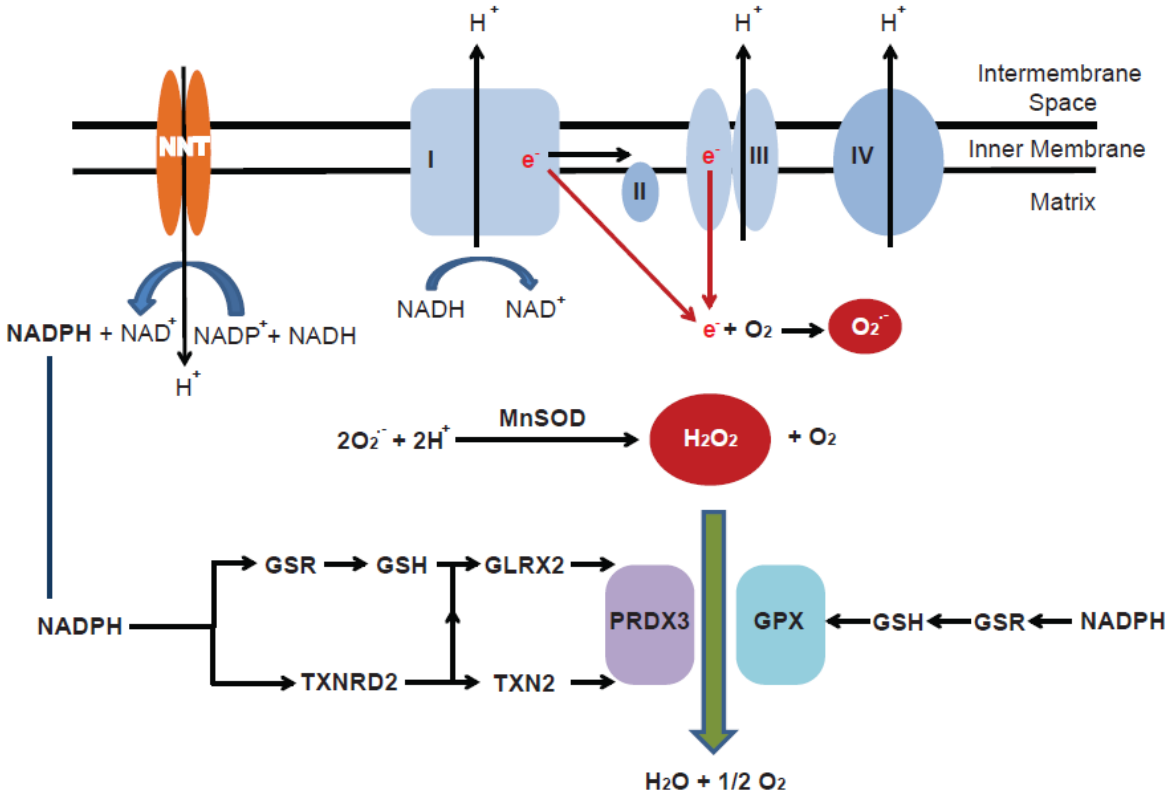

Figure 1. 12: Mitochondrial ROS production and antioxidant defence.

Illustration showing ROS is generated from electron transport chain complexes I and III and may cause oxidative damage to cellular components. Mitochondria have two antioxidant systems: Glutathione and thioredoxin 2. The electron donor system for both antioxidant systems starts with NAPDH, which is generated from NNT. NNT converts $NADP^+$ generated from the TCA and oxidative phosphorylation to NADPH, coupling the activity of antioxidants with energy demand. Electrons are passed from NADPH to antioxidants including glutathione peroxidase and peroxiredoxin 3, which reduce H_2O_2 to water. *GSR*, glutathione reductase; *GSH*, glutathione; *TXNRD2*, thioredoxin reductase 2; *TXN2*, thioredoxin 2; *GLRX2*, glutaredoxin 2; *MnSOD*, manganese SOD. (Image by Prasad *et al. unpublished*)

NADPH is also an electron donor to the mitochondrial specific isoforms of the thioredoxin family of antioxidants (Fig. 1.12). NADPH is a cofactor for selenoprotein thioredoxin reductase 2 (TXNRD2), which reduces thioredoxin 2, which in turn reduces mitochondrial peroxiredoxins PRDX3 and PRDX5. Thioredoxins, like glutathione, are potent redox-active

thiols themselves that scavenges ROS and are upregulated by oxidative stress (Galea *et al.*, 2012). PRDX3 has been reported to consume 90% of ROS generated in the mitochondrion (Cox *et al.*, 2010). In addition to reduction by thioredoxin 2, PRDX3 can be reduced by glutaredoxin 2, a mitochondrial specific GSH dependent enzyme (Hanschmann *et al.*, 2013).

1.8 Oxidative stress in the Adrenal Gland

In steroidogenic cells, the cytochrome P450 (CYP) enzyme family serves as an additional source of oxidative by products. As previously mentioned, the steroidogenic enzymes require electron donors for enzymatic activity. Mitochondrial type 1 CYP enzymes receive electrons from NADPH, which are transferred to ferredoxin reductase, then to ferredoxin and finally to the CYP enzyme (Miller, 2005). ER bound CYP enzymes receive electrons from 2-flavin P450 oxidoreductase (Miller, 2005).

The process of electron transfer is not efficiently coupled, so that electrons leak and react with O_2 to form superoxide. In particular, the final step of cortisol production catalysed by CYP11B1 leaks 40% of its electron flow to ROS, a much higher proportion than that of CYP11A1 (Hanukoglu, 2006; Rapoport *et al.*, 1995). This may explain why glucocorticoids suffer greater depletion than mineralocorticoids in conditions of adrenal insufficiency associated with oxidative stress.

Antioxidant enzymes are highly expressed in the adrenal cortex compared to other tissues and have higher activity, possibly as a compensatory mechanism (Azhar *et al.*, 1995; Hanukoglu, 2006). Moreover, a study by Azhar *et al.* (1995) showed vitamin C was 6-fold higher in the adrenal than in the ovary and 15-fold higher than in the liver. Levels of vitamin E and glutathione were also higher in steroidogenic tissues and antioxidant enzymes CuZn SOD, MnSOD and GPX had high expression and activity in these tissues, with particularly high levels in the ZF and ZR of the adrenal cortex. Furthermore, selenium (Se) levels, which determine GPX activity, have been shown to be preferentially retained in the adrenal and testes following Se deprivation in rats (Behne and Höfer-Bosse, 1984).

Although other antioxidant enzymes such as catalase are capable of detoxifying hydrogen peroxide, a study by Dorval *et al.* (2003) showed that the glutathione redox system was more efficient that catalase in protecting interrenal cells, the fish equivalent of adrenocortical cells, of trout from oxidative stress. Other studies have shown that catalase activity and expression levels are relatively low in the adrenal compared to other antioxidants (Azhar *et al.*, 1995).

In vitro studies on mouse, rat and human leydig tumour cells have shown that administration of oxidative stress in the form of H_2O_2 impairs steroidogenesis (Shi *et al.*, 2010; Tsai *et al.*, 2003), which may explain the necessity for tight redox control within steroidogenic tissues. Similarly another source of oxidative stress, the pesticide endosulfan, reduces cortisol secretion in trout interrenal cells (Dorval *et al.*, 2003).

Two potential mechanisms for this ROS-induced impairment of steroidogenesis are proposed. The first is the suppression of StAR protein functionality. Supporting evidence for this includes functional studies on rat testicular leydig MA-10 cells showing that StAR protein is reduced following exposure to H_2O_2 (Diemer *et al.*, 2003). Similarly, a study by Shi *et al.* (2010) illustrated that perfluorododecanoic acid (PFDoA), an inhibitor of steroidogenesis that increases ROS, acts by reducing expression of StAR in mouse and rat leydig cells. In this study the effects of PFDoA on steroidogenesis and ROS were rescued with a superoxide dismutase analog. Furthermore, Jin *et al.* (2011) showed that 3 week exposure to pro-oxidant cypermethrin causes a decrease in the expression of cholesterol transport and steroid synthesis proteins including StAR. These studies suggest that ROS affects cholesterol transport into mitochondria, an essential step in steroidogenesis. Although these studies examine testicular steroidogenesis, the effect of ROS on StAR in adrenocortical cells may be similar. Furthermore, it has been demonstrated that StAR proteins may preferentially traffic peroxidised cholesterol in steroidogenic tissues which could result in damage and dysfunction selectively targeted to mitochondria (Korytowski *et al.*, 2013; Korytowski *et al.*, 2010).

Alternatively, it has been suggested that ROS affects the activity of steroidogenic enzymes directly. A study by Chanoine (2001) *et al.* demonstrated that Se deficient AN4Rppc7 adrenal cells with minimal GPX1 activity exhibited a marked decrease in corticosterone,

aldosterone and progesterone production after cAMP stimulation compared to Se adequate cells, and StAR mRNA remained unchanged. The authors suggest that GPX1 deficiency impairs steroidogenesis by a mechanism independent of mitochondrial cholesterol import, whereby increased hydrogen peroxide levels affect the activity of one or more CYP enzymes. Similarly, Hornsby *et al.* (1980) showed that cortisol production in bovine adrenocortical cells was decreased in culture because CYP11B1 activity was compromised by lipid peroxidation.

1.9 Aims

Given that 40% of FGD cases have unknown aetiology, the overall aim of this research was to find candidate genes/proteins that might be novel causes of FGD.

The project was split into two approaches:

1) Proteomic arm:

   To search for novel interacting partners of MC2R and MRAP using a tandem affinity purification approach, to disclose interacting proteins that, when defective, might influence MC2R or MRAP function.

   A better understanding of MC2R function may give further insight into the pathogenesis of FGD, and lead to potential candidate genes for FGD. This could reveal proteins that are embryonic lethal when defective and would therefore not be identified by the genetic approach.

2) Genomic arm:

   To investigate the aetiology of one patient with FGD, with a region of linkage on chromosome 3p26-21.

   Candidate genes would be based on previous causes of FGD, for example genes involved in GPCR lifecycle, steroidogenesis or oxidative and replicative stress pathways.

The proband and kindred would be sequenced for mutations in such genes, and disease segregation would be checked. This could reveal genes that are causal for FGD but do not interact with MC2R/MRAP.

Chapter 2: Materials and Methods

2.1 Cell Culture

2.1.1 Maintenance

The following cell lines were used for this project:

H295R: Human Adrenal carcinoma cells

HEK293T: Human Embryonic Kidney cells

H295R cells were obtained from Ian Mason, University of Edinburgh and HEK293T from the European Collection of Cell Cultures (ECACC) at the Health Protection Agency (HPA; Salisbury).

All cell lines were incubated at 37^{o}C in a humidifier with 5% carbon dioxide. Medium was changed every 2-3 days, until the cells reached the desired confluency, upon which cells would be passaged and seeded into new tissue culture flasks or suitable dishes for experiments.

Cell lines were grown in the media as specified below:

<u>H295R</u>

Dulbecco's Modified Eagles Medium (DMEM) with L-glutamine and Ham's F-12 medium (1:1) (Gibco)
2.5% NU serum (BD Biosciences)
Penicillin (0.5u/ml) (Sigma-Aldrich)
Streptomycin (0.5u/ml) (Sigma-Aldrich)
1% ITS+ Premix (6.25µg/ml Insulin, 6.25µg/ml Transferrin, and 6.25ng/ml Selenous Acid) (BD Biosciences)

<u>HEK293</u>

DMEM (Sigma-Aldrich)
10% heat-inactivated Foetal Calf Serum (FCS) (Invitrogen)
Penicillin (0.5u/ml) (Sigma-Aldrich)
Streptomycin (0.5u/ml) (Sigma-Aldrich)

2.1.2 Passaging of cells

Materials

Phosphate Buffered Saline (PBS) (Sigma-Aldrich)
Trypsin/ Ethylenediaminetetraacetic acid (EDTA) (TE) (Sigma-Aldrich)
Cell culture media (section 2.1.1.)

Method

All reagents were warmed to 37°C before use. For a standard T75 flask, culture media was removed and cells were washed in 10 ml PBS. To detach cells from the flask, cells were incubated in 3ml TE. After 2-3 minutes of incubation at 37°C, cells would lift from the surface. 7ml fresh media was added to neutralise the trypsin and the suspension was centrifuged at 200g for 1 minute to pellet the cells. Cells were resuspended in fresh media and plated at the density desired.

2.1.3 Freezing and Storage

Materials

Dimethyl Sulfoxide (DMSO)
Heat-inactivated FCS

Method

Confluent T75 flasks were trypsinised (as above), transferred to 15ml tubes and centrifuged at 200g for 3 minutes to pellet. Media was removed and the pellet was resuspended in a solution of 10% DMSO and 90% FCS. Cell suspensions were transferred to 1ml cryotubes and frozen at -80°C overnight. For long term storage, tubes were moved to a liquid nitrogen tank.

2.1.4 Thawing Cells

Materials

PBS (Sigma-Aldrich)

Cell culture media (section 2.1.1)

Method

Cryotubes containing frozen cells were incubated in the 37°C incubator until thawed. Thawed solutions were centrifuged for 2 minutes at 200g to pellet the cells. Pellets were washed with 10ml PBS and centrifuged for 2 minutes at 200g, then resuspended in 12ml fresh media and transferred to new T75 flasks.

2.1.5 Cell Counting

Materials

Neuberg Haemocytometer

Methods

Cells were trypsinised according to section 2.1.2 and transferred to a 15ml tube. 50µl of the cell suspension was pipetted into a haemocytometer channel (Fig. 2.1). Cells were counted in all four red corners of one grid using a Leica DMIL light microscope with 10x objective. If the number of cells exceeded 500, the cells were diluted further. If the number of cells was fewer than 200, the four red corners in the second grid were also counted. The concentration of cells and volume of the suspension needed to acquire the desired cell density were determined using the following calculations:

Number of cells counted/number red corners counted= number of cells/100nl

Number of cells/100nl x 10^4 = Number of cells/ml (y)

Number of cells required/ y = volume (ml) of cell suspension to seed

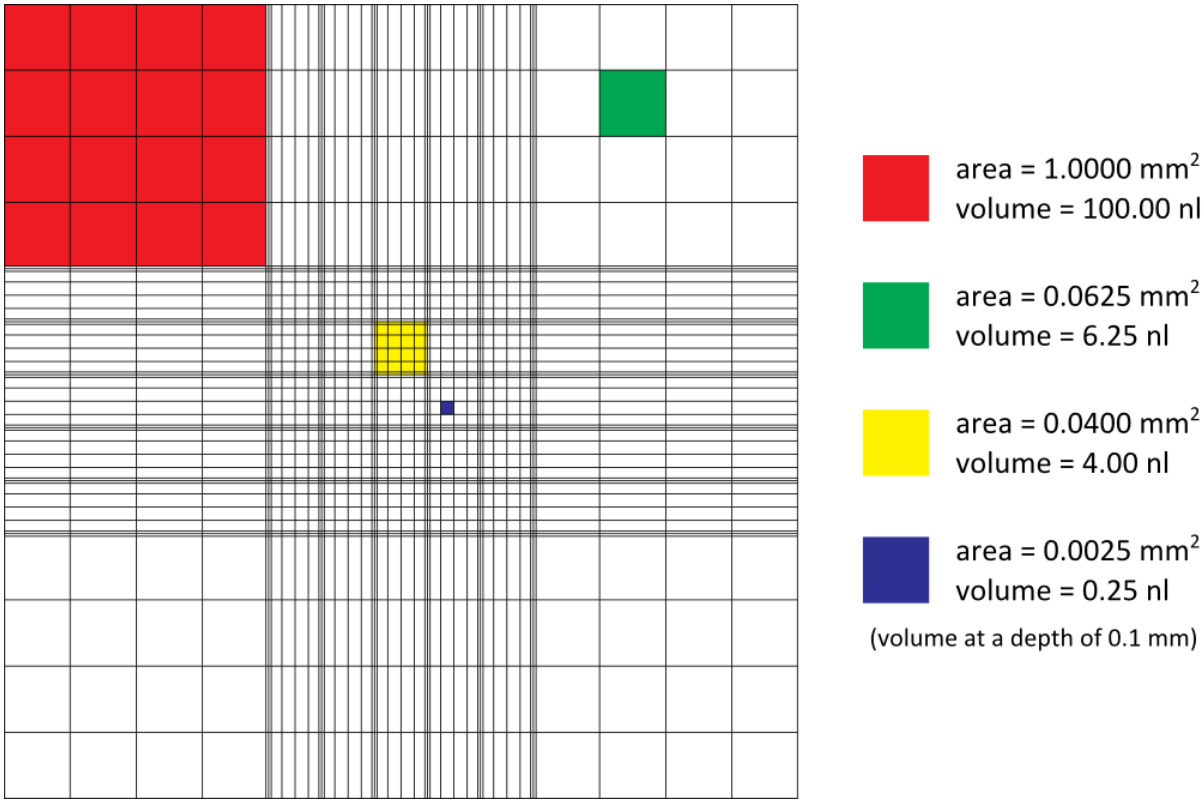

Figure 2. 1: Haemocytometer Grid

The calculated volume of cells was transferred to each well, and media was added to cover cells.

2.1.6 Transient Transfections

For transient transfection of plasmid DNA, lipid based methods were used. Cells were transfected at 80-90% confluency and DNA concentration per transfection was kept constant.

2.1.6.1 Transient Transfection with Lipofectamine and Plus Reagent

Materials

Lipofectamine (Invitrogen)

Plus Reagent (Invitrogen)

Opti-MEM (Serum and antibiotic free medium) (Invitrogen)

2x Cell culture media (section 2.1.1.)

Method

For a standard 6-well plate, 1µg plasmid DNA was diluted in 100µl Opti-MEM with 8µl Plus reagent, mixed gently by pipetting and incubated at room temperature for 20 minutes. Meanwhile, a master mix of Opti-MEM (100µl/well) and Lipofectamine (4µl/well) was prepared. After incubation, the lipofectamine/Opti-MEM solution was mixed slowly with the DNA/Plus reagent solution, and incubated for a further 20 minutes at room temperature.

Media was removed from wells and replaced with 800µl serum-free Opti-MEM. The 212µl DNA/Plus/Lipofectamine solutions were added to wells, and cells were incubated for 3 hours at 37°C with 5% CO_2. After 3 hours, 1ml 2x media was added to each well to given a final concentration of 1x.

Transfections were scaled up and down as follows:

Culture Vessel	**Opti-MEM (µl)**	**DNA**	**Plus reagent (µl)**	**Lipofectamine (µl)**	**Opti-MEM(µl)**
12 well plate + cover slips	50	200ng	4	2	50
6 well plate	100	1µg	8	4	100
10cm^2 dish	250	8µg	20	10	250

2.1.6.2. Transient Transfection with Lipofectamine-2000

Materials

Lipofectamine-2000 (Invitrogen)

Opti-MEM (Invitrogen)

1x Cell culture media (section 2.1.1.)

Method

For a standard 6-well plate, 2µg plasmid DNA was diluted in 100µl Opti-MEM, mixed gently by pipetting and incubated at room temperature for 10 minutes. During incubation, a master mix of Opti-MEM (100µl/well) and Lipofectamine-2000 (10µl/well) was prepared. The lipofectamine 2000/Opti-MEM solution was mixed slowly with the DNA/Opti-MEM solution, and incubated a further 20 minutes at room temperature.

Media was removed from wells and replaced with 800µl fresh cell culture media. The solutions of DNA/Lipofectamine 2000 were added to wells, and cells were incubated overnight at 37°C with 5% CO_2. Media was replaced the following morning. For transfections of *GPX1* HEK293 cell culture media was supplemented with 1% ITS+ premix containing selenous acid to ensure selenocysteine incorporation.

Transfection reagents were scaled up or down, depending upon the culture vessel, as follows:

Culture Vessel	**Opti-MEM (µl)**	**DNA (µg)**	**Lipofectamine 2000 (µl)**	**Opti-MEM (µl)**
6 well plate	100	2	10	100
T25 flask	250	8	15	250
T75 flask	1500	24	40	1500

2.1.7 Lentiviral transduction

2.1.7.1 Generating stable cell lines

Materials

pGIPZ lentiviral vector
Packaging vectors p8.74 (Gag/Po1) and pMDG (VSV-4)
Transfection reagents
Cell culture media

Method

Stable knockdown cell lines were generated using lentiviral transduction. HEK293 cells were used as a packaging cell line in which shRNA plasmids targeting *GPX1* and/or *PRDX3* (Open Biosystems RHS4531-NM_000581 and RHS 54531-EG10935) with an additional GFP tag were transiently transfected. On day 0, HEK293 cells were plated at a density of 7 x 10^5 per well and were transfected 6 hours later with pGIPZshRNA-GFP vectors, packaging vectors p8.74 (Gag/Po1) and pMDG (VSV-4) in a 5:4:3 ratio respectively, according to the transfection protocol in section 2.1.6. On day 1, media was changed to that of the target cell line H295R. On Day 2, 48hrs post transfection, media containing viral particles was collected and concentrated 2x by centrifugation overnight at 5000g and 4°C. On day 3, media containing viral particles was transferred to target H295R cells. HEK293 cells were allowed to grow further and additional viral media was collected and transferred on day 4 to double dose target cells. H295R cells were grown for 4 days before GFP-positive cells were visualised on a fluorescent microscope. Selective pressure (puromycin 4µg/ml) was applied 7 days post transduction.

2.1.7.2 shRNA sequences

Small hairpin shRNA constructs were purchased from Open Biosystems. The pGIPZ lentiviral vector contains a microRNA-adapted shRNA expressed as human microRNA-30

primary transcript (miR-30). The hairpin has a 22 nucleotide dsRNA stem and a 19 nucleotide miR-30 loop, which greatly increases Drosha and Dicer processing compared to previous shRNA designs, leading to increased shRNA production and greater knockdown of target genes (Silva et al., 2005).

Multiple shRNA sequences were available targetting different regions of the genes. The sequences of shRNA are details below:

Gene	ID	Targetted exon	Antisense sequence	Catalogue number
GPX1	07	2	ACATCGTTGCGACACACCG	V3LHS_394707
	09	2	TTCTCGATAAGTAGTACCT	V3LHS_394709
	10	2	TCCAGGCAACATCGTTGCG	V3LHS_394710
PRDX3	1	5	AGTCTGACAAGAGTGCGAT	V2LHS_84099
	2	4	TTCTGTAGGACACACAAAG	V2LHS_84094
	3	4	AGCTTTGTCACTAAAAGCA	V3LHS_384405
	4	3'UTR	TGCCTTCTACAAATAACCA	V3LHS_412107
	5	6	TGATCGTAGGAGAATCCGG	V3LHS_384402
	6	4	TCTGTAGGACACACAAAGG	V3LHS_384404

Table 2. 1: shRNA sequences

2.1.8 Puromycin Kill Curve

Materials

Cell culture media

Puromycin (1mg/ml) (Sigma-Aldrich)

Method

Lentiviral pGIPZ vectors contain resistance genes to puromycin, allowing for selection of cells expressing shRNA. A series of doses were tested ranging from 0 to 10µg/ml**,** which was diluted in cell culture media. H295R cells were seeded in triplicate at a density of 20,000 per well in a 24 well plate, and left to adhere overnight, and were 10% confluent on

day 1. Media was removed from cells and replaced with puromycin containing media, with doses applied, and replenished every 2 days. The minimum concentration of puromycin to cause massive cell death in 3-4 days and to have killed all cells by 7 days was chosen for future selection.

2.2 cDNA synthesis

2.2.1 RNA extraction from cells

Materials

RNeasy mini kit (QIAGEN)

β-Mercaptoethanol (β-ME) (Sigma-Aldrich)

Ethanol (70%) (Fisher-scientific, UK)

Method

For RNA extraction, cells were washed with cold PBS and lysed directly from plates using 350µl buffer RLT (lysis buffer) with β-ME, a reducing agent. Cells were homogenised by passing lysate at least 5 times through a blunt 20-gauge needle fitted to an RNase-free syringe. RNA was purified according to the QIAGEN RNeasy mini kit protocol. Briefly, to each 350µl lysate, one volume of 70% Ethanol was mixed in by pipetting, and the solution was transferred to an RNeasy spin column over a 2 ml collection tube. Lysates were centrifuged at 9000g for 15 seconds through the column. Then, with the through-flow discarded, the column was washed with 700µl buffer RW1. Through flow was again discarded, and the column was washed with 500µl buffer RPE, centrifuged at 9000g for 15 seconds. This step was repeated with a centrifugation time of 2 minutes. The column was then transferred to a clean collection tube, and RNA was eluted with 30µl RNase-free water by centrifugation at 9000g for 1 minute. The RNA yield was quantified using the Nanodrop ND-1000 spectrophotometer measuring absorbance at 260nm. Purity of DNA was

determined by the OD260/OD280 ratio, which should be approximately 1.8 for DNA and 2.0 for RNA. A lower ratio can signify protein or phenol contamination.

2.2.2 DNase Treatment

Materials

Deoxyribonuclease 1 (DNase1) 10,000u/ml (Sigma-Aldrich)
DNase Turbo buffer (Ambion)
RNase inhibitor (40u/µl) (Rnasin, Promega)
RNase free water (Sigma-Aldrich)

Method

RNA from either cell lysates or the human RNA tissue panel was subjected to DNase treatment to cleave and remove genomic DNA. Each reaction mixture contained 1µg RNA, 5µl DNase Turbo buffer, 0.5µl RNase inhibitor (preventing RNA degradation) and 1µl DNase, made up to a volume of 50 µl with RNase free water. Reactions were incubated at 37^{o}C for 15 minutes and then transferred to ice. RNA was purified and precipitated as detailed below.

2.2.3 Phenol extraction and RNA Precipitation

Materials

Phenol pH 7.8 (Sigma-Aldrich)
100% Ethanol (Fisher-scientific, UK)
pH5.3 3M sodium acetate (BDH Chemicals)
5mg/ml glycogen (Ambion)

Method

Phenol is an organic solvent which can be used to remove protein contaminants from nucleic acids. Samples were vortexed with an equal volume of pH 7.8 phenol (under a hood), then spun at 14,000rpm for 1.5 minutes to separate the layers. The top aqueous layer containing purified RNA was transferred to a new tube and precipitated by ethanol precipitation. To each RNA sample, a mixture of 5µl 3M sodium acetate pH5.3 (0.1x volume of RNA), 4µl 5mg/ml glycogen and 125 µl absolute ethanol (2.5x volume of RNA) was added and the samples were incubated at -80^{o}C overnight.

Precipitated RNA was collected by centrifugation at 14,000rpm at 4^{o}C for 10 minutes and the supernatant removed. The pellet was washed with 70% ethanol for a further 5 minutes at 14,000rpm and the supernatant was removed.

The RNA pellet was resuspended in 12.5µl RNase free water. If the sample was not used immediately, it was stored at -80°C.

2.2.4 Reverse Transcription

Materials

5x MMLV RT-buffer (Promega)
DTT 0.1M (Sigma-Aldrich)
dATP, dTTP, dCTP, dGTP (dNTPs) (10mM) (Promega)
RNase inhibitor (40u/µl) (Promega)
MMLV RT-enzyme (200u/µl) (Promega)
Random primers (hexadeoxynucleotides) (500µg/ml) (Promega)

Method

To each 12.5µl RNA sample, 0.25µl random primers were added. The mixture was heated for 10 minutes at 80^{O}C, and then returned to ice. A 1µl aliquot was taken as a pre-reverse

transcription negative control which should not contain cDNA or genomic DNA if DNase treatment was successful.

For reverse transcription, 4µl 5x MMLV RT-buffer, 2µl DTT 0.1M, 1µl dNTPs, 0.5 µl RNase inhibitor, and 1µl MMLV RT-enzyme were added to each RNA/primer mix and incubated for 2 hour at 37^{O}C. Following reverse transcription, cDNA samples were diluted 2x and stored at -20^{o}C.

cDNA samples and pre-RT negative controls were amplified by PCR (section 2.2.4) with GAPDH primers (section 2.7.3.) to confirm successful reverse transcription. The PCR product amplified from cDNA should be approximately 200 base pairs. Presence of a higher molecular weight band would suggest genomic DNA contamination.

2.3 Polymerase Chain Reaction (PCR) and DNA sequencing

2.3.1 Standard PCR

Materials

10 x Standard *Taq* polymerase Buffer (10 mM Tris-HCl, 50 mM KCl, 1.5 mM $MgCl_2$, pH8.3)

dATP, dTTP, dCTP, dGTP (dNTPs) (10mM) (Promega)

Forward and Reverse Primers (10mM) (see section 2.7.3 for specific primers used in amplifications)

Taq polymerase (5000u/ml) (NEB)

Template DNA (100ng)

Nuclease-free H_2O (Sigma-Aldrich)

Method

PCR thermal cycling can amplify specific regions of genes of interest. The technique involves a series of temperature steps that are repeated: Denaturation of DNA at 95^{0}C to separate the double helix, annealing at 50-60^{o}C to bind sequence specific primers to the

template strand, and elongation of complementary strands by DNA polymerase in a 5' to 3' direction at 72^{o}C. The newly synthesised DNA is used as a template in a subsequent cycle, leading to exponential amplification following repeated cycles. The annealing temperature employed is dependent on the melting temperature of the specific primers.

Unless specified, PCR reactions were set up to a volume of 25µl as follows:

	25 µl reaction:	**50 µl reaction:**
10 x Standard PCR Buffer	2.5 µl	5 µl
dNTPs (10mM)	0.5 µl	1 µl
TAQ Polymerase 5000u/ml	0.125 µl	0.25 µl
Forward Primer (10mM)	0.5 µl	1 µl
Reverse Primer (10mM)	0.5 µl	1 µl
DNA	(100ng)	200ng
Nuclease free H_2O	To 25 µl	To 50 µl

Typically, samples underwent PCR cycling in a touchdown program, detailed below:

Touchdown PCR Cycles:

Step	Temperature (^{O}C)	Time (Minutes)	
Denaturation	95	5	1 cycle
Denaturation	95	0.5	10 cycles
Annealing	*	0.5	
Extension	72	1/kb	
Denaturation	95	0.5	20 cycles
Annealing	**	0.5	
Extension	72	1/kb	
Extension	72	5	1 cycle

Dependent on the melting temperature of the primers. * 65 to 55°C ('Touch55') or 60 to 50°C ('Touch50'); **55°C ('Touch55') or 50°C ('Touch50')

2.3.2 Gel Electrophoresis

Materials

Agarose (electrophoresis grade) (Sigma-Aldrich)
10,000x Gel Red (Biotium)
6x Loading Dye (MBI Fermentas)
DNA Ladder (Generuler DNA ladder mix (100-10,000bp 0.5 mg DNA/ml) (MBI Fermentas)
1x TAE Buffer (40mM Tris-acetate, 2mM disodium ethylenediaminetetraacetate (Na_2EDTA),
pH 8.3) (National Diagnostics)

Method

Successful PCR amplification was assessed by agarose gel electrophoresis. DNA samples were loaded into the wells of an agarose gel and an electrical current was applied. Negatively charged DNA molecules migrate through the gel to the anode. The speed of migration depends on size, as larger molecules incur more resistance passing through the porous agarose and migrate more slowly. The size of a PCR product can be estimated by comparison with a DNA ladder containing fragments of known size, run in an adjacent lane.

For a 1% agarose gel, 1g of agarose was mixed with 100ml 1x TAE buffer in a conical flask or bottle. Agarose was dissolved by heating the mixture in a microwave for a few minutes. The solution was cooled until there was no visible steam and 10 µl Gel red was added (10,000x). The mixture was poured into a plastic cast with combs inserted to produce the wells. When the gel had set, the combs were removed and it was transferred to a tank. TAE was poured into the tank to cover the gel.

Blue loading dye was added to each PCR sample in a 1:5 ratio. 7µl DNA ladder was loaded into the first well of each row as a size standard for the other wells. PCR samples were loaded into adjacent wells.

The gel was subjected to a directional electric field with a voltage of 100V for 40 minutes until the blue loading dye had reached 1cm from the end of the gel. Samples were visualised

by UV detection using a Kodak Electrophoresis and Documentation analysis system UV transilluminator (Uvitec)

2.3.3 Gel Extraction

Materials

QIAquick Gel extraction Kit, (QIAGEN)
Isopropanol (100%) (Fisher-scientific, UK)
Nuclease-free water (Sigma-Aldrich)

Methods

To purify DNA from an agarose gel, the bands were visualised under UV light, cut out with a clean blade and transferred to a 1.5ml tube. The weight of the gel slice was determined, and 3 volumes of Buffer QG were added to 1 volume of the gel**.** The mixture was incubated at 50°C for 10 minutes to dissolve the gel, vortexing intermittently. One gel volume of 100% isopropanol was added and mixed to precipitate the DNA. The sample was then transferred to the QIAquick column and centrifuged for 1 minute at top speed to bind the DNA to the silica membrane. Through-flow was discarded and the column was washed with 500µl Buffer QG and centrifuged for 1 minute to remove further agarose. Through-flow was removed and another wash step followed. 750 µl Buffer PE was applied to the column and centrifuged for 1 minute to remove salt. Through-flow was discarded and the column was centrifuged for an additional minute to remove traces of Buffer PE. The column was placed in a clean collection tube, and DNA was eluted with 25µl nuclease free water, centrifuging for 1 minute at top speed. DNA concentration in ng/ml was determined using a Nanodrop ND-1000, measuring absorbance at 260nm (using Beer's Law). The purity of the DNA was determined by calculating the ratio of absorbance at 260nm and A280nm. A ratio of ~1.8 was considered to be pure DNA. Samples were stored at -20°C.

2.3.4 Real time quantitative PCR

Materials

2x SYBR green master mix (KAPA) (SYBR® Green I Dye, AmpliTaq Gold® DNA Polymerase,

dNTPs with dUTP, and optimized buffer components)

R_{-ox} dye (Passive Reference)

Nuclease-free water

Methods

mRNA expression levels were quantified by real time PCR (qRT) using SYBR green 1 fluorescent dye and the Promega MX4000 thermal cycler. Sybr green 1 dye increases its fluorescence when bound to double stranded DNA. The amount of fluorescence is therefore directly proportional to the concentration of amplified template.

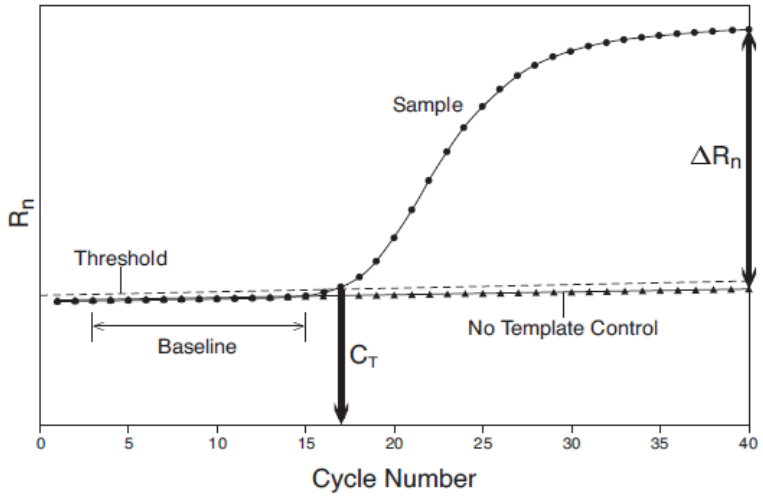

Figure 2. 2: Amplification plot

(Applied Biosystems technical manual 4309155)

The emission intensity of fluorescence during the PCR reaction is plotted against cycle number to produce a sigmoidal amplification plot. It is the density at the threshold cycle (C_T), which is used to calculate the starting concentration of template. This is defined as the cycle at which there is the first significant increase in fluorescence over that of baseline, and is at the start of the exponential phase of the reaction.

The data can be analysed in two ways: either by absolute quantification or relative quantification. Absolute quantification quantifies unknowns by extrapolating from a standard curve of known quantities. Relative quantification quantifies changes in expression in a given sample compared to a reference sample for example an untreated control.

Sybr green fluorescence is normalised to that of a passive reference dye, 'ROX_{low}', which does not intercalate with DNA and increase its fluorescence during the PCR reaction. This is used as an internal reference and to correct for inter-well fluorescent fluctuations.

Each reaction contained the following reagents:

Component	Volume (µl)
KAPA SYBR® FAST qPCR Master Mix (2X) Universal	5
Forward Primer (10 µM)	0.1
Reverse Primer (10 µM)	0.1
Template DNA (variable concentration)	2
ROX_{Low}	0.2
H_2O	2.6

Reactions were run in duplicate in a 96-well plate, including a non-template control to check for contamination. Plates were centrifuged at 1500g to remove bubbles and ensure the reaction mixture was at the bottom of the wells.

Data was analysed using the absolute quantification method. The C_t value of the unknown was quantified absolutely by interpolating the quantity from a standard curve, whose quantities were pre-determined spectrophotometrically.

Standard curves were created using serial dilutions of a known concentration of DNA for the gene of interest, and for *GAPDH*, a house keeping gene. Standard curves with a gradient of -

3.3±0.3 were considered acceptable, which is the number of cycles expected between each standard with a serial dilution of 1 in 10. The r^2 value of the curve was required to be $\geq$0.97, which indicates the relationship between the C_t and the concentration of DNA, and should be linear (1). The concentration of the gene of interest was normalised to *GAPDH* concentration for each sample.

The dissociation curve, which shows the melting temperature (T_m) of PCR products, was used to check nonspecific amplification or contamination. Amplification of specific PCR products should show a single peak at a temperature corresponding to the amplification product's Tm. The non-template control should only show a peak at a temperature corresponding to the Tm of primer dimers, typically much lower than a specific amplification product.

The following cycles were used for all reactions:

Temperature (^{O}C)	Time (Minutes: seconds)	Cycles
95	3:00	1
95	00:03	40
60	00:20	
68	00:01	
95	1:00	1
60	00:30	
68	00:30	

2.3.5 DNA sequencing

Materials

Big Dye 3.1 cycle sequencing kit (Applied Biosystems, UK)

Method

Sequencing of PCR products or cloned constructs was performed by the Genome centre (Barts and the London, Queen Mary, University of London). The centre used BigDye 3.1 chemistry to sequence samples, which is a form of Sanger sequencing based on the dideoxy-mediated chain termination method (Sanger *et al.*, 1977). The sequencing results were analysed on BioEdit software (Hall, 1999).

2.3.6 Whole exome sequencing

Materials

Agilent V4 (51mbp) exome enrichment kit

Illumina HiSeq2000

Methods

5µg of high quality genomic DNA with an OD_{260}/OD_{280} of >1.8 was required for enrichment using the Agilent V4 (51Mbp) exome enrichment microarray. The enrichment and exome sequencing was performed by Otogenetics. Briefly, DNA was fragmented and a library was created using standard techniques including end repair, A-tailing and paired adaptor ligation. DNA was hybridised to the array, washed to remove un-tethered strands, and then enriched, eluted and amplified. The enriched DNA was subjected to massively parallel sequencing on the Illumina HiSeq 2000.

Nucleotide level variation was analysed using DNAnexus online software (https://www.dnanexus.com/). A filtration strategy was employed to minimise the number of

variants for analysis (Fig. 2.3), removing variants that were heterozygous and known SNPs, selecting variants that were non-synonymous coding, splice site mutations, insertions or deletions (indels) with a coverage of >20. Variants were checked against the Ensembl SNP database, release 54. The remaining variants were assessed for FGD candidate genes prioritising those that would have a role in oxidative stress.

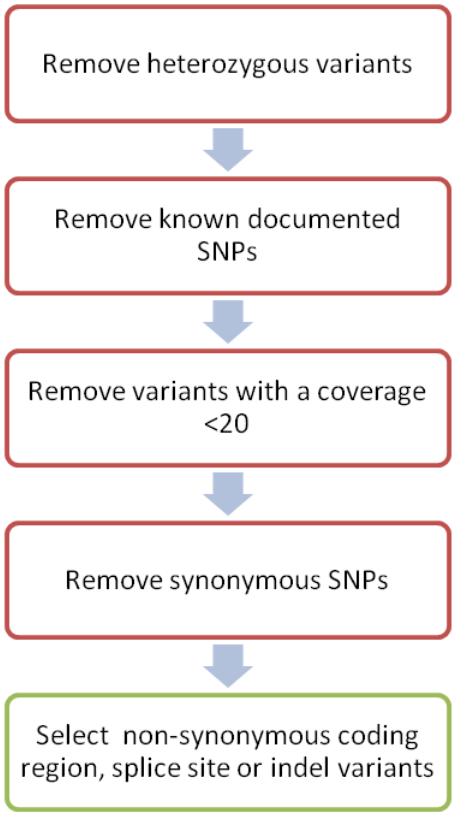

Figure 2. 3: Whole exome sequencing filtration strategy

Variants were filtered to remove heterozygous variants, known documented SNPs, variants with coverage less than 20 and synonymous variants. Non-synonymous coding region, splice site and indel variants were selected for analysis. It was hypothesised that candidate genes would have a role in oxidative stress.

2.3.7 Primer sequences for cloning, PCR, RT-PCR and sequencing

Description	FP(a)	RP(b)	
Incorporate BamH1 and EcoR1 sites to *MC2R* for CTAP vector	CTAGTGGGCGGATCCATGAAGCACATTATCAACTCGTAT	CTAGTGGAATTCCCAGTACCTGCTGCAGAAG	Cloning TAP-tag vectors
Incorporate BamH1 and EcoR1 sites to *MC2R* for NTAP vector	CTAGTGGGATCCCATGAAGCACATTATCAACTCGTATG	CTAGTGGAATTCCTACCAGTACCTGCTGCAGAAG	
Incorporate BamH1 and EcoR1 sites to *MRAP* for CTAP vector	CTAGTGGGCGGATCCATGGCCAACGGGACCAAC	CTAGTGGAATTCGCTCTGCAATTGAGAGGTC	
Incorporate BamH1 and EcoR1 sites to *MRAP* for NTAP vector	CTAGTGGGATCCCATGGCCAACGGGACCAACGC	CTAGTGGAATTCTCAGCTCTGCAATTGAGAGGTC	
GPX1 from initial methionine to exon 1 and 2 junction	ATGTGTGCTGCTCSGCYAGCG	CTTGGCGTTCTCCTGATGCCCAAA	Fusion PCR
GPX1 from exon 1 and 2 junction to end of 3'UTR	TTTGGGCATCAGGAGAACGCCAA	TTCTGCTGACACCCGGCACTT	
GPX1 from initial methionine to p.129 (start of R130-L133del)	ATGTGTGCTGCTCSGCYAGCG	CTGGGAGCTGGCAGGAAGGCGAA	
GPX1 from p.134 (end of R130-L133del) to end of 3'UTR	TTTGGGCATCAGGAGAACGCCAAG	TTCTGCTGACACCCGGCACTT	
GPX1 incorporation of *Bam*H1 at 5' and *Hind*III at 3'	CGGATCCATGTGTGCTGCTCGGCCAGCG	GATAAGCTTTTCTGCTGACACCCGGCACTTTAT	Cloning *GPX1* for pCMV-tag3B vector
Correct unknown SNP at position 110 (p.Gly110Cys) in GPX1-pGEM-Te vector to wild type sequence	GCTCCCTGCGGGGCAAGGTACTACT	AGTAGTACCTTGCCCCGCAGGGAGC	Site directed mutagenesis
GPX1 correcting frameshift in *GPX1*-FLAG vector	TTGCGGCCGCGGTGAATTCGATTAT	ATAATCGAATTCACCGCGGCCGCAA	
Real time PCR primers for *GPX1*	TGCGGGGCAAGGTACTACTT	ATGAGCTTGGGGTCGGTCAT	Real time PCR
Real time PCR primers for *GAPDH*	TGCACCACCAACTGCTTAG	GAACATCATCCCTGCATCC	

Real time PCR primers for *PRDX3*	CGAGACTACGGTGTGCTGTT	AGAATCCGGTGTCCAGTTCG	
Real time PCR primers for *STAR*	GACATTCAAGCTGTGCGCTG	TGTAGAGAGTCTCTTCTAGCCGAG	
Real time PCR primers for *GPX2*	TGAGGCACAACCACCCGGGA	TCCACCCCCAGGACGGACAT	
Real time PCR primers for *GPX3*	ACGAGTACGGAGCCCTCACCA	TGGTTGCAGGGAAAGCCCAGA	
Real time PCR primers for *GPX4*	TCCGCCAAGGACATCGACGG	GGGAAGGCCAGGATCCGCAA	
Real time PCR primers for *NNT*	GGGTCATGTCATTAGAGG	CAGTATCCCTGTGAGACC	
T3	GCAATTAACCCTCACTAAAGG	CCTTTAGTGAGGGTTAATTGC	Sequencing primers
T7	TAATACGACTCACTATAGGG	CCCTATAGTGAGTCGTATTA	
SP6	ATTTAGGTGACACTATAG	CTATAGTGTCACCTAAAT	

2.4 Cloning

2.4.1 Cloning TAP-tag vectors

Materials

pcDNA3.1+MC2R (cDNA.org)

p3xFLAG-CMV14-MRAP (backbone Sigma-Aldrich)

InterPlay mammalian TAP vectors pCTAP and pNTAP

Method

MC2R and *MRAP* inserts were amplified by PCR from pcDNA3.1+MC2R and p3xFLAG-CMV-14-MRAP (MRAP-FLAG) (appendix 7.1), using the standard reaction mix (section 2.3.1) and the following cycles:

Step	Temperature (^{O}C)	Time (Minutes)	Cycles
Denaturation	94	5	1
Denaturation	94	0.5	30
Annealing	64	0.5	
Extension	72	1	
Extension	72	5	1

Primers incorporating *Bam*H1 and *Eco*R1 sites were used to amplify genes for subsequent cloning into pCTAP and pNTAP (pTAP) vectors (section 2.3.7). Amplified fragments and the pTAP vectors were digested using *Bam*H1 and *Eco*R1 for 2 hours in a 40 µl reaction mixture, and treated with Antarctic phosphatase to prevent religation (section 2.4.7).

Digested products were visualised by gel electrophoresis, gel extracted and purified using the QIAGEN gel extraction kit (sections 2.3.2. and 2.3.3). Inserts were ligated into the pTAP vectors at *Bam*H1 and *Eco*R1 sites using T4 ligase (Promega) at 4 ^{O}C (section 2.4.4).

After which, ligation reactions were transformed into JM109 competent cells and grown on LB agar plates with 50µg/ml kanamycin (section 2.4.6). Plasmid DNA was purified from transformation clones and screened for inclusion of the insert by digesting with *Bam*H1 and *Eco*R1 (section 2.4.3).

2.4.2 Cloning GPX1 vectors

Materials

pGEM-T easy (pGEM-Te) (Promega)
p3xFLAG-CMV10 (Sigma-Aldrich)
pCMV-tag3B (Agilent)

Method

Wild type and R130-L133del *GPX1* were cloned into p3xFLAG-CMV10 and pCMV-tag3B mammalian expression vectors (appendix 7.1). GPX1 was amplified from HEK293 cDNA using a two-step fusion PCR method, due to difficulties in amplifying the full transcript. The fused fragments were ligated into pGEM-Te using conventional a/t cloning, before transfer to p3xFLAG-CMV and pCMV-tag3B. Cloning was confirmed by DNA sequencing using sequencing primers details in section 2.3.7.

2.4.2.1 Sub-cloning into pGEM-Te vector

Materials

5x One*Taq* GC reaction buffer (NEB)
dNTPs (10mM) (Promega)
Forward and Reverse Primers (10mM)
One*Taq* polymerase (5000u/ml) (NEB)
Nuclease free water (Sigma-Aldrich)
pGEM-Te vector (Promega)

Method

Wild-type and R130-L133del *GPX1* were amplified from HEK293 cDNA in a two-step overlap PCR method in which two fragments were amplified separately in an initial PCR, then fused in a subsequent PCR reaction. For both wild-type and R130-L133del *GPX1*, cDNA was amplified from the first initiating methionine to the end of the 3' untranslated region (3'UTR), in order to include the SECIS element required for translation of selenoproteins.

Primers were designed to amplify exon 1 and 2 of *GPX1* separately using exon junction spanning primers (Fig. 2.4.) (section 2.3.7) in a 50µl PCR reaction mix described below and the touch 55 program described in section 2.3.1. The exon 1 fragment was 69% GC-rich, hence a commercially optimised PCR reaction buffer was used for initial amplification of the two fragments.

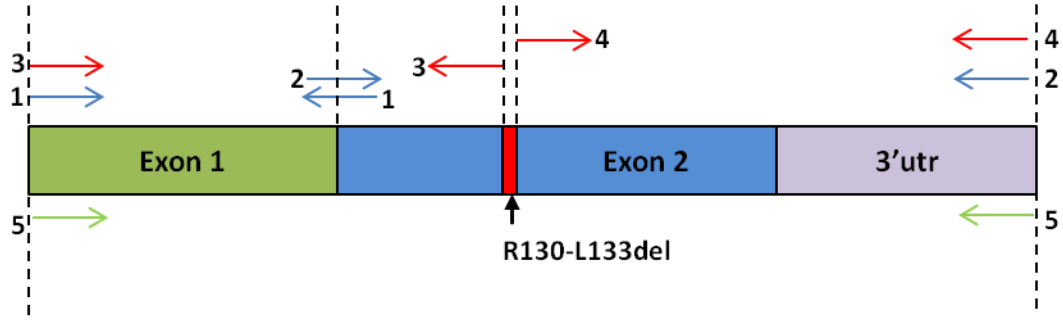

Figure 2. 4: Fusion PCR

Illustration showing primer pairs used to amplify wild-type and R130-L133del *GPX1* using two-step fusion PCR method. In the first step, exon 1 and 2 of wild-type *GPX1* were amplified separately using primers pairs 1 and 2. R130-L133del *GPX1* was amplified in two segments before and after the deletion, using primer pairs 3 and 4. In the second step fragments were fused using primer pair 5.

Reaction:

5x One*Taq* GC reaction buffer	10µl
10mM dNTP	1µl
10µm FP	1µl
10µm RP	1µl
One*Taq* polymerase	0.25µl
Template DNA	200ng
Nuclease-free water	To 50µl

The amplified products were analysed by gel electrophoresis (section 2.3.2) and bands were gel extracted (section 2.3.3), then mixed in equal concentration by vortexing in nuclease free water. The cDNA mix was amplified using the standard touch 55 program and a 50µl reaction mix with standard *Taq* polymerase (section 2.3.1). The standard *Taq* polymerase amplifies DNA to include dA overhangs which is a requirement for subcloning into the pGEM-Te vector. Amplification fused the two fragments into one 824bp product, which was confirmed by gel electrophoresis (section 2.3.2).

The 824bp fragment was gel extracted and subsequently subcloned into the pGEM-Te vector which is initially a linear vector with T-overhangs (appendix 7.1). Sequencing revealed an unknown SNP at position 110 (p.Gly110Cys) which was rectified by site directed mutagenesis (section 2.4.9) in order to establish a wild-type construct.

The mutant R130-L133del *GPX1* transcript was amplified from the wild-type pGEM-Te-*GPX1* construct through similar methodology. Two fragments were amplified using primers spanning either side of the 12 base pair deletion (Fig. 2.4.2.1) (section 2.3.7) using a touch 55 program and standard *Taq* 50µl reaction mix (section 2.3.1). The PCR products were analysed by gel electrophoresis and gel extracted, then fused in a second PCR reaction with the same reaction conditions (Fig. 2.4.2.1).

Full length fragments were ligated into the pGEM-Te vector using 2x rapid lipase buffer (section 2.4.4), transformed into JM109 *E.coli* competent cells and colonies were screened for presence of the insert by digesting with *Not1* (section 2.4.3)

2.4.2.2 Cloning into pCMV-FLAG *GPX1*

To generate FLAG-tagged GPX1, pGEM-Te vectors containing wild-type and R130-L133del *GPX1* and p3xFLAG-CMV10 were digested with *Not1* for 2hr at 37°C (section 2.4.3) and the linearised p3xFLAG-CMV10 vector was treated with Antarctic phosphatase. Digested products were subjected to gel electrophoresis, purification, ligation and transformation as above. Sequencing the construct revealed a frameshift which was corrected by site directed mutagenesis according to section 2.4.9 using primers detailed in section 2.3.7.

2.4.2.3 Cloning pCMV-tag3B *GPX1*

To generate myc-tagged wild type and R130-L133del *GPX1*, primers were designed to introduce *Bam*H1 and *Hind*III restriction sites 5' and 3' to *GPX1*, to enable direct cloning into pCMV-tag3B (primers detailed in section 2.3.7). PCR was used to amplify fragments from wild type and R130-L133del pGEM-Te-*GPX1* vectors using a touch 55 program and the following reaction mixture:

Component	
5x Q5 reaction buffer	10µl
10mM dNTP	1µl
10µM FP	2.5ng
10µM RP	2.5ng
Q5 HF Hot start polymerase (2000U/ml)	0.5
Template DNA	200ng
Nuclease-free water	To 50µl

PCR products were visualised by gel electrophoresis and gel extracted for purification. The purified products were digested with *Bam*H1 and *Hind*III for 1 hr at 37°C (section 2.4.3), in addition to the pCMV-tag3b vector. The linearised vector was treated with Antarctic phosphatase (section 2.4.3).

As above, digested products were checked by gel electrophoresis and purified. The purified products were ligated as described in section 2.4.4 with 2x Quick buffer and Quick ligase (NEB). Ligations were transformed into JM109 competent cells, grown overnight and plasmid DNA was purified. Plasmid DNA was digested with *Bam*H1 and *Hind*III to check for insert release.

2.4.3 Restriction Digest

Materials

Restriction endonucleases (Promega)
100x Bovine Serum Albumin (BSA) (Promega)
10x Buffer (dependent on the optimal buffer for each enzyme/enzyme combination) (NEB)
Antarctic Phosphatase (5000u/ml) (NEB)
1x Antarctic Phosphatase buffer (NEB)

Methods

Restriction endonucleases were used to digest inserts and vectors in order to prepare insert sticky ends and linearise vectors before ligation. Restriction digests were also used at the end of the cloning process to screen transformed colonies for release of an insert. Colonies displaying drop out of the correct size fragment on digestion were sent for Sanger sequencing to confirm the insert was in frame with the correct orientation.

DNA was digested using appropriate restriction enzymes for 2 hours unless otherwise stated, in a 10µl reaction mixture for checking insert release, and 40 µl reaction mixture for digesting inserts and vectors before ligation as indicated below:

	Screening colonies for insert	Preparing insert and vector for ligation
DNA Template	100ng	1 µg
100x BSA	0.1 µl	0.4 µl
10x Buffer 1-4 (NEB Biolabs)	1 µl	4 µl
Enzyme 1 (NEB Biolabs)	1 µl	1 µl
Enzyme 2 (NEB Biolabs)	1 µl	1 µl
ddH_2O to a total volume of	To 10 µl	To 40µl

Digested products were analysed by gel electrophoresis. If preparing DNA for ligation, an additional step was required before gel electrophoresis. Reaction mixtures containing linearised vectors were treated with Antarctic phosphatase to dephosphorylate the 5' end preventing religation of the empty vector. 1µl Antarctic phosphatase and 10x Antarctic phosphatase buffer were added to these reaction mixtures by pipetting, and samples were incubated for a further 30 min at 37°C, then heated to 65°C to deactivate the enzyme. After gel electrophoresis digested inserts and vectors were gel extracted and purified (sections 2.2.6 and 2.2.7) for ligation.

2.4.4 Ligation

Materials

Vectors

Control insert DNA (4ng/µl) (Promega)

T4 DNA ligase 100u (Weiss units) (Promega)

Either T4 DNA 10x DNA ligase buffer (Promega), 2x rapid ligase buffer (Promega) or 2x Quick ligase buffer (NEB)

Nuclease free water (Sigma-Aldrich)

Method

The concentration of insert required for ligation was calculated using the following equation:

ng vector x kb insert)/kb vector x insert: vector ratio = ng insert

Various insert to vector ratios were used to increase the likelihood of successful ligation. Ligation reaction mixes were prepared as follows:

	Sample reaction	Positive control	No insert control	No ligase control
2X Rapid Ligation Buffer,2 x Quick buffer or 10x ligation buffer	5µl/5µl/1µl	5µl/5µl/1µl	5µl/5µl/1µl	5µl/5µl/1µl
Vector	1µl	1µl	1µl	1µl
PCR product	Xµl	-	-	-
Control Insert DNA	-	2 µl	-	-
T4 DNA Ligase (400,000u/ml) or Q5 ligase	1µl	1µl	1µl	-
Deionised water to a final volume of	10µl	10µl	10µl	10µl

A Promega control insert DNA was used as a positive control to give an indication of the number of colonies expected after transformation for a successful ligation, and a no insert, negative control was used as a background check to assess background due to religation of

linear vectors, which should produce few colonies after transformation. The no ligase control gives an indication of the number of background colonies due to uncut vector and should also produce few colonies

Tubes were briefly centrifuged, and reactions were incubated overnight at 4^{o}C when utilising 10x ligation buffer, for three hours at room temperature when using 2x rapid ligation buffer or 10 minutes at room temperature when using 2x Quick ligase buffer.

2.4.5 Preparation of LB agar plates

Materials

LB broth
Agar (Sigma-Aldrich)
Antibiotic (Sigma-Aldrich)
X-Gal (5-bromo-4-chloro-3-indolyl-beta-D-galactopyranoside (Promega)
0.1 M Isopropylβ-D-1-thiogalactopyranoside (IPTG) (Promega)

Method

10g LB broth and 7.5g agar were dissolved in 500ml water, autoclaved to sterilise and cooled to approximately 37°C. Once cooled, antibiotic was added to the solution at a concentration of 100µg/ml for ampicillin or 30µg/ml for kanamycin, and the solution was poured into 10cm^2 plates under sterile conditions. Plates were left to set at room temperature, and stored at 4°C.

For plates being used to grow competent cells transformed with pGEM-Te vectors, 20µl X-Gal and 20µl IPTG were poured onto plates and spread using a sterile Pasteur pipette. The pGEM-Te vector contains a segment of the LacZ gene that encodes the N-terminal fragment of β-galactosidase which converts X-Gal to a blue product. The gene segment is located in the multiple cloning site, hence ligation of DNA into the vector disrupts the gene preventing β-galactosidase activity, resulting in no blue product. Based on this principle, colonies can be

screened by colour, where white colonies contain the DNA insert, and blue colonies do not because they maintain β-galactosidase activity.

2.4.6 Transformation

Materials

JM109 *E.coli* highly competent cells (Promega)

LB Broth (Sigma-Aldrich)

Method

JM109 highly competent cells (>10^8 cfu/µl) were defrosted on ice and gently mixed by flicking the side of the tube. In a 1.5ml tube, 50µl competent cells were mixed with 10µl plasmid DNA and incubated on ice for 20 minutes. The cells were then heat shocked in a 42^{o}C water bath for 45 seconds, to uptake the DNA, and returned to ice for 2 minutes. 950 µl LB broth was added to the cells, which were then shaken at 230rpm for 1.5 hours at 37^{o}C.

The cells were pelleted by centrifugation at 4000g for 5 minutes and supernatant was removed. Cells were resuspended in 200µl LB broth and spread over an agar plate containing the appropriate antibiotic with a sterilised glass rod. The plate was incubated at 37^{o}C overnight to grow colonies.

Individual colonies were picked using a sterile pipette tip, and transferred to a 50ml tube containing 10ml LB Broth with the appropriate antibiotic. For pGEM-Te cloning, colonies that were white in colour were selected to be grown, and blue colonies were disregarded.

Cells were grown for 16 hours in a shaking incubator (37^{o}C), then centrifuged at 4000g for 20 minutes to collect the pellet and supernatant was discarded. Plasmid DNA was extracted and purified according to section 2.4.3.

2.4.7 Plasmid Purification

Materials

QIAGEN Miniprep kit

Methods

Cell pellets were resuspended in 250µl cold buffer P1 and transferred to a 1.5ml tube. Cells were lysed in 250µl alkaline buffer p2, mixing by inversion. 350µl acidic buffer N3 was added and mixed to neutralise the solution. Samples were then centrifuged for 10 minutes at 13,000rpm and supernatant was collected and transferred to a QIAprep spin column, which was centrifuged for one minute to bind DNA to the silica membrane. Through-flow was discarded and the 750µl buffer PE was added to wash the column of endonucleases and salt, again spinning for one minute. Through-flow was again discarded and the column was transferred to a clean 1.5ml collection tube. DNA was eluted in 30µl nuclease free water by centrifuging at 13,000rpm for one minute. For purification of larger plasmid preps, the QIAGEN Plasmid Midiprep kit was used according to manufacturer's instructions.

2.4.8 Glycerol stocks

Materials

100% glycerol (Sigma-Aldrich)

LB broth (Sigma-Aldrich)

Method

A 700µl suspension of transformed JM109 cells was pipetted into a sterile 1.5ml tube. 300µl of 100% glycerol was added and mixed, and stocks were stored at -70°C.

2.4.9 Site directed mutagenesis

Materials

QuikChange XL Site-Directed Mutagenesis Kit (Promega):
10 x Reaction buffer (Promega)
dNTP mix (Promega)
PfuTurbo DNA polymerase (2.5U/µl) (Promega)
Dpn1 (10U/µl) (Promega)
Primers
Nuclease free water (Sigma-Aldrich)

Method

An unknown SNP at position 110 (p.Gly110Cys) was identified in the wild type GPX1-pGEM-te construct, and a frameshift was apparent in GPX1-FLAG vectors. In order to correct sequence anomalies, site directed mutagenesis (SDM) was employed. The QuikChange® II XL Site-Directed Mutagenesis Kit was used to change the cysteine residue to a glycine, using two complementary primers containing the mutation desired flanked by unmodified sequence complementary to the wild type sequence (section 2.3.7). Similarly the frameshift was corrected by SDM. The primers were required to be 25-45bp in length with a Tm $\geq$78°C. The following reaction was prepared:

Component	
10 x reaction buffer	5µl
dNTP mix	1µl
FP	125ng
RP	125ng
Template DNA	50ng
Nuclease-free water	To 50µl
Add last: *PfuTurbo* DNA polymerase (2.5U/µl)	1µl

The following cycles were used for site directed mutagenesis:

Temperature (°C)	Time (Minutes)	Cycles
95	1	1
95	0.5	18
62	1	
68	1/kb	
68	5	1

Following amplification, the reaction mix was incubated on ice for 2 minutes, and then 1µl restriction endonuclease *Dpn1* was added to the reaction and mixed by pipetting. The reaction was incubated at 37°C for 2 h to digest parental DNA. The digested DNA was transformed into NEB 5-alpha Competent *E.coli* (high efficiency), grown and purified as described below. To check for release of the insert, plasmid DNA was digested with *Not1* restriction endonuclease as described in section 2.4.3.

2.4.10 Transformation using NEB 5-alpha Competent *E.coli* (high efficiency) cells

Materials

NEB 5-alpha Competent *E.coli* (NEB)

SOC medium (NEB)

Method

Tubes containing 50µl NEB 5-alpha Competent *E.coli* cells were thawed on ice for 10 minutes. 5µl of *Dpn1*-digested DNA reaction was added to the competent cells and gently mixed by flicking the tube. The mixture was incubated on ice for 30 minutes, then heat shocked at exactly 42°C for 30s using a water bath, and returned to ice for 5 min. 950µl SOC medium was pipetted into the mixture and incubated at 37°C for 60 min at 250rpm.

Following incubation transformation reaction mixtures were centrifuged at 1000g for 10 min. 800µl supernatant was aspirated and discarded. The cell pellet was resuspended in the remaining supernatant and 100µl was transferred to LB agar plates containing 100µg/ml ampicillin.

Plates were incubated overnight at 37°C, after which colonies were picked and cultured in 10ml LB broth overnight at 37°C with 230rpm shaking. The cultured cells were centrifuged for 20 minutes at 4000g to form a pellet, then purified according to section 2.4.7.

2.5 Protein Analysis and Protein-Protein interaction protocols

2.5.1 Protein extraction for Western blotting

Materials

RIPA buffer (Sigma-Aldrich)

complete, Mini, EDTA-free Protease Inhibitor Cocktail Tablets (Roche)

2x Laemmli buffer (Sigma-Aldrich)

Methods

To prepare lysates, media was removed by pipetting and cells were washed 3x in cold PBS. For a 6 well plate, cells were lysed in 200µl RIPA buffer (containing protease inhibitor), scraped off the plate, and transferred to 1.5ml tubes. Tubes were left on ice for 30 minutes, then centrifuged at 13,000rpm for 12 min at 4^{o}C to pellet cell debris. Supernatant was collected and added to an equal volume of 2x Laemmli buffer, containing SDS and β-ME, then boiled for 10 minutes to denature proteins prior to gel loading

2.5.2 Bradford Protein Assay

Materials

Protein Assay Dye (Coomassie Brilliant Blue G-250) (5x)(Biorad)
Phosphate Buffered Saline (PBS) (Sigma-Aldrich)
Bovine serum albumin (BSA) (Sigma-Aldrich)

Method

The Bradford protein assay was used to determine protein concentration of cell lysates. The assay is based on the maximum absorbance shift from 465nm to 595nm of Coomassie Brilliant Blue G-250 when bound to a protein. Serial dilutions of BSA ranging from 0 to 1mg/ml in concentration were used as protein standards. The protein assay dye was diluted 1 in 5 with PBS prior to the assay. 10 µl of standard or test sample were added in triplicate to each well of a 96-well plate, plus 200µl protein assay dye. The samples were left to incubate at room temperature for 5 minutes, then absorbance was read using a standard plate reader. A standard curve was produced by plotting OD595 against concentration of the BSA standard, and the protein concentration of each sample was determined by extrapolating from the linear equation.

2.5.3 Western blotting

Materials

Kaleidoscope prestained Protein Marker (Biorad)
50x 3-(N-morpholino)propanesulfonic acid (MOPS) running buffer (50 mM MOPS, 50 mM Tris Base, 0.1% SDS, 1 mM EDTA, pH 7.7)
SDS PAGE precast NuPage BisTris gels (4-12%, 10% or 12%) (Invitrogen)

Methods

A pre-cast gel was briefly rinsed with distilled water and inserted into the gel tank. The tank was filled with 1x MOPS buffer to cover the gel, and the comb removed. The protein ladder was loaded into the first well of the gel (10µl for 10 well gel, 8 µl for 15 well gel). Samples prepared in 2x Laemmli buffer (section 2.5.1) were centrifuged for 1 minute at 13,000g and loaded into adjacent wells, typically between 20 and 30µl depending on the protein content of the lysate. The gel was run for 30 minutes at 70V and an hour at 160V.

2.5.4 Semi-dry Transfer of Proteins from Gel to Membrane

Materials

0.1µm pore nitrocellulose membrane
1x Transfer Buffer (0.9% glycine (w/v), 0.242% Tris (w/v), 20% Methanol (v/v))
Extra thick filter paper (Biorad)
Trans-Blot SD semi-dry transfer cell (Bio-Rad)

Methods

A square segment of nitrocellulose membrane was cut to the dimensions of the gel using the extra thick filter paper as a template. The membrane was soaked in transfer buffer for 10 minutes prior to the transfer procedure. A sandwich of filter paper-membrane-gel-filter paper

was assembled in the transfer cell (Fig. 2.5). First, filter paper was briefly soaked in transfer buffer and placed on the transfer cell, pressed with a roller to remove excess buffer. Next the membrane was placed on top of the filter paper, and then the gel was soaked and placed on top of the membrane. Bubbles were removed by gently pressing the gel from the centre to the corners. Finally, the second filter paper was soaked and placed on top of the gel. The sandwich was pressed again with the roller to remove excess buffer. The transfer cell was set to 15V for 40 minutes for one blot or 50 minutes for two blots.

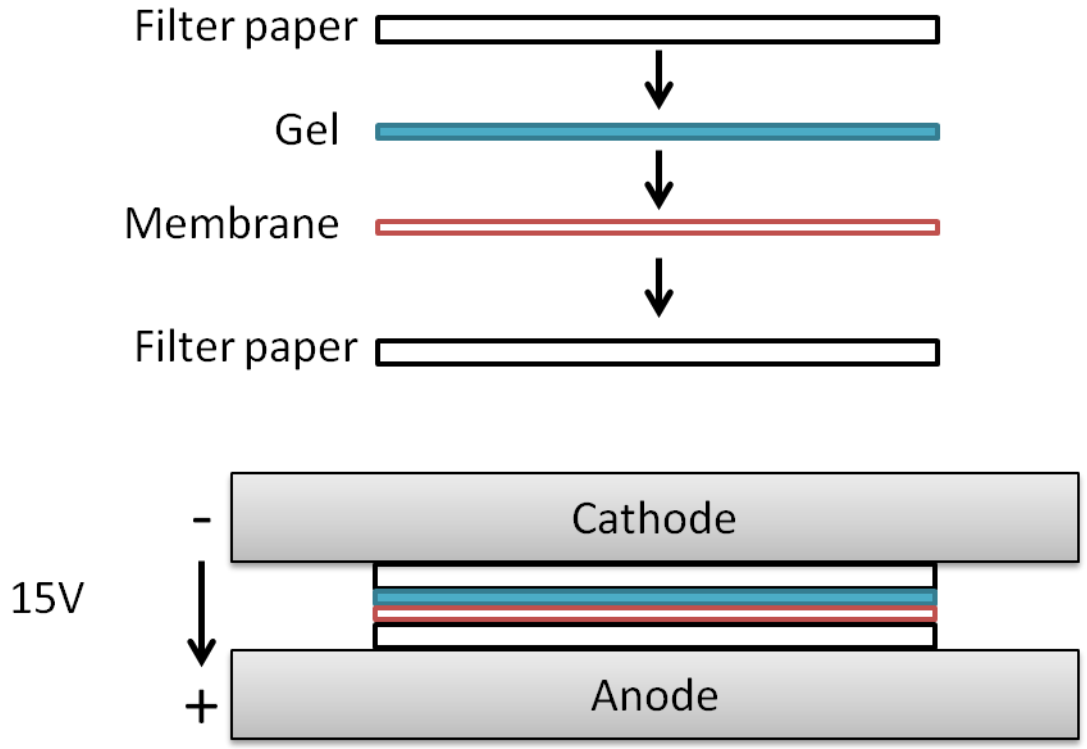

Figure 2. 5: Semi-dry Transfer.

Illustration showing assembly of filter paper, nitrocellulose membrane and polyacrylamide gel on the transfer cell.

After transfer, the gel was discarded and the membrane was subjected to Ponceau-S staining to determine efficiency of the transfer.

2.5.5 Ponceau-S staining

Materials

Ponceau-S (0.2% Ponceau-S and 1% Acetic acid) (Sigma-Aldrich)
Washing buffer (1x PBS + 0.1% (v/v) Tween20) (PBS-Tw) (Sigma-Aldrich)

Method

Ponceau-S is a dye that reversibly stains protein bands without any adverse effects on the proteins. Staining membranes with Ponceau-S reveals any regions where the transfer has failed (seen as bubbles) as well as the amount of protein loaded per lane, and the efficiency of the transfer. Membranes were placed in small containers, covered with Ponceau-S and left on a shaker for two minutes. Ponceau-S was removed and the membrane was washed with PBS-Tw. After one wash, protein bands became visible. Ponceau-S staining was then removed with further washes in PBS-Tw.

2.5.6 Immunoblotting

Materials

Blocking buffer (5% non-fat dried powdered milk (Asda) in PBS-Tw (0.1%))
Primary antibody
HRP conjugated Secondary antibody (Odyssey)
Washing buffer (0.1% PBS-Tw)

Method

A blocking buffer was prepared by dissolving 5% powdered milk in PBS-Tw and mixing by inversion. Nitrocellulose membranes were transferred to 50ml tubes with 10ml blocking buffer for one hour, to prevent non-specific binding of the antibody. Tubes were rotated on a roller. After blocking, membranes were incubated in milk containing relevant dilutions of primary antibodies overnight at 4°C.

The following day, membranes were subjected to 3x 10 minutes washes in PBS-Tw, incubated in milk containing fluorophore-conjugated secondary antibodies (goat rabbit 800 1:5000, goat mouse 680 1:20,000) for 1 hour and wash steps were repeated. Bands were detected using an Odyssey scanner at wavelengths 800 and 680.

2.5.7 Antibodies for Western blotting

	Antigen/ Fluorophore	Species	Company	Dilution
1°	β-actin	Mouse monoclonal	Sigma-Aldrich	1 in 10,000
1°	SOD2	Rabbit polyclonal	Abcam	1 in 5000
1°	NRF2	Rabbit polyclonal	Abcam	1 in 1000
1°	GPX1	Rabbit polyclonal	Abcam	1 in 1000
1°	FLAG	Mouse monoclonal	Sigma-Aldrich	1 in 2000
1°	PRDX3	Rabbit polyclonal	Proteintech	1 in 500
1°	PRDX-SO2/3	Rabbit polyclonal	Abcam	1 in 2000
1°	Calmodulin binding protein	Rabbit polyclonal	Millipore	1 in 500
1°	GAPDH	Rabbit polyclonal	Abcam	1 in 5000
1°	PARP	Rabbit polyclonal	Cell Signalling Technology	1 in 1000
1°	StAR	Mouse monoclonal	Abcam	1 in 500
1°	Myc	Rabbit monoclonal	Sigma-Aldrich	1 in 1000
1°	p38-MAPK	Rabbit polyclonal	Cell Signalling Technology	1 in 1000
1°	ph-p38MAPK	Mouse monoclonal	Cell Signalling Technology	1 in 2000
2°	IRDye®680LT	Goat anti-mouse	Li-cor	1 in 20,000
2°	IRDye®800CW	Goat anti-rabbit	Li-cor	1 in 5000

2.5.8 Deglycosylation

Materials

N-Glycosidase F (PNGase F) (500,000 U/ml) (NEB)

Buffer G7 (NEB)

Method

Hek293 cells were transfected with MRAP-CTAP, MRAP-NTAP or empty vector in 6 well plates and lysed as above (2.5.1). 10µl of lysate was subjected to digestion by PNGase in the following reaction mix:

Component	
Protein lysate	10µl
PNGase F	1µl
Buffer G7 10x	1.5µl
Lysis buffer to a total volume of	15 µl

Reactions were mixed, briefly centrifuged and incubated at 37°C for 2 hr. The samples were then analysed by Western blot according to section 2.5.3.

2.5.9 Tandem affinity purification (TAP)

Materials

InterPlay mammalian TAP system (Agilent):

Streptavidin binding buffer (SBB)

Streptavidin elution buffer (SEB)

Calmodulin binding buffer (CBB)

EDTA 0.5M

14.4M β-ME

Method

Tandem affinity purification is an immunoprecipitation technique that utilises a double epitope-tag to isolate proteins in two successive purification steps.

For TAP, 1 x 10^8 HEK293 and H295R cells (8 x $10cm^2$ plates) were transfected with TAP-tagged *MC2R*, *MRAP*, *NTAP-MEF2* (myocyte enhancer factor-2) as a positive control or empty vector as a negative control (section 2.1.6.1). After 48h, cells were harvested using 400µl/$10cm^2$ plate of the lysis buffer provided supplemented with protease inhibitors, and transferred to 1.5ml tubes on ice (section 2.5.1). A 20µl aliquot of lysate was stored at -80°C to use as an input during Western blot analysis.

Prior to purification steps 500 µl/sample of the streptavidin resin slurry was centrifuged at 1500g for 5 minutes and the supernatant comprising an ethanol storage buffer was removed by pipetting. The streptavidin resin was washed twice in 1ml SBB and after each wash the resin was centrifuged for 5 minutes at 1500g. After wash steps, streptavidin resin was resuspended in a small volume of SBB to cover the resin and transferred to 15ml tubes. Lysate pooled from $10cm^2$ dishes was transferred to the streptavidin resin and topped up with 500µl SBB. A further 40µl 0.5M EDTA and 7µl 14.4M β-ME were added per ml lysate and samples were placed on a rotator overnight at 4°C.

Following overnight incubation the resin was centrifuged at 1500g for 5 min and an 80µl aliquot of supernatant was separated and stored at -80°C for Western blot analysis to determine the amount of target protein that did not bind the resin. The remaining supernatant was aspirated and the resin was washed three times with 1ml SBB for 20min on a rotator at 4°C. On the final wash step, supernatant was removed and 1 ml SEB was added to the streptavidin resin to elute associated proteins. Samples were placed on a rotator for 1h 15min at 4°C.

The resin was collected by centrifugation at 1500g for 5 min and supernatant containing eluted proteins was transferred to 250µl calmodulin resin in a 15ml tube, which had been pre-washed three times in CBB. A 20µl aliquot was taken at this stage for Western blot analysis,

which would show the amount of target protein recovered by the first purification step. 4ml CBB with 20 µl streptavidin supernatant supplement were added to each sample and rotated at 4°C overnight.

Following the second overnight incubation, samples were centrifuged at 1500g for 5 minutes to collect the resin. The resin was washed 3 times in 1ml CBB and on the last wash supernatant was removed leaving enough to cover the beads. An equal volume of Laemmli buffer was added and samples were boiled to detach and denature proteins bound to the calmodulin resin.

The efficiency of the double purification was analysed by Western blot, using aliquots taken from each step of the purification. The intensity of the bands and level of background gave an indication of the success of the purification.

2.5.10 Coomassie Blue staining

Materials

Coomassie Brilliant Blue G-250 Colloidal concentrate (Sigma-Aldrich)
Methanol (Fisher-scientific)
Acetic acid (Sigma-Aldrich)

Method

Coomassie brilliant blue is a triphenylmethane dye that stains proteins in polyacrylamide gels. Lysates containing TAP-tagged MC2R or MRAP isolated by tandem affinity purification were run on a 4-12% Bis-Tris 1D SDS-PAGE gradient gel. The gel was fixed in a solution containing 7% acetic acid and 40% methanol, then stained with a solution of Coomassie Blue (colloidal concentrate with deionised water (1:4)) and 20% methanol overnight. After bands became visible, the gel was destained with 25% methanol and 7% acetic acid for 5 minutes, and then 25% methanol and 2% acetic acid for a minimum of 10

minutes until the bands appeared in good contrast against the background. The gel was stored in deionised water. Chosen bands were excised and analysed by mass spectrometry at KCL Proteomics Facility, Institute of Psychiatry.

2.5.11 Mass spectrometry

Method

Coomassie Blue stained SDS-PAGE containing lysates purified by TAP were analysed by mass spectrometry at KCL Proteomics Facility, Institute of Psychiatry, using their optimised protocol:

In-gel reduction, alkylation and digestion with trypsin were performed prior to subsequent analysis by mass spectrometry. Cysteine residues were reduced with dithiothreitol and derivatised by treatment with iodoacetamide to form stable carbamidomethyl derivatives. Trypsin digestion was carried out overnight at room temperature after initial incubation at 37^{o}C for 2 hours.

Peptides were extracted from the gel pieces by a series of acetonitrile and aqueous washes. The extract was pooled with the initial supernatant and lyophilised. Each sample was then resuspended in 23μL of 50mM ammonium bicarbonate and analysed by LC/MS/MS. Chromatographic separations were performed using an Ultimate LC system (Dionex, UK). Peptides were resolved by reversed phase chromatography on a 75 μm C18 PepMap column using a three step linear gradient of acetonitrile in 0.05% formic acid. The gradient was delivered to elute the peptides at a flow rate of 200nL/min over 30 min. The eluate was ionised by electrospray ionisation using a Z-spray source fitted to a QTof-micro (Waters Corp.) operating under MassLynx v4.0. The instrument was run in automated data-dependent switching mode, selecting precursor ions based on their intensity for sequencing by collision-induced fragmentation. The MS/MS analyses were conducted using collision energy profiles that were chosen based on the mass-to-charge ratio (*m/z*) and the charge state of the peptide.

Acquisition parameters were optimised for high coverage and full characterisation, which included a reduced ion exclusion time for MS/MS from 2 min to 20 sec to promote re-sequencing of peptides.

The mass spectral data was processed into peak lists using ProteinLynx Global Server v2.2.5 with the following parameters:

MS survey – No background subtraction, SG smoothing 2 iterations 3 channels, peaks centroided (top 80%) no de-isotoping.

MS/MS – No background subtraction, SG smoothing 2 iterations 4 channels, peak centroiding (top 80%) no de-isotoping.

The peak lists was searched against the Swiss Prot and r2 sequence specific databases using Mascot software v2.2 (http://www.matrixscience.com) using the following parameter specifications:

Precursor ion mass tolerance 1.2 Da
Fragment ion mass tolerance 0.6 Da
Tryptic digest with up to three missed cleavages
Variable modifications: Acetyl (Protein N-term), Carbamidomethylation (C), Gly->pyro-glu (N-term Q), Oxidation (M) and Phosphorylation (S, T &Y).

Database generated files were uploaded into Scaffold 3 software (www.proteomesoftware.com) to align samples for easier interpretation. Protein identifications were automatically accepted if they contained at least two unique peptide assignments and were established at 100% identification probability by the Protein Prophet algorithm (Nesvizhskii, *et al.*, 2003). Mass spectra for all other protein identifications were manually validated according to accepted procedures.

2.6 Imaging of cells

2.6.1 Immunocytochemistry

Materials

4','6-diamido-2-phenylindole stain (DAPI) (Sigma-Aldrich)
Primary and secondary antibodies (Section 2.6.2)
3.7% paraformaldehyde (Sigma-Aldrich)
0.025% Triton X-100 (Sigma-Aldrich)
PBS (Sigma-Aldrich)
0.1% (v/v) Triton-100 in PBS (PBS-Tr) (Sigma-Aldrich)
Blocking buffer (3% (w/v) Bovine Serum Albumin (BSA), 10% Normal Goat serum (NGS) in 0.1% PBS-Tr)
Fluorescent Mounting Media (Dako)

Methods

HEK293 cells were transfected with appropriate vectors in 12 well plates containing 10mm cover slips. Cells were transfected at 50% confluence, and cultured until 60-70% confluent in order to distinguish and analyse single cells by microscopy. Media was then discarded and cells were washed twice with PBS. To fix, cells were incubated in 3.7% paraformaldehyde for 10 minutes, followed by a 2 minute wash in PBS. Cell were permeabilised with 0.025% TritonX-100 in PBS for 10 minutes, and then blocked in 3% BSA and 10% NGS in 0.1% PBS-Tr for an hour. After blocking cells were stained with appropriate primary antibodies in blocking buffer for 1.5 hours, washed twice in PBS for 10 minutes, incubated with species specific cy2 or cy3 conjugated secondary antibodies in blocking buffer for 1.5 hour, and washed again three times in PBS for 10 minutes. Cells were briefly incubated with 2μg/ml DAPI (1 minute) to stain nuclei, and washed again for 10 minutes in PBS. Cover slips were removed with forceps and mounted onto 1mm thick clear slides using one drop of fluorescent mounting media. Slides were stored at 4°C in the dark. Immunostained cells were visualised

on the Zeiss LSM510 laser scanning confocal microscope. Images were taken using a 63x objective.

2.6.2 Antibodies for immunocytochemistry

	Antigen/Fluorophore	Species	Company	Dilution
1°	Calmodulin binding protein	Rabbit polyclonal	Millipore	1 in 100
1°	FLAG	Mouse monoclonal	Sigma-Aldrich	1 in 500
1°	HA	Mouse monoclonal	Sigma-Aldrich	1 in 500
2°	AF488-Green	Donkey Mouse	Invitrogen	1 in 1000
2°	AF546-Red	Donkey Rabbit	Invitrogen	1 in 5000
2°	AF488-Green	Goat anti-mouse	Invitrogen	1 in 1000
2°	AF568-Red	Goat anti-rabbit	Invitrogen	1 in 1000

2.6.3 Confocal microscopy

Fluorescent and RBG colour imaging was performed on the Zeiss LSM 510 inverted confocal laser scanning microscope (Carl Zeiss Ltd, UK). Objectives used were either 10x, 20x, 40x or 63x. The pinhole was set to 1 Airy unit, with Cy2 green fluorophore detected by the 458nm Argon laser, Cy3 red fluorophore detected by the 543 HeNe laser and blue wavelengths such as that emitted by DAPI detected by the 405nm Diode laser. Images were acquired at 1024x1024 pixels, averaging 8, bit data depth 16**.** Image processing was performed using Zen lite software (Carl Zeiss Ltd, UK).

2.7 Functional assays

2.7.1 Cycloheximide treatment to assay half-life of proteins

Materials

Cell culture media

ITS premix (BD biosciences)

Cycloheximide (CHX) 50mg/ml (Sigma-Aldrich)

MG132 10mM (Sigma-Aldrich)

Dimethyl sulfoxide (DMSO) (Sigma-Aldrich)

Method

The half-life of a protein can be assayed using CHX, a eukaryotic protein synthesis inhibitor, to determine the degree of degradation of a protein. CHX blocks translation of mRNA on 80S ribosomes in the cytosol. MG132 is a 26S-proteosome inhibitor, preventing degradation of ubiquitin-conjugated proteins.

HEK293 cells were seeded in 12-well plates and grown overnight to a confluency of 70%. In initial experiments, cells were transfected with 1µg R130-L133del-FLAG or 25ng WT-FLAG, and DNA concentration was kept constant using an empty vector. Untransfected cells were used as a negative control. 24h after transfection, cells were treated either 25 µg/ml cycloheximide, 25µM MG132, both or DMSO as a vehicle control for 4h. CHX, MG132 and DMSO were diluted in DMEM cell culture media supplemented with 1% ITS premix but no serum. Following treatment, media was removed and cells were washed with cold PBS, then lysed for Western blot analysis using FLAG antibody (Sigma-Aldrich) and GAPDH as a loading control.

In later experiments, cells were transfected with 10ng WT-FLAG to gain similar protein levels to R130-L133del-FLAG. Cells were treated with 50µg/ml CHX, 25µM MG132 or both for 10h and lysed at 1, 2, 5, and 10h after treatment. Lysates were analysed by Western blot analysis using antibodies to FLAG and GAPDH as a loading control to normalise data.

In order to calculate half-life, the percentage of protein remaining (Y) was plotted again time (X) for WT and R130-L133del. GraphPad Prism 4 software was used to create a nonlinear regression model with an exponential curve to fit data, with the equation:

$$\mathbf{Y=Y_0e^{-KX}}$$

Y_0= Value of Y at time 0

K= Rate constant

X= Time

The half-life was calculated using the equation ln(2)/K.

2.7.2 cAMP luciferase assay

Materials

Dual-luciferase reporter system (Promega):

Luciferase assay buffer II

Luciferase assay substrate (lyophilized)

Stop & Glo® Buffer

50x Stop & Glo® Substrate

5x Passive lysis buffer

pRL-CMV Renilla luciferase plasmid

α-GSU-846 plasmid

Method

cAMP production was measured using the Promega Dual-Luciferase Reporter assay system in which the activities of Firefly (*Photinus pyralis*) and Renilla (*Renilla reniformis*) luciferases are measured sequentially from a single sample. To measure the cAMP response to ACTH in the presence of TAP-tagged MC2R or MRAP, *MC2R* and *MRAP* constructs were co-transfected with an 'experimental' α GSU-846 luciferase reporter, containing a luciferase driven by the cAMP responsive promoter α GSU-846, and a 'control' reporter pRL-CMV *Renilla* luciferase plasmid, driven by the CMV immediate-early enhancer/promoter. The two

luciferases respond to different substrates, hence the Firefly reaction can be quenched whilst simultaneously initiating the Renilla reaction.

The following bioluminescent reactions are catalysed by Firefly and *Renilla* luciferases:

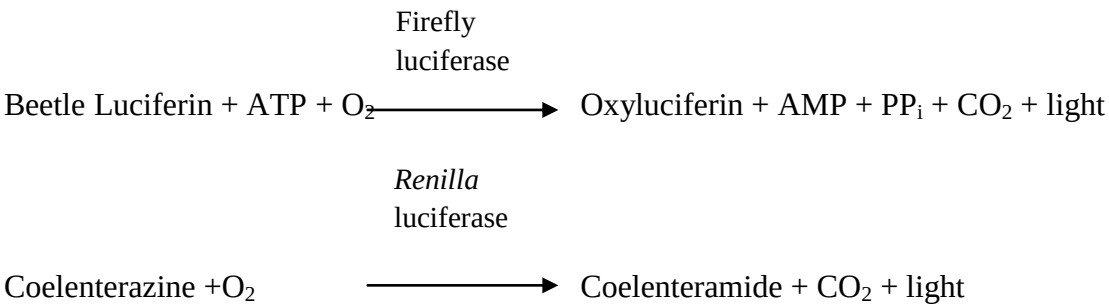

HEK293 cells were seeded in 6-well plates and grown overnight to 80% confluency. Cells were transfected with either 1µg MC2R-TAP with 1µg MRAP-FLAG, MRAP-TAP or empty vector, 1µg MRAP-TAP with 1µg HA-MC2R, or 2µg empty vector alone. All cells were transfected with 900ng α GSU-846 and 100ng pRL-CMV luciferase reporter plasmids. 48h after transfection, cells were stimulated for 6h with ACTH ranging from 10^{-6} to 10^{-11}M concentration.

Following stimulation, media was removed and cells were washed twice in PBS. Cells were harvested in 100µl 1x passive lysis buffer which promotes rapid lysis, left on a rocker for 10 minutes at 4°C, then transferred to a 1.5ml tubes and incubated on ice for 30 minutes. Tubes were centrifuged at 13,000rpm for 2 minutes to pellet cell debris.

Before starting the assay, Luciferase assay reagent II (LAR II) was prepared by resuspending the lyophilized luciferase assay substrate in 10ml of luciferase assay buffer II. Both reagents were warmed to room temperature before use. For Stop & Glo® reagents, 1 volume of 50x Stop & Glo® substrate was added to 50 volumes of Stop & Glo® Buffer in a glass tube.

25µl of the cell lysate supernatant was transferred to a white-walled 96-well plate and inserted into the BMG Labtech Omega luminometer to measure luciferase activities. The BMG Labtech Omega luminometer was programmed to inject 80µl of LARII into each well,

followed by 80µl Stop & Glo® reagent. The reaction was initiated by the addition of LARII following which luminescence from the Firefly luciferase activity is quantified. The reaction is then quenched by adding Stop & Glo® which simultaneously initiates *Renilla* luciferase activity leading to luminescent signal which is subsequently measured.

Data obtained from the illuminator is analysed by dividing the Firefly luciferase activity values by those obtained by *Renilla* luciferase. Luciferase activity is proportional to cAMP production, because cAMP activates protein kinase A (PKA) which phosphorylates cAMP response element binding protein (CREB) which is expressed by the α GSU-846 construct. CREB binds co-activators and in turn recruits RNA polymerase II to the αGSU promoter initiating transcription of the luciferase.

Hence, Firefly luciferase is activated on ACTH stimulation due to cAMP generation, whereas the *Renilla* luciferase activity acts as an internal control.

2.7.3 Glutathione Peroxidase (GPX) assay

GPX activity was measured using continuous spectrophotometric rate determination, based on a coupled assay of NADPH oxidation, (Sigma-Aldrich protocol EC 1.11.1.9). As GPX1 detoxifies hydrogen peroxide, glutathione is oxidised (Fig. 1.5.4.). In a second reaction, glutathione reductase uses NADPH to return glutathione to its reduced state. Oxidation of NADPH to $NADP^+$ results in a decreased absorbance at 340nm. This decrease is inversely proportional to the level of GPX activity.

As all GPXs will detoxify hydrogen peroxide, it is not possible to differentiate between different GPX activities in this assay. One would only be able to discriminate between GPX4 and total GPX activity, by using a phospholipid hydroperoxide.

2.7.3.1 In house assay GPX assay

Materials

Sodium Phosphate (Sigma-Aldrich)

Dithiothreitol (DTT) (Sigma-Aldrich)

Sodium Azide (Sigma-Aldrich)

Reduced Glutathione (Sigma-Aldrich)

B-Nicotinamide dinucleotide 2-phosphate reduced tetrasodium salt (NADPH) (Sigma-Aldrich)

GPX1 enzyme from bovine erythrocytes (lyophilised powder ≥300u/mg) (Sigma-Aldrich)

30% Hydrogen peroxide (Sigma-Aldrich)

Deionised water (Sigma-Aldrich)

Method

Cells were grown in 6 well plates to 90% confluency. To harvest, cells were scraped off plates using a rubber police man, with 10mM sodium phosphate with 1mM DTT buffer pH7 at 4^{o}C, and were homogenised using a sonicator. The homogenised lysate was centrifuged at 10,000g for 15 minutes at 4^{o}C to pellet the cell debris and supernatant was transferred to 1.5ml tubes and kept on ice.

The following cocktail was prepared and equilibrated to 25^{o}C:

Cocktail components	
50mM Sodium Phosphate Buffer with 0.4mM EDTA, 1mM Sodium Azide pH7	9.2ml
100u/ml Glutathione Reductase	0.1ml
200mM Reduced Glutathione (GSH)	0.05ml
NADPH	1mg

150µl cocktail and 25µl homogenised lysate were pipetted into the wells of a 96-well plate. As a positive control, purified GPX1 enzyme from bovine erythrocytes was diluted in sample buffer at concentrations ranging from 0.5 to 5u/ml to acquire a standard curve. For a negative control, sample buffer with no cell lysate was used to calculate background activity.

Absorbance at 340nm (A340nm) was monitored using a thermostatted spectrophotometer until it reached a steady state. Following equilibration, 25µl 0.042% hydrogen peroxide was added to each well using a multichannel pipette and A340nm was recorded immediately for 5 minutes at 30 second time intervals.

To calculate units per ml of enzyme in the samples, the maximum ΔA_{340nm} was determined for both test and blank samples and entered into the following equation:

Units/ml enzyme = (A340nm/min Test - A340nm/min Blank)(2)(0.2)(df)/ (6.22) (0.025)

Where 2 = 2 µmoles of GSH produced per µmole of β-NADPH oxidized, 0.2 = Total volume (in millilitres) of assay, df = Dilution factor, 6.22 = Millimolar extinction coefficient of ß-NADPH at 340 nm and 0.025 = Volume (in millilitres) of enzyme used

The units/ml GPX1 were measured relative to protein concentration, calculated using the Bradford assay.

2.7.3.2 Commercial Assay

Materials

Glutathione peroxidase assay kit (Abcam):
GPX Assay buffer
Cumene hydroperoxide
Glutathione
GPX1 positive control
NADPH

Method

Cells were grown in T25 flasks to 90% confluency, and scraped off in 300µl cold assay buffer supplemented with protease inhibitors. For the commercial assay standards were prepared before the assay by diluting NADPH to a range of concentrations between 0.1 to 1mM. 100µl of NADPH standards were plated in duplicate in a clear 96 well plate and A_{340}nm was measured using a thermostatic spectrophotometer. A standard curve was generated by plotting A_{340}nm against NADPH concentration.

After the standard curve had been generated, test wells were prepared. 50µl of each lysate, GPX1 positive control and assay buffer (background control) were added in duplicate to the wells of a 96-well plate.

The following reaction mixture was prepared for each test reaction:

Assay Buffer	33 µl
40 mM NADPH solution	3 µl
GR solution	2 µl
GSH solution	2 µl

40µl reaction mixture was added to each test well and incubated for 20 minutes to deplete GSSG in samples. 10µl cumene hydroperoxide solution was added samples to start the reaction, and A_{340}nm was measured for 10 minutes with readings taken at 30 second intervals. The total change in A_{340}nm within the linear range was calculated for each sample, and the NADPH standard curve was used to extrapolate the concentration of NADPH in the sample. The GPX activity then was calculated using the following calculation:

GPX Activity = B / T1 – T2 x V x Sample Dilution = nmol/min/ml = mU/ml

Where B is the NADPH amount that was decreased between T1 and T2 (in nmol), T1 is the time of first reading (A1) (in min), T2 is the time of second reading (A2) (in min) and V is the pre-treated sample volume added into the reaction well (in ml).

The units/ml GPX1 were estimated relative to protein concentration, calculated using the Bradford assay.

One unit is defined as the amount of enzyme that will cause the oxidation of 1.0 μmol of NADPH to NADP+ under the assay kit condition per minute at 25°C.

2.7.4 MTS (3-(4,5-dimethylthiazol-2-yl)-5-(3-carboxymethoxyphenyl)-2-(4-sulfophenyl)-2H-tetrazolium) assay

Materials

CellTiter 96® AQueous Non-Radioactive Cell Proliferation Assay (Promega)
MTS/PMS solution
30% Hydrogen peroxide

Method

Cell viability was determined using the CellTiter 96® AQueous Non-Radioactive Cell Proliferation Assay (Promega), a colorimetric assay based on the conversion of MTS (an electron coupling reagent) into formazan, catalysed by dehydrogenase enzymes found in metabolically active cells. Conversion of MTS into formazan results in an increase in absorbance at 490nm (A490nm).

Cells were seeded in triplicate in a 96 well plate at a density of 5000 cells and allowed to grow for 24 hours before treatment with 100μM H_2O_2 for a further 24 hours. On the morning of the assay, a further subset of cells were seeded at densities of 0 to 30,000 cells per well in triplicate to create a standard curve which was used as a positive control. Cells were allowed an hour to adhere, then media was removed from all wells and replaced with 100μl fresh media and 20μl MTS/PMS solution. After 2 hours incubation at 37°C in darkness, absorbance at 490nm was measured using the Wallac spectrophotometer. The number of metabolically active cells in test wells could be calculated using the linear equation of the

standard curve. Alternatively, the A490nm of samples could be compared directly, which was directly proportional to the number of metabolically activity cells.

2.7.5 GSH assay

Materials

Menadione 40µM

Total Lysis buffer

Oxidised Lysis buffer

Luciferin generation reagent

Luciferin detection reagent

Method

Glutathione is potent and abundant antioxidant that reduces toxic ROS. It acts as an electron donor, which on reducing disulfide bonds between proteins becomes oxidised (GSSG). The ratio of reduced to oxidised glutathione (GSH/GSSG) is therefore an indicator of cell toxicity.

The GSH/GSSG-Glo assay is a luciferase based assay with an output measure of luminescence. The assay principle is that the conversion of Luciferin-NT to Luciferin by glutathione-s-transferase, is dependent on GSH. This reaction is coupled to a Firefly luciferase reaction producing light, hence GSH is proportional to luminescence.

Samples are plated twice for two separate treatments. In one subset, all glutathione is converted to the reduced form GSH by a reducing agent, to calculate total glutathione. In the second subset, a reagent is used to block all reduced GSH. Remaining GSSG is then converted to GSH by the reducing agent and luminescence is quantified. From measuring the total and oxidised glutathione, the GSH/GSSG ratio can be calculated using the following calculation:

(Net total glutathione RLU- Net GSSG RLU)/(Net GSSG/2)

10,000 cells seeded in duplicate in a 96 well plate with white walls, to protect from inter-well cross-talk. Cells were seeded in duplicate twice for separate total and oxidised glutathione measurements, and were grown for 48 hours in normal media. For a positive control, a subset of cells were treated with 40µM menadione, a synthetic compound which increases levels of GSSG, for 1 hour prior to lysis (Sun *et al.*, 1997).

Buffers for the assay were made a maximum of 30 minutes before use as follows:

Volume per reaction (96-well plate):

	Total Lysis Buffer (µl)	**Oxidised Lysis Buffer (µl)**
Luciferin-NT	1	1
Passive Lysis Buffer 5x	10	10
NEM, 25mM	-	0.5
Water	39	38.5
Total volume:	**50**	**50**

Luciferin Generation Reagent	**(µl)**
100mM DTT	1.25
Glutathione-S-Transferase	3
Glutathione Reaction Buffer	45.75
Total volume	50

One subset of cells was lysed in 50µl total lysis reagent and the other in 50µl oxidised lysis reagent. As a background control, 50µl total lysis buffer was added to one well with no cells.

The plate was shaken gently for 5 minutes at room temperature. Luciferin generation buffer was added to all wells, shaken briefly, and incubated at room temperature in the dark for 30 minutes. Finally, 100µl luciferin detection buffer was added to wells, shaken briefly and incubated for 15 minutes in the dark. Luminescence was then read using the BMG Labtech OMEGA machine.

2.7.6 Enzymatic immunoassay

Materials

Cortisol Assay (Parameter):
Wash buffer
Stop Solution
Calibrator Diluent RD5-43
Colour reagent A
Colour reagent B
Primary antibody solution
Conjugate

Methods

Cortisol levels were measured using an enzymatic immunoassay, which is a competitive binding technique. Lysates are incubated with mouse-monoclonal antibody to cortisol and horse radish peroxidase (HRP)-conjugated cortisol, hence endogenous cortisol in the lysate must compete with HRP-conjugated cortisol for binding sites of the antibody. The incubation occurs in a goat anti-mouse coated microplate, to which the mouse monoclonal antibody becomes bound. Wash steps remove unbound sample and a substrate solution is added to determine bound enzyme activity which is measured by an increase in absorbance at 450nm. The absorbance at 450nm is inversely proportional to the concentration of endogenous cortisol in the lysate.

To measure cortisol levels, 800,000 cells were plated in 6 well plates and grown for 48 hours. Media was removed and replaced with serum free media either with no additives or containing 100µM H_2O_2 or 10^{-5}M forskolin. Cells were incubated for 6h, after which media was removed and stored in 1.5ml tubes at -80°C. Cells were lysed and subjected to Bradford assay for protein quantification.

Prior to the cortisol assay, samples were diluted 10-fold in calibrator diluent RD5-43 reagent. All assay reagents were warmed to room temperature before use. 20ml wash buffer concentrate was diluted in deionised water to prepare 500ml of wash buffer. The substrate solution was made 15 minutes prior to the assay procedure by mixing equal volumes of colour reagents A and B, enough for 200µl per well. The cortisol standard was reconstituted in 1ml deionised water to form a stock solution of 100ng/ml concentration and allowed to stand for 15 minutes. A standard curve was generated by making serial dilutions of the stock and was used within 1h of preparation.

To begin the assay, 150µl calibrator diluent RD5-43 was added into non-specific binding (NSB) wells and 100µl into zero standard wells (blank), standard wells and sample wells of the microplate. 100µl standard or sample was added to appropriate wells in duplicate. 50µl of cortisol conjugate was added to all wells, producing a red colour. A further 50µl primary antibody solution was added to all wells except NSB wells, changing the colour of wells to violet. The plate was incubated in the dark for 2h at room temperature on a shaker.

Following incubation wells were washed with 400µl wash buffer four times, each time aspirating and after the final step blotting against paper towel. 200µl substrate solution was added to each well and incubated a further 30 minutes at room temperature in darkness, the 50µl stop solution was added changing the colour from blue to yellow. The optical density of each well was measured within 30 minutes of adding the Stop Solution with a wavelength set at 450nm. The reading was corrected by subtracting readings at 570nm.

For data analysis, the optical density was plotted against cortisol concentration and a standard curve was generated using the mean of each standard. The sample values were obtained by

extrapolating from the standard curve and multiplying by the dilution factor. All values were normalised to protein concentration.

2.8 *in vivo* techniques

2.8.1 Mouse lines

Adrenals from *GPX1*$^{-/-}$ mice of a mixed genetic background were obtained as a kind gift of Xingen Lei from Cornell University.

2.8.2 Paraffin Embedding

Materials

4% paraformaldehyde (Sigma-Aldrich)
Ethanol (Fisher-scientific)
Xylene (Fisher-scientific)
Paraffin wax

Method

Adrenal glands from WT and *GPX1*$^{-/-}$ KO mice were fixed in 4% paraformaldehyde and stored in PBS at 4^{o}C overnight. Adrenals were incubated in increasing concentrations of ethanol (50-100%) for 1 hr intervals, and then xylene for 1-2 minutes, to dehydrate the tissue. Following dehydration adrenals were embedded in paraffin wax by incubating for 6 hours at 56^{o}C, and allowed to cool to room temperature in plastic moulds.

2.8.3 Sectioning

Materials

3-triethoxysilylpropylamine (TESPA) (VWR)
Superfrost Plus slides (VWR)

Method

8µm cross sections were cut using a microtome (Leitz 1512) and mounted onto TESPA treated 1mm thick superfrost plus slides. TESPA leaves the slide with a coating of positively charged ions, creating an adhesive surface for the section to bind. A few drops of distilled water were placed on the slide and the paraffin section was laid on top. A gentle heat was applied to soften the wax and remove crinkles. Water was aspirated by pipetting, leaving the section adhered to the slide surface. Slides were left to dry at 37^{o}C overnight.

2.8.4 Deparaffinisation

Materials

Ethanol (Fisher-scientific)

Xylene (Fisher-scientific)

Method

Before staining, sections were deparaffinised and rehydrated. Paraffin is insoluble and would inhibit staining if not removed. Sections were deparaffinised in a series of 10 minute incubations through the following solutions: 3x Xylene, 2x 100% EtOH, 1x 90% EtOH, 1x70% EtOH, 1x 50% EtOH and 2x H_2O.

2.8.5 Haematoxylin and Eosin (H&E) staining

Materials

Haematoxylin (Lamb Laboratories)

Acid alcohol (75% EtOH, 0.04% HCL) (Sigma-Aldrich)

Ammonia solution (0.084% ammonium hydroxide) (Sigma-Aldrich)

Eosin (Lamb Laboratories)

EtOH (Fisher-scientific)

Xylene (Fisher-scientific)

DPX Fluorescent mounting media (Lamb Laboratories)

Method

For H&E staining, slides were incubated in Haematoxylin dye for 2 minutes, washed for 2 minutes in running water, dipped 10 times in Acid Alcohol, washed, dipped 10 times in ammonia solution and left under running water for 5 minutes. Then, slides were dipped 10 times in 80% EtOH, 15 seconds in Eosin dye, 20 times in 90% ETOH, 100% EtOH and incubated twice for 3 minutes in Xylene. Cover slips were mounted with DPX mounting media, and slides were visualised with the confocal laser scanning microscope (Carl Zeiss Ltd, UK).

2.8.6 Immunofluorescent staining of adrenal sections

Materials

0.5M Sodium Citrate
normal goat serum
PBS-Tr
Antibodies
DAPI

Method

For immunofluorescence, slides were boiled in 0.5M Sodium Citrate (BDH Chemicals) for antigen masking, blocked in 10% normal goat serum for 1 hour to reduce non-specific binding of secondary antibodies. Slides were then incubated in PBS-Tr (0.1%) with antibodies to side chain cleavage, cleaved caspase-3 or inner zone antigen (IZA-1) overnight (section 2.8.6). The following day, slides were washed in PBS triton three times, and incubated in secondary antibodies, goat anti-mouse Alexa Fluor 488 and goat anti-rabbit Alexa Fluor 568 (section 2.8.6) in PBS-Tr for 2 hours. Slides were washed 3 times in PBS-Tr for 10 minutes and treated with DAPI for one minute and washed once more. Cover slips were mounted with glycerol in PBS (1 in 5). Slides were visualised using the confocal laser scanning microscope (Carl Zeiss Ltd, UK).

2.8.7 Antibodies for immunostaining

Ab	Antigen/ Fluorophore	Species	Company	Dilution
1°	SCC	Rabbit polyclonal	Millipore	1 in 1000
1°	IZA-1	Mouse monoclonal	Kind gift of Professor Gavin Vinson, QMUL	1 in 10
1°	Cleaved Caspase-3	Rabbit polyclonal	Santa-cruz	1 in 1000
2°	AF488-Green	Goat anti-mouse	Invitrogen	1 in 1000
2°	AF568-Red	Goat anti-rabbit	Invitrogen	1 in 1000

2.8.8 Radioimmunoassay

Materials

Steroid Diluent

corticosterone_125I

Corticosterone antibody

Precipitant Solution

Method

Corticosterone measurements were made using a radioimmunoassay which was performed by collaborators Xingen Lei and colleagues, Cornell University. The principle of the radioimmunoassay is similar to the enzymatic immunoassay used to measure cortisol, where a radioactive label is used instead of a colorimetric signal. Samples containing corticosterone are incubated with a known concentration of radioactive-labelled corticosterone and antibody to corticosterone, so that endogenous corticosterone from samples has to compete with the radioactive labelled form for binding of the antibody. After incubation the unbound proteins are removed and the radioactivity is measured, which is inversely proportional to corticosterone levels.

All reagents were brought to room temperature before the procedure. Serums from WT and $GPX1^{-/-}$ mice were diluted 1 in 200 with Steroid Diluent before addition to assay tubes. 300µl Steroid Diluent was added to NSB tubes and 100µl to zero standard tubes. 100µl each standard and 100µl diluted serum samples were added to appropriate tubes in duplicate.

200µl corticosterone_125I was added to all tubes and 200µl anti-corticosterone was added to the zero standard tubes to stop the assay. The zero standard tube (B_0) would have 100% binding of corticosterone_125I. Tubes were incubated for 2h at room temperature, after which 500 µl Precipitant Solution was added to all tubes and vortexed thoroughly. Tubes were then centrifuged at 1000g for 15 min, and supernatant was aspirated removing unbound sample.

The precipitate was counted on a gamma counter. To calculate corticosterone levels the following calculation was made:

% B/Bo (percentage bound) = mc(sample)- mc(NSB) / mc(zero standard)-mc(NSB) x 100

Mc=mean counts

The standard curve was plotted with percent bound versus the concentration of corticosterone from which the concentration of corticosterone in samples was extrapolated.

2.9 Statistical Analysis

Statistical analysis was performed on PRISM4 software and significance was determined by the student's t-test. Experiments that were analysed with statistics were performed in duplicate or triplicate and represent 3 independent experiments. Error bars represent the standard deviation of the mean taken from individual experiments. A *p* value under 0.05 was taken as statistically significant.

Chapter 3: Tandem Affinity Purification to identify interacting proteins of MC2R and MRAP in human adrenocortical cells

3.1 Introduction

In 2005, Metherell *et al.* identified *MRAP* as a causal gene for FGD, accounting for 20% of the patient cohort. Investigation into the role of MRAP revealed that the protein co-localised with MC2R at the ER and cell surface membrane, and co-IP showed the two proteins form a complex that was functionally receptive to ACTH when co-transfected into heterologous chinese hampster ovary (CHO) or neuroblastoma 'SK-N-SH' cells.

Like MC2R, some other GPCRs require accessory factors for trafficking for example a *Drosophila* cyclophilin gene *NinaA* is implicated in the transportation of RH1, the predominant rhodopsin, to rhabdomeres where it functions in phototransduction (Colley *et al.*, 1991). In the absence of NinaA, RH1 accumulates in the ER and is eventually degraded, and hence, *NinaA* mutants have low levels of rhodopsin (Cooray *et al.*, 2009). Other examples include the receptor activity-modifying proteins (RAMPs) which are required for expression of calcitonin and calcitonin-like receptors at the cell surface, and the receptor expression-enhancing proteins (REEPS) which are thought to be involved in the folding and trafficking of odorant receptors (Cooray et al., 2009); (Hay et al., 2006; McLatchie et al., 1998; Saito et al., 2004; Webb et al., 2009).

Interacting accessory factors can aid different aspects of the receptor cell cycle, for example correct folding, docking, ligand specificity, anchoring/stabilisation and endocytosis. It is therefore possible that in addition to MRAP there are other, unknown, interacting partners of MC2R which regulate its function.

Given that approximately 50% drugs target GPCRs, gaining understanding of their interacting partners could provide valuable information (Daulat *et al.*, 2007; Participants, 2004). Likewise, revealing further players in MC2R regulation could pinpoint genes involved in the pathogenesis of FGD. I therefore hypothesised that MC2R and MRAP are only two parts of an interacting complex of proteins that are necessary for the correct functioning and signalling of MC2R. In order to disclose potential interacting partners of MRAP and/or MC2R, a proteomic approach was employed.

Techniques that decipher protein interactions include the yeast 2 hybrid assay, and more recently tandem affinity purification (TAP). Currently, TAP is the most efficient technique for bait protein purification because of its quick, simple, generic protocol and flexibility meaning it can be used for any organism and a multitude of applications. Coupled with other techniques it has proven to be more informative than previous methods (Xu *et al.*, 2010).

3.1.2 Tandem Affinity Purification

Tandem Affinity purification was initially developed by Rigaut and colleagues of the European Molecular Biology Laboratory, Germany (Rigaut *et al.*, 1999). Previous protein purification techniques, including the Yeast 2 Hybrid screen (Y2H), have been limited by high levels of false positives and negatives as well as a lack of information regarding stoichiometry. The flexibility of such techniques was poor, with only a certain set of conditions testable (Puig *et al.*, 2001). Generating a generic protein purification technique to isolate protein complexes had not been possible due to the variability of protein properties. To resolve this Rigaut *et al.* chose to tag target proteins with peptides or protein domains so that a standardised purification strategy could be employed for all proteins, based on the tag. To retain protein complex integrity and to eliminate false positives such as non-physiological complexes, the tagged target protein would have to be expressed as close as possible to native levels. This meant a high affinity tag would be needed for purification and hence a double tag was developed.

The Tandem Affinity Purification tag (TAP-tag) forms the basis of the TAP method. Various different tags now exist, but the first tag developed consisted of calmodulin binding peptide (CBP), a tobacco etch virus (TEV) cleavage site and protein A (from *Staphylococcus aureus*, containing two IgG binding domains) at the C-terminus, or the same proteins in reverse at the N-terminus (Fig. 3.1). These tags were chosen over others because they purified the highest percentage of target protein from cell extracts (Rigaut *et al.*, 1999).

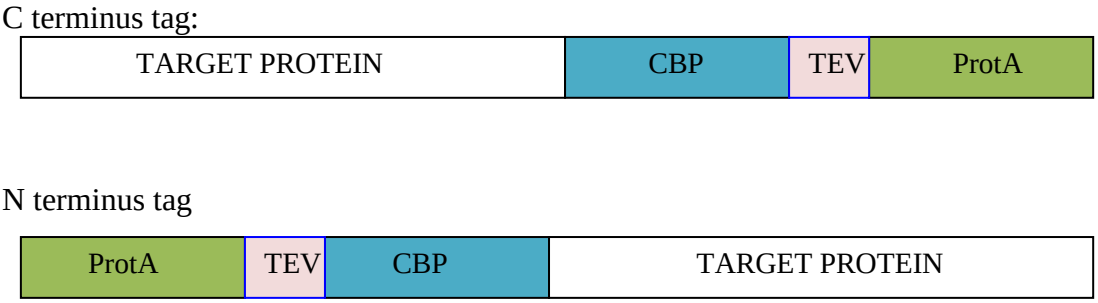

Figure 3. 1: Original tandem affinity purification tag

Illustration showing the first tandem affinity purification tag designed by Rigaut *et al.*, with protein A and calmodulin binding peptide tags at either the C (upper panel) or N (lower panel) terminus. The Prot A and CBP tags are separated by a TEV cleavage site. After the first purification step with IgG matrix the ProtA tag is cleaved with TEV protease. Therefore, the CBP tag is always closest to the inserted gene. (Based on Puig *et al.* (2001)

To summarise, the method consists of fusing the target protein to the affinity tags, introducing the construct into the host cell, maintaining native expression levels, and then recovering the target protein and its interactants via two purification steps (Fig. 3.2) (Rigaut *et al.*, 1999). In the first purification step, lysates are passed through an IgG matrix for which the Protein A has a high affinity. The target and associated proteins are captured by the IgG matrix and washed before being eluted. Protein A can only be detached from the IgG matrix under denaturing conditions. To overcome this, Rigaut *et al.* designed the TAP-tag to have a TEV protease recognition site between ProtA and CBP, enabling the target protein and its associated factors to be released by adding TEV protease (Rigaut *et al.*, 1999). In the second purification step, the eluate is incubated with calmodulin beads in the presence of calcium, and then eluted with EGTA in gentle conditions. However, EGTA can affect the stability of some proteins (Rigaut *et al.*, 1999), a factor that has been overcome in later developments of the tag.

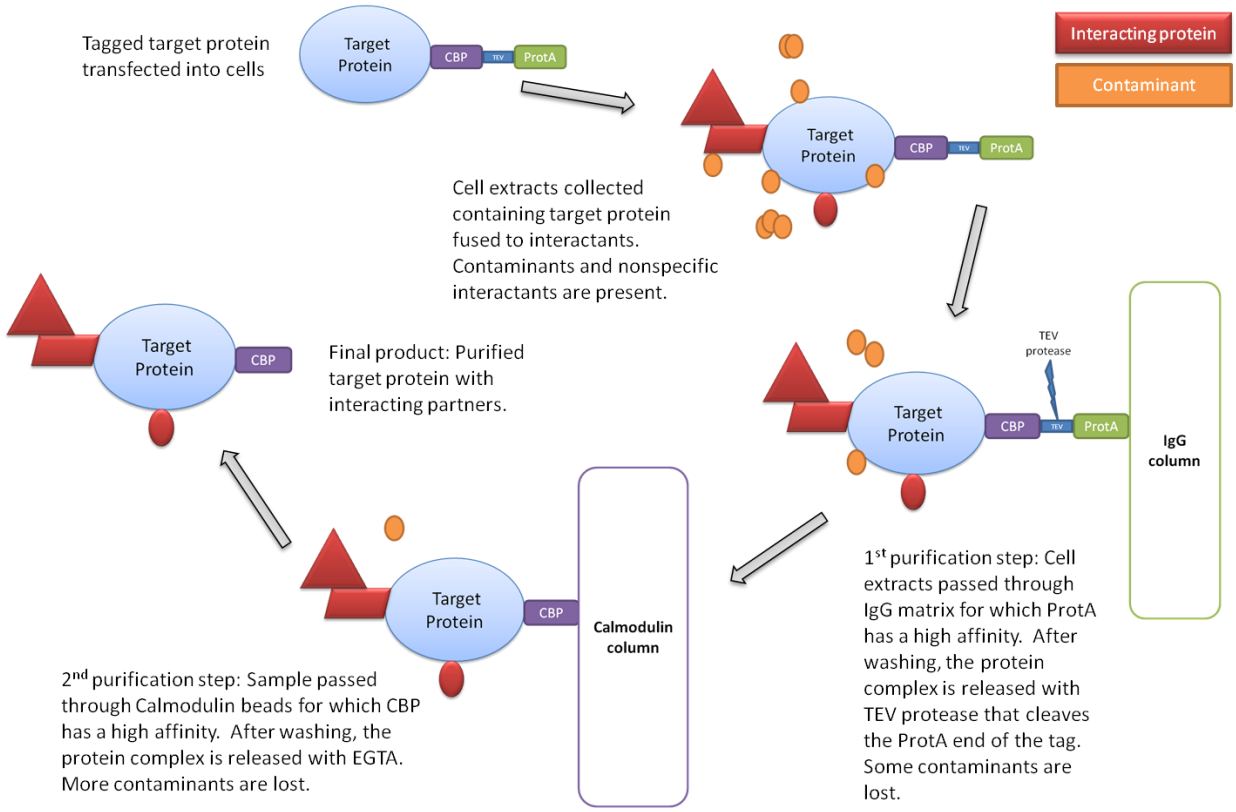

Figure 3. 2: Tandem Affinity Purification, an Overview

Based on Xu. *et al.* (2010)

Following two step purification, proteins recovered can be analysed in different ways. One can either simply identify interactants, or examine the structure or activity of the complex. To identify protein complex components, the purified material can be fractionated, for example by centrifugation and gel filtration, for further enrichment and to separate complexes by organelle/compartment. This is an optional step however stoichiometry cannot be determined without fractionation (Puig *et al.*, 2001). Samples are loaded on to a gradient polyacrylamide SDS gel which denatures the proteins and separates them by mass. The bands can be visualised by coomassie blue or silver staining and cut from the gel for protein identification via mass spectrometry (Puig *et al.*, 2001). Alternatively, if the structure is to be investigated, purified proteins are concentrated and then examined by electron microscopy. Finally, because tandem affinity purification is such a gentle technique, the activity of the intact protein complex can be tested by suitable assays (Puig *et al.*, 2001).

3.1.3 Yeast-2-hybrid Assay

The yeast two hybrid screen also caters for high throughput screening and, to its merit, was the starting point for interactome mapping. In contrast to TAP, it has the advantage of detecting less stable interactions that are less likely to be picked up by TAP (Gingras *et al.*, 2007). It is based on the activation of a reporter gene, for example LacZ, which is activated when a bait protein of interest interacts with a prey protein. In one strain, a bait protein is fused to a binding domain of a transcriptional activator for a region upstream of the gene. In a second, a prey protein is fused to an activating domain of a transcriptional activator. When strains are mated, the reporter gene can only be activated when the binding and activating domains are within close proximity. Therefore the gene is only activated if an interaction has taken place (Johnsson and Varshavsky, 1994). Despite discovering a multitude of interactions, this technique fails to give consistent data and is riddled with false positives and negatives. Numerous low and high throughput studies do not show overlap, to a greater extent than TAP (Parrish *et al.*, 2006). Other factors also bring fault, such as the fact that only isolated domains of proteins, and not the full length are used for bait and prey, which could cause false negatives (Daulat *et al.*, 2007). Testing mammalian proteins that usually succumb to post translation modifications is not possible in yeast and could miss interactions (Johnsson and Varshavsky, 1994). Finally, and quite simply, the technique is a lot more time consuming than TAP.

Conventional Y2H systems are not ideal for studying the interaction of membrane bound proteins since they rely on transcription factor activation and must therefore be performed in the nucleus. Previously this has been circumvented by studying the interaction of a portion of the membrane protein that is not embedded in the membrane, such as its N- or C- terminus, that can be relocalised to the nucleus. Such studies may not accurately reflect the situation in living cells because the conformation of the protein may be altered and interactions with other membrane proteins may be missed in the nucleus. Several variations on the Y2H strategy have been developed to overcome these problems including the Ras recruitment system and the Cytotrap assay. However a particularly efficient variation that overcomes

these difficulties is the split ubiquitin MbY2H assay. This is based on split-ubiquitin technique (Johnsson and Varshavsky, 1994) in which the reassociation of N- and C-terminal halves of ubiquitin allows the release of reporter gene(s). This system allows the screening of both full-length integral membrane and membrane-associated proteins, the interactions occur in their natural environment and post-translational modifications such as glycosylation and disulphide bonds are preserved. Several different groups have successfully applied this technique to detect protein-protein interactions in a wide range of organisms (Thaminy *et al.*, 2003; Wang *et al.*, 2003; Wang *et al.*, 2004)

3.2 Aims

The aim of this section was to identify novel interacting partners of MC2R and MRAP, in order to unveil proteins potentially involved in the pathogenesis of FGD. To overcome the limitations of the yeast two hybrid system, the tandem affinity purification technique was employed to isolate interacting proteins. Before performing purification steps, TAP-tagged proteins of interest would be cloned and their functional expression validated. The double purification technique would be carried out on lysates from cultured H295R adrenocortical carcinoma cells (H295R) transfected with target genes, and purified complexes would be detected by mass spectrometry.

3.3 Results

3.3.1 Construction of TAP-tag vectors

For the purposes of this project I employed the Stratagene Interplay Mammalian TAP system in which target protein is fused to streptavidin binding peptide (SBP) and calmodulin binding peptide (CBP) tags. The SBP tag is a 38aa synthetic sequence obtained from a random peptide library with an affinity of ~2 x10^{-9}M for the streptavidin resin. The tag is eluted from the resin with biotin. The 26aa CBP tag is derived from the C-terminus of muscle myosin

light-chain kinase, and in the presence of calcium, has an affinity of ~$1x10^{-9}$M for the calmodulin resin. The tagged protein is eluted by removing calcium with a chelating agent. Unlike previous TAP methods, the Stratagene Interplay system does not require protease digestion to cleave tags for elution. Furthermore, the TAP expression vectors contain a human cytomegalovirus (CMV) promoter which drives the insert expression in most mammalian cell lines.

MC2R and MRAP were cloned both into the N-terminal (NTAP) and C-terminal (CTAP) TAP-tag vectors. For NTAP the SBP and CBP tags were 5' to the gene and for CTAP 3' to the gene (Fig. 3.3A-B). As described in section 2.4.1, cDNA protein coding regions for *MC2R* and *MRAP* were amplified from pcDNA3.1+ and p3xFLAG-CMV14-vectors containing the genes previously constructed in our laboratory, with primers containing *Bam*H1 and *Eco*R1 restriction sites (Fig 3.3C). Purified PCR fragments were digested with *Bam*H1 and *Eco*R1, and ligated into the vectors, then transformed into bacterial cells for amplification. Clones positive for the TAP vector were selected with 50µg/ml kanamycin, and extracted plasmid DNA was digested with *Bam*H1 and *Eco*R1 to check for the release of the insert (Fig. 3.3D). Plasmid DNA from selected clones expressing the insert was sequenced using T3 and T7 sequencing primers to confirm the insert was in frame and had no sequence anomalies. More details are found in section 2.4.1.

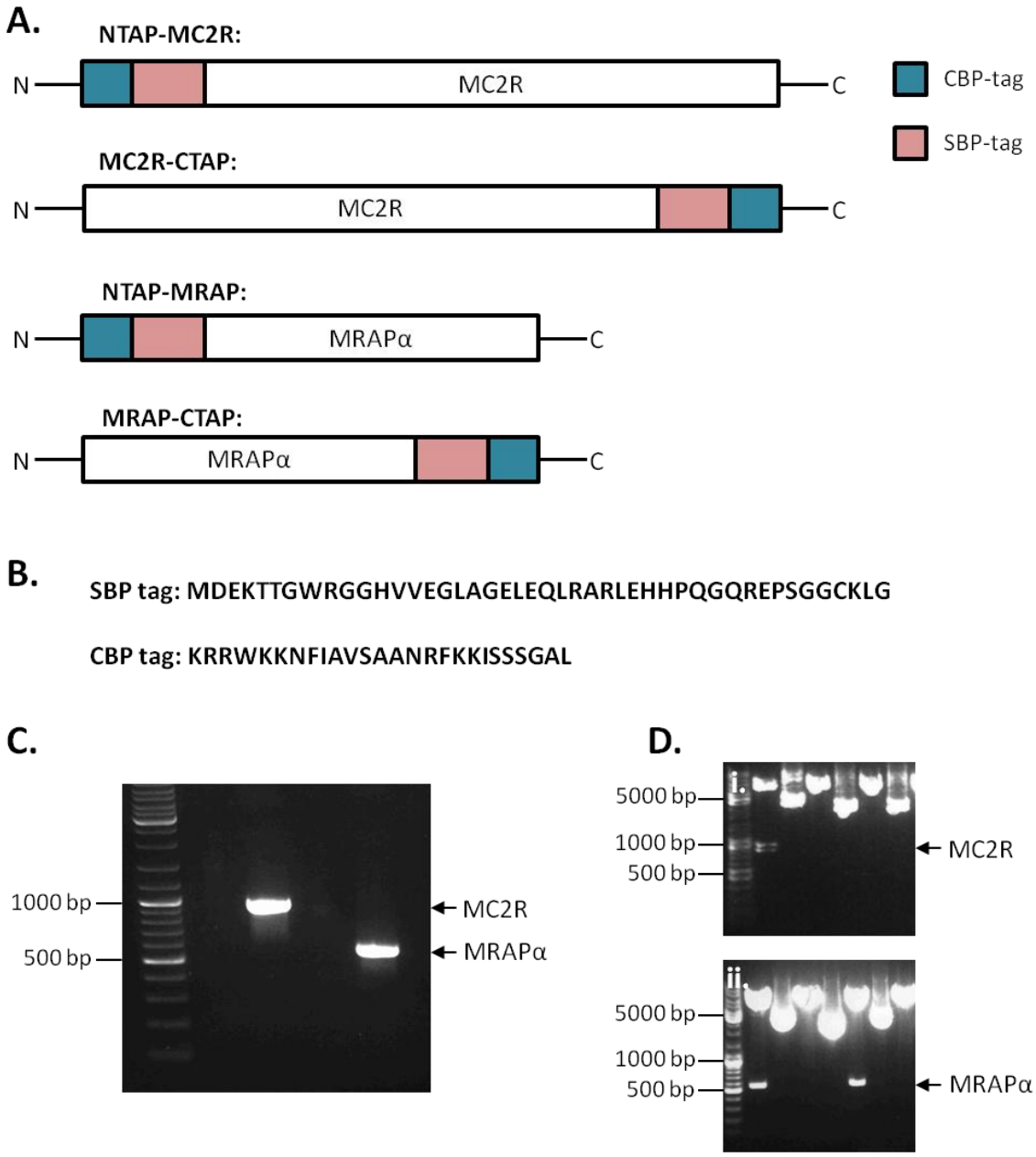

Figure 3. 3 Cloning TAP-Tag constructs

A. Schematic diagram of MC2R and MRAP TAP-tag constructs. The TAP-tag, consisting of streptavidin binding peptide and calmodulin binding peptide, was 5' in NTAP constructs and 3' in CTAP constructs. *MC2R* and *MRAP* were cloned into vectors through conventional cloning strategies. B. Amino acid sequences for SBP and CBP tags, 38 and 26 residues in length respectively. C. PCR amplification of *MC2R* and *MRAP* cDNA from pcDNA3.1+–MC2R and MRAP-FLAG constructs. D. Restriction digests of plasmid DNA extracted from transformed clones, screening for release of MC2R (i.) or

MRAP (ii.) insert from the CTAP vector. Image representative for CTAP and NTAP clones.

3.3.2 Validation of TAP-tag vectors

3.3.2.1 Expression levels

To determine protein expression of NTAP and CTAP tagged MC2R and MRAP, constructs were transiently transfected into HEK293 cells seeded in 6-well plates and grown for 24 hours, then lysed for protein extraction. In adjacent wells, empty CTAP vector was transfected as a negative control and NTAP-MEF2 (myocyte enhancer factor-2) as a positive control for protein detection. Cell lysates were subjected to Western blot analysis detecting TAP-tagged proteins using a calmodulin binding peptide antibody (anti-CBP) at a dilution of 1:500 (Millipore).

Endogenous MRAPα has a predicted MW of 19kDa. It has previously been demonstrated that C-terminal tagged MRAP-FLAG, with a predicted MW of 24kDa, migrates as several bands between 16-32kDa on SDS-PAGE (Webb *et al.*, 2009). These bands are thought to be products of glycosylation, post-translation modifications and/or cleavage products. Indeed MRAP has one glycosylation site situated at the N-terminus (Sebag and Hinkle, 2007). MC2R has a predicted MW of 33kDa but has previously been shown to migrate as a smear (Webb *et al.*, 2009). The NTAP affinity tag will add 8kDa so the expected sizes of MC2R and MRAP constructs would be 41kDa and 27kDa respectively. The CTAP affinity tag will add 9kDa hence the expected sizes of MC2R and MRAP constructs would be 42kDa and 28kDa respectively.

In agreement with previous reports neither MC2R-NTAP nor -CTAP presented a clear banding pattern on Western blot but migrated as a smear, typical of many GPCRs (Fig. 3.4A) (Webb *et al.*, 2009). Similarly MRAP-CTAP showed a banding pattern consistent with Webb *et al.*, whereby several protein species are resolved believed to be post-translationally modified possibly by glycosylation. In contrast the N-terminal tagged NTAP-MRAP presented a distinct single band at the predicted size of the monomer (approx. 27kDa) (Fig.

3.4A). It is therefore possible the N-terminal tag in NTAP-MRAP interferes with post-translational modifications.

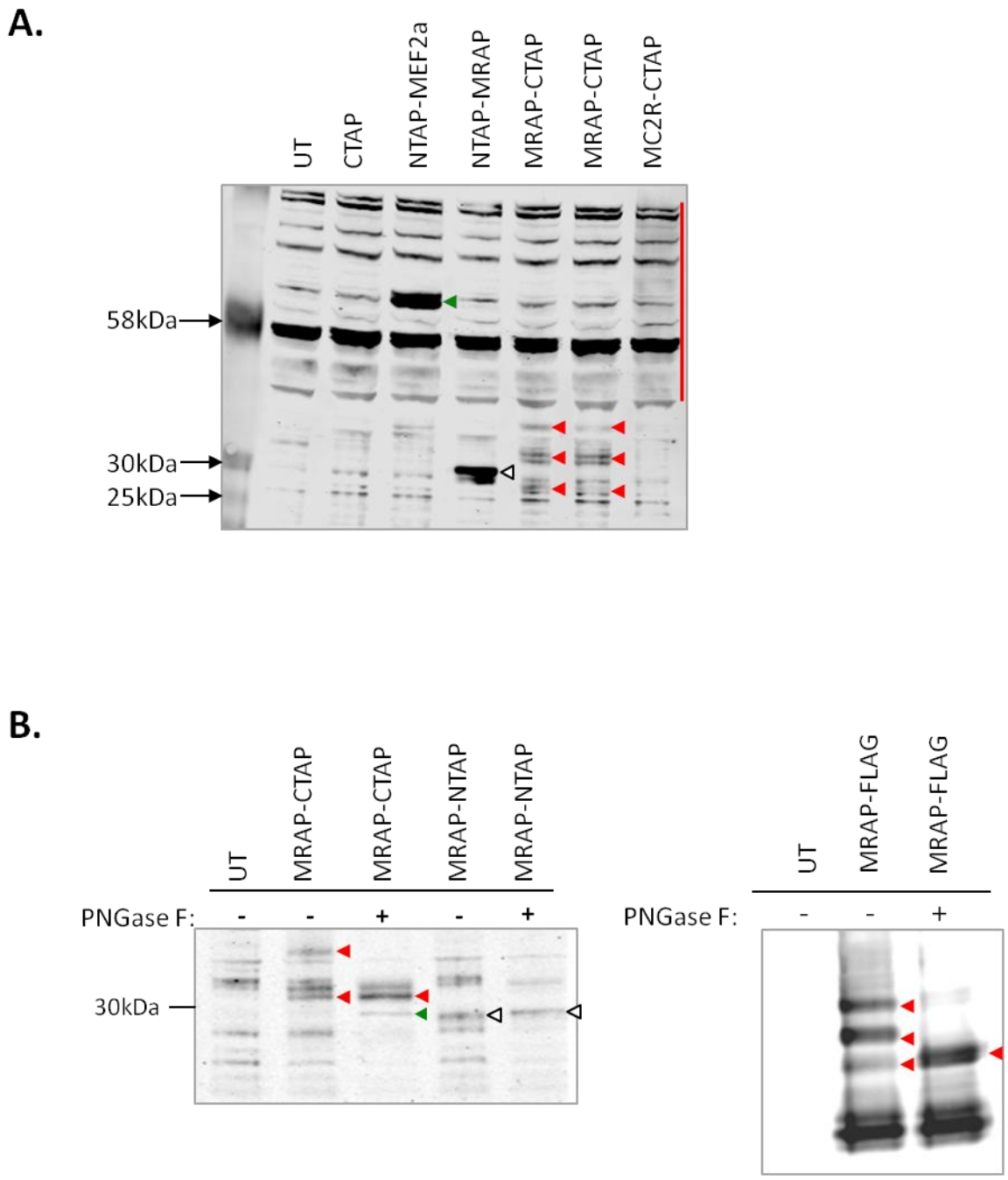

Figure 3. 4: Validating protein expression of TAP-tag vectors:

(A) Western blot showing expression of transfected TAP-tag constructs in HEK293 cells, blotting with anti-CBP antibody. MC2R-CTAP (representative for NTAP-MC2R) migrates as a smear (*Vertical bar*). NTAP-MRAP migrates as one 27kDa band (*white*

arrow head) **whereas MRAP-CTAP migrates as three species (*red arrow heads*). NTAP-MEF2a was used as a positive control, detected at 62kDa (*green arrow head*). Unlabelled bands are non-specific. (B) Western blot analysis of transfected cells treated with PNGaseF to remove glycosylation. Left panel shows treatment of MRAP-CTAP transfected cells with PNGaseF resulted in the addition of a lower molecular weight band *(green arrow head)* and the removal of the higher MW band, suggesting removal of glycosylation (*red arrow heads* represent higher MW bands). Treatment of NTAP-MRAP transfected cells with PNGaseF did not change the size of the protein suggesting it had no post-translational modification (*white arrows heads)*. MRAP-FLAG was subjected to equivalent treatment as a positive control (right panel) where the two higher MW, glycosylated species disappear on PNGaseF treatment *(red arrow heads* represent MRAP-FLAG*).***

To determine whether MRAP-CTAP and NTAP-MRAP were glycosylated, HEK293 cells were transfected with one or the other construct and lysates were digested with Peptide-N-Glycosidase F (PNGaseF) or left untreated (Fig. 3.4B left panel). PNGaseF is an endoglycosidase that cleaves N-terminal linked oligosaccharides, removing glycosylation. As a positive control, a subset of cells were transfected with MRAP-FLAG, an N-terminally tagged construct which is known to be glycosylated, and lysates treated similarly (Fig. 3.4B right panel). The MW of MRAP recombinant proteins was determined by Western blot analysis, running lysates on a 4-12% SDS-PAGE gel and detecting with anti-CBP antibody. As a negative control, lysates from untransfected cells were run in parallel.

Figure 3.4B shows that treatment with PNGaseF resulted in a reduction in the intensity of the highest molecular mass band believed to be MRAP-CTAP and the addition of a lower molecular weight band, suggesting that MRAP-CTAP is glycosylated. The molecular weight of NTAP-MRAP did not decrease following PNGaseF treatment, consistent with the theory that the TAP-tag had hindered post-translational glycosylation of NTAP-MRAP.

The above experiments suggest both NTAP-MRAP and MRAP-CTAP constructs express proteins at the correct predicted MW, but the N-terminal tag may interfere with glycosylation. The expression of MC2R in both NTAP (not shown) and CTAP vectors was not clearly detected by Western blot, a common issue encountered when immunoblotting GPCRs, however, other methods such as immunocytology and activity assays can be used to determine their expression and functionality as detailed below.

3.3.2.2 Subcellular localisation

In order to check TAP-tagged MC2R was expressed at the cell surface, NTAP-MC2R or MC2R-CTAP constructs were co-transfected with MRAP-FLAG into HEK293 cells and analysed by immunocytochemistry. MRAP-FLAG was previously constructed in our laboratory by directional cloning of MRAPα cDNA into the *Hin*dIII and *Eco*R1 restriction sites of the p3xFLAGCMV-14 expression vector (Sigma, Poole, UK) (Chan *et al.*, 2009b). HEK293 cells have no endogenous MC2R or MRAP but have been shown to express all the other proteins required for a fully functional MC2R (Rached et al., 2005). HEK293 cells were chosen over an adrenocortical cell line, such as H295R, as they are easier to transfect, achieving 80-90% transfection efficiency.

12 well plates containing coverslips were seeded with HEK293 cells and grown to 50% confluency, then transfected according to section 2.1.6.1 with either single constructs or co-transfected with MRAP and MC2R constructs in various combinations to assess protein function (Fig. 3.5). Cells were fixed and either permeabilised by the addition of Triton or untreated, then stained with anti-CBP, anti-FLAG, and fluorescently labelled secondary antibodies. Nuclei were stained with DAPI, and coverslips were mounted to slides.

When transfected alone MRAP-TAP constructs were retained intracellularly (Fig. 3.5 B-C) similar to the localisation seen with the MRAP-FLAG construct previously investigated in our laboratory (Fig. 3.5A).

Co-transfection of HA-MC2R and MRAP-CTAP or HA-MC2R and NTAP-MRAP showed localisation of both proteins to the perinuclear region and cell surface in permeabilised cells (Fig. 3.5F) (NTAP-MRAP not shown) with good cell surface expression of MC2R in unpermeabilised cells (D-E), suggesting both MRAP-TAP constructs were capable of trafficking MC2R to the cell surface.

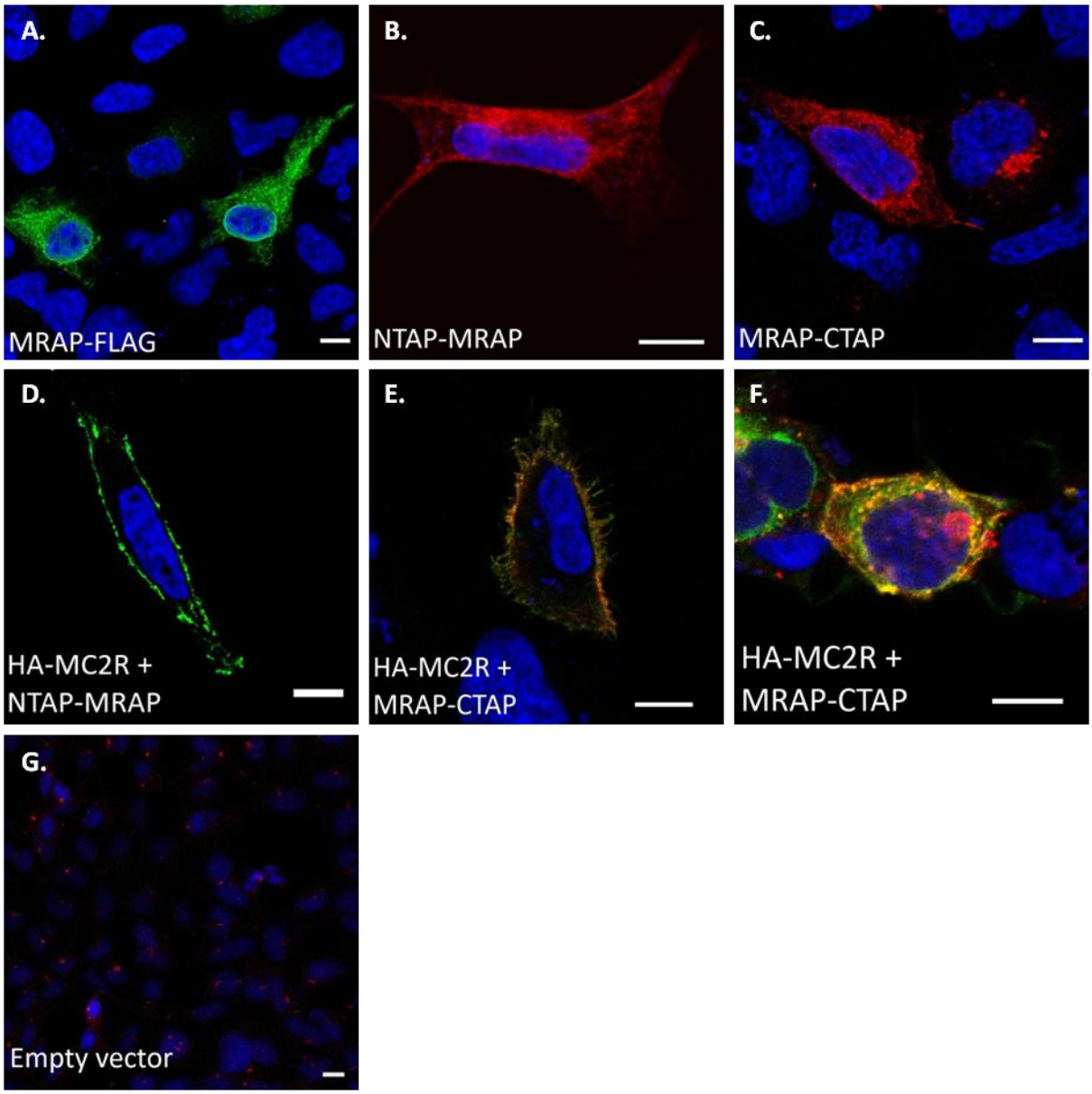

Figure 3. 5: Subcellular localisation of TAP-tagged MRAP proteins.

Subcellular localisation was determined by immunofluorescent staining of HEK293 cells transfected with MRAP-FLAG (A), NTAP-MRAP (B), MRAP-CTAP (C), HA-MC2R in

combination with NTAP-MRAP (non-permeabilised) (D), HA-MC2R in combination with MRAP-CTAP (non-permeabilised) (E), HA-MC2R in combination with MRAP-CTAP (permeabilised) (F) or empty vector alone (G). Cells were fixed, permeabilised (unless stated), and stained with anti-HA, anti-FLAG or anti-CBP antibodies and viewed by confocal microscopy. NTAP-MRAP (B) and MRAP-CTAP (C) had similar subcellular localisation to MRAP-FLAG (A) when transfected alone. In non-permeabilised cells, HA-MC2R (*green*) localised to the cell surface when cotransfected with NTAP-MRAP (D) or MRAP-CTAP (*red*) (E). In permeabilised cells, proteins colocalised to the cell surface and perinuclear area (F), (representative of HA-MC2R + NTAP-MRAP). CBP antibody staining of cells transfected with empty TAP-tag vectors were used as negative controls (F).

MC2R-TAP constructs were also retained intracellularly when transfected alone, similar to the localisation seen with the HA-MC2R construct previously investigated in our laboratory (Fig. 3.6A).

Co-transfection of NTAP-MC2R with MRAP-FLAG saw a substantial amount of the NTAP-MC2R pool shift to the cell surface, the rest remaining intracellularly in a pattern consistent with endoplasmic reticulum staining, however markers were not used (Fig. 3.6D). These data suggest that NTAP-MC2R is capable of trafficking to the cell surface without interference from the double tag.

When MC2R-CTAP was cotransfected with MRAP-FLAG, it was expressed intracellularly, but cell surface expression was not apparent (Fig. 3.6E). This could be because the C-terminus of MC2R and hence the tag itself is intracellular.

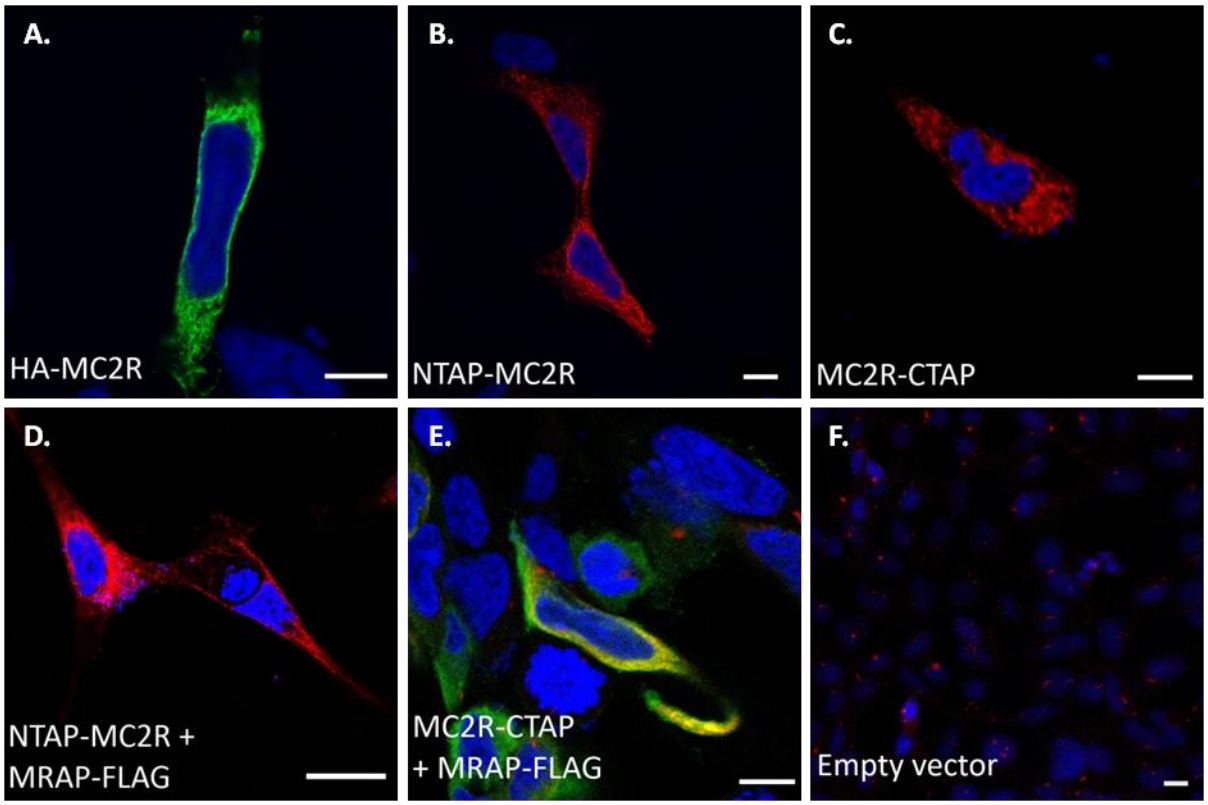

Figure 3. 6: Subcellular localisation of TAP-tagged MC2R proteins.

Subcellular localisation was determined by immunofluorescent staining of HEK293 cells transfected with HA-MC2R (A), NTAP-MC2R (B), MC2R-CTAP (C), NTAP-MC2R with MRAP-FLAG (D), MC2R-CTAP with MRAP-FLAG (E) or empty vector alone (F). Cells were fixed, permeabilised (unless stated), and stained with anti-HA, anti-FLAG or anti-CBP antibodies and viewed by confocal microscopy. NTAP-MC2R (B) and MC2R-CTAP (C) had similar subcellular localisation to HA-MC2R (A) when transfected alone. When co-transfected with MRAP-FLAG, NTAP-MC2R was localised to the cell surface and perinuclear area (D), whereas MC2R-CTAP in combination with MRAP-FLAG was detected intracellularly (E). CBP antibody staining or cells transfected with empty TAP-tag vectors were used as negative controls (F).

These data confirms that NTAP-MC2R and MC2R-CTAP constructs express the protein, which had not been clearly detected by Western blot. Overall the localisation of TAP-tag

proteins mirror that of HA-MC2R and MRAP-FLAG proteins, used in previous studies (Chan *et al.*, 2009b; Metherell *et al.*, 2005; Webb *et al.*, 2009) which suggests that the proteins are localising correctly. However, it was unclear whether MC2R-CTAP was able to reach the cell surface when co-transfected with MRAP-FLAG. I further investigated the functionality of these proteins in the following section.

3.3.2.3 Functional cell surface expression and ACTH Response

Functional studies into MC2R and MRAP function suggest that MRAP interacts with MC2R through its TMD, and a 15aa tyrosine rich region in the N-terminus of MRAP can influence MC2R trafficking. This region has been suggested to either play a role in stabilising the MRAP/MC2R interaction or interact with another protein that regulates MRAP/MC2R cell surface expression (Webb *et al.*, 2009). Increasing the length of the C-terminus of MRAP reduces the amount of MC2R that reaches the cell surface and hence the ACTH responsiveness of the cells. Therefore, it was necessary to check whether the presence of the 9kDa TAP-tag added to MRAP and MC2R would influence the ACTH responsiveness of the receptor.

As previously described, when ACTH binds to and activates MC2R, a series of downstream signalling events occur including the generation of cAMP, which through a number of routes, stimulates the induction of cortisol genesis. cAMP activates PKA, which phosphorylates and activates StAR protein in the acute phase of ACTH stimulation. In the later stages of ACTH stimulation cAMP also activates the transcriptional upregulation of steroidogenic genes through binding to cAMP response element binding proteins (CREB).

To measure ACTH responsiveness of cells transfected with NTAP or CTAP-tagged MC2R and MRAP, a dual reporter cAMP luciferase assay was employed, which is described in detail in section 2.7.2. HEK293 cells containing no endogenous MC2R or MRAP were seeded in 6 well plates and grown for 24h. As a positive control, HA-MC2R and MRAP-

FLAG vectors were used, which when co-transfected have previously been demonstrated to elicit a cAMP response (Chung *et al.*, 2008; Webb *et al.*, 2009).

To test the functionality of NTAP-MC2R (Fig. 3.7A) cells were cotransfected with NTAP-MC2R and either MRAP-FLAG, NTAP-MRAP or for a negative control empty vector. In all wells, equal concentration of α-GSU and Renilla were transfected. 48h after transfection, cells were stimulated with doses of ACTH ranging from 10^{-6} to 10^{-11}M in order to create dose response curves. Cells were stimulated for 6h, then lysed and the luminescence was read on a luminometer in duplicate. The experiment was duplicated with CTAP constructs (Fig. 3.7B).

Dose response curves were generated and EC_{50} measurements for each transfection using Prism (Prism Software Corp.). The EC_{50} or the half maximal effective concentration is defined as the concentration of ACTH when 50% of its maximal effect is observed.

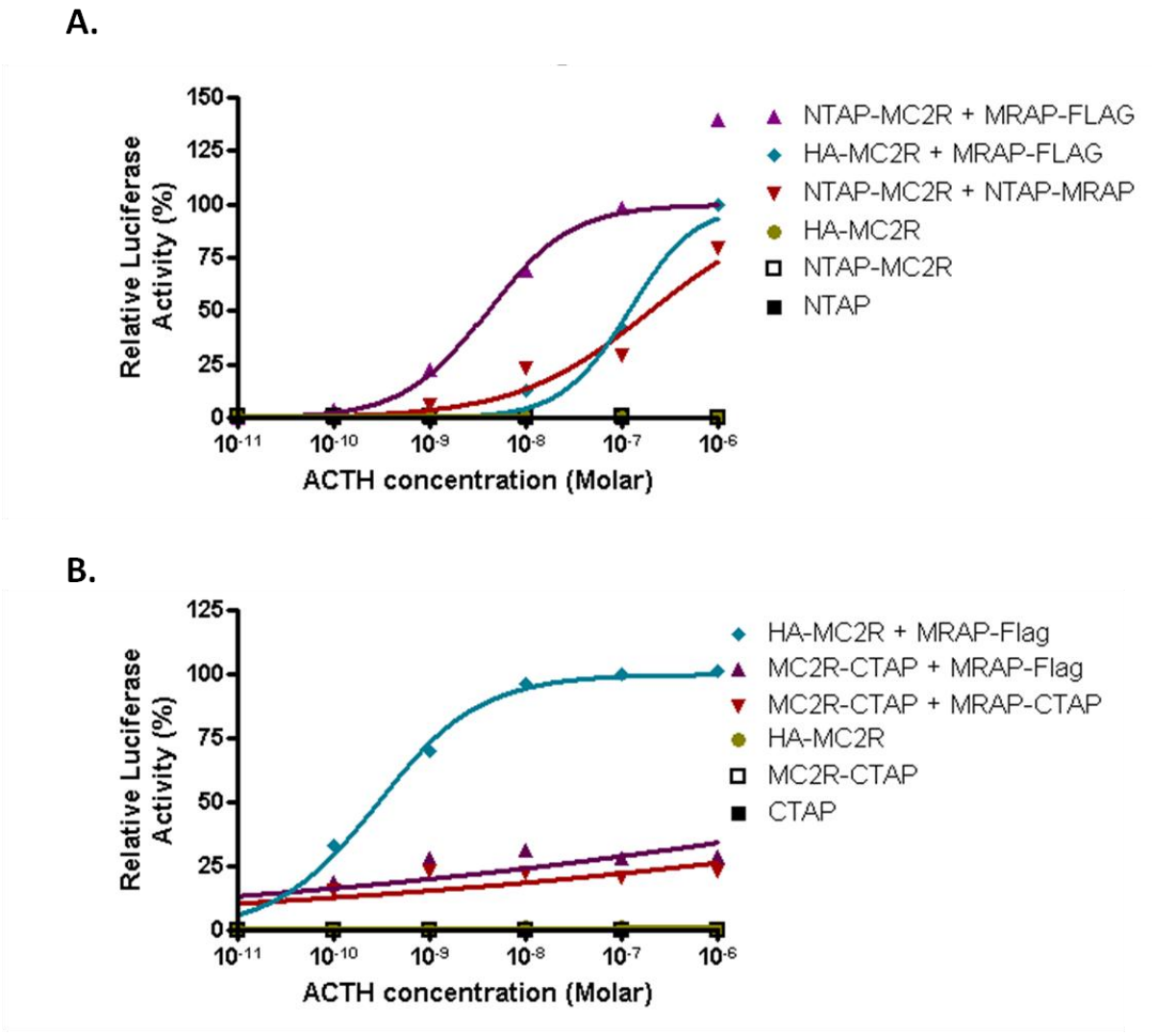

Figure 3. 7: TAP-tag constructs express functional proteins.

Graph showing dose response curves for TAP-tagged MC2R and MRAP normalised to 100% HA-MC2R and MRAP-FLAG. HEK293 cells were transfected with MC2R-NTAP/CTAP in combination with MRAP-FLAG, NTAP-MRAP/CTAP or empty vector and reciprocally MRAP-CTAP was also transfected with HA-MC2R. All cells were co-transfected with α-GSU and Renilla, and stimulated with ACTH (1-39) for 6h. As negative controls, single construct or empty vectors were transfected alone. Luciferase activity was assessed as the relative light units (RLU) of reporter α-GSU Firefly luciferase relative to internal control Renilla. Both NTAP- (A) and -CTAP (B) MC2R and MRAP proteins elicited a cAMP response that was ACTH dose dependent,

indicating the constructs expressed functional proteins that were able to interact, traffic to the cell surface and signal.

The cAMP response elicited by co-transfecting NTAP-MC2R with NTAP-MRAP (EC_{50} 1.98 x 10^{-7}M) was similar to that of HA-MC2R and MRAP-FLAG (EC_{50} 1.17 x 10^{-7}M), suggesting NTAP-MRAP is able to bind and traffic NTAP-MC2R to the cell surface and facilitate its response to ACTH (Fig. 3.7A). In cells co-transfected with NTAP-MC2R with MRAP-FLAG there was a higher cAMP response and the dose response curve shifted to the left (EC_{50} 4.00 x 10^{-9}M).

Similarly, co-transfection of MC2R-CTAP and MRAP-CTAP also elicited a cAMP response curve compared to negative controls (Fig. 3.7B). However, cAMP response was reduced by addition of the CTAP tag. The combination of HA-MC2R and MRAP-FLAG produced the highest cAMP response (EC_{50} 2.97 x 10^{-10}M), followed by MC2R-CTAP and MRAP-FLAG (EC_{50} 4.81 x 10^{-4}M) and MC2R-CTAP and MRAP-CTAP elicited the lowest response (EC_{50} 3.98 x 10^{-2}M).

These data suggest that both MC2R and MRAP are hindered by the CTAP-tag, to a greater degree than NTAP. As mentioned above, the increased length of the C-terminus of MRAP can decrease cell surface expression, and hence an extra length of the CTAP tag may have this effect. For MC2R, the extension of the C-terminus has been reported to have differing effects, for example, Fridmanis et al. (2010) found fusion of eGFP to the C-terminus decreased receptor activity, whereas Noon et al. (2002) found no effect.

To summarise, in cells co-transfected with TAP-tag MC2R and MRAP, ACTH stimulated a cAMP response in a concentration dependent manner, suggesting the proteins are functional. Based on these data, tandem affinity purification was attempted with these constructs.

3.3.3 Tandem Affinity Purification

After verifying that NTAP- and -CTAP constructs expressed functional proteins, the constructs were used to express target proteins for tandem affinity purification.

Constructs were transfected in both HEK293 cells, detailed above, and also H295R human adrenocortical cells, as I hypothesized that some interacting partners of MC2R/MRAP might be adrenal specific like MC2R.

For both cell lines, cells were seeded at a density of $1x10^8$ cells and transfected with either NTAP-MC2R, NTAP-MRAP or empty NTAP vector as a negative control. After 48h lysates were collected and subjected to the double purification steps detailed in section 2.5.9. Briefly, lysates were incubated with beads coated in a streptavidin resin overnight, then washed and eluted and transferred to beads coated in calmodulin resin and incubated a further 24h. The purified lysate bound to the calmodulin resin was washed and then detached from the beads with Laemmli buffer containing β-ME and SDS. The experiment was repeated with CTAP constructs.

The efficiency of purification was analysed by Western blot, using aliquots taken from each step of the purification process. The transfection efficiency for H295R cells is relatively low, and this is reflected in the poor detection of NTAP-MC2R/MRAP in transfected H295R cells with anti-CBP antibody (Fig. 3.8Ai). Similarly, the CTAP proteins were not detected in transfected H295R lysates (Fig. 3.8Bi).

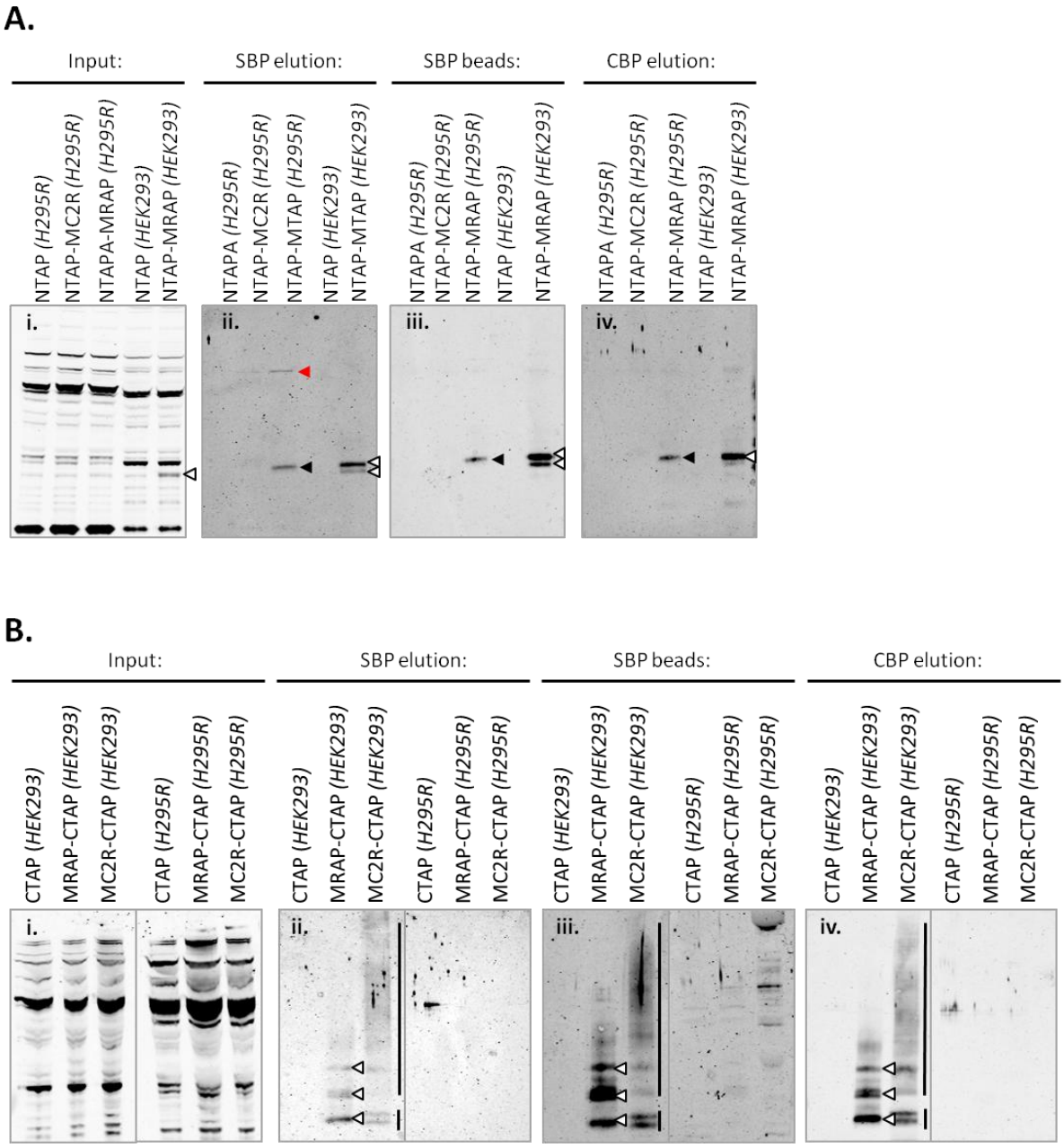

Figure 3. 8: Tandem Affinity Purification of MC2R and MRAP

Proteins captured by TAP from HEK293 and H295R cells transfected with (A) empty NTAP vector, NTAP-MRAP or NTAP-MC2R, or (B) empty CTAP vector, MRAP-CTAP or MC2R-CTAP. Images show Western blot analysis of lysates from protein inputs (i), proteins eluted from streptavidin beads (ii), proteins remaining on the streptavidin beads after elution (iii), and proteins detached from calmodulin beads after elution with Laemmli buffer (iv), immunoblotted with CBP antibody. NTAP-MRAP was detected in both HEK293 (*white* arrows) and H295R lysates (*black* arrows)

following affinity purification (Aiv). An additional higher molecular weight band (*red* arrow) was observed in HEK293 lysates following the first purification step (Aii). MRAP-CTAP and MC2R-CTAP were detected in HEK293 lysates following purification (*white arrows* depict MRAP-CTAP, *black lines* depict MC2R-CTAP), but not in H295R lysates (Biv). Failure to detect MRAP-CTAP or MC2R-CTAP in H295Rs could be due to low expression levels. A considerable amount of protein was left on streptavidin beads following the first purification step which could decrease total yield (Aiii & Biii).

In HEK293 cells, NTAP-MRAP was readily detectable at 27kDa from input lysates (Fig. 3.8Ai *white arrow*), but the anti-CBP antibody detected a lot of background from nonspecific proteins. MRAP-CTAP was not detected in HEK293 inputs due to high background and possibly low expression levels (Fig. 3.8Bi).

Following elution from streptavidin resin, immunoblotting with anti-CBP antibody showed the first purification step had eradicated most non-specific bands. In HEK293 cells, NTAP-MRAP was detected as a doublet (Fig. 3.8Aii *white arrows*) after this first elution and MRAP-CTAP as three species (Fig. 3.8Bii *white arrows*) confirming our findings in section 3.3.2. As previously mentioned, MRAP has previously been demonstrated to migrate as multiple species, which have described to be products of glycosylation, post-translational modifications and/or cleavage products (Metherell *et al.*, 2005; Webb *et al.*, 2009).

In H295R cells, NTAP-MRAP was not detected from input lysates using anti-CBP, only after purification with the streptavidin resin, which revealed a 27kDa band (Fig. 3.8Aii *black arrow*) and a slower migrating band (Fig. 3.8 Aii *red arrow*), possibly the SDS resistant homodimer previously described (Cooray *et al.*, 2008). MRAP-CTAP was not detected in H295R lysates after this purification step (Fig. 3.8Bii).

Western blot analysis of streptavidin coated beads resuspended in Laemmli buffer showed that a lot of protein remained on the beads following the elution step, suggesting some inefficiency in the protocol/purification process (Fig. 3.8Aiii and Biii *white arrows*).

Following purification with calmodulin resin, Western blot analysis showed the higher molecular weight species of NTAP-MRAP in H295R cells was absent, suggesting the band was not specific to MRAP (Fig. 3.8Aiv). The lighter species of the doublet in HEK293 cells was also absent and hence may also have been non-specific (Fig. 3.8Aiv). The other possibility is that the washes were too stringent, removing interactors.

NTAP-MC2R was not detected with anti-CBP antibody for either cell line after two-step TAP (Fig. 3.8Aiv). It is well documented that GPCRs do not form a clear banding pattern, and often migrate as a smear (Webb *et al.*, 2009). However, one would expect to see a banding pattern after double purification, as seen for MC2R-CTAP in HEK293 cells (Fig. 3.8Biv *black lines*). Furthermore, after 2-step purification, neither MC2R-CTAP nor MRAP-CTAP was detected in H295R lysates using anti-CBP antibody (Fig. 3.8Biv).

All lysates from transfected H295R cells were run on 4-12% SDS-PAGE in parallel with lysates from cells transfected with empty vectors. The gel was then fixed and stained with Coomassie blue to make proteins visible. The resultant banding patterns were compared to select protein bands to send for mass spectrometric (MS) analysis (Fig. 3.9A). For gel A the NTAP vector lane and NTAP-MC2R lanes showed very similar banding patterns in keeping with the suspicion that the NTAP-MC2R purification had failed. For this reason no bands were sent for analysis from NTAP-MC2R. Bands EM1_1, EM1_2, EM1_3 and EM1_4 from the NTAP-MRAP purification, that differed from the vector alone lane, were submitted for MS. For gel B bands EM2_1, EM2_2, EM2_3, EM2_7, EM2_8, EM2_9, EM2_10 that differed from the control lane were submitted for MS (Fig. 3.9B). We speculated that bands EM2_7, EM2_8 and EM2_9 might harbour MRAP. Bands EM2_4, EM2_5 and EM2_6, that presented similar banding patterns across all three lanes, were also sent for MS in the anticipation of finding MC2R somewhere within the smears for EM2_5 and EM2_6 with the expectation it would be absent in EM2_4.

For detection of interacting partners, gel slices were digested and analysed by mass spectrometry which was carried out by the KCL proteomics facility (detailed methodology section 2.5.10). The full list of proteins detected from bands labelled in figure 3.9 is shown in table 3.1.

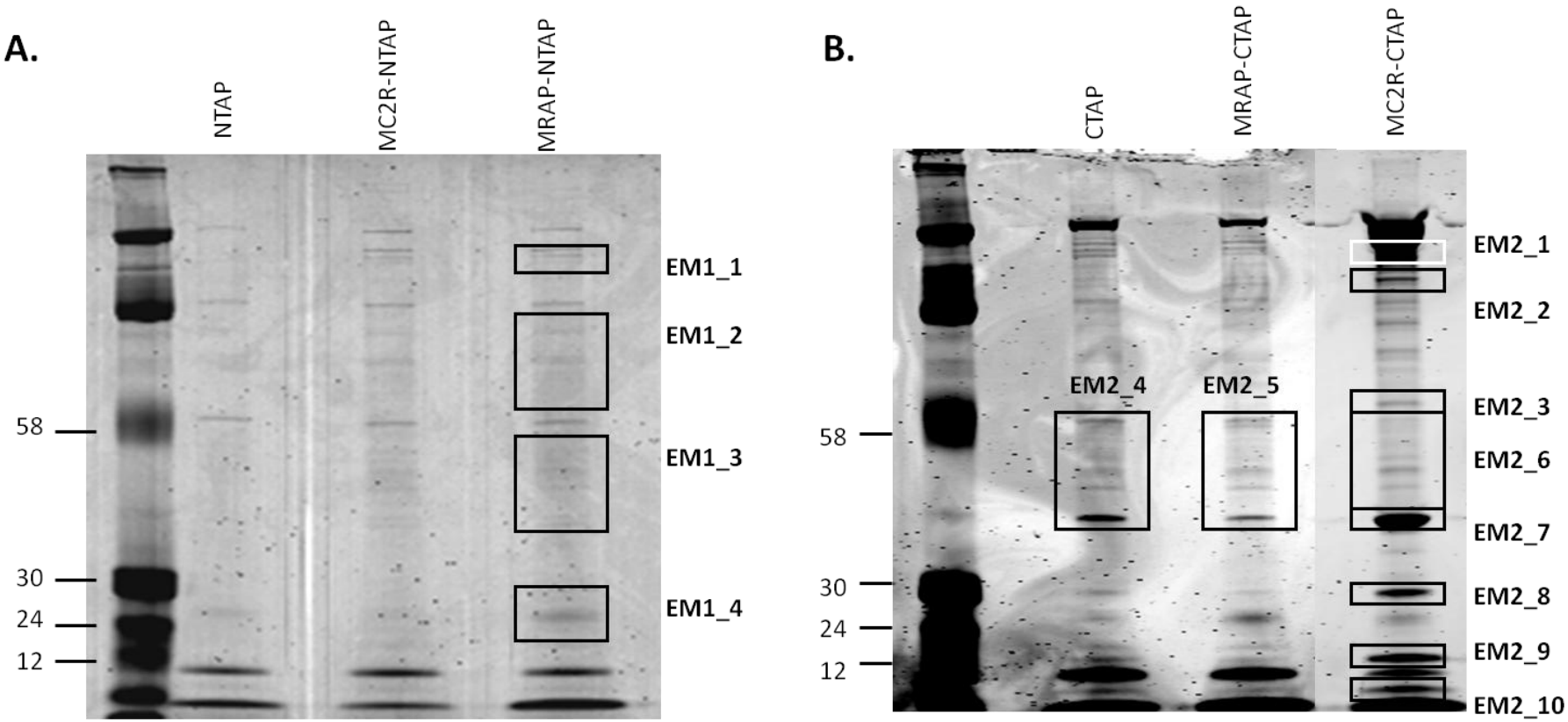
A.
NTAP
MC2R-NTAP
MRAP-NTAP
58
30
24
12
EM1_1
EM1_2
EM1_3
EM1_4
B.
CTAP
MRAP-CTAP
MC2R-CTAP
58
30
24
12
EM2_4
EM2_5
EM2_1
EM2_2
EM2_3
EM2_6
EM2_7
EM2_8
EM2_9
EM2_10

Figure 3. 9: Coomassie blue staining of affinity purified lysates

Affinity purified protein complexes from H295R cells transfected with either empty vector, MC2R or MRAP flanked by N-terminal (A) or C-terminal (B) TAP-tag were separated on a 4-12% 1D SDS-PAGE and detected by Coomassie Blue staining of the gel. Purified extracts from cells transfected with empty TAP-tag vector were ran in parallel as a negative control. Bands that were present in either MC2R or MRAP lanes but absent from the empty vector purification were considered for LC/MS/ analysis. The bands labelled were excised for digestion and LC/MS/MS analysis.

3.3.4 Identification of interacting partners by mass spectrometry

Band ID.	Protein I.D.	Species	Uni-prot Access. No.	MW (Da)	pI	No. Pep.	No. Uniq.	% Cov.
EM1_1	Serum albumin	Bovine	P02769	69248	5.82	4	2	4%
	GTPase-activating-like protein IQGAP2	Human	Q13576	180465	5.47	8	1	1%
	GTPase-activating-like protein IQGAP1	Human	P46940	189134	6.08	7	1	1%
	Ig kappa chain C region	Human	P01834	11602	5.58	2	1	13%
	Lysozyme C	Human	P61626	16526	9.38	2	1	8%
EM1_2	Serum albumin	Bovine	P02769	69248	5.82	9	4	8%
	Heat shock protein HSP 90-beta	Human	Q4R4T5	83185	4.97	7	3	6%
EM1_3	60kDa heat shock protein,	Human	P10809	61016	5.7	3	2	4%

	mitochondrial							
	Tryptophanase	*E.coli*	P0A853	52740	5.88	3	2	5%
	NADPH: adrenodoxin oxidoreductase, mitochondrial	Human	P22570	53803	8.72	3	2	4%
EM1_4	Serum albumin	Bovine	P02769	69248	5.82	7	6	12%
	Purine nucleoside phosphorylase deoD-type	*E.coli*	Q0T8S9	25919	5.42	4	2	10%
	Streptavidin	*S.avidini*	P22629	18822	7.93	2	2	16%
EM2_1	Myosin-9	Human	P35579	226392	5.5	221	102	45%
	Myosin-10	Human	P35580	228858	5.44	63	26	20%
	Clathrin heavy chain 1	Human	Q00610	191493	5.48	10	8	8%
	Myosin-14	Human	Q7Z406	227863	5.76	14	4	3%
	Ras GTPase-activating-like protein IQGAP1	Human	P46940	189134	6.08	2	1	2%
EM2_2	Myosin-9	Human	P35579	226392	5.5	31	19	14%
	Myosin-10	Human	P35580	228858	5.44	7	4	4%
	LIM and calponin homology domains-containing protein 1	Human	Q9UPQ0	121762	6.1	2	2	2%
	Protein AMBP	Human	P02760	38974	5.95	1	1	7%
EM2_3	Myosin-9	Human	P35579	226392	5.5	15	10	8%
	Myosin-10	Human	P35580	228858	5.44	3	2	2%

	Protein AMBP	Human	P02760	38974	5.95	3	1	7%
EM2_4	*60 kDa heat shock protein, mitochondrial*	*Human*	*P10809*	*61016*	*5.7*	*12*	*8*	*23%*
	Tubulin alpha-1B chain	*Human*	*P68363*	*50120*	*4.94*	*3*	*2*	*8%*
	Actin, cytoplasmic 2	*Human*	*P63261*	*41766*	*5.31*	*3*	*1*	*9%*
	Actin, cytoplasmic 1	*Human*	*P60709*	*41710*	*5.29*	*3*	*1*	*5%*
	Tubulin beta chain	*Human*	*P07437*	*49639*	*4.78*	*3*	*1*	*3%*
	Putative elongation factor 1-alpha-like 3	*Human*	*Q5VTE0*	*50153*	*9.15*	*2*	*1*	*2%*
	Protein AMBP	*Human*	*P02760*	*38974*	*5.95*	*2*	*1*	*7%*
	Vimentin	*Human*	*P08670*	*53619*	*5.06*	*2*	*1*	*3%*
	Pyruvate kinase isozymes M1/M2	*Human*	*P14618*	*57900*	*7.96*	*1*	*1*	*3%*
EM2_5	*60 kDa heat shock protein, mitochondrial*	*Human*	*P10809*	*61016*	*5.7*	*17*	*8*	*21%*
	Tubulin alpha-1B chain	*Human*	*P68363*	*50120*	*4.94*	*4*	*3*	*12%*
	Tubulin beta chain	Human	P07437	49639	4.78	4	2	
	Vimentin	*Human*	*P08670*	*53619*	*5.06*	*6*	*1*	*3%*
	Pyruvate kinase isozymes M1/M2	*Human*	*P14618*	*57900*	*7.96*	*1*	*1*	*3%*
	Putative elongation factor 1-alpha-like 3	Human	Q5VTE0	50153	9.15	2	1	2%
	Methylcrotonyl-CoA carboxylase beta	Human	Q9HCC0	61294	7.57	1	1	3%

	chain, mitochondrial							
EM2_6	*Actin, cytoplasmic 1*	Human	P60709	41710	5.29	13	9	31%
	Myosin-9	Human	P35579	226392	5.5	10	6	5%
	Tubulin beta chain	Human	P07437	49639	4.78	5	5	17%
	Tubulin alpha-1B chain	*Human*	*P68363*	*50120*	*4.94*	*4*	*3*	*12%*
	Vimentin	*Human*	*P08670*	*53619*	*5.06*	*4*	*3*	
	Myosin-10	Human	P35580	228858	5.44	3	2	2%
	60 kDa heat shock protein, mitochondrial	Human	P10809	61016	5.7	2	1	4%
	Actin, cytoplasmic 2	Human	P63261	41766	5.31	13	1	5%
EM2_7	*Actin, cytoplasmic 1*	Human	P60709	41710	5.29	15	10	34%
EM2_8	*Actin, cytoplasmic 1*	Human	P60709	41710	5.29	7	6	25%
	Protein AMBP	Human	P02760	38974	5.95	3	1	7%
EM2_9	*Actin, cytoplasmic 1*	Human	P60709	41710	5.29	83	22	67%
	Tropomodulin-3	Human	Q9NYL9	39570	5.08	5	5	21%
	Myosin regulatory light chain 12B	Human	O14950	19767	4.71	6	3	34%
	Myosin-9	Human	P35579	226392	5.5	2	2	1%
	Protein AMBP	Human	P02760	38974	5.95	1	1	7%
EM2_10	Tropomyosin alpha-4 chain	Human	P67936	28504	4.67	45	23	79%
	Tropomyosin alpha-3 chain	Human	P06753	32799	4.68	36	8	25%
	Actin, cytoplasmic 1	Human	P60709	41710	5.29	5	4	16%
	Putative	Human	A6NL28	26253	4.47	8	3	20%

	tropomyosin alpha-3 chain-like protein							
	Myosin-9	Human	P35579	226392	5.5	2	2	2%
	40S ribosomal protein S3	Human	P23396	26671	9.68	4	1	11%
	THO complex subunit 4	Human	Q86V81	26872	11.2	1	1	7%

Table 3. 1: LC/MS/MS analysis of 1D SDS gel bands EM1_1 – EM2_10 from a transfected H295R cells

Rows highlighted in *grey* represent common false positives such as ribosomal proteins, heat shock proteins, cytoskeletal proteins or proteins that associate with the cytoskeleton. *Blue* represents proteins frequently pulled out since they are interactors with the affinity tags. In the species column non-human contaminants are represented by red shading. *Italicised* proteins represent those present in empty vector preparations. Parameters analysed were peak intensity (pI), molecular weight (MW), number of peptides aligned (No. pep.), the number of peptides unique to protein of interest (no. uniq.) and percentage coverage (% cov.)

Mass spectrometry identified heat shock proteins, ribosomal proteins and a large number of cytoskeletal proteins, often reported as false positives in TAP-tag studies, these are highlighted in grey in Table 3.1. Other proteins included those known to interact with the cytoskeleton, for example IQGAP1&2, tropomodulin-3, LIM and calponin homology domains-containing protein 1 and myosin which were also considered false positives.

Although it is likely MRAP and MC2R interact with cytoskeletal proteins during trafficking, it is unlikely these proteins are specific to MC2R function. Furthermore, it is through elimination of common false positives that putative candidate proteins can be identified. Proteins detected from band 2_4 (Fig. 3.9) containing empty vector lysates included cytoskeletal and heat shock proteins, as well as mitochondrial pyruvate kinase.

Protein I.D.	Uniprot Accession No.
60 kDa heat shock protein, mitochondrial	P10809
Tubulin alpha-1B chain	P68363
Actin, cytoplasmic 2	P63261
Actin, cytoplasmic 1	P60709
Tubulin beta chain	P07437
Putative elongation factor 1-alpha-like 3	Q5VTE0
Protein AMBP	P02760
Vimentin	P08670
Pyruvate kinase isozymes M1/M2	P14618

Table 3. 2: False positives isolated by TAP

Table listing proteins purified from cells transfected with empty TAP-tag vector. H295R cells transfected with empty vector alone were subjected to tandem affinity purification and MS analysis. Proteins purified from empty vector preparations included cytoskeletal proteins, proteins that interacted with calmodulin binding peptide (protein AMBP), and mitochondrial pyruvate kinase.

The bands EM2_5 and EM2_6 contained a similar list of proteins and crucially did not contain MC2R. Disappointingly MRAP was not identified in any of the MC2R-CTAP bands either. A list of proteins detected from lysates transfected with CTAP is shown in table 3.2. For the purposes of establishing potential candidate proteins, all cytoskeletal, heat shock and ribosomal proteins and proteins detected in EC 2_4 were filtered out. Proteins known to interact with CBP and SBP affinity tags were also eliminated, and finally any non-human contaminants were excluded.

A list of the remaining proteins identified and their known functions is shown in Table 3.3. Importantly this list did not include the expected reciprocal positive interactors MC2R and MRAP themselves. As a crucial validation of the system we would expect the MRAP

constructs to pull out MC2R and vice versa. I hypothesised that the candidate protein would be involved in the life cycle of MC2R, which could include folding, dimerisation, trafficking, docking or endocytosis. To ascertain if this was likely for the candidates listed I searched for their functions in online databases.

	Protein I.D.	Uniprot Accession No.	Function
MC2R-CTAP	Clathrin heavy chain 1	Q00610	Intracellular trafficking
	THO complex subunit 4	Q86V81	Nuclear chaperone
MRAP-CTAP	Methylcrotonyl-CoA carboxylase beta chain, mitochondrial	Q9HCC0	Leucine catabolism
NTAP-MRAP	Lysozyme C	P61626	Bacteriolysis
	NADPH:adrenodoxin oxidoreductase, mitochondrial	P22570	Electron transfer

Table 3. 3: Candidate proteins following elimination of common contaminants

MS data was filtered by eliminating common contaminants of TAP, and proteins that interacted with affinity tags, non human proteins, and proteins that were detected in lysates purified from cells transfected with empty vector.

3.4. Discussion

Proteomic techniques that reveal protein-protein interactions are important tools for understanding the organisation and mechanics of cellular processes. Genetic approaches that produce gene and protein lists do not always provide enough insight into how these processes are conducted or managed.

This chapter aimed to use a proteomic technique to uncover interacting partners of MC2R and MRAP, which when dysfunctional, may contribute to the pathogenesis of FGD. It was also important to increase our understanding of MC2R regulation, as until the discovery of MRAP it was not possible to express the fully functional receptor in heterologous cell lines. Other factors may exist that regulate MC2R lifecycle, and these may interact with MC2R or MRAP. We therefore hypothesised that MC2R and MRAP were two parts of a greater complex.

The tandem affinity purification (TAP) technique, followed by mass spectrometry (MS) was employed to uncover interacting partners because it offered several advantages over the traditional yeast two hybrid screen. TAP allows for purification of protein complexes under native conditions and cellular compartment, a consideration required when investigating transmembrane proteins (Puig *et al.*, 2001; Rigaut *et al.*, 1999; Xu *et al.*, 2010). It allows the full length protein to be expressed with post-translational modifications maintained, and has reduced background from contaminants compared to the Y2H (Daulat *et al.*, 2007; Xu *et al.*, 2010).

The Stratagene Interplay mammalian tandem affinity purification system is a commercial kit specifically developed to isolate interacting proteins from mammalian cells. The double tag includes a 38aa streptavidin binding peptide with a high affinity to streptavidin which is eluted with biotin, and a 26aa calmodulin binding peptide tag that binds to calmodulin in the presence of calcium and is eluted with a chelating agent such as EGTA. This system has been previous used to successfully isolate a number of proteins (Ahlstrom and Yu, 2009; Bradley *et al.*, 2007; Chiu *et al.*, 2006; Gallois-Montbrun *et al.*, 2007; Griffin *et al.*, 2007; Haag Breese *et al.*, 2006; Hentschke *et al.*, 2010; Juillard *et al.*, 2009; Li *et al.*, 2011; Medina-Palazon *et al.*, 2007; Park *et al.*, 2011; Wei *et al.*, 2007; Wiederschain *et al.*, 2007; Xie *et al.*, 2009). Compared to other TAP systems, its main advantage is the gentle elution conditions. Fusion proteins can be eluted with small molecules under mild conditions (Li, 2011) with no need to use protease cleavage enzymes to release protein complexes during the

first elution. Protease cleavage usually results in a significant loss of yield, therefore dispensing with this step is a clear advantage (Li, 2011).

MC2R and MRAP TAP-tag constructs were successfully cloned and expressed functional proteins, with correct subcellular localisation. Staining patterns mirrored that of previous studies, however a future consideration would be to use compartmental markers to confirm this data. The Western blot banding pattern of NTAP-MRAP differed to that previously published for MRAP-FLAG, presenting as one band compared to the 3 bands ranging from 16-32kDa observed when transfecting MRAP-FLAG into CHO cells (Webb *et al.*, 2009). In contrast, MRAP-CTAP shared a similar banding pattern to MRAP-FLAG, with three distinct bands absent from control lysates. NTAP-MRAP was however expressed at the correct predicted MW (TAP-tag approximately 8kDa), and hence it was possible that the N-terminal TAP tag interfered with post-translational modifications. MRAP is known to be glycosylated at the N-terminus (Sebag and Hinkle, 2007). Digesting with PNGaseF confirmed NTAP-MRAP was not glycosylated, and in our initial cAMP assay, we found no major differences between NTAP-MC2R/NTAP-MRAP and HA-MC2R/MRAP-FLAG cAMP responses, however in order to determine statistical significance more experimental repeats would be required.

Western blot analysis at each step of tandem affinity purification showed a marked reduction in background protein patterning and enhanced purification of target product. The purification process therefore appeared to be efficient. However, a large amount of fusion protein was left bound to streptavidin beads following elution, a problem that has been encountered previously with elution from streptavidin with biotin (Li, 2011). This would have decreased the final yield, and therefore this step requires further optimisation.

It was hypothesised that candidate proteins acquired from the affinity purification and Mass Spectrometry (MS) would have a role in MC2R life cycle, for example folding, trafficking, docking or endocytosis. MS analysis of TAP-tagged MRAP and MC2R transfected cell lysates extracted from coomassie blue stained gels identified a very small number of putative

interacting partners; however, most of these were not considered good candidate proteins for MC2R regulation.

MS analysis identified cytoskeletal and scaffolding proteins as well as heat shock protein 60, all of which are abundant proteins and common false positives in the TAP technique (Gingras *et al.*, 2007). These were excluded these from the final list of candidate proteins because of this reason, however, many studies have implemented cytoskeletal proteins as regulators of steroidogenesis, and hence these proteins should not be completely overlooked. In the 1960's it was demonstrated that stimulating adrenocortical cells with ACTH resulted in a change in cell morphology, which was found to be due to paxillin (Han and Rubin, 1996; Vilgrain *et al.*, 1998; Yasumura *et al.*, 1966). Many studies, the first by Crivello and Jefcoate (1978), have used inhibitors of cytoskeletal protein polymerisation to investigate the effects on steroidogenesis in adrenal cells. Generally, inhibiting polymerisation prevents cAMP dependent steroidogenesis at the stage before delivery of cholesterol to the mitochondria (Sewer and Li, 2008).

The final list of the candidate proteins remaining following the exclusion of common false positive such as those described above is given in table 3.2. Of the 5 proteins listed, the most fitting candidate gene, based on the criteria detailed above, was clathrin heavy chain 1, which was isolated from lysates of H295R cells transfected with MC2R-CTAP, and excised from gel slice EM2_1. It has previously been demonstrated by our own laboratory, that clathrin is implicated in the internalisation of MC2R (Baig et al., 2001; Baig et al., 2002). Baig *et al.* showed that internalisation of MC2R in Y1 cells is halted when cells are treated with concanavalin A or hypertonic sucrose, which inhibit clathrin-mediated endocytosis. Baig and colleagues also confirmed that MC2R is not internalised through the caveolae mechanism because inhibitors filipin and nystatin had no effect on internalisation. Kilianova *et al.* (2006) also confirmed these results using immunofluorescence on M3 cells, showing that β-arrestin-2-GFP colocalises with myc-hMC2R in endocytic compartments following incubation with ACTH. hMC2R did not colocalise with caveolin-1 either with or without ACTH incubation. The detection of clathrin by affinity purification may suggest that MC2R and clathrin interact

directly, however this finding would need to be investigated by reciprocal immunoprecipitation in order to confirm an interaction.

MC2R-CTAP also pulled out THO complex subunit 4 encoded by *ALYREF*, also named ALY, which is forms part of the THO/TREX complex. The THO/TREX complex is involved in mRNA processing and export from the nucleus (Masuda *et al.*, 2005; Umlauf *et al.*, 2013). The complex associates with the splicing machinery, and along with UAP56, recruits mRNA export receptor NXF, which has been suggested to transport messenger ribonucleoprotein particles (mRNP) containing processed mRNA to the nuclear pore complex (NPC) where they are exported to the cytoplasm for translation on ribosomes (Umlauf *et al.*, 2013). As the THO complex is involved in mRNA processing, it is unlikely the THO complex interacts with MC2R at a protein level, suggesting this could be a false positive. However, it is interesting that conditions of adrenal insufficiency have been associated with defects in genes involved at a nuclear level, for example, 90% of patients with Triple A syndrome, a condition of adrenal insufficiency and neurological defects (described in section 1.5), have mutations in AAAS, a nuclear pore protein (Prasad *et al.*, 2013; Storr *et al.*, 2009). Furthermore, the genetically isolated Irish traveller community that harbour FGD, have mutations in *MCM4*, a DNA helicase involved in DNA replication (Hughes *et al.*, 2012).

A slightly unsuspected finding from the purification process was the detection of mitochondrial proteins from purified lysates of H295R cells transfected with NTAP-MRAP or MRAP-CTAP. In NTAP-MRAP lysates, NADPH dependent adrenodoxin oxidoreductase (FDXR) was detected. Nuclear encoded FDXR is an important mitochondrial enzyme for multiple biological processes but is particularly important in the adrenal cortex for its role in steroid biosynthesis (Ewen *et al.*, 2012). FDXR receives electrons from NAPDH which it transfers to adrenodoxin which then reduces type 1 mitochondrial steroidogenic CYP enzymes, including CYP11A1, CYP11B1 and CYP11B2 (Sparkes *et al.*, 1991). Deficiency of p450 oxidoreductase, an electron donor to type 2 ER-bound CYP enzymes is associated with congenital adrenal hyperplasia (Arlt et al., 2004; Flück and Miller, 2006; Flück et al., 2008). In light of this finding, a co-immunoprecipitation of FDXR and MRAP was carried

out to confirm the interaction, however the FDXR did not immunoprecipitate with MRAP or vice versus (data not shown), suggesting the detection of FDXR by TAP-MS was a false positive, most likely due to high expression levels of the enzyme.

In MRAP-CTAP lysates, the β-subunit of mitochondrial 3-Methylcrotonyl-CoA carboxylase 2 (MCCC2) was co-purified, which is a biotin containing enzyme that catalyses the conversion of 3-methylcrotonyl-CoA to 3-methylglutaconyl-CoA (Gallardo *et al.*, 2001). MCCC is from a family of biotin containing carboxylases including acetyl-Co-A carboxylase and pyruvate carboxylase, which catalyse one step in leucine catabolism ultimately leading to the production of acetyl-CoA which is used in the citric acid cycle (Chu and Cheng, 2007). Whereas the biotin containing alpha unit binds ATP and HCO_3^-, the β-unit binds the acyl-CoA substrate (Gallardo *et al.*, 2001). Patients with mutations causing deficiency in either subunit have 3-Methylcrotonylglycinuria, in which acute metabolic decomposition leads to convulsions, coma or death typically at 6 months to 3 years of age (Gallardo *et al.*, 2001; Holzinger *et al.*, 2001)

To our best knowledge, MRAP resides at the cell surface and intracellularly at the ER (Chung *et al.*, 2008; Metherell *et al.*, 2005). However, with no mitochondrial markers used in these studies, it is not yet been determined whether MRAP is also present in mitochondria. NTAP-MRAP also pulled out lysozyme C, an enzyme that cleaves the beta-(1,4)-glycosidic bond between N-acetylmuramic acid and N-acetylglucosamine in peptidoglycans in bacterial cell walls (Callewaert and Michiels, 2010), and therefore not a credible candidate protein for MRAP interaction.

Overall, the TAP-tag technique identified mostly common false positives and poor candidate proteins. Crucially, TAP-MS failed to detect MC2R and MRAP in H295R adrenocortical cell lysates, which would be present both as target proteins and as endogenous interactors. Furthermore, the potential interaction between MRAP and FDXR was found to be a false positive when validated. These data suggest the TAP-MS process was not efficient in identifying interactors of MC2R and MRAP and may indicate a need to optimise my protocol to gain a better yield and recovery of proteins.

Although assessing cAMP response by luciferase assay provided evidence to suggest TAP-tagged MC2R and MRAP could interact, an important control that should be implemented in future before proceeding with 'bait and prey' experiments is to coimmunoprecipitate MC2R and MRAP, using the TAP technique, for example by pulling down with TAP-tagged MC2R and probing for FLAG tagged MRAP. The lysates would be subjected to Western blot analysis to confirm the proteins interact, and the gel would be stained and subjected to MS analysis to confirm whether MS was sensitive enough to detect the isolated proteins.

Several studies that employed the same Interplay Mammalian TAP system to isolate proteins have made interesting adjustments to the original protocol which may prove useful for future experiments. Ahlstrom *et al.* (2009) used the Interplay Mammalian TAP system to successfully isolate and recover full length N-terminal tagged WNK4 from HEK293 cells and examine its kinase activity against OSR1 and SPAK. The original protocol was adapted by introducing a high salt and detergent lysis buffer and increasing the number of wash steps following precipitation from the streptavidin resin (using the high salt buffer), in order to dissociate weakly interacting proteins. Comparing preparations separated on a silver stained SDS gel taken from the regular and HSD protocols showed a great reduction in background in HSD preparations.

Although Ahlstrom *et al.* (2009) successfully purified their target protein WNK4, they were unable to identify a novel interacting partner by MS, a 40kDa protein kinase that copurified with WNK4 and was absent from empty vector preparations. Similarly to my results, mass spectrometry detected mostly highly abundant proteins such as tubulin and heat shock proteins. Ahlstrom *et al.* used 1 x 10cm^2 plate per transfection, whereas other studies made larger preparations from 10 x 15cm^2 plates (Griffin et al., 2007; Xie et al., 2009), and successfully identified novel interacting partners. In my protocol, I used 8 x 10cm^2 dishes to purify extracts from cells. Bearing in mind the purification of NTAP-MRAP was detected by Western blot, and MS did not detect known interacting partners, a problem with my protocol could be that MS is not sensitive enough to detect low abundance proteins. Therefore, a

future consideration would be to scale up my experiment. This may also increase the likelihood of detecting interacting partners.

More recent studies implementing Interplay technology have used the latest version of the system, the Interplay 'Adenoviral TAP system' (InterPlay), which uses viral infection to increase transfection efficiency (Li, 2011). This could be an important consideration for future attempts to find interacting partners of MC2R and MRAP as the H295R line used for this project has a low transfection efficiency. Another advantage being the likelihood of gaining expression levels closer to physiological levels, which has been argued to reduce false positives and encourage only true interactions (Bradley et al., 2007; Chen et al., 2005; Li, 2011; Puig et al., 2001; Rigaut et al., 1999).

Taking these options into account, there is potential to improve the quality of my data in future experiments. However, the efficiency of the TAP-MS technique as a whole remains questionable considering the number of adjustments made by researchers to improve efficiency. Common adaptations to the original protocol include substituting the CBP tag, which has been reported to produce poor yield/recovery (Li, 2011) and bind endogenous calmodulin, interfering with binding of the CBP-tag to the calmodulin resin. Other adaptations include reducing tag size to prevent interference with protein complex formation or protein complex function (Xu *et al.*, 2010), and introducing triple tags to increase yield (Li *et al.*, 2011).

Despite these many improvements false positives remain. TAP-MS has the ability to generate high-throughput data however studies do not show a great deal of overlap in the interactions reported. Two of the first high-throughput studies employing TAP-MS to map the multi-protein complex networks of yeast *Saccharomyces cerevisiae* were deemed highly successful, allowing deep insight into the organisational network of proteins in yeast (Gavin et al., 2006; Gavin et al., 2002; Krogan et al., 2006). However, the two datasets showed high levels of noise from non-specific interactions and despite employing statistical algorithms and scoring systems there was very low overlap between the datasets (Collins *et al.*, 2007; Xu *et al.*, 2010).

Further limitations of the TAP-MS technique include its unsuitability for detecting transient interactions. This could introduce false negatives into the technique, which could explain why control proteins were not isolated for my experiments. To rectify this, methods such as crossing linking could be used in future to stabilise interactions (Gingras *et al.*, 2007).

To conclude, other proteomic techniques have previously been used within our laboratory to find interacting partners of MC2R, including the yeast-2-hybrid and bacterial-2-hybrid screen, neither of which identified clear candidate proteins for investigation. Although TAP-MS has been associated with limitations which question its reliability, coupled with other techniques it has proved to be more informative than previous methods. My application of the TAP technique to search for novel candidates of MRAP and MC2R did not generate valuable data suggesting it could be optimised in future, for example by stably expressing TAP proteins and scaling up experiments to increase the overall yield and abundance of low level proteins for MS detection. Following these adjustments, it is possible the TAP-tag technique could disclose interesting proteins involved the MC2R lifecycle and potentially novel candidate genes for FGD.

During the proteomic arm of this project mutations in nicotinamide nucleotide transhydrogenase (NNT) were recognised as a novel cause of FGD and, further, a variant in another antioxidant gene glutathione peroxidase 1 (*GPX1*) was identified, the consequence of which was unclear. The remainder of my PhD focussed on the investigation of this variant as a possible cause of FGD.

Chapter 4: Investigation of *GPX1* as a putative candidate gene for FGD

4.1 Background

4.1.1 Identification of *GPX1* as a putative candidate gene for FGD

50% of FGD cases have mutations in genes in the ACTH signalling or steroidogenic pathway, namely *MC2R*, *MRAP* or *STAR*. The discovery of FGD-causing *NNT* mutations introduced a novel pathway into the pathogenesis of FGD suggesting adrenal steroidogenesis is affected by changes in antioxidant machinery. For the second part of this project I undertook the functional characterisation of further candidate genes.

As discussed in section 1.4.17, NNT is an inner mitochondrial membrane enzyme that supplies mitochondria with NADPH, required for regeneration of reduced glutathione, a potent antioxidant and co-substrate for multiple antioxidant enzymes. Of the nine probands with unknown aetiology analysed by SNP array genotyping, three had chromosome 5 linkage (leading to the discovery of *NNT* mutations), and one had a large region of homozygosity on chromosome 3p26-21. Following the investigation of *NNT*, this latter region was re-examined for putative candidate genes. An antioxidant enzyme, glutathione peroxidase 1 (*GPX1)* was identified based on the known function of *NNT*.

Sequencing the affected individual (#1; Fig. 4.1C arrowed) with chromosome 3 linkage revealed a twelve base pair in-frame deletion in exon 2 of *GPX1*; c.del388-399; p.Arg130-Leu133del (p.R130-L133del) (Fig. 4.1A-B, E), which was heterozygous in the parents and the unaffected sibling (#2; Fig. 4.1C). This mutation was absent from SNP databases. Post mortem analysis of the deceased 5 month old sibling (#3; Fig. 4.1C) revealed small adrenals with loss of the ZF, but it is unknown whether she carried the *GPX1* mutation since DNA was unavailable for study. Sequencing 100 FGD patients with unknown aetiology revealed three further heterozygous missense mutations: p.Ala132Thr, p.Ala140Ser and p.Leu168Gly in different individuals, but no other homozygous or compound heterozygous mutations were found. R130-L133del is at alpha helix-2, a stretch of sequence at the subunit interface of the tetrameric protein (Fig. 4.1D) so it is possible it affects oligomerisation.

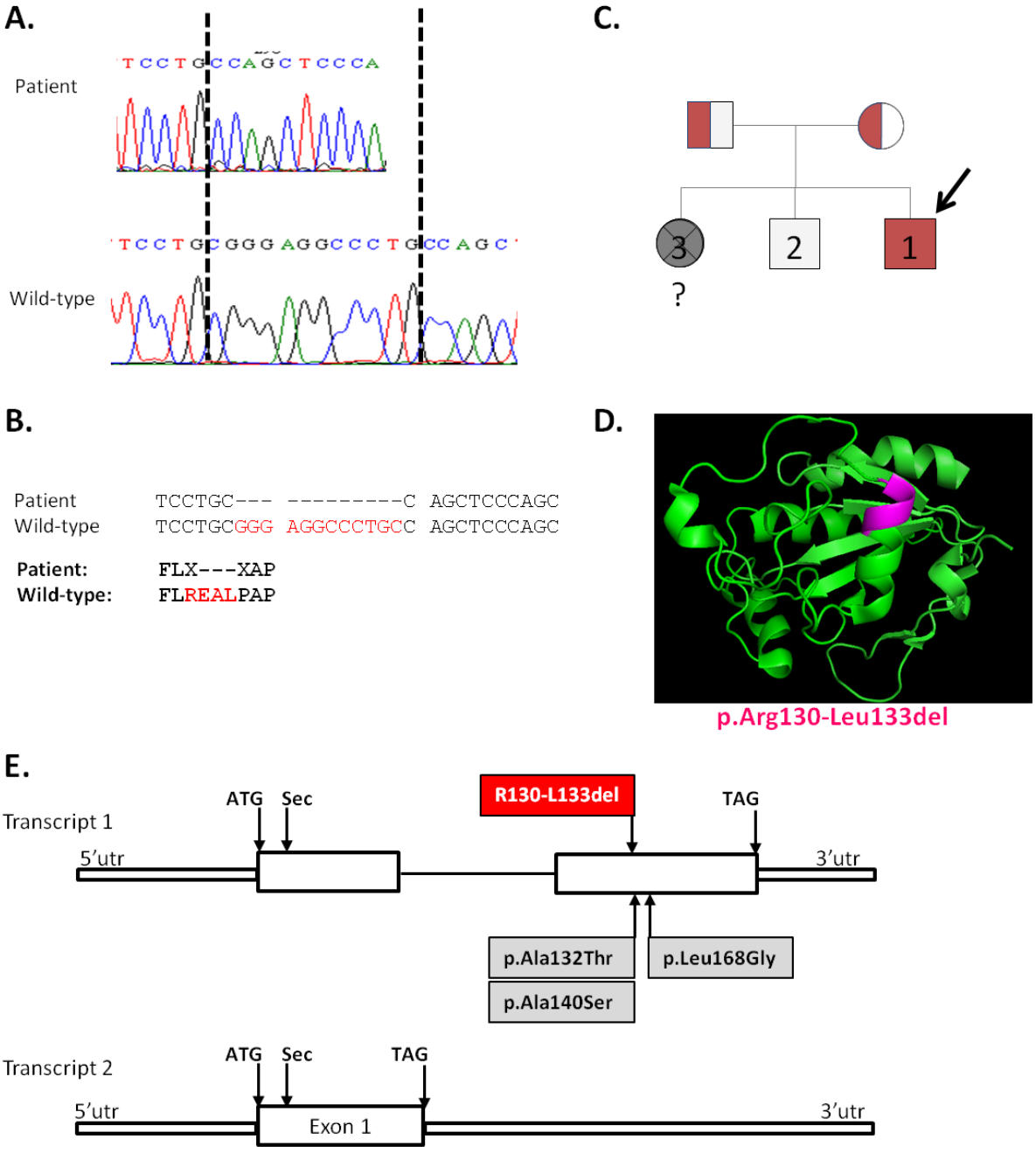

Figure 4. 1: *GPX1* mutation c.del388-399; p.Arg130-Leu133del in proband (arrowed)

A. Partial DNA sequence electropherograms for the affected patient and a wild-type control. The dashed line indicates the site of the homozygous in-frame deletion. B. Alignments of genomic DNA and corresponding protein sequences. C. Pedigree of the family with one affected individual with homozygosity on chromosome 3. 1=proband (depicted by arrow); 2= unaffected sibling; 3=deceased sibling with unknown genotype (denoted by '?'). D. A ribbon diagram of the GPX1 monomer highlighting segment

p.Arg130-Leu133del in pink, which is at the start of a long loop responsible for oligomerisation of the protein. E. Location of p.Arg130-Leu133del in second exon of transcript 1 (upper panel) depicted by red box and heterozygous mutations depicted by grey boxes. Transcript 2 in lower panel. Start codons (ATG), the selenocysteine codon (Sec) and stop codons (TAG) are labelled accordingly.

4.1.2 Clinical Phenotype

The proband was diagnosed with familial glucocorticoid deficiency at 2 years of age after collapsing. His synacthen test revealed 248-331nmol/l cortisol (normal range >550nmol/l) and 145pg/ml ACTH (normal range <50pg/ml). Other biochemistry results showed low DHEAS, slightly high sex hormone-binding globulin, low free androgen index (FAI) and he was negative for adrenal antibodies. He was also vitamin D deficient. Other investigations have included an adrenal scan, which was normal, and genetic diagnostic tests which showed a 46XY karyotype and no mutations in *MC2R*, *MRAP*, *STAR* or *NNT*.

The patient has a body mass index (BMI) of 17.9 and is tall at 1.77m final height, his father and mother at 1.7m and 1.68m respectively. His parents are first cousins and both suffer dylipidemia. The father experienced a heart attack at the age of 67. The proband has one brother who has congenital deafness but no glucocorticoid deficiency and is of normal weight. His sister died aged 5 months of adrenal insufficiency with hypoplasia of the ZF and ZR, but preservation of the ZG.

The proband has previously undergone surgery for an inguinal hernia in 1983 and testicular torsion reduction in right testicle in 1988. For FGD, the proband was treated with hydrocortisone as glucocorticoid replacement therapy, and the dose was reduced following an improvement in 2003. Treatment was stopped for 6 months between September 2011 and February 2012 due to nausea, and is now at 10mg in the morning.

4.1.3 *GPX1* encodes Glutathione Peroxidase 1

The glutathione peroxidases are a group of enzymes that use glutathione as an electron donor to reduce toxic hydrogen peroxide to water. GPX1 was first discovered by Mills *et al.* in 1957, in erythrocytes, where it was found to act to protect haemoglobin from oxidative damage.

GPX1 is located on chromosome 3p21.3, and has two isoforms (Fig. 4.2). Isoform 1 is 1146bp, 2 exon transcript, translated as a 203aa protein with a predicted molecular weight of 22kDa. The protein forms a tetramer with a predicted weight of approximately 85-93kDa (Awasthi *et al.*, 1975). Isoform 2 is 1106bp transcript lacking an intron, which reads through into intron 1 to form a shorter coding region. It has an additional stretch of coding sequence absent from the first transcript, which shifts the open reading frame resulting in a shorter C-terminus but longer 3' untranslated region (3'UTR). This transcript is poorly documented in literature. *GPX1* also has a pseudogene on the X chromosome which is conserved back to the chimpanzee/human split. The active site, surrounding residues and 3'UTR are homologous to functional *GPX1*, however, a premature stop codon is present at position 161 downstream of the active site. Lack of EST data suggests the gene is not expressed (Mariotti *et al.*, 2012).

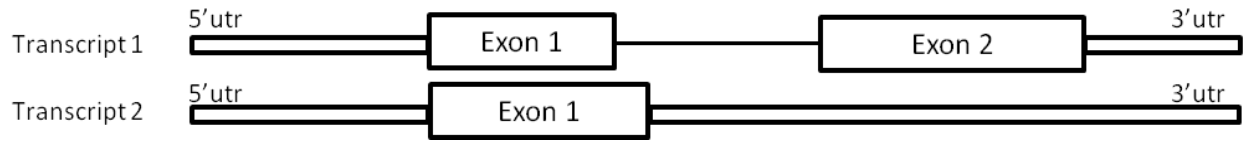

Figure 4. 2: *GPX1* transcripts.

Illustration showing two coding transcripts for *GPX1*. Transcript 1 has two exons and is 1146bp in length. Transcript 2 has one exon and is 1106 in length. In transcript 2, the exon reads through into intron 1 up to the next TAG codon, and the rest of the transcript is untranslated. Intron depicted by single line and UTRs by double line.

4.1.4 GPX1 is a Selenoprotein

A decade after its discovery, purification of GPX1 established it as a selenium (Se) containing enzyme, which was dependent on the trace element for peroxidase activity (Flohe, Rodtruck 1973). Mass spectrometric analysis revealed the presence of a selenocysteine residue in the middle of exon 1, sometimes referred to as the '21stamino acid' (Kraus *et al.*, 1983). The selenocysteine residue (Sec) is similar to a cysteine with Se replacing the sulphur moiety in the amino acid side chain (Lubos *et al.*, 2011). Sec, like Cys is redox active and forms the active site of the enzyme. Both Sec and non-Sec containing glutathione peroxidases exist with the same catalytic function. However, replacing the Sec in GPX1 with a Cys lowers the rate of catalysis by a few orders of magnitude (Rocher *et al.*, 1992). Sec is deprotonated at a normal physiological pH making it a stronger nucleophile, which could partly account for this difference (Lubos *et al.*, 2011), and is also less sensitive to inactivation by hyperoxidation (Rocher *et al.*, 1992).

Se as a trace element is found in various chemical forms in the body but probably confers its main biological function through its incorporation into proteins as an amino acid (Lei *et al.*, 2007). There are 25 selenoproteins in the human genome, (Kryukov et al., 2003; McCann and Ames, 2011). Most are enzymes that have significant roles in redox regulatory pathways and thyroid metabolism (McCann and Ames, 2011).

Following the molecular cloning of *GPX1* in mice, sequence analysis revealed the selenocysteine was encoded by a TGA opal stop codon in the middle of exon 1 (Chambers *et al.*, 1986). For the stop codon to be translated as a selenocysteine, a number of factors are required:

The 3'UTR sequence is essential for the correct translation of the UGA codon (Berry *et al.*, 1991; Shen *et al.*, 1993). Deleting the 3' UTR in thyroid selenoprotein 5' deiodinase (5'DI) abolishes the enzymes activity, but does not alter the activity of the cysteine-mutant 5'DI (Berry *et al.*, 1991). The 3' UTR sequence is not particularly conserved amongst selenoproteins or between species. However, a stem-loop secondary structure named the

selenocysteine insertion element (SECIS), is highly conserved and required for selenocysteine incorporation (Shen *et al.*, 1993). Despite sequence differences, SECIS elements of GPX1, 5'DI and GPX4 can be interchanged without reducing selenocysteine incorporation (Berry *et al.*, 1991; Weiss and Sunde, 1998). The sequence of the SECIS stem loop can be altered providing the secondary structure is maintained (Shen *et al.*, 1995). Only a change to the conserved 'AAR' apical loop sequence would affect enzymatic activity without changing the secondary structure (Budiman et al., 2009; Shen et al., 1995).

The role of the SECIS element is to recruit binding proteins that facilitate Sec incorporation (Fig. 4.3). These binding proteins include SECIS-binding peptide 2 (SBP2), which recruits elongation factor eEFSec and a specific $tRNA^{(Ser)Sec}$ to the ribosome(Donovan et al., 2008) (Donovan 2009). Other binding proteins have also been discovered. In a model proposed by Chavatte *et al.* (2005), after associating with the ribosome, SBP2 is exchanged for ribosomal L30, and a conformational change in the SECIS loop triggers the release of $tRNA^{(Ser)Sec}$ and GTP hydrolysis. Another binding factor involved is nuclease sensitive element binding protein 1 which increases translation efficiency by stabilising the complex (Shen *et al.*, 2006).

The importance of selenoproteins as a whole is highlighted by studies examining defects in the selenocysteine incorporation machinery. Mutations in the *SBP2* gene in humans lead to a multisystem disorder, including azoospermia, impaired thyroid function, axial muscular dystrophy, increased susceptibility to ultraviolet radiation and enhanced insulin sensitivity (Schoenmakers *et al.*, 2010) and $tRNA^{Sec[Ser]}$ knockout mice are embryonic lethal (Bosl *et al.*, 1997).

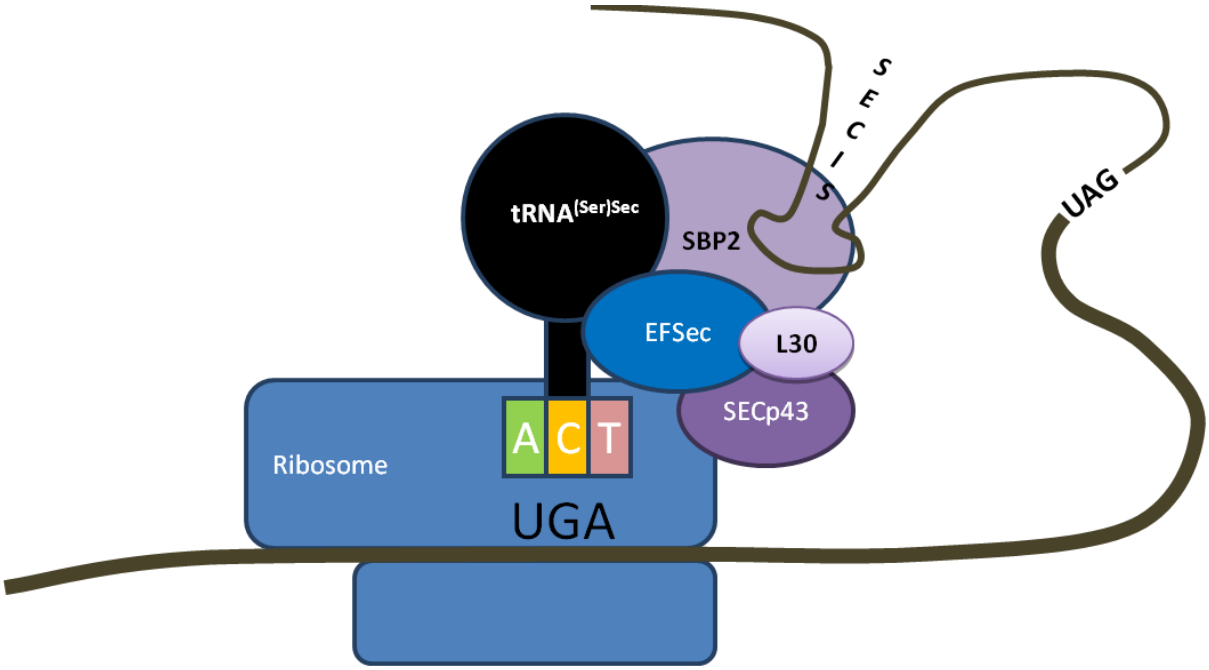

Figure 4. 3: Selenocysteine incorporation

Illustration of selenocysteine incorporation machinery. The stem-loop SECIS element situated in the 3' UTR, recruits binding proteins SBP2 and EFsec to facilitate incorporation of Sec at the ribosome. After associating with the ribosome, L30 competes with SBP2 for binding of SECIS, releasing the tRNA$^{[Ser]Sec}$.

4.1.5 GPX1 Catalytic Cycle

The catalytic heart of GPX1 is not only comprised of the redox active Sec, as crystallography studies reveal the involvement of glutamine (Gln) and tryptophan (Trp) residues in substrate interaction (Epp *et al.*, 1983) . This triad of residues is highly conserved amongst glutathione peroxidases and has been shown to be essential for catalytic function (Maiorino *et al.*, 1998). An additional fourth residue, asparagine (Asn), is thought to form a tetrad with these residues based on molecular modelling and mutational analysis of *D.melanogaster* non-Sec GPX4 (Toppo *et al.*, 2009; Tosatto *et al.*, 2008). The conservation of these residues is illustrated in figure 4. 4, which shows an alignment of all 8 human GPXs.

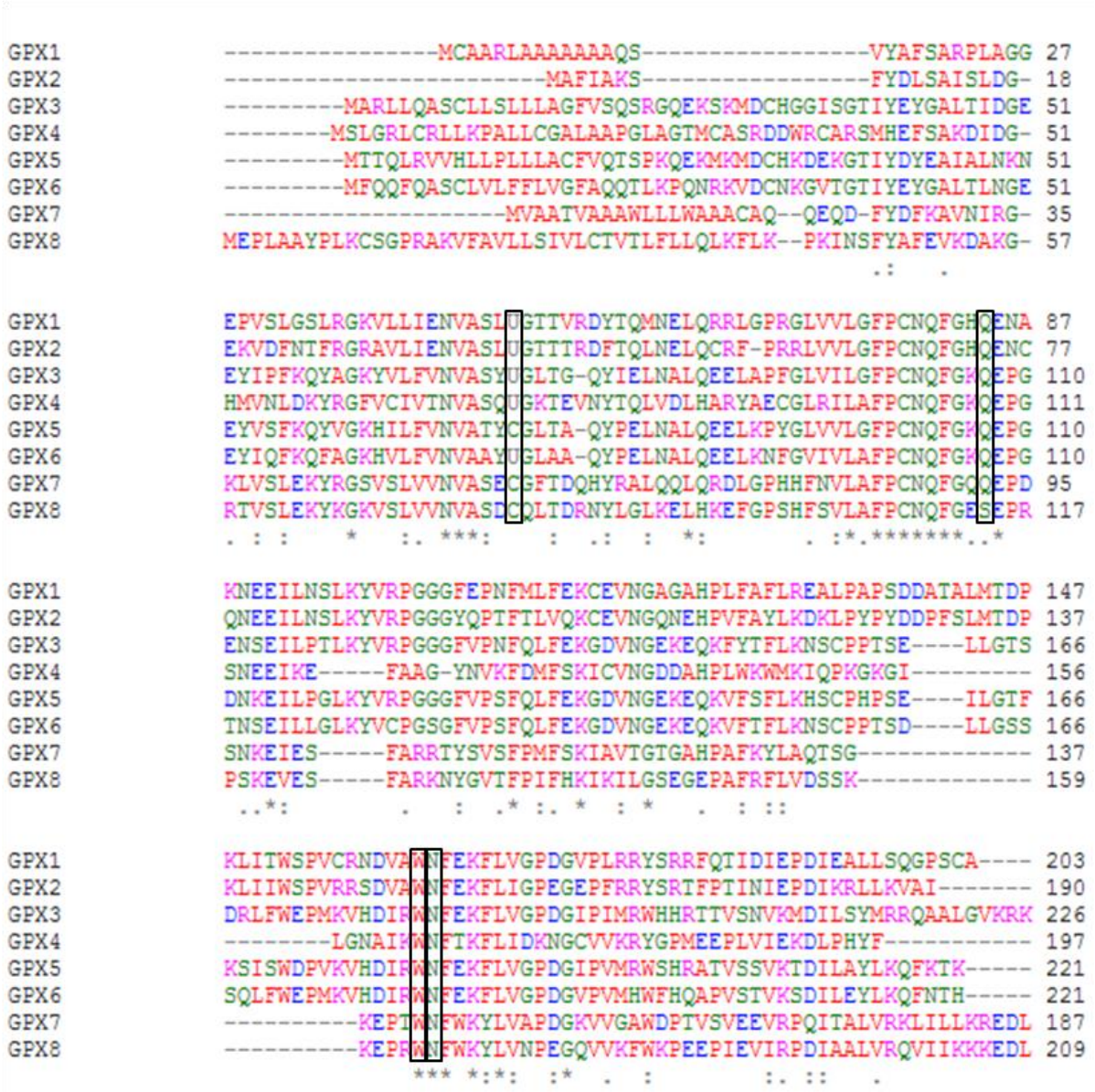

Figure 4. 4: Multiple sequence alignment of human GPX1-8

The GPX active site tetrad of residues includes Sec (U), glutamine (Q), tryptophan (W) and asparagine (N) depicted by boxes. Only GPX8 varies in substitution of glutamine (Q) for a serine (S). Consensus symbol '*' indicates positions with a fully conserved residue; ':' conservation between groups of strongly similar properties; and '.' conservation between groups of weakly similar properties. Residues highlighted *Red* depict small and hydrophobic residues; *blue* acidic residues; *magenta* basic residues, *green* hydroxyl, sulfhydryl and amine residues; and *grey* unusual amino acids

GPX1 confers its catalytic action by a ‘ping-pong’ mechanism consisting of peroxidatic and reductive steps with an intermediate bond (Brigelius-Flohé and Maiorino, 2013). As illustrated in figure 4.5, in step 1 when a hydroperoxide binds to the Sec active site it oxidises the selenol moiety (Se-H) to selenic acid (Se-OH) (Flohe *et al.*, 1973). In the second step selenic acid is reduced by glutathione to form a glutathionylated selenol (Se-SG), releasing oxygen in the form of water. In the third reaction Se-SG is reduced by a second glutathione molecule back to selenol (Se-H), producing oxidised glutathione (Brigelius-Flohé and Maiorino, 2013; Flohé *et al.*, 2011; Lubos *et al.*, 2011). Because the abundance of glutathione outweighs the concentration of hydroperoxides in the cell, saturation kinetics are never met (Brigelius-Flohé and Maiorino, 2013; Lubos *et al.*, 2011). The overall reaction is seen in figure 4.5B.

A.

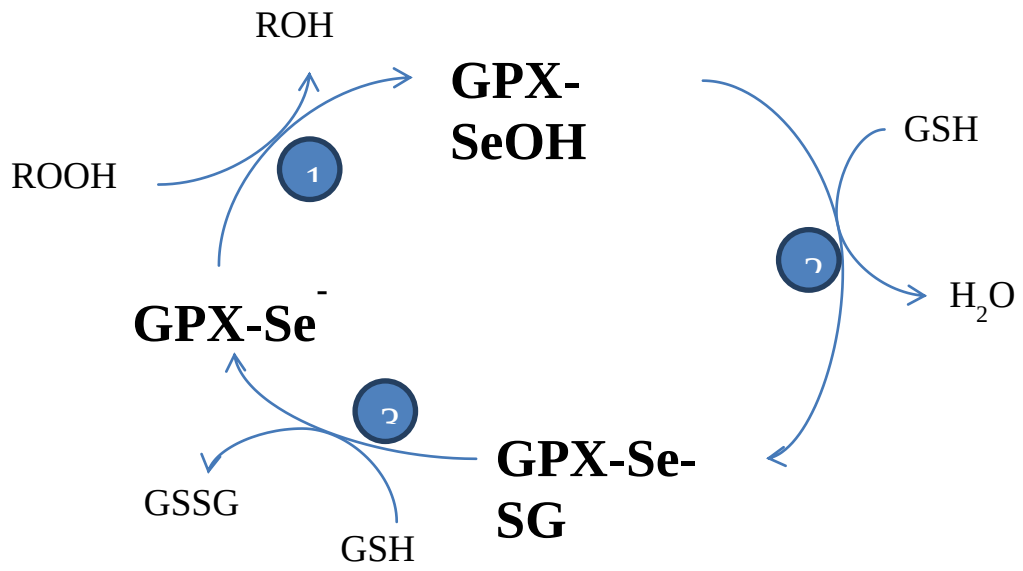

(1) $GPX\text{-}Se^- + H_2O_2 \longrightarrow GPX\text{-}SeOH + OH^-$

(2) $GPX\text{-}SeO^- + H^+ + GSH \longrightarrow GPX\text{-}Se\text{-}SG + H2O2$

(3) $GPX\text{-}Se\text{-}SG + GSH \longrightarrow GPX\text{-}Se^- + H^+ + GSSG$

B. $ROOH + 2GSH \longrightarrow ROH + GSSG + H_2O$

(Brigelius-Flohé and Maiorino, 2013)

Figure 4. 5: GPX1 catalytic cycle

A. Diagram showing GPX1 catalytic cycle with corresponding equations for each step.

B. Overall equation for GPX1 catalysis of H_2O_2

4.1.6 GPX Enzyme family

There are eight *GPX* genes (*GPX1-8*), five of which are selenoproteins (Kasaikina *et al.*, 2011). *GPX5*, *GPX7* and *GPX8* instead have a cysteine residue at their active site (Brigelius-Flohé and Maiorino, 2013; Ghyselinck and Dufaure, 1990). The enzyme family are thought

to have evolved in three distinct groups: *GPX1/GPX2*, which are enzymatically very similar but have different tissue expression (Chu *et al.*, 1997), *GPX3/GPX5/GPX6*, the latter two formed by duplication of *GPX3* and *GPX4/GPX7/GPX8*, with *GPX4* as the ancestral gene which are all monomeric unlike the other GPXs which are tetrameric (Fig. 4.6) (Brigelius-Flohé and Maiorino, 2013; Mariotti *et al.*, 2012). The active site tetrad of residues is conserved between all mammalian GPXs except GPX8 in which one residue is substituted (Fig. 4.6) (Lubos *et al.*, 2011; Tosatto *et al.*, 2008).

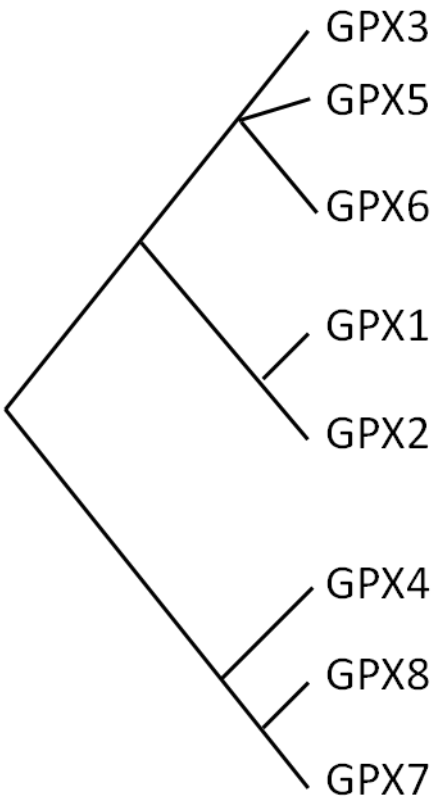

Figure 4. 6: Phylogenetic tree for human GPX family.

GPX1 is widely expressed in all tissues, whereas the other genes are more tissue specific (Lei *et al.*, 2007)**.** *GPX2* is expressed exclusively in the gastrointestinal tract in rats but in humans also the liver and colon (Chu *et al.*, 1997). It is thought to be an extra source of antioxidant defense from gut derived pathogens and can be induced by NRF2, a transcription factor upregulated by oxidative stress (Banning *et al.*, 2005). *GPX3* is expressed predominantly from the kidneys but is also secreted into extracellular fluid as a glycoprotein (Takahashi *et*

al., 1987; Yoshimura *et al.*, 1991). *GPX4* is expressed in most tissues, however its activity is generally lower than GPX1, excluding the testes, where it is highly expressed. *GPX5* is an epididymis-specific GPX found in humans, primates, pigs and rodents (Brigelius-Flohé and Maiorino, 2013) and it is thought to have a role in maintaining sperm integrity, as mating *GPX5*$^{-/-}$ male mice with WT females increases the incidence of miscarriage (Chabory *et al.*, 2009). Relatively few details are known about the remaining GPXs, but GPX6 has been shown to be expressed in olfactory glands (Kryukov *et al.*, 2003), GPX7 in oesophageal epithelial cells (Peng *et al.*, 2012) and GPX8 in the lung (Yamada *et al.*, 2012).

Most GPXs are cytosolic, but the isoforms do vary in cellular compartment. GPX1 is predominantly cytosolic but also resides in mitochondria and peroxisomes (Lubos *et al.*, 2011). *GPX4* can be alternatively spliced into cytosolic, mitochondrial (mt*GPX4*) and sperm nuclear (sn*GPX4*) isoforms (Brigelius-Flohé *et al.*, 1994)**.** The mitochondrial isoform has been reported to have a structural function in midpiece of spermatozoa where it is enzymatically inactive (Ursini *et al.*, 1999), and knockout of mt*GPX4* renders mice infertile (Schneider *et al.*, 2009). As the name suggests, snGPX4 resides in the nuclei of spermatozoa where it has been suggested to protect the structural integrity of sperm chromatin in conjunction with epididymis expressed *GPX5* (Puglisi *et al.*, 2012). GPX7 and 8 have been reported as ER residing proteins, specifically GPX7 in the lumen and GPX8 in the membrane (Nguyen *et al.*, 2011)

GPX4 is unique amongst the GPXs, in that it is the only enzyme capable of reducing complex phospholipid hydroperoxides and cholesterol hydroperoxides in membranes (Arai *et al.*, 1999). One theory is that the peroxidatic moiety is more exposed in the monomer allowing increased accessibility by larger phospholipid substrates, although GPX7 and 8, which are also monomeric have only been reported to reduce H_2O_2 (Brigelius-Flohé and Maiorino, 2013).

4.1.7 Regulation of GPX1

4.1.7.1 Regulation of GPX1 by Selenium

The principal regulator of GPX1 expression and activity is Se. Se is required for $tRNA^{(Ser)Sec}$ synthesis, hence Se deficiency greatly diminishes GPX1 activity by halting the selenocysteine incorporation process at the translational level (section 4.1.4). In addition, selenium deficiency reduces transcript stability as the TGA is then read as a stop codon leading to nonsense mediated decay. Converting the Sec codon (TGA) to either a stop (TAA) or cysteine (TGC) will stop regulation by Se, as demonstrated in rat hepatocytes, and substituting Sec for a TAA stop codon decreases *GPX1* mRNA levels, indicating possible nonsense mediated decay (Moriarty *et al.*, 1998).

The regulation of *GPX1* mRNA levels by Se has been demonstrated both *in vitro* and *in vivo* (Baker *et al.*, 1993; Bermano *et al.*, 1996; Sun *et al.*, 2000; Weiss Sachdev and Sunde, 2001). However, the mRNA stability of other selenoproteins is not as severely affected by Se depletion (Sunde *et al.*, 2009), even when the selenoprotein is as likely a candidate to undergo nonsense mediated decay (Sunde *et al.*, 2009).

Se regulates each selenoprotein to a different degree, in a tissue dependent manner. For example, severe Se deficiency can result in a total loss of *GPX1* mRNA expression and activity in rat liver. In contrast only 75% loss of GPX4 activity is seen with no changes to *GPX4* mRNA expression (Bermano *et al.*, 1995).

The preferential protection of certain selenoproteins under Se deficiency has been reviewed by McCann and Ames (2011), who suggest that a hierarchy of selenoproteins exists, where those classed as ‘essential’ are more resistant to Se deficiency than those that classed as non-essential. A protein is essential if it is required for survival or reproduction, (its absence causing embryonic lethality or infertility in mice). Under this assumption, *GPX4* is essential and *GPX1* is not, which is reflected in their respective resistances to Se deficiency (McCann and Ames, 2011).

The mechanisms behind this preferential regulation at the translational level are not completely understood, however several studies suggest selenoproteins more resistant to Se deficiency have greater binding affinity to Sec incorporation machinery such as SBP2 (Low *et al.*, 2000; Schoenmakers *et al.*, 2010; Squires *et al.*, 2007). In keeping with this, SBP2 is constrained to the nucleus under oxidative conditions, forcing selenoproteins in other cellular compartments to compete for its binding when there is limited availability (Papp *et al.*, 2006).

It has also been suggested that SECIS element variation is a contributing factor which alters translation efficiency (Latreche *et al.*, 2009; Low *et al.*, 2000; Squires *et al.*, 2007). Two types of SECIS elements exist the difference between the two lying in the positioning of the adenine-adenine-purine (AAR) motif, a highly conserved sequence in all SECIS elements (Budiman *et al.*, 2009). Replacing the 3' UTR of 5'DI1 with either the *GPX1* or *GPX4* 3' UTR alters translational efficiency under Se deprivation, with the *GPX1* 3' UTR proving least efficient (Bermano *et al.*, 1996).

Another mechanism involves eIF_{4a3}, a eukaryotic initiation factor released during Se deprivation. eIF_{4a3} binds to type 1 SECIS elements, competing with SBP2 for binding thereby inhibiting translation (Budiman *et al.*, 2009). Selenoproteins with type 1 SECIS elements include GPX1 and other selenoproteins at the bottom of the hierarchy (Budiman *et al.*, 2009).

Finally, a number of studies have indicated that regulation by Se is dependent on the methylation of the Sec $tRNA^{Sec[Ser]}$. Selenoproteins such as GPX1 that are more sensitive to Se deprivation appear to require the Sec $tRNA^{Sec[Ser]}$ to be methylated at position 34 (Um34) for successful Sec incorporation. Methylation of Um34 is decreased by Se deprivation. Selenoproteins GPX1, GPX3, SelR and SelT were not detected in Sec $tRNA^{Sec[Ser]}$ knockout mice engineered to express the unmethylated form (Carlson *et al.*, 2005).

4.1.1.1 Se Independent Regulation of GPX1

Non-Se regulators of GPX1 expression include adenosine and nucleolin. Adenosine is involved in numerous biological functions including the protection again ischemia/reperfusion injury and apoptosis (Lee and Emala, 2002). In human primary pulmonary endothelial cells, adenosine treatment can regulate GPX1 by increasing mRNA stability and GPX activity, which could explain its protective role (Zhang *et al.*, 2005). Similarly, nucleolin has been shown to bind the 3' UTR of many selenoproteins including GPX1 to increase mRNA stability (Wu *et al.*, 2000). Knockdown of nucleolin decreases protein levels of selenoproteins in a selective manor, where GPX1 is least affected (Miniard *et al.*, 2010; Wu *et al.*, 2000).

GPX1 is also regulated at the transcriptional level, for example paraquat can stimulate *GPX1* promoter activity (de Haan *et al.*, 1998). The *GPX1* promoter contains binding sites for many transcriptional regulators involved in the cellular response to oxidative stress including P53 (Tan *et al.*, 1999), NFκB and AP-1 (Zhou *et al.*, 2001) and oxygen response elements (Cowan *et al.*, 1993). P53, a tumour suppressor that is pro-apoptotic, surprisingly upregulates *GPX1* transcription, but may do this in the initial stages of activation before it induces ROS production (Tan *et al.*, 1999). The pro-survival transcription factor NFκB, has been implicated in upregulation of *GPX1* during oxidative stress. Inhibitors of NFκB prevent the typical ROS induced increase in *GPX1* expression in skeletal muscle cells, indicating NFκB mediates this response (Zhou *et al.*, 2001).

GPX1 can also undergo post-translational modifications that regulate its activity. It is a substrate for c-Abl and Arg tyrosine kinases, which interact and phosphorylate GPX1 increasing its activity. Under lethal doses of hydrogen peroxide, c-Abl and Arg promote apoptosis, but the abundance of GPX1-kinase complexes is low. Under lower doses, c-Abl and Arg activate GPX1 to protect against apoptosis. c-Abl/Arg deficient cells treated with hydrogen peroxide have an increased apoptotic response, suggesting increased sensitivity to ROS in the absence of GPX1 activation by these kinases (Cao *et al.*, 2003a).

4.1.8 Functional Role of GPX1: Protection Against Oxidative Stress

Despite the abundance and distribution of *GPX1*, the knock-out (KO) mice are normal, viable and fertile with no histopathologies until 15 months of age (Esposito *et al.*, 2000). For an enzyme that reduces hydrogen peroxide, it is also surprising that KO mice show no abnormalities when exposed to hyperbaric oxygen, a form of oxidative stress (Cheng *et al.*, 1997b). It is possible that residual glutathione peroxidase activity is maintained by other members of the enzyme family, preventing lethality.

However, a number of independent *GPX1* KO mice lines have shown GPX1 to play a major role in protection against oxidative stress. Studies indicate that *GPX1* KO mice are more susceptible to hydrogen peroxide and paraquat induced lethality (Cheng *et al.*, 1998; de Haan *et al.*, 1998) and diquat-induced oxidative stress (Fu *et al.*, 1999) when compared to wild-type (WT) mice. In keeping with this, *GPX1* overexpressing mice are more resistant to paraquat induced lethality (Cheng *et al.*, 1998).

Knockout mice are generally smaller and have increased levels of lipid peroxidation, mitochondrial hydrogen peroxide production, and a decreased mitochondrial control ratio (less ATP production) in the liver (Esposito *et al.*, 2000; Esposito *et al.*, 1999). When injected with paraquat, KO mice have an increased NADPH/NADP ratio and higher levels of protein and lipid peroxidation compared to WT (Cheng *et al.*, 1999). Therefore GPX1 protects against oxidative stress by attenuating levels of oxidation and maintaining a balanced redox status.

4.1.9 *GPX1* Polymorphisms and Disease

GPX1 KO mice show no gross abnormalities, and no human mutations have been described to date however, variants in *GPX1* have been implicated in the increased risk of various disease states in humans. The deficiency of Se, considered a trace element, has health implications, presumably due to loss of selenoprotein(s) activity. Low Se dietary intake can

result in Keshan disease, a cardiomyopathy, or Keshan-Beck disease, an osteoarthropathy, both due to increased oxidative stress (Lei *et al.*, 2009; Reeves *et al.*, 1989; Wu and Xu, 1987).

The antioxidant effects of Se have been recognised for years and it is thought to have anticarcinogenic properties (Lei *et al.*, 2007). In fact, a clinical trial by Clark *et al.* (1996) showed daily supplementation with Se reduced mortality rates significantly (Clark *et al.*, 1996). However, other studies such as the SELECT trial by Lippman *et al.* found Se had no beneficial effect on cancer risk (Lippman *et al.*, 2009).

The two most common sequence polymorphisms in *GPX1* associated with increased susceptibility to disease are a proline to leucine substitution at position 198, and a variation in the number of alanine repeats (5 to 7) in exon 1 with five alanines found most commonly (Moscow *et al.*, 1994; Shen *et al.*, 1994). A high incidence of the P198L SNP has been identified in patients with lung cancer (Moscow *et al.*, 1994), bladder cancer (Ichimura *et al.*, 2004) and colon cancer (Hu and Diamond, 2003). Furthermore, expression of *GPX1* is decreased in breast and prostate cancer cell lines (Gladyshev *et al.*, 1998; Hu and Diamond, 2003) and in a liver cancer mouse model (Esworthy *et al.*, 1995).

The sequence polymorphisms described are known to affect enzyme activity. A recent study by Zhou *et al.* (2009) showed *GPX1* with 5 alanines and a leucine at position 198 had significantly higher activity than other alleles when transiently transfected into Se treated MCF-7 cells which have low levels of GPX1. However the authors only investigated the activities of 5 and 7 alanines in combination with proline or leucine residues and did not investigate the activity of a 6 alanine/leucine combination. Moreover, other studies have suggested the leucine allele at 198 gives lower GPX activity due to reduced responsiveness to Se (Hamanishi *et al.*, 2004; Lei *et al.*, 2009), and the number of alanines has no effect on activity (Moscow *et al.*, 1994; Shen *et al.*, 1994).

Loss of heterozygosity at this locus is common in cancer (Hu and Diamond, 2003; Moscow *et al.*, 1994). It is therefore interesting that naked mole rats, that have a naturally occurring

mutation in *GPX1* causing a premature stop codon and minimal expression, do not develop cancer and have an unusually long life span for rodents of 28 years (Kasaikina *et al.*, 2011).

In addition to cancer, *GPX1* polymorphisms have been associated with increased susceptibility to cardiovascular disease, neurodegenerative diseases such as Parkinson's (Damier *et al.*, 1993), Alzheimer's (Paz-y-Mino *et al.*, 2010), osteoporosis (Mlakar *et al.*, 2010) and decreased activity has been associated with early onset type 1 diabetes mellitus (Dominguez *et al.*, 1998).

4.2 Aims

The genomic arm of this project focused on the discovery of *GPX1* as a novel candidate gene for FGD. The aim of this chapter was to uncover the mechanism through which a mutation in *GPX1* may cause FGD, and to investigate the role of *GPX1* in the adrenal cortex by:

(1) Functionally characterising R130-L133del *in vitro*
(2) Analysing *GPX1* expression levels in the adrenal cortex relative to other tissues by real time PCR
(3) Knocking down *GPX1* with shRNA in human adrenocortical cells and assessing cellular and steroidogenic function.
(4) Assessing differences in adrenal morphology and corticosterone production in *GPX1* KO mice compared to WT by immunohistology and radioimmunoassay

4.3 Results

4.3.1 Analysis of *GPX*$^{-/-}$ Mouse Adrenals

GPX1 is one of the most abundant antioxidant enzymes in mammals and is ubiquitously expressed throughout the body. *GPX1*$^{-/-}$ mice show no obvious phenotype and naked mole rats, which lack a functional GPX1, have no reported abnormalities. It was therefore

questionable whether GPX1 deficiency could be the cause of the adrenal phenotype in our patient. In humans, post mortem histological analyses of adrenals from FGD patients show small adrenals, with disorganised glomerulosa cells and absent fasciculata and/or reticularis cells (Clark and Weber, 1998). An autopsy of the deceased 5 month old sibling of the proband (no 1 Fig. 4.1C) revealed small adrenals with loss of the ZF, but it is not known whether the individual carried the *GPX1* mutation. To address this question I employed a mouse model with loss of *GPX1*, to analyse adrenal gland histology for abnormalities.

Adrenals from 4 month old WT and *GPX1*$^{-/-}$ mice were obtained courtesy of Xingen Lei, Cornell University (Esworthy *et al.*, 1997). Mice were from a mixed genetic background. The adrenals from WT and *GPX1*$^{-/-}$ were of similar size. Adrenals were embedded in paraffin and sectioned into 8µm slices as described in section 2.8.3.

Haematoxylin and eosin staining (H&E) was used to inspect gross adrenal morphology. *GPX1*$^{-/-}$ mice showed normal adrenal morphology compared to WT mice (Fig. 4.7A).

To check steroidogenic capacity cells were immunostained with side chain cleavage enzyme (CYP11A1) antibody. CYP11A1 converts cholesterol to pregnenolone in the first and only rate limiting step of steroidogenesis, and is therefore expressed in all steroid producing cells. Immunofluorescent analysis showed typical CYP11A1 staining in all adrenal cortex zones, for both WT and *GPX1*$^{-/-}$ mice, suggesting loss of GPX1 does not affect adrenal morphology (Fig. 4.11B). The intensity of CYP11A1 staining was not distinctly different. Sections were counterstained with zonal marker inner-zone antigen 1 (IZA-1), a protein expressed only in the zona fasciculata and reticularis. WT and *GPX1*$^{-/-}$ mice both showed typical zonation with no abnormalities in the knockout (Fig. 4.7B).

Loss of *GPX1* in previous mouse studies has been associated with increased levels of apoptosis, and mice with a spontaneous *NNT* mutation show greater levels of cleaved caspase-3, a marker of apoptosis, in the ZF (Meimaridou *et al.*, 2012b). We hypothesised that loss of *GPX1* may present a similar phenotype. Immunostaining WT and *GPX1*$^{-/-}$ sections with cleaved caspase-3 antibody showed an unusual phenotype, with staining apparent

between steroidogenic cells possibly staining blood vessels (Fig. 4.7C). This staining pattern was characteristic of capillary wall vascular endothelial cells that run through the adrenal cortex. The intensity of staining was much higher in the *GPX1*$^{-/-}$ mice perhaps indicating higher levels of apoptosis in these cells. Unfortunately further analysis of *GPX1*$^{-/-}$ mouse adrenals was not possible due to a lack of supply.

NNT mutant mice also had significantly lower corticosterone levels than WT (Meimaridou *et al.*, 2012b), consistent with FGD patients who present with low or undetectable levels of cortisol. Therefore basal corticosterone levels were measured for 6 WT and *GPX1*$^{-/-}$ mice by radioimmunoassay, which was performed by colleagues at Cornell University, US. *GPX1* $^{-/-}$ mice showed a trend towards lower basal corticosterone levels than WT (Fig. 4.7D), but the difference was not significant. Should further mice become available increasing the numbers assayed may enable significance of this difference to be established.

To summarise, the adrenals of *GPX*$^{-/-}$ mice had normal histology compared to WT, with no morphological and zonal differences or changes to *CYP11A1* expression pattern. The adrenals did however have increased cleaved caspase-3 staining in an unusual pattern that appeared vascular. Measurement of basal corticosterone concentration showed a trend towards lower levels in *GPX*$^{-/-}$ mice however there was no statistical significance.

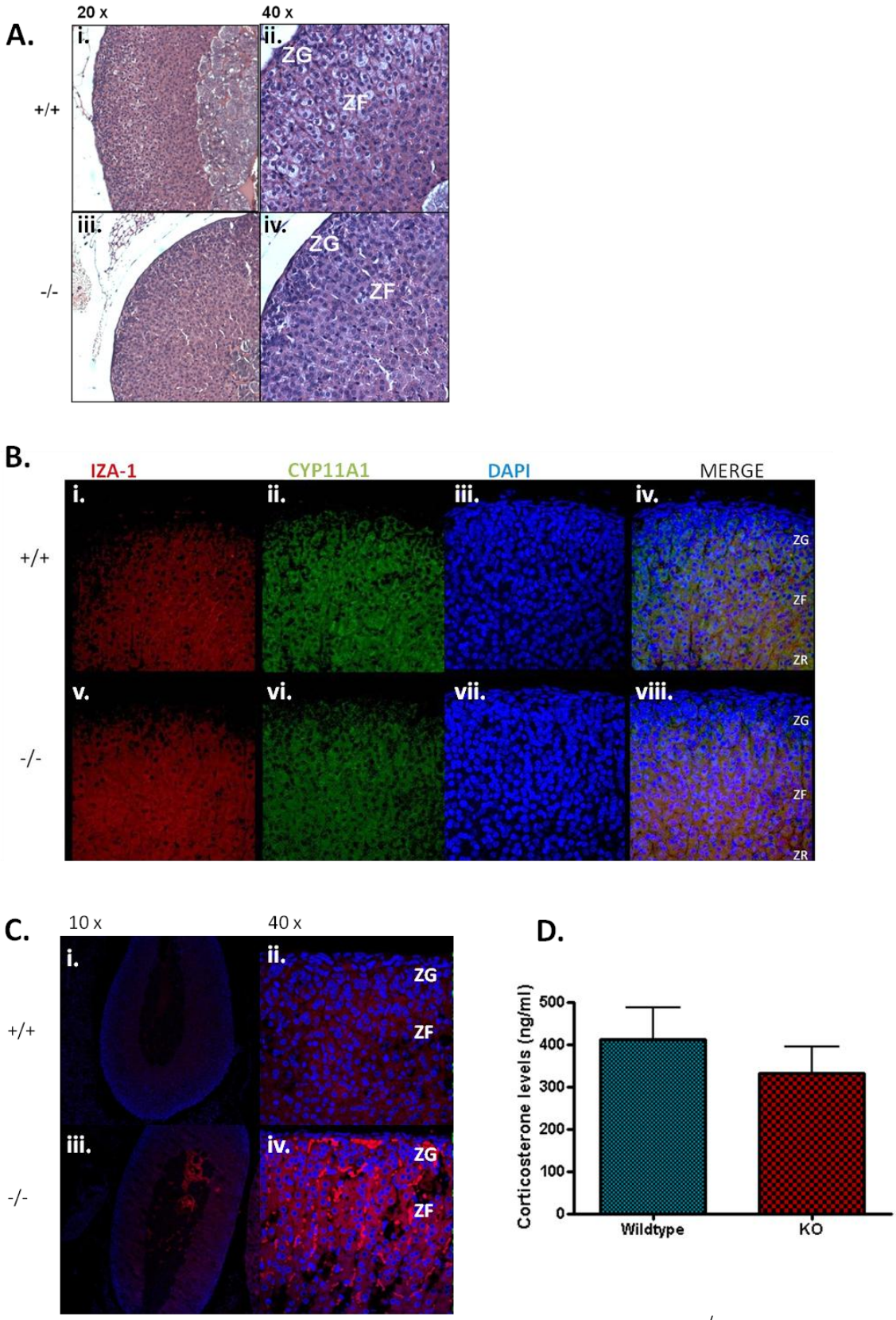

Figure 4. 7: Analysis of adrenals from 4 month old WT and *GPX1*$^{-/-}$ mice.

A. H&E staining of wild-type (i and ii) and *GPX1*$^{-/-}$ mice (iii and iv). Adrenals from *GPX*$^{-/-}$ mice had grossly normal morphology . B. *GPX1*$^{-/-}$ adrenals had normal zonation,

depicted by immunofluorescent staining for zonal markers CYP11A1 (ii and vi) and IZA-1 (iii and vii) which was similar to WT. C. Increased immunofluorescent staining with apoptotic marker cleaved caspase-3 showed staining characteristic of vascular endothelial cells in *GPX1*$^{-/-}$ mice adrenal (iii and iv) which was absent from WT adrenals (i and ii)(n=2). D. Basal corticosterone levels in wild-type and *GPX*$^{-/-}$ mice, measured by radio-immunoassay. *GPX*$^{-/-}$ mice had lower corticosterone levels but the difference did not reach statistical significance (n=6). Abbreviations: ZG, Zona Glomerulosa; ZF, Zona Fasciculata; CYP11A1, p450 side chain cleavage enzyme; IZA-1, Inner Zone Antigen 1.

4.3.2 Tissue Distribution of *GPX1* Expression in Humans

Expression levels of a gene can give an indication of tissue specific functional significance. To investigate *GPX1* expression in the adrenal cortex relative to other tissues, tissue distribution of *GPX1* mRNA was analysed using cDNA synthesised from a panel of human tissue RNA samples of trauma patients with no underlying health issues (Ambion). Real time quantitative PCR using primers targeting *GPX1* and *GAPDH* (section 2.3.7) was carried out on this panel.

Data was analysed using the absolute quantification method. The C_t value of the unknown was quantified absolutely by interpolating the quantity from a standard curve, whose quantities were pre-determined spectrophotometrically. Gene expression of the house keeping gene *GADPH* was used for normalisation.

Analysing the mRNA expression of *GPX1* relative to *GAPDH* in each tissue, showed *GPX1* was highest in the adrenal cortex, suggesting it has an important role there. Following the adrenal, mRNA expression was highest in the spleen and adipose tissue (Fig. 4.8A). Comparing tissue distribution of *NNT*, a known FGD causing gene, did not show a similar expression pattern however both were highly expressed in adipose tissue with substantial expression of *NNT* in the adrenal (Fig. 4.8C).

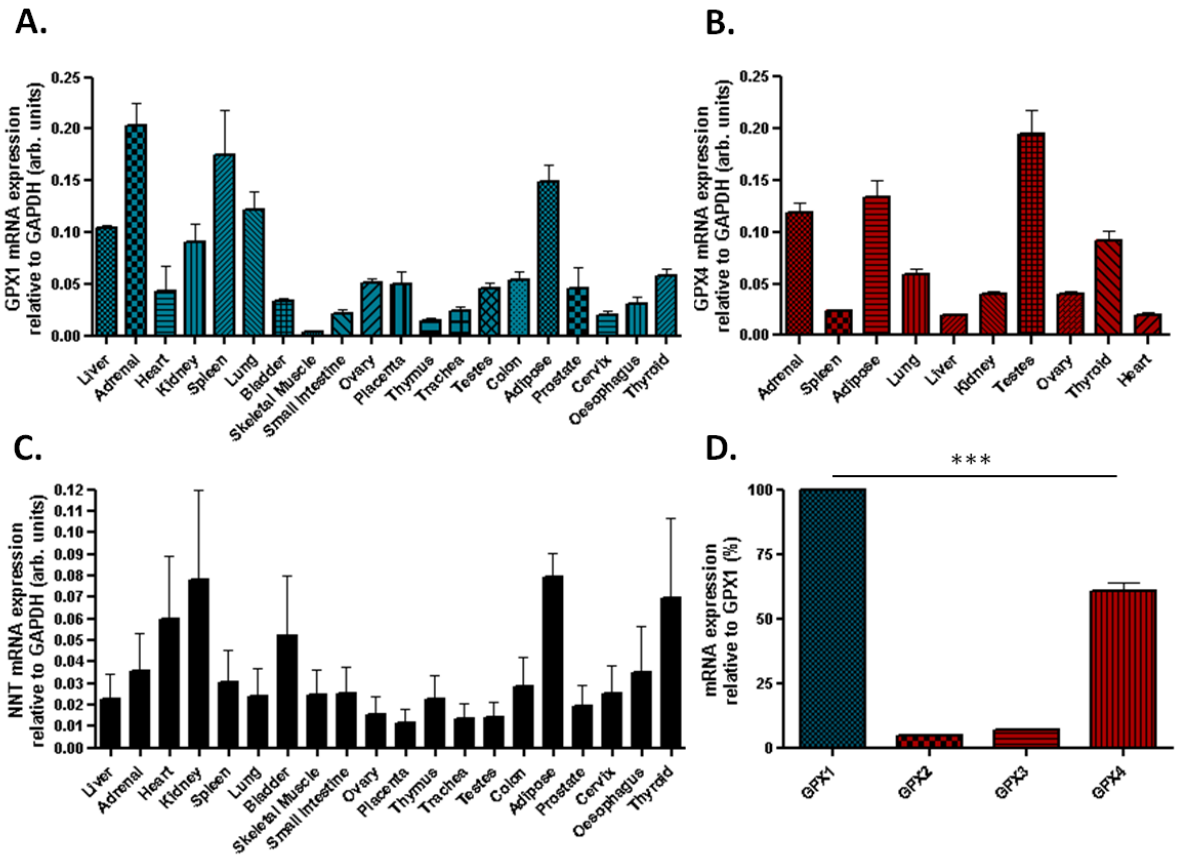

Figure 4. 8: Quantitative Real time PCR analysis of *GPX1* mRNA expression in humans

Real time PCR analysis of mRNA expression of *GPX1* (A), *GPX4* (B) and *NNT* (C) normalised to *GAPDH* using cDNA derived from a panel of 20 human tissues. A. *GPX1* is highly expressed in the adrenal, spleen and adipose tissue. B. *GPX4* is highly expressed in the testes, adipose tissue and adrenal. C. *NNT* is highly expressed in adipose tissue, kidney and thyroid. D. Real time PCR analysis of relative mRNA expression of *GPX1-4* in adrenal cortex, using adrenal cortex cDNA, normalised to *GAPDH*. *GPX4* mRNA levels were significantly lower than *GPX1* (*$p<0.001$) (A-C n=3 mean ± SD, D *GPX1* and 4 n=3, GPX2 and 3 n=1).**

The second most abundant glutathione peroxidase in mammals is GPX4, which is also ubiquitously expressed, but predominantly in the testes where it has a role in spermatogenesis. To determine whether *GPX1* was the predominant glutathione peroxidase in the adrenal cortex, *GPX4* mRNA expression was quantified by qRT-PCR in a subset of

tissues. As predicted, *GPX4* mRNA expression peaked in the testes, but was also high in adipose tissue and the adrenal cortex (Fig. 4.8C). *GPX1* mRNA expression was significantly higher than *GPX4* expression in the adrenal cortex, suggesting it is the predominant GPX in this tissue. Preliminary data (n=1) suggested GPX2 and 3 expression was much lower than that of *GPX1* and 4 in the adrenal cortex, similar to most tissues (Fig. 4.8D).

These data suggest *GPX1* is highly expressed in the adrenal cortex compared to other tissues and is more highly expressed than *GPX4* in the adrenal cortex.

4.3.3 Generation of stable knockdown H295R cell lines using a lentiviral delivery system

4.3.3.1 H295R Human Adrenal Carcinoma Cell line

H295R cells were chosen as a human adrenal model because they express all of the necessary steroidogenic enzymes for glucocorticoid, mineralocorticoid and androgen steroid production, secreting 20 steroids in total, representing all three adrenal zones (Wang and Rainey, 2012). The cell line is derived from an adrenocortical carcinoma belonging to a 48 year old black female and was originally established as the NCI-H295 cell line (Wang and Rainey, 2012). These cells are aneuploid hypertriploid with a modal chromosome number of 62 (Wang and Rainey, 2012). The H295R cell line is a substrain developed for a lower doubling time and greater attachment. H295Rs are supplemented with Nu serum or Ultra-G to increase growth rate, leading to a doubling time of 2 days (Wang and Rainey, 2012). For cell maintenance conditions see section 2.1.1.

H295Rs are not responsive to ACTH due to low expression of *MC2R*, however these cells do respond to forskolin treatment, a cAMP pathway activator (Wang and Rainey, 2012). Forskolin can induce the production of cortisol, 11β-hydroxyandrostenedione, DHEA, DHEAS, corticosterone, 11-deoxycortisol and androstenedione (Wang and Rainey, 2012). Hence, the cell line makes a good model for steroid synthesis.

To investigate the role of GPX1 in the adrenal cortex, *GPX1* expression was knocked down in human adrenocortical cells (H295R). Poor transfection efficiency is a common difficulty associated with the H295R cell line when using traditional cationic lipid transfection methodology. Therefore, stable cell lines were generated using lentiviral transduction, using pGIPZ plasmids expressing shRNAs targeting one or more regions of the *GPX1* gene.

4.3.3.2 Optimisation of puromycin selection

The pGIPZ shRNA lentiviral vectors used for stable KD cells lines contain not only the shRNA but also a puromycin resistance gene, making it possible to select cells which express the shRNA and a GFP tag allowing easy identification of transfected cells. Before generating stable cell lines, the optimal concentration of selection antibiotic puromycin was determined by a kill curve. The kill curve was designed to quantify the minimum concentration of puromycin needed to cause significant cell death in 3-4 days and to have killed all cells by day 7. H295R cells were seeded in triplicate in 24-well plates and subjected to doses of puromycin ranging from 0 to 10µg/ml.

From observation it was evident that a dose above 2.5µg/ml was neccessary to cause cell death in 3 days (Fig. 4. 9). Based on these data, selection was started at 4µg/ml, which could be increased to 5µg/ml if required. The efficiency of the treatment was easily determined by visualising the cells under a fluorescent microscope, as the shRNA are expressed with a GFP tag.

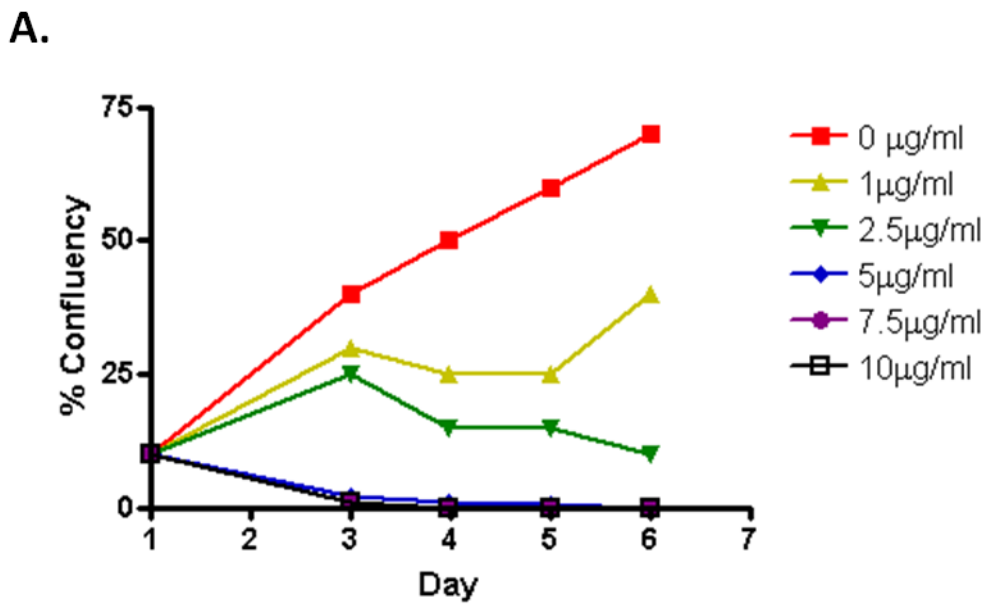

Figure 4. 9: Puromycin Kill curve.

Cells plated at a density of 20,000 were subjected to doses of puromycin ranging from 0 to 10µg/ml. Massive cell death was observed for doses of 5µg/ml and above, suggesting a dose between 2.5µg/ml and 5µg/ml was suitable for puromycin selection. Data is based on visual observation of cells treated in triplicate.

4.3.3.3 Generating stable cell lines

Three stable cell lines were created using lentiviral transduction (section 2.1.7.), each expressing different combinations of shRNAs targeting one or more regions of the *GPX1* gene. An additional 'scrambled' (SCR) cell line was created as a negative control, which stably expressed a shRNA targeting a nonspecific sequence.

The following combinations of shRNA were used to create the respective cell lines:

Cell line:	shRNA ID:
KD-10	#10
KD-0910	#09 and #10
KD-070910	#07, #09 and #10

(Sequences detailed in section 2.1.7.2)

To determine knockdown efficiency, mRNA expression of *GPX1* relative to *GAPDH* was measured by quantitative real time PCR (qRT) using primers specific to *GPX1* and *GAPDH*. SCR and *GPX1* knockdown (KD) cells, were seeded in 6 well plates and grown to 90% confluency, then lysed for RNA extraction and cDNA synthesis. qRT-PCR showed that mRNA levels were reduced by approximately 50% in *GPX1* KD cell lines compared to SCR, with the highest KD of 54% seen in KD-10 cells (Fig. 4.10Ai).

shRNA sequences were chosen that were specific to *GPX1*, however mRNA levels of *GPX4*, the second most highly expressed GPX, were checked by qRT-PCR to confirm any experimental findings from functional assays were the result of *GPX1* KD alone. mRNA levels of *GPX4* were unchanged in *GPX1* KD cells compared to SCR (Fig. 4.10Aii). This also suggests that *GPX4* is not upregulated in absence of *GPX1* expression. The subsequent effect of mRNA KD on protein levels was determined by Western blot. Cell lysates from 6 well plates were collected and immunoblotted using anti-GPX1 and anti-actin antibodies. Western blot analysis showed an >80% decrease in GPX1 protein abundance in all three *GPX1* KD cell lines compared to SCR with KD070910 cells showing the highest knockdown of 92% (Fig. 4.10B).

These data show successful generation of *GPX1* KD model in H295R cells with no compensatory increase in *GPX4* mRNA expression.

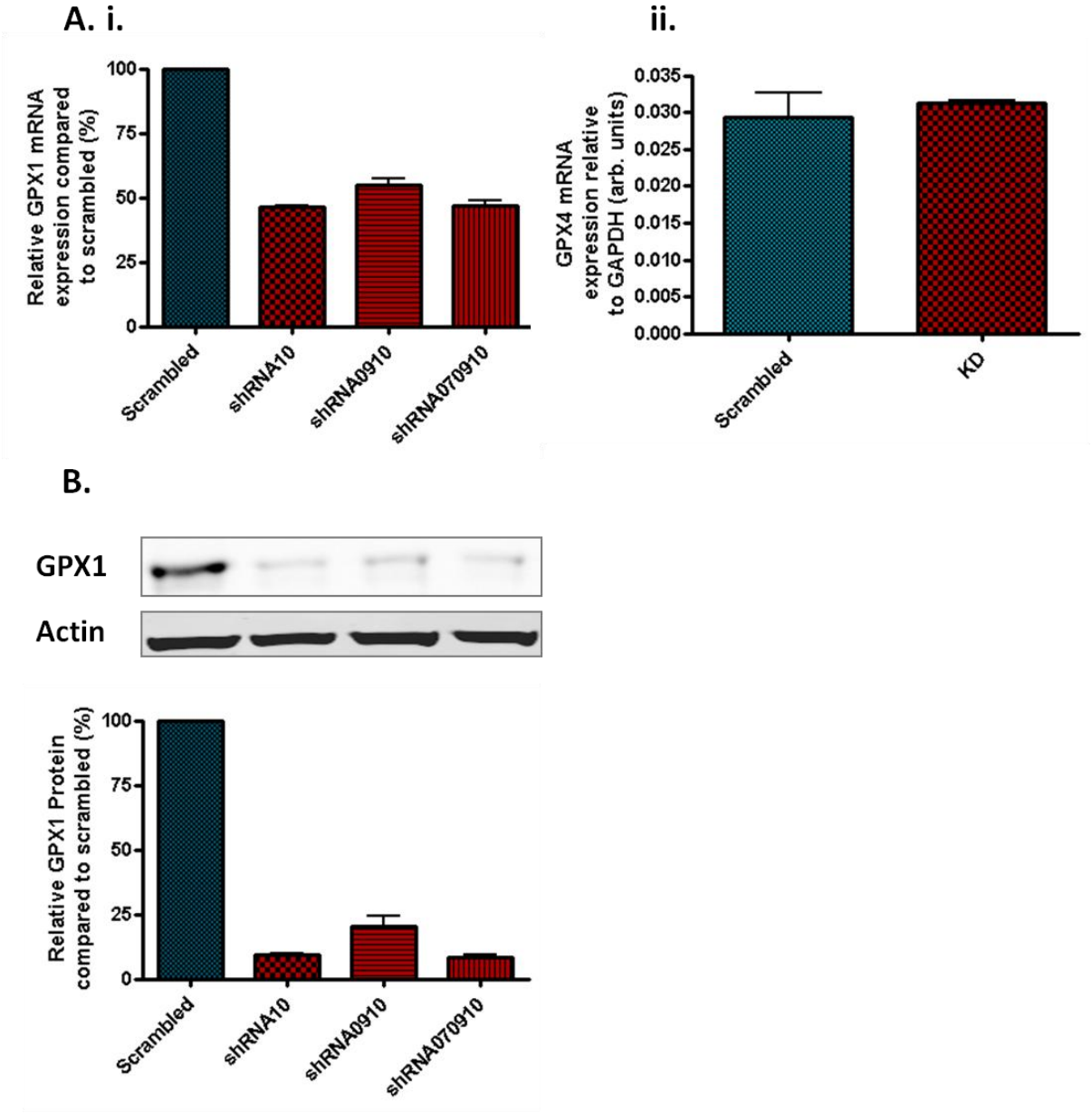

Figure 4. 10:*GPX1* knockdown in human adrenocortical carcinoma cells

RNA and protein extracts were collected from cells harvested after stable transduction of shRNA and cDNA was generated. mRNA and protein knockdown were assessed relative to a scrambled negative control. A. Knockdown validation by real time PCR analysis measuring *GPX1* mRNA expression relative to *GADPH* (n=3 ± s.d.) B. Knockdown validation by Western blot and densitometric analysis of GPX1 protein levels relative to β-actin loading control (n=4 ± s.d.). C. Real-time PCR analysis of *GPX4* mRNA levels relative to *GAPDH* following *GPX1* knock down (n=3 ± s.d.) .

4.3.4 Total GPX activity in *GPX1* Knockdown cells

As described above, GPX1 is one of 8 glutathione peroxidases capable of reducing hydrogen peroxide in conjunction with several other antioxidant systems. It is therefore uncertain whether loss of GPX1 alone would compromise antioxidant defense in the adrenal cortex. To investigate the GPX1 contribution to total GPX activity in the adrenal, SCR and *GPX1* KD cell lines were assessed for total GPX activity by an NADPH coupled assay system.

The GPX assay is a commonly used technique based on the original method established by Paglia and Valentine (1967). The protocol can be used on homogenised tissue, plasma or cell lysates. Details of the protocol used for this chapter are described in section 2.7.3.1. All GPXs reduce hydrogen peroxide using glutathione as a co-substrate. In a coupled reaction, glutathione reductase reduces oxidized glutathione simultaneously oxidizing NADPH to $NADP^+$ (Fig. 4.11). This replenishes the glutathione store, ready for GPX1 to recycle. NADPH absorbs UV light in its reduced form but not its oxidised form, hence the decrease in reduced NADPH levels following GPX activity is associated with a decrease in absorbance at 340nm. The assay is based on this inverse relationship between activity of GPX and levels of NADPH.

To determine GPX activity, the absorbance of NADPH (A340nm) was plotted against time, with the rate of reaction equal to the maximum change in absorbance between two time points within linear regression (V_{max}). The units of enzyme per milligram protein were calculated using the extinction coefficient of NADPH at 340nm (section 2.7.3.1). Purified GPX enzyme was used as a positive control.

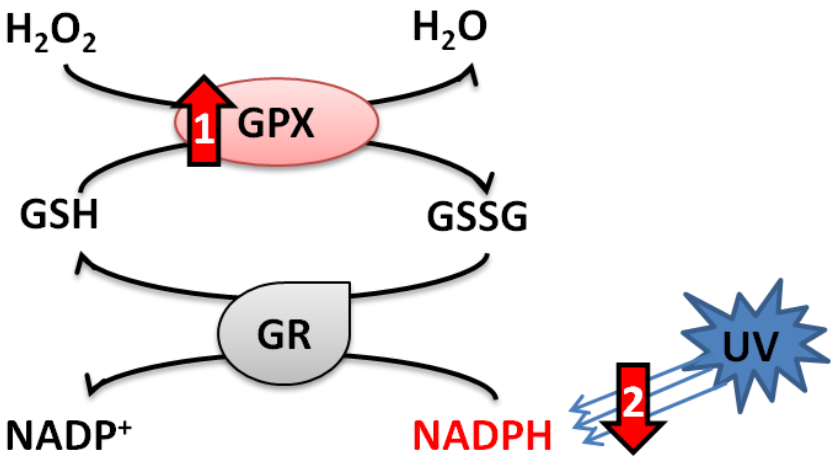

$$2GSH + H_2O_2 \xrightarrow{GPX} GSSG + 2H_2O$$

$$GSSG + \beta\text{-}NADPH \xrightarrow{GR} \beta\text{-}NADP^+ + GSH$$

Figure 4. 11: Spectrophotometric NADPH-coupled GPX assay.

GPXs reduce H_2O_2 simultaneously consuming glutathione (GSH) as an electron donor. Oxidised glutathione (GSSG) is reduced by glutathione reductase which uses NADPH as a donor. The subsequent decrease in reduced NADPH, which absorbs light at 340nm, can be measured as an indicator of GPX activity. The higher the GPX activity, the more GSH oxidised leading to greater GR activity and increased oxidation of NADPH to $NADP^+$. GSH, reduced glutathione; H_2O_2, hydrogen peroxide; GPX, glutathione peroxidase; GSSG, oxidised glutathione; β-NADPH, β-nicotinamide adenine dinucleotide phosphate, reduced form; β-nicotinamide adenine dinucleotide phosphate, oxidised form.

Different cell types have different levels of GPX activity (Sandström *et al.*, 1987), therefore it is important to optimise the assay to ensure appropriate sensitivity. High concentrations of reducing agents such as DTT can reduce GPX activity, and increasing pH will increase the spontaneous reaction between hydrogen peroxide and reduced glutathione. Indeed, initial

assay test runs presented a high level of background activity in the blank sample, which contained only reagents from the cocktail and hydrogen peroxide. The assay cocktail was a sodium phosphate buffer containing all proteins needed for the enzymatic reaction including; NADPH, GSH and glutathione reductase, as well as sodium azide, to inhibit catalase activity.

To find optimal assay conditions, three variables were investigated: concentration of H295R cell lysates, concentration of DTT, and pH.

For a positive control in all conditions, purified glutathione peroxidase from bovine erythrocytes was used. Figure 4.12A shows that in positive control samples (GPX1), a pH greater than 7 leads to a decreased rate of reaction (V_{max}), and an increased rate of reaction in the blank (Fig. 4.12A), suggesting a spontaneous reaction between hydrogen peroxide and glutathione is occurring. Generally, a higher concentration of DTT (1mM), gave higher GPX activity for H295R lysates (Fig. 4.12A).

In terms of assay sensitivity, the optimal cell density in 1mM DTT/sodium phosphate buffer appeared to be between variable**,** but concentration higher than 3.6 x 10^6 lead to a reduced reaction rate. This trend was seen in lysates at pH6.5, 7 and 7.5 in 1mM DTT. The highest detection of activity was in pH7.5 with 1mM DTT and 2.4 x 10^6 cells**,** with the largest difference between the sample and the blank (Fig. 4.12B). However, the rate of reaction in the blank sample at this pH was very high (Fig. 4.12A), with the linear phase of the reaction ending in one minute (not shown). With the reaction ending too quickly, it could be possible that data from the start of the reaction would be lost.

Based on the above data, it was decided that the optimum conditions for the GPX assay were sodium phosphate buffer (pH 7.0) with 1mM DTT and lysate from 3.6 x10^6 H295R cells.

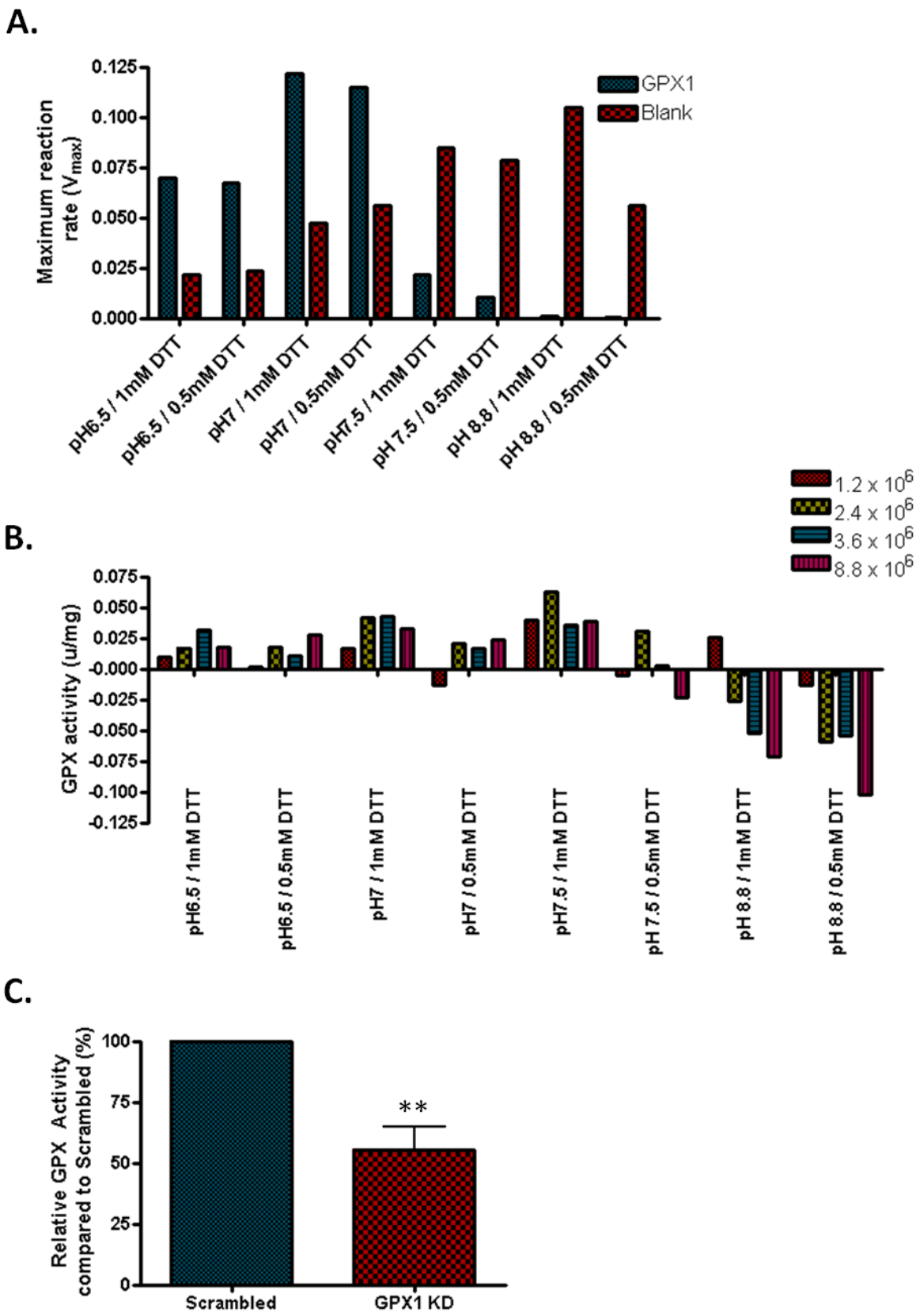

Figure 4. 12: NADPH coupled assay for total GPX activity in *GPX1* KD cells.

Spectrophotometric enzymatic assay for total GPX activity following treatment with substrate H_2O_2. Cells harvested in sodium phosphate buffer were sonicated and protein

extracts mixed with GSH, NADPH, glutathione reductase and sodium azide. Reactions were started with the addition of H_2O_2 (0.042%). Rate of absorbance of NADPH at 340nm over a 5 min period was determined and normalised to total protein concentration (mg) using a Bradford assay. A. Maximum rate of reaction (V_{max}) for purified GPX1 (3u/ml) positive control and blank (no GPX/cell lysate) negative control samples in 8 different sodium phosphate buffers, calculated as the maximum change in absorbance/time (performed in duplicate). B. Total GPX activity per mg total protein for lysates of different cell densities in 8 different sodium phosphate buffers (performed in duplicate). Cell density indicated by colour: red, 1.2 x 10^6 cells; yellow, 2.4 x 10^6 cells; blue 3.6 x 10^6 cells; purple, 8.8 x 10^6 . C. Percentage total GPX activity in *GPX1*-KD cells relative to in SCR control (normalised to total protein concentration). GPX activity was significantly lower in the knockdown cell line ($p<0.01$; n=3 ± s.d.).**

Using the optimised conditions, lysates from SCR and KD10 cells were collected and assayed (section 2.7.3.1). Data analysis showed 50% less GPX activity (u/ml) in the KD cell line calculated from the rate of absorbance over a 5 minute period following addition of H_2O_2 (Fig 4.16C). This suggests that GPX1 accounts for the remaining 50%, and is the predominant GPX in the adrenal cortex. It also suggests that the other GPXs cannot compensate for loss of GPX1. Hence, a significant portion of antioxidant defense in the adrenal cortex would be lost with a non-functional GPX1.

4.3.5 Effect of *GPX1* knockdown on cell viability

Evidence suggests GPX1 can modulate both cell proliferative and apoptotic pathways. A catalogue of studies investigating *GPX1*$^{-/-}$ *in vivo* and *in vitro*, have shown that loss of GPX1 increases apoptosis (de Haan *et al.*, 2004; Faucher *et al.*, 2005; Fu *et al.*, 2001). I therefore hypothesised that *GPX1* KD would increase oxidative stress in the adrenal and could lead to increased apoptosis and hence a decrease in cell viability in H295R KD cell lines.

To test whether *GPX1* KD has an effect on cell viability and proliferation, SCR and KD cells were plated at a density of 5000 cells per well, and grown for 24 hours, then subjected to 100µM H_2O_2 and grown for a further 24 hours. Cell proliferation was determined by spectrophotometric MTS assay (section 2.7.4), measuring the number of viable, metabolically active cells.

The MTS assay showed no difference in the number of metabolically active cells between SCR and KD cell lines when untreated, however a marked decrease in viability was seen in KD cells when subjected to H_2O_2 treatment (Fig. 4.13A) suggesting that KD cells are more susceptible to cell death when exposed to oxidative stress.

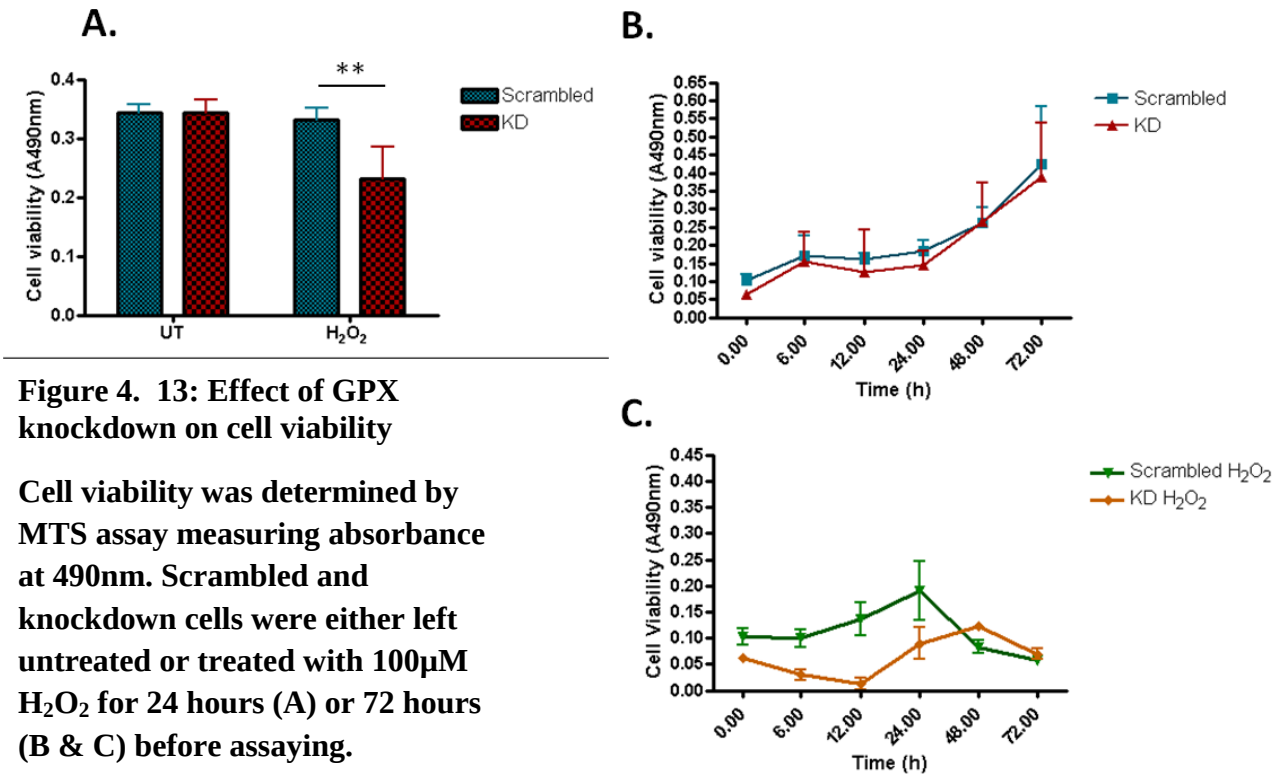

Figure 4. 13: Effect of GPX knockdown on cell viability

Cell viability was determined by MTS assay measuring absorbance at 490nm. Scrambled and knockdown cells were either left untreated or treated with 100µM H_2O_2 for 24 hours (A) or 72 hours (B & C) before assaying.

A. At 24 hours post treatment there were significantly less metabolically active KD cells than SCR ($p<0.01$, n=6 ±s.d). B.*GPX1* knockdown cells grow at a similar rate to scrambled when untreated (n=3 ±s.d) C. Scrambled cells have a delayed response to hydrogen peroxide treatment compared to *GPX1* knockdown cells (n=3 ±s.d)**

To examine this effect further, 3000 cells were plated and grown for 24 hours, then treated with H_2O_2 for 72 hours, to observe a trend in cell viability. When untreated, SCR and KD cells grew at a similar rate (Fig. 4.13B). Differences were seen after H_2O_2 treatment, when the number of metabolically active KD cells dropped between 0 and 12 hours, and slowly recovered by 48 hours (Fig. 4.13C). SCR cells also reacted to H_2O_2, but after 24 hours (Fig. 4.13C). This delayed response could suggest SCR cells are better protected from hydrogen peroxide than the *GPX1* KD cells.

The decrease in viability could suggest an increase in apoptotic cell death. To test whether *GPX1* KD cells had higher levels of apoptosis, KD and SCR cells seeded in 6 well plates were subjected to acute oxidative stress in the form of 1mM H_2O_2 for 30 minutes and left to recover for 24 hours. Cell lysates were assayed by Western blot for cleaved poly (ADP-ribose) polymerase (PARP) protein, which is a marker of cell death by apoptosis.

Basal untreated levels of cleaved PARP were significantly higher in KD cells compared to SCR. When treated with H_2O_2, both SCR and KD cells showed a marked increase in cleaved PARP relative to actin (Fig. 4.14A-B). The data suggests that absence of GPX1 may cause an increase in pro-apoptotic signaling under normal physiological conditions.

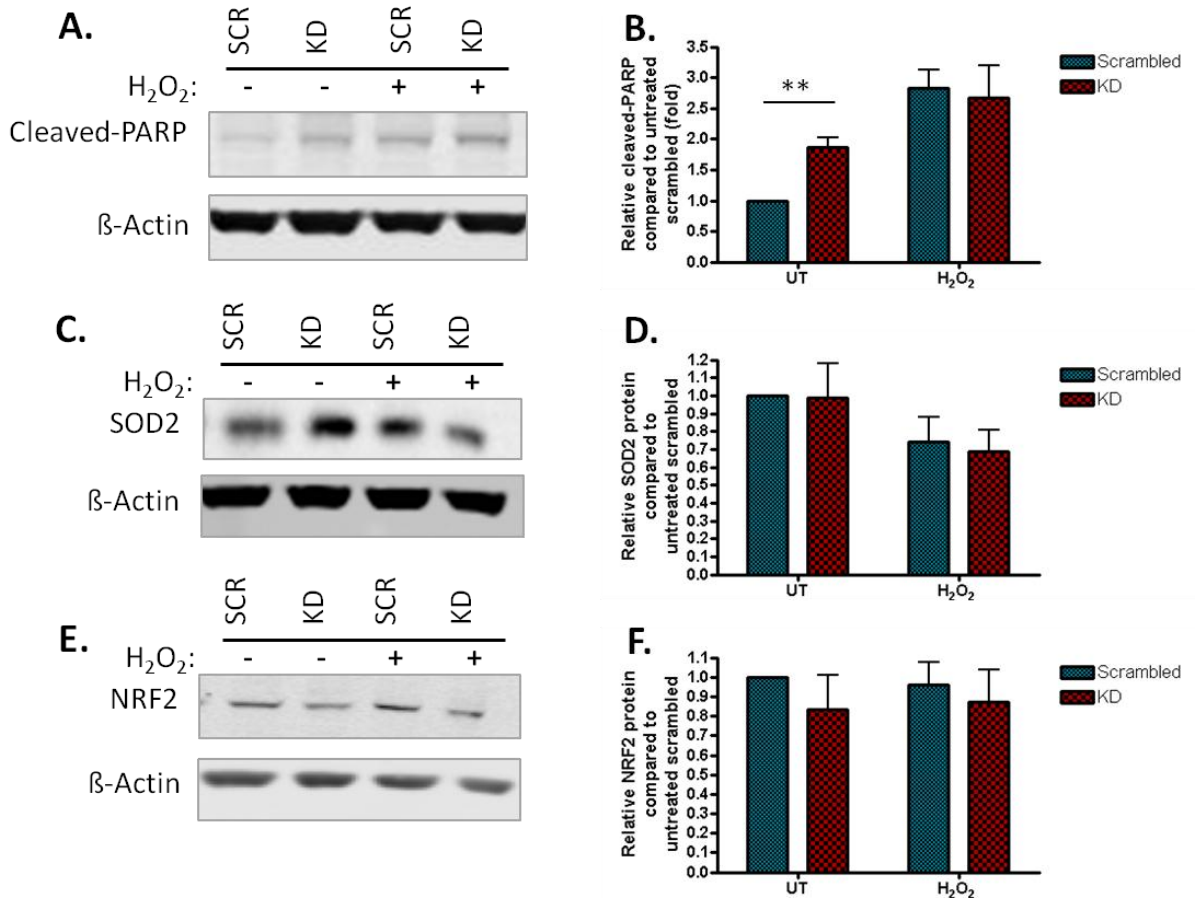

Figure 4. 14: Expression levels of markers of oxidative stress

Scrambled and knockdown cells were either untreated or subjected to 1mM H_2O_2 for 30 minutes and left to recover overnight. Lysates from scrambled and knockdown cells were immunoblotted with antibodies to cleaved-PARP (A), SOD2 (C), NRF2 (E) and protein levels were quantified relative to an internal control, β-actin, by densitometric analysis (B, D, F). There were significantly higher basal levels of cleaved-PARP ($p<0.01$) (A), but no significant differences in SOD2 (C) or NRF2 (E). (n=3, mean ±sd)**

To further investigate the effect of *GPX1* KD on oxidative stress in adrenal cells, the protein levels of several antioxidants were determined by Western blot. Increased levels of ROS may activate nuclear factor, erythroid 2-like 2 (NRF2), a redox sensitive transcription factor. NRF2 acts on antioxidant response elements in the promoters of many antioxidant genes to upregulate their transcription (Fig. 4.14), and inhibition of NRF2 can increase apoptosis in

lung cancer cell lines (Wang *et al.*, 2008). Previous studies have shown that NRF2 protein levels are upregulated by oxidative stress (Purdom-Dickinson *et al.*, 2007), however immunoblotting SCR and *GPX1* KD lysates with NRF2 antibody did not show any consistent differences between the cell lines (Fig. 4.14E-F). Analysing protein levels does not however consider the level of NRF2 activity, which is dependent on subcellular localisation as described in figure 4.15.

SOD2 is a potent antioxidant that converts superoxide radicals to H_2O_2 (Fig. 4.14) which goes on to be reduced by GPXs. It is therefore plausible, that loss of GPX1 activity would alter the balance of this reaction. An imbalance of GPX1/SOD2 is seen in the aldosterone switch off phenomenon, where chronic ACTH stimulation results in increased *SOD2* and decreased *GPX1* mRNA levels, leading to higher levels of H_2O_2, and down regulation in *CYP11B2* (Suwa *et al.*, 2000). Levels of SOD2 were determined for SCR and KD cell lines by immunoblotting lysates with anti-SOD2 antibody. Levels of SOD2 were reduced by H_2O_2 treatment in all cell lines, but there was no difference between SCR and KD cells (Fig. 4.14C-D).

To summarise, the data suggest no difference in cell viability between SCR and KD cells under normal conditions however a KD cells show greater vulnerability to H_2O_2 toxicity. *GPX1* KD lysates had a higher concentration of cleaved-PARP, an apoptotic marker, however there was no compensatory increase in protein abundance of antioxidants NRF2 or SOD2, which are upregulated on oxidative stress.

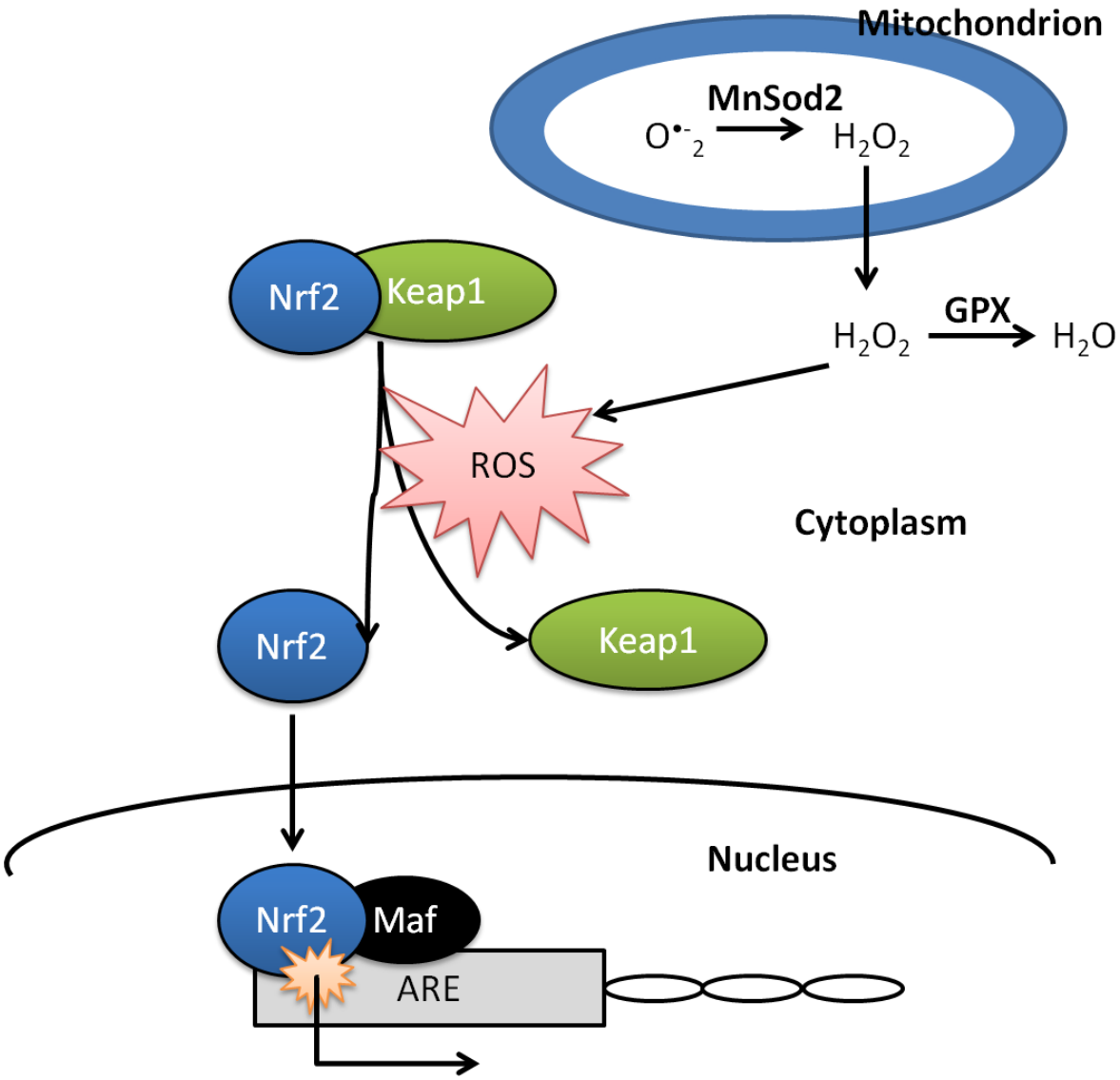

Figure 4. 15: Illustration of Nrf2 activation by ROS.

Under normal physiological conditions Nrf2 is bound to a repressor molecule KEAP1, however under increased oxidative stress Nrf2 dissociates from KEAP1 and translocates to the nucleus where it dimerises with other transcription factors such as small Maf. Nrf2 binds to antioxidant response elements (AREs) in the promoters of antioxidant genes and activates their transcription. Nrf2, nuclear factor, erythroid 2-like 2; Maf, small Maf; ARE, antioxidant response element; ROS, reactive oxygen species; $O^{\bullet -}_2$, superoxide anion; H_2O_2, hydrogen peroxide; MnSOD, manganese SOD; KEAP1, Kelch-like ECH-associated protein 1 Adapted from (Kensler *et al.*, 2003; Kim and Vaziri, 2010)

4.3.6 Assessing steroidogenic capacity in knockdown cells

In vitro studies on human Leydig tumour cells have shown that H_2O_2 administration impairs steroidogenesis through reducing protein levels of StAR (Diemer *et al.*, 2003; Shi *et al.*, 2010; Tsai *et al.*, 2003). For insight into a mechanism through which a mutation in *GPX1* causes FGD, the protein levels of StAR were checked in KD and SCR lysates by Western blot. Cells were grown in 6 well plates, treated with 1mM H_2O_2 for 30 minutes and left to recover overnight, and lysates were immunoblotted with anti-StAR and anti-actin antibodies.

StAR protein levels were significantly decreased in *GPX1* KD cells both when untreated and when treated with H_2O_2 suggesting that absence of GPX1 affects StAR protein levels, potentially by increasing levels of H_2O_2 (Fig. 4.16A-B). Quantifying mRNA expression of StAR by qRT showed no difference between SCR and KD cell lines, suggesting StAR levels were modulated by GPX1 post-transcriptionally (Fig. 4.16C).

These data suggest a potential mechanism whereby absence of GPX1 reduces StAR protein abundance potentially through increasing levels of H_2O_2.

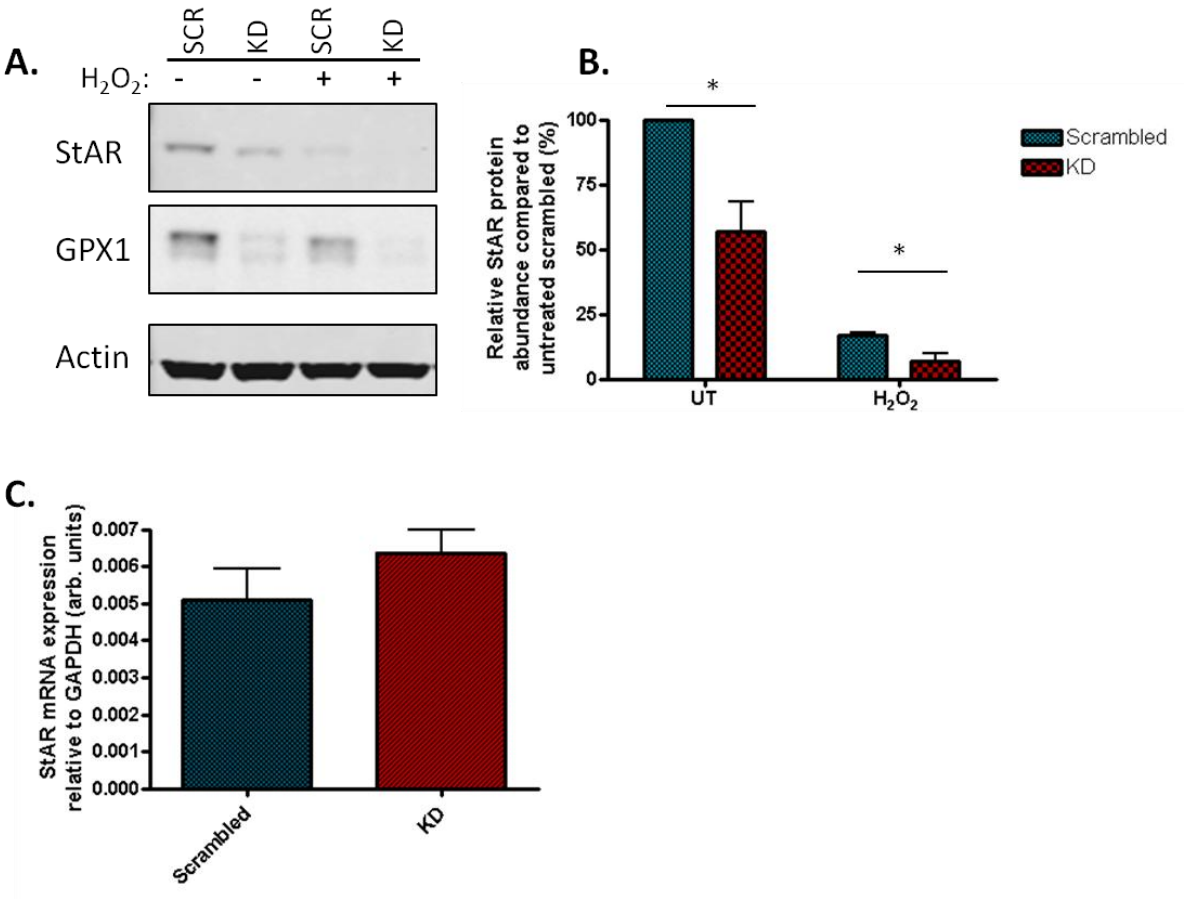

Figure 4. 16:*GPX1* Knockdown cells have decreased StAR protein levels

Scrambled and knockdown cells were treated with 1mM H_2O_2 for 30min and allowed to recover overnight. A. Lysates were immunoblotted with anti-StAR antibody, anti-GPX1 to illustrate *GPX1* knockdown, and anti-actin as a loading control. StAR protein levels were significantly decreased in *GPX1* knockdown cells either when treated with H_2O_2 or untreated (*$p<0.05$). B. Densitometric analysis of Western blot. (*$p<0.05$, n=3 ± SD) C. qRT PCR analysis of StAR mRNA expression in scrambled and knockdown cells showed no differences in expression. cDNA was generated from RNA extracts (n=3 mean±sd)

4.3.7 Functional characterisation of *GPX1* mutation

This is the first description of a 12bp deletion in *GPX1*. I explored the effect of the deletion on expression and function of the enzyme, by overexpressing epitope tagged WT and R130-L133del genes in HEK293 cells. The expression, subcellular localisation and ability to oligomerise were tested.

4.3.7.1 Cloning *GPX1* constructs

To investigate R130-L133del protein expression, WT and mutant *GPX1* were cloned into p3XFLAG-CMV and pCMV-tag3B (Myc-tag) mammalian expression vectors.

Following difficulties amplifying full length WT *GPX1*, the gene was amplified from HEK293 cDNA using a two-step overlap PCR method, where exon 1 and 2 were amplified separately using exon spanning primers, and then fused in a subsequent PCR reaction, illustrated in figure 4.17. Primers were designed to include the 3' UTR, which contains the SECIS sequence vital for incorporation of the selenocysteine residue. See detailed methodology in section 2.4.2.

GPX1 was subcloned into pGEM-Te (Promega) by conventional a/t cloning strategies. Sequencing revealed an unknown SNP at position 110 (p.Gly110Cys) which was rectified by site directed mutagenesis in order to establish a WT construct.

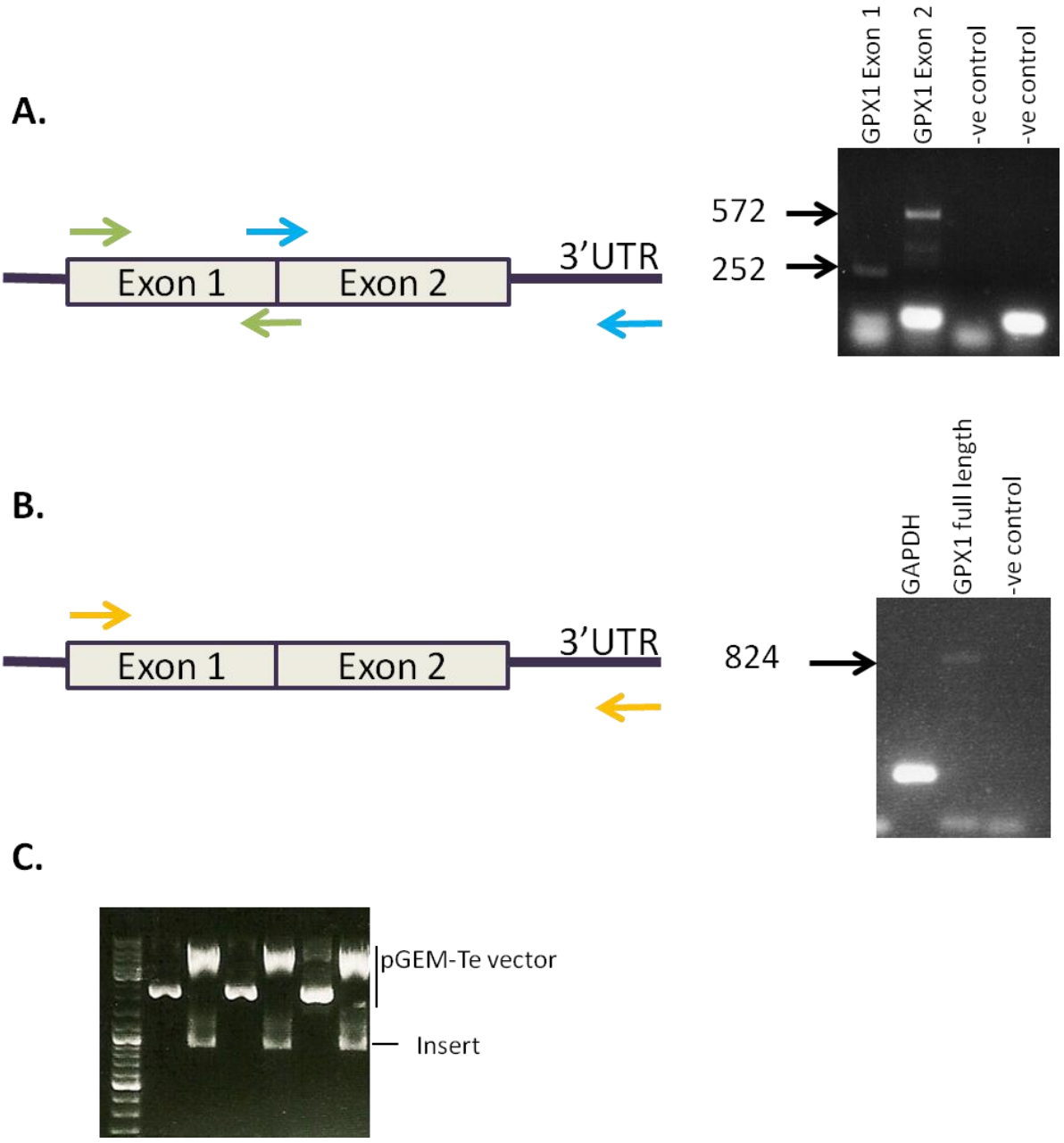

Figure 4. 17: Cloning of WT and R130-L133del *GPX1*-FLAG constructs

Wild-type and R130-L133del vectors were constructed by 2-step overlap PCR (A & B) and subcloned into pGEM-Te (C) vector then transferred to pCMV-3xFLAG and pCMV-tag3B). A. WT gene was amplified in two sections: exon 1 and exon 2-3' UTR, including SECIS element. B. Two amplified fragments fused in second PCR. The R130-L133 deletion was created using the same strategy with primers bordering the deletion. C. Wild-type gene subcloned into pGEM-Te. Plasmid DNA was extracted from positive

clones and digested with *Not1* restriction endonuclease to release *GPX1* insert. Clones that released inserts were sequenced.

R130-L133del was created by fusion PCR using the WT vector as a template. Initially two fragments were amplified either side of the deletion, which were fused in a second PCR and religated into PGEM-T easy vector.

GPX1 WT and R130-L133del genes were subsequently cloned into p3xFLAG-CMV vector at *Not1* sites and pCMV-tag3b at *Bam*H1 and *Hind*III sites. Inserting fragments at *Not1* sites led to a frameshift which was corrected by site directed mutagenesis (section 2.4.9).

4.3.7.2 Expression of *GPX1* constructs

GPX1 p3xFLAG-CMV constructs (WT-FLAG and R130-L133del-FLAG) were tested for expression by Western blot analysis using FLAG antibody, 48h after transfection into HEK293 cells. Western blot analysis showed that the WT gene was expressed as a 25kDa protein, the predicted molecular weight of GPX1 plus the triple FLAG tag. The R130-L133del GPX1 was also expressed, however at a slightly lower molecular weight, consistent with 4aa deletion, and presenting a lower intensity band relative to the loading control GAPDH (4.18A).

The expression of WT and R130-L133del genes was investigated over time. HEK293 cells transfected with one or other vector were lysed at 6, 12, 24, 48 and 72 hours. The abundance of the R130-L133del protein was lower than the WT throughout the time course (Fig. 4.18B).

To compare the function of these proteins in future experiments, for example enzymatic activity, it would be necessary to gain similar protein levels. In order to optimise a transfection protocol where this would be achieved, HEK293 cells were transfected with different quantities of the WT plasmid DNA to produce a similar intensity band as R130-L133del at 24 hours. These experiments showed that the input of WT plasmid had to be reduced 100x to gain similar protein levels to R130-L133del (Fig. 4.18.C-D).

To summarise, both WT-FLAG and R130-L133del-FLAG constructs express proteins, the latter detected at much lower abundance following transfection at the same DNA concentration.

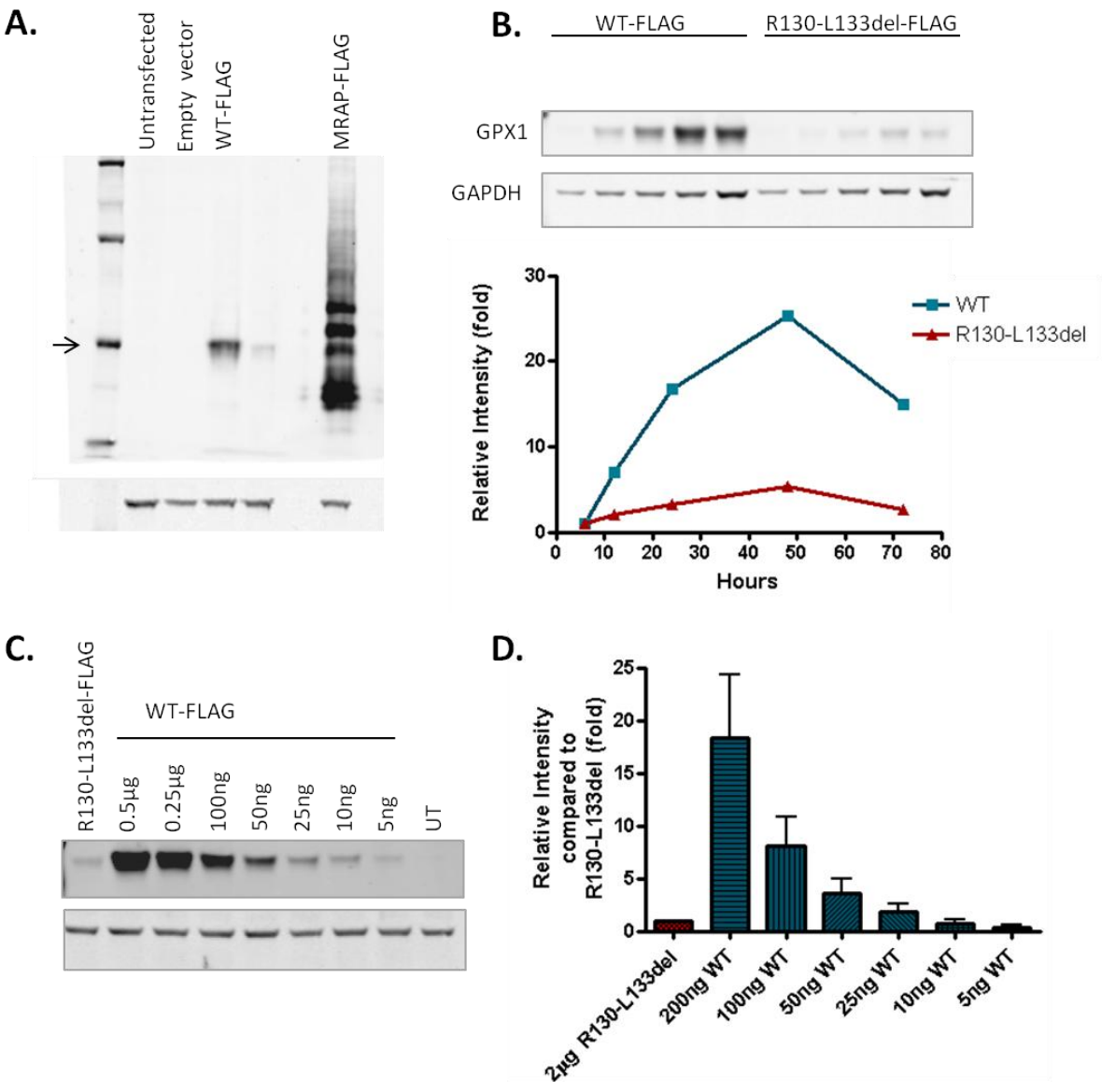

Figure 4. 18: Expression of WT-FLAG and R130-L133del-FLAG in HEK293 cells

***GPX1* wild-type and R130-L133del FLAG-tagged constructs were expressed in HEK293 cells, and lysates were immunoblotted for anti-FLAG and anti-GADPH as a loading control. A. WT-FLAG is expressed at 25kDa. Lower protein levels were seen for R130-L133del-FLAG at a slightly lower molecular weight. B. GPX1 protein expression over**

time relative to GAPDH loading control. Upper panel showing Western blot with FLAG and GAPDH antibodies. Lower panel showing densitometric analysis of GPX1 protein levels relative to GADPH loading control, at time points 6, 12, 24, 48 and 72h C. Upper panel showing Western blot with GPX1 antibody of an assay to reduce the quantity of wild-type DNA transfected to gain similar expression levels to R130-L133del-FLAG, lower panel GAPDH loading control. (n=3, mean ±sd). D. Densitometric analysis of GPX1 relative to GAPDH loading control.

4.3.7.3 Subcellular localisation of R130-L133del

Following the discovery that R130-L133del protein is found at lower concentrations than WT, I explored whether the mutation altered the subcellular localisation of the protein. GPX1 is a predominantly cytosolic enzyme but also resides in mitochondria and peroxisomes (Lubos *et al.*, 2011). HEK293 cells transfected with either WT or mutant vector and the mitochondrial fluorescent marker MitoDSred were stained with antibody to FLAG and cy-labelled secondary antibody, in addition to DAPI, which stains nuclei.

Confocal analysis revealed the R130-L133del protein had similar staining patterns to wild-type (Fig. 4.19), suggesting the mutation did not affect subcellular localisation. For both WT and R130-L133del proteins mitochondrial staining was minimal. This could be due to the low percentage of protein localised to this organelle.

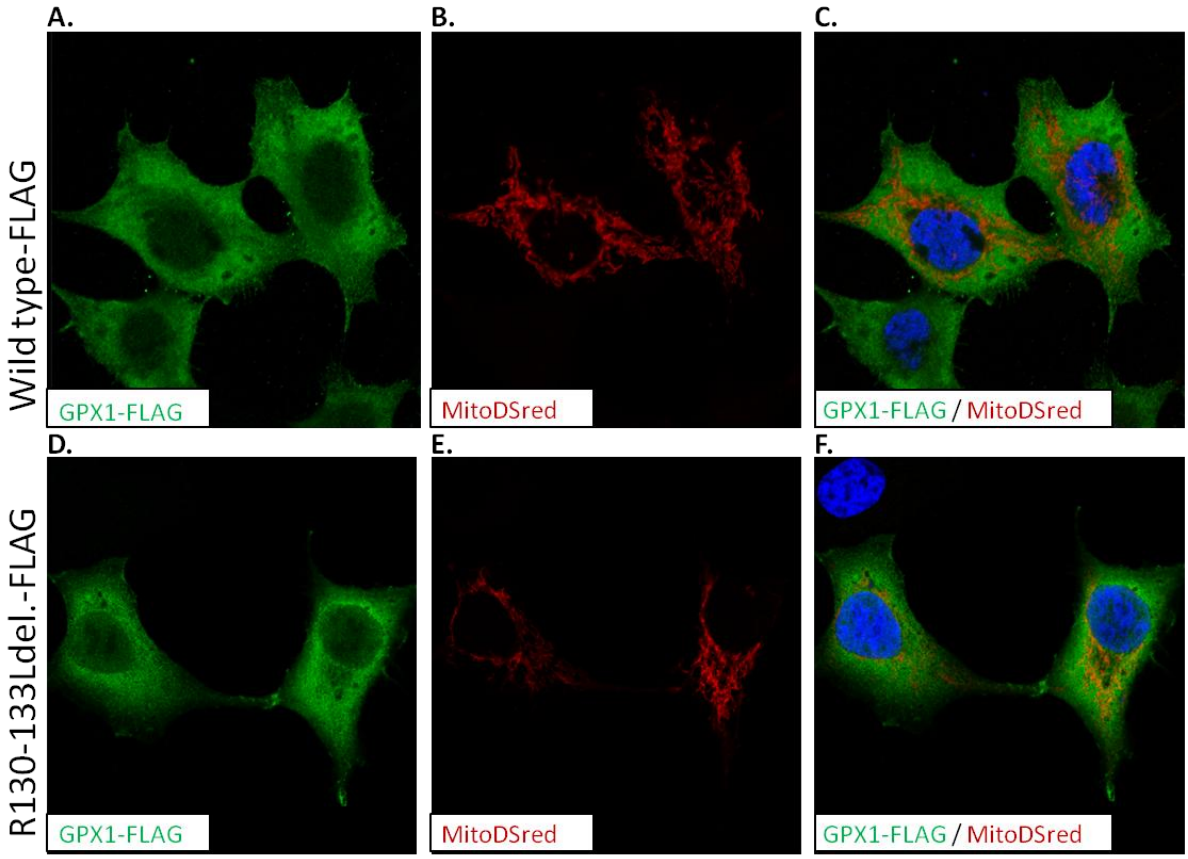

Figure 4. 19: Subcellular localisation of R130-133Ldel-FLAG in HEK293 cells

Images show expression of wild-type (A-C) and R130-133Ldel (D-F) FLAG-tagged vectors in fixed and permeabilised HEK293 cells. Cells were stained with anti-FLAG antibody and Cy2 secondary antibody (green), cotransfected with fluorescent mitochondrial marker MitoDSred (red) and nuclei stained with DAPI (blue).

4.3.7.4 Degradation of R130-L133del.

The effect of the R130-L133del mutation on *GPX1* is unknown, but the reduced protein abundance suggest that there is either translational repression or that the protein is inappropriately targetted for degradation. GPX1 fills the criteria for nonsense mediated decay because it has a UGA codon in the middle of an exon that is at least 50 bp away from the intron (Lubos *et al.*, 2011; Silva and Romão, 2009). However, the SECIS sequence in the 3' UTR prevents nonsense mediated decay. To assess the R130-L133del degradation, HEK293

cells in 12 well dishes were transfected with either WT or R130-L133del-FLAG, or an empty vector as a negative control. Cells were grown overnight, then treated to compare the half-life of the proteins with either protein synthesis inhibitor cycloheximide (CHX), to halt protein synthesis or MG132, a 26S proteasome inhibitor, to inhibit degradation. As a vehicle control, cells were treated with DMSO. After 4 hours treatment with 25µg/ml CHX a reduction in WT and R130-L133del protein abundance was seen (Fig. 4.20A), consistent with inhibition of protein synthesis. Similarly treatment with 25µM MG132 clearly increased abundance of R130-L133del, consistent with blockade of the degradation pathway.

To investigate further, the experiment was repeated with 100X less WT plasmid DNA to gain similar protein levels to R130-L133del before treatment. A higher concentration of CHX was used to increase the effect seen, based on optimisation experiments using the WT protein (data not shown). Cells were lysed at 1, 2, 5 and 10 hours after treatment and the percentage of GPX1 protein remaining was analysed by Western blot. After CHX treatment, the abundance of both WT and R130-L133del diminished, but a significant decrease in protein abundance was only seen for R130-L133del suggesting levels were decreasing at a faster rate (Fig. 4.20C-D and I). In support of this there was virtually no R130-L133del protein in CHX treated cells after 10 hours (Fig. 4.20C). The half life, calculated from 0.69/K where K is the rate constant in $Y= Y_0e^{-kx}$, was far shorter for R130-L133del than WT, at 2.714 hours compared to 11.15 hours respectively. However, there was no significant difference between the reduction in WT and R130-L133del by 10 hours (Fig. 4.20I).

MG132 alone increased R130-L133del protein levels significantly compared to DMSO treatment (Fig. 4.20I-J), but reduced WT protein levels significantly, possibly due to the toxicity of MG132. Why this should not affect the R130-L133del is not clear. MG132 did increase the intensity of a band between 10 and 15kDa for R130-L133del, however expressing R130-L133del with a myc epitope tag did not produce a similar band, suggesting it was an artifact, perhaps a degradation product, of FLAG (Fig. 4.20B).

To summarise R130-L133del had a shorter half-life than WT GPX1, and responded to MG132 treatment inhibiting the 26S proteasome, suggesting it was degraded at a faster rate.

CHX treatment significantly reduced R130-L133del protein abundance compared to DMSO treated cells, but had no significant effect on WT abundance. Despite this, there was no significant difference between WT and R130-L133del abundance after 10h CHX treatment. This may suggest R130-L133del undergoes some degree of degradation to exhibit a shorter half-life than WT, but the low abundance of R130-L133del seen upon transfection may also be due to poor translation.

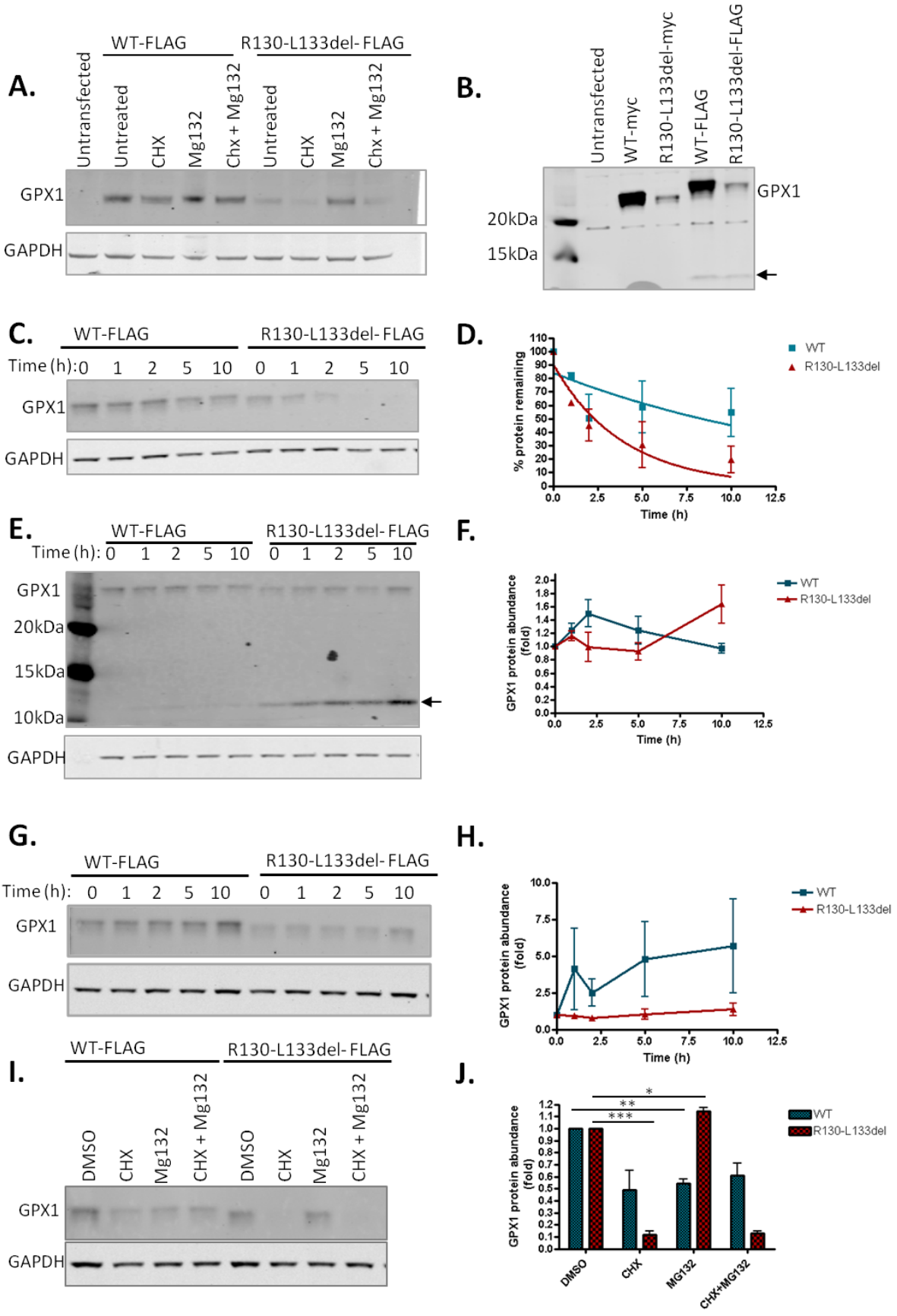

Figure 4. 20: Degradation of R130-L133del-FLAG in HEK293 cells.

A. HEK293 cells transfected with 25ng WT or 2µg R130-L133del-FLAG treated for 4h with 25µg/ml CHX, 25µM MG132, both or DMSO as a vehicle control. An increase in R130-L133del protein levels is seen following treatment with MG132. B. Expression of WT and R130-L133del FLAG and MYC-tag vectors in HEK293 cells, lysates immunoblotted with anti-FLAG and anti-MYC. C-J. Cells transfected with 1µg R130-L133del-FLAG plasmid DNA and 10ng WT to gain similar protein concentration, were treated with 50µg/ml CHX, 25µM MG132, both, or DMSO as a vehicle control for 10 hours. Lysates were collected at 0, 1, 2, 5 and 10 hours after treatment and immunoblotted with anti-FLAG antibody and anti-GAPDH antibody as a loading control (C, E, G, I). Protein concentration was quantified by densitometric analysis normalising to GAPDH intensity (D, F, J). Images show protein abundance of WT and R130-L133del-FLAG over time following CHX (C&D), MG132 (E&F) and DMSO (G&H) treatment. The half-life of R130-L133del was 2.714h compared to 11.15h for WT. A 12kDa band (indicated by arrow) was present for R130-L133del which increased in intensity after MG132 treatment (E), this is likely an artifact (see B). At 10 hours (I&J), protein concentration of R130-L133del was significantly lower with CHX treatment and significantly higher with MG132 treatment compared to DMSO treated cells, however there was no significant difference between R130-L133del and WT protein concentration (I&J). (n=3 ±sd *p<0.05, **p<0.01, ***p<0.001)

4.3.7.5 Oligomerisation of GPX1

R130-L133del is located in alpha helix-3 and the beginning of a region before β-strand 6 which is associated with oligomerisation (Fig. 4.21). This region shows structural variability which ultimately determines whether the GPX is a monomer like GPX4, a dimer like GPX5 in plants or a tetramer like the majority of GPXs. Within dimeric and tetrameric proteins this loop is conserved. It contains two flat regions allowing an interface for adjacent monomers, and also stabilises interactions with the other two monomers forming the tetramer. Tetramerisation is primarily determined by the presence of the 'PGGG' motif

which is upstream of alpha helix-3, and forms a hairpin-like structure which through hydrophobic interactions and hydrogen bonds stabilises tetramer formation.

The deletion R130-L133del, would effectively remove one loop of alpha-helix-3 and the first residue of the oligomerisation domain (Fig. 4.21). It is therefore unclear whether the mutation would affect oligomerisation. To further investigate the effect of this mutation, I intended to perform co-immunoprecipitation of WT and R130-L133del proteins, by cloning the genes in both FLAG and myc tagged vectors. Unfortunately, initial experiments to optimise coimmunoprecipitation with WT proteins, were not successful. In search of alternative methods, cells were transfected with WT- and R130-L133del-FLAG plasmids, lysed in a non-reducing sample buffer and immunoblotted with anti-FLAG and anti-GPX1 antibodies to detect native GPX1 complexes.

A.

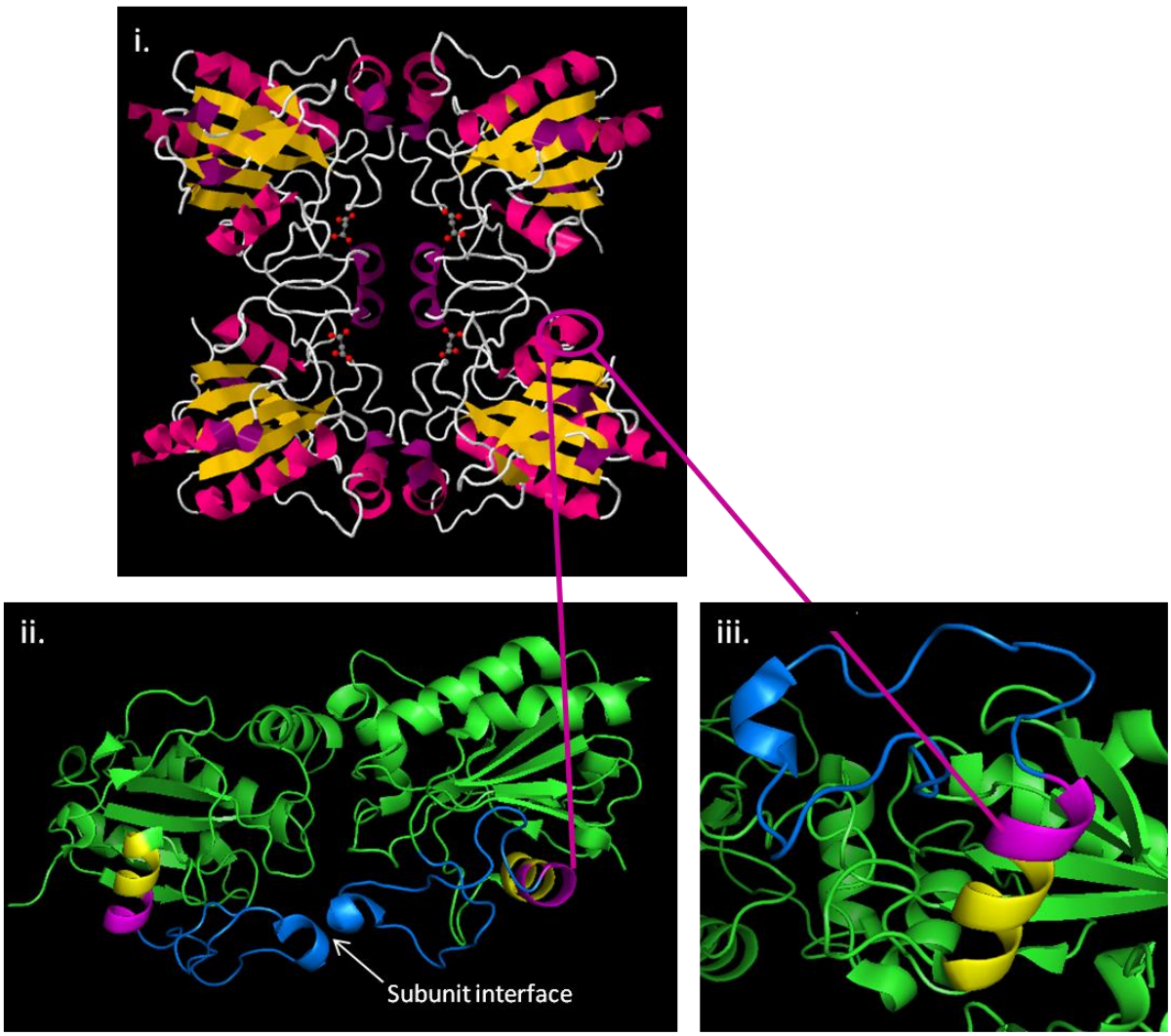

Figure 4. 21: Ribbon diagram of glutathione peroxidase 1.

Positions 130-133, affected by R130-L133del, are in alpha-helix 3 and an adjacent oligomerisation domain, a region responsible for subunit interface. (i.) GPX1 tetramer with positions 130-133 depicted by pink circle. (ii.-iii). GPX1 dimer showing positions 130-133 in pink, alpha-helix 3 in yellow and oligomerisation domain in blue with subunit interface indicated by an arrow. Deletion R130-L133del removes one loop of the alpha helix (depicted in pink). Diagrams of GPX1 crystal structure obtained from Tetramer image obtained from protein data bank (Kavanagh et al.). Dimer illustrated using PyMol software.

GPX1 migrated as a smear, possibly due to posttranslational modifications or ubiquitination. Blotting with FLAG antibody showed the most striking bands were between 22kDa and 25kDa, consistent with the monomer (Fig. 4.22A). An additional band is seen between 75-100kDa that may represent the tetramer, with a predicted molecular weight of 83-95kDa (Flohé *et al.*, 1971). This band is detected with both FLAG and GPX1 antibodies meaning it is specific for the FLAG-tagged GPX1 and is similar for both the WT and R130-L133del proteins, suggesting the R130-L133del protein is capable of forming a tetramer (Fig. 4.22B). Interestingly, with the GPX1 antibody alone a strong band is seen just below, which may represent the endogenous tetramer (Fig. 4.22B red arrow). In addition to these bands, a strong band is seen in both WT and R130-L133del channels between 50-75kDa, presumably a dimer, which may form before tetramerisation (Fig. 4.22B).

To summarise, R130-L133del migrates in a similar pattern to WT GPX1, showing bands consistent with the predictive molecular weight of the tetramer. Hence, this data suggests R130-L133del is capable of oligomerisation.

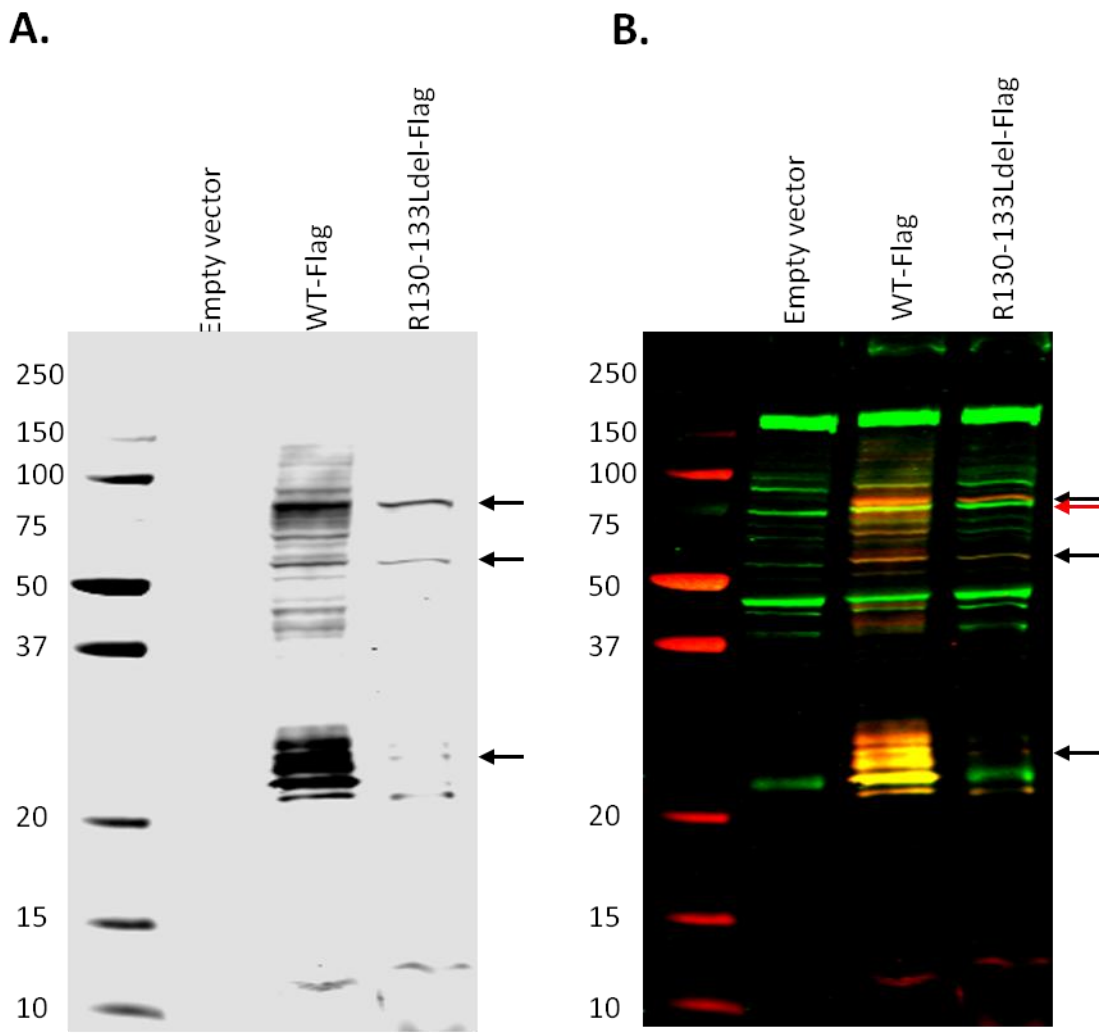

Figure 4. 22: R130-133Ldel can form a tetramer when expressed in HEK293 cells. **HEK293 cells were transfected with WT- or R130-L133del-FLAG tagged GPX1 vectors or an empty vector negative control. Lysates were collected in a non-reducing sample buffer and run on SDS-PAGE, then blotted with anti-FLAG and anti-GPX1 antibodies. A. Image showing FLAG detection only. Recombinant WT GPX1 is detected with strong bands between 22-25kDa, the monomer, and between 75-100kDa, potentially the tetramer (*black arrows)*. A strong band is also seen at approximately 50-60 kDa perhaps the dimer *(black arrow)*. No bands were seen for the empty vector negative control. B. Image shows co-staining with anti-FLAG in red and anti-GPX1 in green, with overlap in yellow. Overlap of FLAG and GPX1 detection confirms bands are specific for GPX1. A band that may correspond to the endogenous protein tetramer is depicted by the red arrow.**

4.4 Discussion

In the search for novel causes of FGD, a mutation in the antioxidant gene *GPX1* was discovered in a FGD patient with unknown aetiology.

4.4.1 *GPX1*$^{-/-}$ Mouse Model

An autopsy on the 5 month old sibling of the affected individual revealed small adrenals with loss of the ZF and disorganised cells in the ZG. Adrenals from *GPX1*$^{-/-}$ mice were analysed to check for a similar phenotype. However, immunostaining with zonal markers IZA-1 and CYP11A1 showed no abnormalities in 4 month old *GPX1* $^{-/-}$ mouse adrenals compared to WT and *GPX1*$^{-/-}$ cells had steroidogenic capacity. The mice were however, relatively young, and it has been documented in past literature that *GPX1*$^{-/-}$ mice do not show abnormalities until over a year of age (Esposito et al., 2000). H&E staining also confirmed normal morphology, in contrast to *NNT* deficient mice which have been previously noted to show a mild display of overcrowded and disorganised cells (Meimaridou *et al.*, 2012b).

Immunofluorescent staining for cleaved caspase-3, a marker of apoptosis, presented an unusual staining pattern in the *GPX1* knockout mouse adrenal, characteristic of vascular endothelial cells. Interestingly, *GPX1*$^{-/-}$ mice have an impaired ability to promote angioneogenesis, and isolated endothelial progenitor cells from *GPX1*$^{-/-}$ mice are more susceptible to hydrogen peroxide mediated apoptosis than WT cells (Galasso *et al.*, 2006). GPX1 is known to protect against vascular endothelial dysfunction, characterised by increased levels of ROS reducing the bioavailability of nitric oxide (NO), which mediates vasorelaxation. Agonists of NO that usually cause vasorelaxation, cause vasoconstriction in *GPX1* deficient (+/-) mice, and these mice have increased structural abnormalities in myocardial vasculature (Forgione *et al.*, 2002). Furthermore, the effect of angiotensin II, a ROS-inducing agent in vascular endothelial cells that leads to dysfunction, can be rescued by overexpression of *GPX1*, but augmented by GPX1 deficiency in mice (Chrissobolis *et al.*, 2008). It is interesting that angiotensin II acts on the zona glomerulosa in which most of the cleaved caspase-3 positive staining is seen. However, in order to confirm that the staining is

specific to vascular endothelial cells, counterstaining for endothelial cell marker PECAM-1 would be needed. By comparison, mice harbouring a natural loss of function mutation in antioxidant enzyme *NNT* elicit increased cleaved caspase-3 staining within the ZF cells of the adrenal cortex, from which corticosterone is secreted (Meimaridou *et al.*, 2012b). The effect of increased apoptosis in the vasculature supplying the adrenal is unknown.

GPX1$^{-/-}$ mice also showed a trend towards less corticosterone production, but this was not significant. The mouse model does not therefore recapitulate the human condition but displays a milder phenotype. This is similar to the situation seen with other knockout models used to study adrenal insufficiency syndromes, for example the *AAAS*$^{-/-}$ knockout mouse, has no adrenal abnormalities (Huebner *et al.*, 2006) and *NNT* knockout mice also show no major histopathologies (Meimaridou *et al.*, 2012b). Although *NNT* knockout mice had a 50% reduction in corticosterone levels, these mice were ACTH responsive and had relatively high basal and stimulated corticosterone levels (Meimaridou *et al.*, 2012b) in contrast to human FGD patients. It is also worth noting that in our experiment corticosterone levels were high for unstimulated mice, suggesting the mice were stressed before the assay.

4.4.2 Tissue Distribution of *GPX1*

In humans, previous studies have shown *GPX1* mRNA levels to be high in the liver, heart and kidney (Atanasova *et al.*, 2006). The quantitative real time PCR data showed that *GPX1* is ubiquitously expressed in human tissues, similar to the situation in marmoset and mouse tissues (Atanasova et al., 2006; Cheng et al., 1998). My data revealed *GPX1* expression to be highest in the adrenal cortex followed by spleen and adipose tissue. It has been suggested that the adrenal cortex has a greater need for antioxidant defense than other tissues, due its additional sources of reactive oxygen species from steroid biosynthesis (Azhar *et al.*, 1995). During steroidogenesis, electron transfer by CYP enzymes from the donor system is not completely coupled, leading to leakage of electrons and generation of ROS. 40% of electron flow from NADPH is lost to ROS in the hydroxylation of steroids by CYP11B1, which could explain why FGD patients with *NNT* mutations have isolated glucocorticoid deficiency

(Hanukoglu, 2006). High *GPX1* expression in the adrenal gland may act as a compensatory mechanism to tackle excess hydrogen peroxide generated by steroidogenesis.

Compared to GPX1, *GPX4* mRNA expression was also ubiquitous but generally lower in all tissues apart from the thyroid and testes. Highest expression was seen in the testes, in accordance with previous data (Atanasova *et al.*, 2006), as GPX4 is involved in spermatogenesis and acts as a structural component of the sperm midpiece (Imai and Nakagawa, 2003). Following the testes, expression was highest in adipose tissue and the adrenal gland.

Levels of *GPX1* mRNA were significantly higher than GPX4 in the adrenal, suggesting GPX1 is the predominant form in this tissue. Initial tests (n=1), suggest that GPX2 and 3 are expressed at low levels in comparison to GPX1 and 4. GPX2 is predominantly expressed in the gastrointestinal tract but also the liver (Chu *et al.*, 1997; Wingler *et al.*, 1999), whereas GPX3 is a glycoprotein expressed and secreted from the kidney (Avissar *et al.*, 1994).

Both GPX1 and 4 were highly expressed in the adrenal compared to other tissues. Although GPX1 is considered to be the predominant GPX, GPX4 has been well characterised in the literature as an important antioxidant that protects membranes from oxidative damage. Unlike GPX1, GPX4 is a monomer with 3 alternative splicing forms: cytosolic, mitochondrial and sperm-nuclear (Maiorino *et al.*, 2003). *GPX4*$^{-/-}$ mice are embryonic lethal, due to its unique ability to reduce complex membrane bound phospholipid and cholesterol hydroperoxides. Like GPX1, overexpression of *GPX4* can protect against apoptosis (Nomura *et al.*, 1999). Interestingly, although cGPX4 and mtGPX4 are ubiquitously expressed, mtGPX4 is predominantly expressed in the testes with limited expression elsewhere. This suggests that GPX1 is the predominant mitochondrial form in other tissues (Brigelius-Flohé and Maiorino, 2013)

The role of glutathione peroxidase in adipose tissue has been recently explored. Oxidative stress has been implicated in the pathogenesis of obesity-associated metabolic diseases. GPX1 overexpressing mice are insulin resistant with hyperinsulinaemia and hyperglycemia

(McClung *et al.*, 2004), whereas *GPX1*$^{-/-}$ mice have enhanced insulin sensitivity (Loh *et al.*, 2009). GPX1 can regulate insulin signalling through modulating H_2O_2 levels in pancreatic islets. An increase in hydrogen peroxide in *GPX1*$^{-/-}$ mice leads to the inactivation of redox sensitive PTEN, which is an inhibitor of insulin signalling. Thus, loss of GPX1 increases insulin signalling by increasing hydrogen peroxide levels. It is therefore surprising that *GPX1* is highly expressed in adipose tissue. Interestingly, the affected FGD patient with the *GPX1* mutation has been described as underweight.

One should also consider, that the adrenal is surrounded by a layer of adipose tissue. A study by Li *et al.* (2009), investigated whether adipocyte secretory products could influence adrenocortical steroidogenesis, and found in Y1 mouse adrenocortical cells, adiponectin reduced ACTH-stimulated secretion of corticosterone and changed the expression of steroidogenic genes (Li *et al.*, 2009). This is interesting considering human hepatic mRNA expression of adiponectin receptors has been shown to correlate with mRNA expression of *GPX1* (Carazo *et al.*, 2011).

4.4.3 *GPX1* Knockdown Model in Human Adrenal H295R cells

Given the high expression of *GPX1* in the adrenal cortex, it was hypothesised that *GPX1* has an essential role in the adrenal cortex in detoxifying ROS. The effect of *GPX1* knock down in human adrenocortical H295R cells was analysed to gain insight into its function in the adrenal. Stable lentiviral transduction of shRNA was carried out to maximise KD of *GPX1*. Three stable cell lines were generated achieving 50% mRNA and 90% protein KD, with cell lines 10 and 7910 showing the highest KD. The total GPX activity was measured by an NADPH coupled spectrophotometric assay, to determine the percentage to which GPX1 contributes in adrenocortical cells. There are 8 glutathione peroxidases in mammals which all reduce hydrogen peroxide to water. KD of *GPX1* by shRNA lead to 50% loss of total GPX activity in the human adrenocortical cell line, suggesting GPX1 is the predominant form of GPX in the adrenal, accounting for a large degree of hydrogen peroxide detoxification. mRNA levels of *GPX4* were unchanged by *GPX1* KD, suggesting its expression is independent of GPX1 and not upregulated by absence of GPX1. Similar findings are

reflected in other cell culture (Kelner et al., 1995; Lei et al., 1995), and mouse models (Cheng *et al.*, 1997a; Cheng *et al.*, 1997b). *GPX1* $^{-/-}$ or overexpressing mice show no differences in GPX3 and 4 mRNA expression compared to WT (Cheng *et al.*, 1997b). Taken together, this data suggests that GPX1 is the predominant form of GPX in the adrenal cortex, and its loss is not compensated for by the other GPXs.

GPX1 KD cells showed increased basal levels of cleaved PARP, a marker of apoptosis, and decreased cell viability when treated with hydrogen peroxide. Similarly, many cell lines cultured from *GPX1*$^{-/-}$ mice have increased susceptibility to ROS induced apoptosis, including astrocytes (Liddell *et al.*, 2006b), embryonic fibroblasts (De Haan *et al.*, 2003), hepatocytes (Fu *et al.*, 1999; Fu *et al.*, 2001) and at low oxidative conditions (6% O_2) in myoblasts (Lee *et al.*, 2006). *GPX1*$^{-/-}$ mice injected with paraquat have increased mRNA levels of pro-apoptotic markers GADD45, Bax, Bcl-w, cMyc, and pro-caspase-3 and decreased levels of apoptosis inhibitor BCl-2 compared to WT (Cheng *et al.*, 2003), and overexpressing *GPX1* protects against these effects, for example in breast carcinoma cells (Gouaze *et al.*, 2001).

Despite significantly higher basal levels of cleaved PARP in *GPX1* KD cells, there was no difference in viability seen between SCR and KD cells measured by MTS assay. This may suggest a subtle phenotype. The level of cleaved PARP increased after acute oxidative stress in both SCR and KD cells, but there was no significant difference between the cell lines. On the other hand, the MTS assay showed exposure to H_2O_2 significantly reduced viability in *GPX1* KD cells compared to SCR. This latter discrepancy could be due to different experimental conditions, as cleaved PARP was detected after acute stress (1mM H_2O_2) and a recovery period, whereas viability was measured after 24 hours in 100µM H_2O_2. A difference in levels of cleaved-PARP after H_2O_2 was apparent between cell lines, but there was so significant difference. An effect may have been seen with a lower dose of H_2O_2, to which SCR cells may have been more resistant.

GPX1 has been repeatedly demonstrated to influence apoptotic pathways through modulating levels of hydrogen peroxide, predominantly to promote survival (Emerling et al., 2005; Li et

al., 2001; Taylor et al., 2004). Furthermore, the antioxidant and anti-apoptotic effects of Se are mediated in part through GPX1 (Cheng et al., 2003; Kasaikina et al., 2011; Kayanoki et al., 1996; Kretz-Remy and Arrigo, 2001) . *GPX1*$^{-/-}$ mice have over 50% less Se in the liver than WT, suggesting the remaining Se is used by GPX1 (Cheng et al., 1997a; Cheng et al., 1997b). Paraquat induced liver aponecrosis is attenuated by Se injection in Se deficient WT mice to a greater degree than in Se deficient *GPX1*$^{-/-}$ mice, presumably due to increased GPX1 activity (Cheng *et al.*, 2003).

Previous studies have demonstrated that excess ROS in different forms can impair steroidogenesis (Diemer et al., 2003; Dorval et al., 2003; Shi et al., 2010). Mechanisms for impairment include the suppression of StAR protein, which has been shown in Leydig cells following exposure to hydrogen peroxide or perfluorododecanoic acid (PFDoA) (Diemer et al., 2003; Shi et al., 2010); and in mice after exposure to pro-oxidant cypermethrin (Jin *et al.*, 2011). However, the influence of ROS on StAR mRNA expression is not clear, as studies show opposing findings. Another theory is that ROS affects steroidogenesis directly by influencing the activity of steroidogenic enzymes (Chanoine *et al.*, 2001). My data show a 40% decrease in StAR protein abundance in *GPX1* KD cells compared to SCR at baseline and 90% decrease when treated with hydrogen peroxide, with no changes to StAR mRNA expression, suggesting that StAR is inhibited post-transcriptionally. StAR is expressed in three forms: a 37kDa precursor, 32kDa intermediate and a mature 30kDa form. The 37kDa form contains a mitochondrial targetting sequence that is proteolytically cleaved when it enters the mitochondrial matrix (Miller and Auchus, 2011). The 37kDa is considered to be the active form of StAR, but the conversion of StAR to its intramitochondrial forms is the final step of cholesterol transfer process (Diemer *et al.*, 2003). Hence the finding of a decrease in the 30kDa form suggests that loss of GPX1 increases levels of ROS that inhibits cholesterol transport.

GPX1 has already been linked to the regulation of steroidogenesis. Adrenocortical cells deprived of Se with subsequently lower *GPX1* expression levels have decreased steroid production after cAMP stimulation (Chanoine *et al.*, 2001), suggesting *GPX1* expression

influences steroid output. Azhar *et al.* (1995) also show that an age-associated decrease in corticosterone in rats is correlated with a decrease in mRNA and protein levels of several antioxidants, including *GPX1*.

The above data may give insight into a potential disease mechanism whereby loss of *GPX1* function leads to increased levels of hydrogen peroxide, inhibiting StAR, resulting in reduced steroidogenesis. Alternatively, I did not explore the possibility, that the disease mechanism could also act before steroidogenesis, affecting MC2R signalling directly. A study by Wiseman *et al.* (2011), showed trout exposed to dietary selenomethionine (Se-Met) had greater plasma corticosterone levels with increased transcript levels of *mc2r* but not *star*, *cyp11A1* or *cyp11b1*, which are usually up regulated on ACTH stimulation. This suggests that the Se-Met dependent increase in plasma corticosterone was independent of ACTH, but acting on the MC2R signalling pathway (Wiseman *et al.*, 2011). Furthermore, cadmium, a toxic ROS inducing endocrine disrupter, suppresses ACTH stimulated cortisol production by reducing *MC2R*, *StAR* and *CYP11A1* transcript levels in trout. The inhibition of ACTH-induced cortisol production was rescued by a cAMP analog, suggesting it exerted its effect upstream on MC2R signalling (Sandhu and Vijayan, 2011). Therefore, it would be interesting to explore the effects of oxidative stress on MC2R signalling and its expression at the cell surface.

4.4.4 Functional Characterisation of R130-L133del

To further characterise a disease mechanism, it was necessary to functionally characterise the R130-L133del mutation in *GPX1*. Expressing the R130-L133del gene in mammalian HEK293 cells showed reduced protein levels compared to WT, which suggested the protein was being degraded. In order to gain similar levels of the WT protein 24 hours after transfection, 100x less of the WT plasmid DNA was needed. Treating transfected cells with cycloheximide showed that the R130-L133del protein had a shorter half-life than WT, and treatment with MG132 to inhibit the 26S proteasome increased R130-L133del protein levels. Furthermore, CHX treatment significantly reduced R130-L133del abundance by 10h compared to DMSO treated cells, but did not significantly reduce WT abundance. Despite

these findings, there was no significant difference between WT and R130-L133del protein abundance 10 hours after cycloheximide treatment. It is therefore unclear whether the low protein levels of R130-L133del are due entirely to degradation, or whether other mechanisms such as poor translation may also contribute.

The protein could be degraded for a number of reasons. Even small changes to *GPX1* primary structure can change the functioning of this enzyme, for example the Pro198Leu mutation in exon 2 and a varying number of alanine repeats at the start of the protein, both affect enzymatic activity. The R130-L133del mutation is on alpha-helix3 and a stretch of sequence responsible for subunit interface, so it was predicted to affect oligomerisation. However, Western blot analysis of lysates run in a non-reducing buffer showed high molecular weight bands between 75-100kDa for the R130-L133del that mirrored that of WT, suggesting it was able to form the tetramer, discounting this theory.

Other possible reasons for degradation include changes to tertiary structure, for example the 12 base pairs of R130-L133del sit between the Trp and Gln residues of the predicted tetrad that form the GPX1 active site hence the deletion would change the distance between these residues, which could affect the final tertiary structure of the protein, and the positioning of the tetrad residues in the active site (Fig. 4.23). The region deleted also over crosses a c-Abl/Arg tyrosine kinase phosphorylation site at positions 132-145 key to GPX activity.

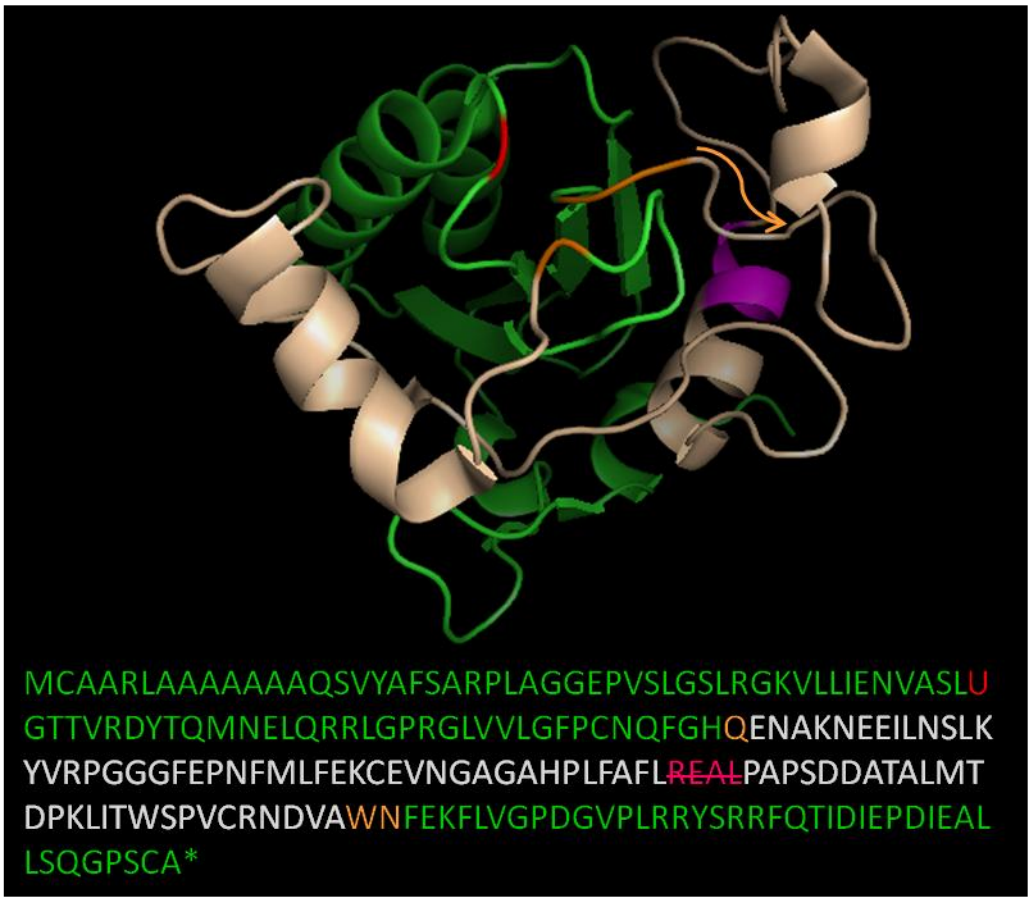

Figure 4. 23: GPX1 monomer and catalytic tetrad.

R130-L133del highlighted in pink, the catalytic tetrad residues Sec in red; glutamine, tryptophan and asparagine in orange; and region between catalytic tetrad residues altered in length by R130-L133del highlighted in white. The R130-L133del deletion would shift tryptophan and asparagine residues away from the active site, as indicated by the orange arrow.

Alternatively R130-L133del protein abundance may be low due to poor translation. *GPX1* is already a likely candidate for nonsense mediated decay, and selenocysteine incorporation is an inefficient process. Interestingly, naked mole rats have a naturally occurring premature stop gain mutation in *GPX1* at the end of exon 2, which is only five codons premature of the existing TAG codon. This mutation similarly results in a low protein levels when expressed in mammalian cells. Kasaikina *et al.* (2011), show that the enzymatic activity of the protein was unchanged compared to WT, however, mutating the selenocysteine to a cysteine at the active site, rescued protein levels. This suggests that the mutation affected selenocysteine

incorporation, leading to the reading of Sec as a stop, and subsequent nonsense mediated decay. It would therefore be of great interest to see whether the R130-L133del has a similar effect on selenocysteine incorporation, which could lead to reduced translation and explain low protein levels.

4. 4. 5 Conclusions

The majority of mutations causing FGD are in genes involved in the ACTH signalling-steroidogenic pathway. The discovery of a FGD patient with a mutation in *GPX1*, and the previous findings of FGD causing *NNT* and *TXNRD2* mutations, suggests that oxidative stress also plays a role in this disease pathogenesis. Oxidative stress has also been implicated in the pathogenesis of Triple A syndrome, another adrenal insufficiency disorder, and adrenoleukodystrophy, which involves the build-up of very-long chain fatty acids. The antioxidant genes causing these conditions are ubiquitously expressed, but impact specifically on the adrenal. The pathogenic mechanisms include peroxisomal dysfunction and a failure to import antioxidant DNA repair proteins. Therefore, disruption to redox status in several different compartments can impair steroidogenesis in the adrenal cortex.

Taken together, the data from this chapter suggests GPX1 has an important role in preventing oxidative stress in the adrenal cortex. R130-133Ldel renders GPX1 a shorter half-life, resulting in low protein levels, however the percentage of protein remaining after CHX treatment was not significantly different to WT, suggesting translational inefficiency is also involved. Low levels of GPX1 may cause FGD by increasing oxidative stress in the adrenal cortex, potentially by reducing StAR protein levels, inhibiting the first step of steroidogenesis. However, overall analysis of *GPX1*$^{-/-}$ adrenals and adrenocortical cells with *GPX1* KD revealed a relatively mild phenotype, raising the question of causality in the patient and the possibility that the disease might be di- or oligogenic.

Chapter 5: Digenic inheritance of mutations in antioxidant pathway genes in the proband with Familial Glucocorticoid Deficiency

5.1 Background

In the previous chapter, a mutation in *GPX1* in a patient with FGD of unknown aetiology was investigated. *GPX1* was a valid candidate gene because of the previous finding of mutations in antioxidant gene *NNT* causing FGD, however, investigation into the disease mechanism revealed that loss of *GPX1* presents a mild phenotype in adrenocortical cells. Although *GPX1* knockdown cells had increased susceptibility to hydrogen peroxide induced cell death and lower protein levels of StAR, $GPX1^{-/-}$ mice had relatively normal adrenal glands. At basal levels, *GPX1* knockdown cells had increased levels of apoptosis, but there was no difference to viability in normal conditions, which could suggest the effect of loss of GPX1 is subtle.

In addition to the above findings, sequencing 100 FGD patients of unknown aetiology did not reveal any homozygous or compound heterozygous mutations in *GPX1*, raising the possibility that *GPX1* was not the causal gene in our proband. Alternatively, it was worth considering that the disease in this proband was di- or oligogenic with *GPX1* in addition to other genes, perhaps in the same pathway.

5.2 Aims

This chapter aimed to clarify whether *GPX1* was the causal gene in the proband, or a second gene defect was present, by carrying out whole exome sequencing of the proband and his brother. The function of the second candidate gene identified would be explored in the context of the human adrenal cortex by shRNA knockdown of the gene, alone and in combination with *GPX1* in H295R human adrenocortical cells, gaining insight into a potential disease model of digenic inheritance.

5.3 Whole exome sequencing

5.3.1 An Introduction to Exome Sequencing

Next generation sequencing is now an accessible and accurate way of discovering disease causing mutations behind Mendelian disorders, and has the potential to accelerate biological

and medical research (Shendure and Lieberman Aiden, 2012). Given that 85% of disease causing mutations in Mendelian disorders are in protein coding regions or canonical splice sites (Cooper *et al.* 1995) , which cumulatively comprise only 1% of the human genome, exome sequencing is an efficient and cost effective technique for revealing novel candidate genes and mutations. Additionally, whole exome sequencing bypasses the need for linkage data and does not require large cohorts (Ng *et al.*, 2010; Ng *et al.*, 2009).

Exome capture and targeted enrichment by hybridisation can be achieved with the use of programmable microarrays. This method has been demonstrated in a proof-of-concept study by Ng *et al.* who used exome sequencing followed by a filtration strategy to accurately identify the known causal gene of Freeman-Sheldon syndrome (FSS) (Ng *et al.*, 2009). The authors also demonstrated the first successful application of exome sequencing to discover a causal gene for a Mendelian disorder of unknown aetiology, identifying *DHODH* as the causal gene for Miller's syndrome. Exome sequencing also has clinical implications as discussed by Choi *et al.* (2009) who illustrated the value of the technique in making an unanticipated genetic diagnosis of congenital chloride diarrhoea in a suspected Bartter syndrome patient.

Several cycle-array sequencing technologies have been developed in the past decade including 454 pyrosequencing, AB SOLiD and the Illumina Genome Analyser (SOLEXA technology), which all have the same basic work-flow. A 'shot gun' DNA library (of the individual to be sequenced) is prepared by DNA fragmentation and common adaptor sequences with sticky ends are ligated *in vitro*. Clonal 'sequencing features' or 'amplicons' are then generated in clusters by emulsion or bridge PCR (described below), attached to a substrate coated platform or micrometer sized beads. Clusters are then sequenced using alternating cycles of DNA synthesis catalysed by a polymerase or ligase and image acquisition of fluorescently labelled nucleotides (Shendure, 2011).

454 pyrosequencing uses emulsion PCR to generate amplicons bound to 28µm beads. Adaptor-flanked library fragments are amplified by PCR within a water-oil emulsion with the forward primer tethered to the bead. The template concentration is low enough to ensure a

maximum of one library fragment per bead. Once the emulsion is broken, beads are washed with a denaturant to remove unbound DNA strands, and a universal sequencing primer is hybridised to the common adaptor on all fragments for enrichment by hybridisation. Beads are pre-incubated with *Bst* polymerase and single stranded binding protein and transferred to an array of pico-litre sized wells containing ATP sulfurylase and luciferase. Sequencing involves the addition of one nucleotide per cycle, with incorporation leading to pyrophosphate release with subsequent ATP and luciferin production, generating light which is detected as a signal (Ng et al., 2009; Shendure, 2011). 454 pyrosequencing enables read lengths of 400bp within one day, however it comes at a price, costing >1$ per megabase, greater than other technologies (Shendure and Lieberman Aiden, 2012).

AB SOLiD technology also utilises emulsion PCR to enrich adaptor flanked sequence features, however beads are magnetic and 1µm in diameter. Once the emulsion is broken, the beads are washed and immobilised to a substrate coated planar platform. For sequencing, a universal primer is hybridised to all adaptors, and at every cycle DNA ligase ligates one of a mixture of octamers to the sequence feature. Fluorescent labels within the octamer correspond to the base identity at the octamer centre. At the end of each cycle images are taken in four channels corresponding to each base fluorescent label, and the label is then chemically cleaved between base positions 5 and 6 in the octamer. In the cycles that follow, octamers are ligated every 5 bases until the extended primer is denatured. The process is then repeated with ligation of the sequencing primer at a different position (eg. +1 or-1) in the adaptor allowing sequencing of bases between those already sequenced (Shendure, 2011). SOLiD technology is significantly cheaper than 454 pyrosequencing at <$0.10 per megabase but read length is a short as <200bp.

For this project, I employed SOLEXA technology, also known as the Illumina genome analyser. In contrast to the above techniques, amplified sequence features are generated by bridge PCR, in which forward and reverse primers are bound by linkers to a solid substrate platform resulting in clusters at specific locations on the surface. For sequencing, features are linearised to single strands and sequencing primers hybridise to the common adaptor regions,

then amplification occurs through *Bst* polymerase. Sequencing involves the addition of four chemically modified nucleotides, which each possess a 'reversible terminator' cleavable moiety that only allows a single incorporation per cycle. Each type of nucleotide is labelled with a different fluorescent wavelength which is detected through four channels. After extension and image acquisition, the reversible terminator and fluorescent label are cleaved by denaturation with formaldehyde and the next cycle begins. The Illumina Genome analyser has 8 lanes on a single flow cell, which can be used to sequence 8 libraries at once (Shendure, 2011). Similar to SOLiD technology, Illumina sequencing is <$0.10 per megabase, however reads are longer between 200-400bp.

All the above sequencing technologies have the ability to generate millions of sequencing reads that can be enzymatically manipulated *in vitro*, which was not possible for Sanger sequencing. The disadvantages of next generation sequencing compared to Sanger sequencing is the lower accuracy and short read length, features that may be optimised in time (Shendure, 2011).

5.3.2 Whole exome sequencing of the proband

To search for alternative candidate genes, next generation whole exome sequencing was employed, sequencing all protein coding regions in the proband and his brother. For exome capture, 5µg genomic DNA was required to be fragmented and hybridised to the Agilent V4 (51 Mbp) exome enrichment microarray and washed to remove un-tethered strands. The targeted DNA was then enriched, eluted and amplified. Massively parallel resequencing of the enriched DNA was employed using one lane of the Illumina HiSeq2000 platform with SOLEXA technology.

For the proband a total of 49,087,900 reads, averaging 100bp in length, were mapped to the GRCh37/hg19 2009 human reference sequence, revealing 267,711 variants compared to wildtype, with an average coverage of 4.58. A filtration strategy was employed to minimise the number of variants for analysis. Typical of FGD, the inheritance pattern in this kindred

appeared to be autosomal recessive as both parents were unaffected and there was known consanguinity; hence, heterozygous variants were eliminated. FGD is a rare disorder and we hypothesized that, like all the mutations in *NNT*, the causal variant would be novel. We therefore searched for novel variants removing all common SNPs recorded in SNP databases. Synonymous coding variants were also removed, as were variants outside coding regions and splice sites. Variants with a coverage lower than 20 were excluded. This gave a total of 80 variants for analysis.

Of the 80 variants, 72 were non-synonymous coding region missense mutations (appendix 1.1), 5 were in-frame deletions (appendix 1.2), 1 was a frameshift mutation (appendix 1.3.), and 2 were stop gain mutations (appendix 1.4). Candidate genes were selected based on their known biological function. I hypothesised that the 'second hit' candidate gene would have a role in oxidative stress, similar to that of *NNT* or *GPX1*.

Only one variant fulfilled this criteria, with a coverage of 20 reads, a stop gain mutation (c.C199T; pQ67X (CAG>TAG); chromosome 10: 120,933,975) in exon 1 of peroxiredoxin 3 (PRDX3) (Fig. 5.1C). PRDX3 is a strong candidate gene because of its role as an antioxidant enzyme. Like the glutathione peroxidases, peroxiredoxins catalyse the reduction of toxic hydrogen peroxidase to water (Fig. 5.1B). PRDX3 is the mitochondrial isoform and a 2-Cysteine (2-Cys) subtype, utilising 2 cysteine residues for catalysis; an N-terminal peroxidatic redox active cysteine which functions as the active site, and a C-terminal 'resolving' cysteine (Cys_R) which reduces the oxidised Cys_p on an adjacent subunit, a crucial part of the catalytic cycle.

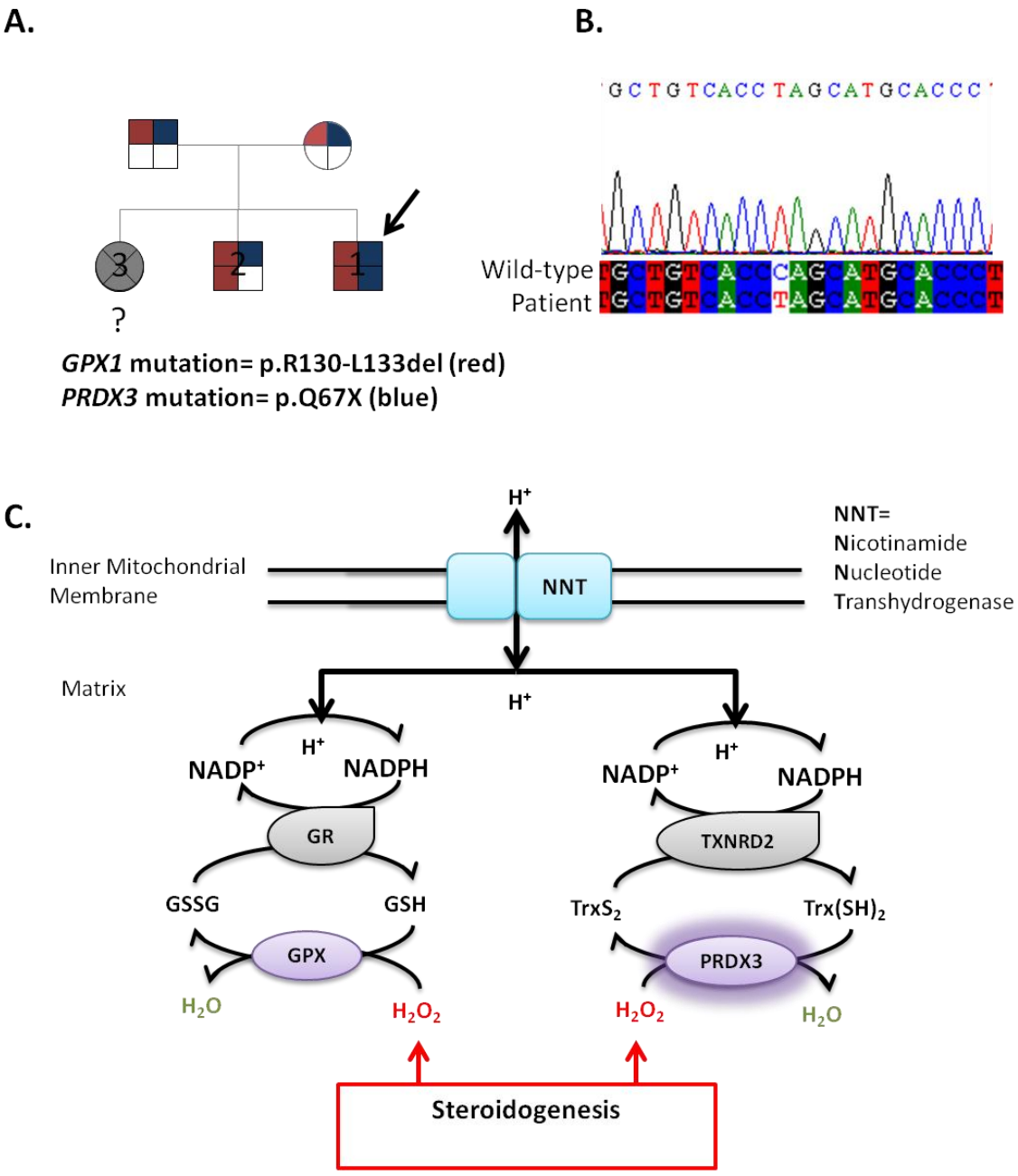

Figure 5. 1: A homozygous mutation in *PRDX3*

A. Pedigree of the family with the affected proband, homozygous for *GPX1* (red) and *PRDX3* (blue) mutations, and the unaffected sibling heterozygous for the *GPX1* mutation but homozygous for the *PRDX3* mutation. B. Partial DNA sequence

electropherogram for the affected patient and a wild-type control. C. Illustration of the NNT antioxidant pathway in mitochondria, with the candidate gene PRDX3 emphasized. Abbreviations include nicotinamide transhydrogenase (NNT), nicotinamide adenine dinucleotide phosphate ($NAPD^+$/NADPH), glutathione reductase (GR), thioredoxin reductase 2 (TXNRD2), glutathione peroxidase (GPX) and peroxiredoxin 3 (PRDX3). D. Illustration of *PRDX3* gene with c.C199T; p.Q67X mutation depicted by arrow and red box (introns not to scale).

The mutation results in the substitution of a glutamine residue for an amber stop codon, leading to an early truncation at position 67 of a 256aa protein and the ablation of the Cys_R residue key to the enzyme's function as a 2-Cys peroxiredoxin. The Q67X mutation was confirmed by PCR and Sanger sequencing with primers targeting exon 1. This variant was not present in SNP databases including dbSNP (www.ncbi.nlm.nih.gov/SNP/) and NHLBI GO-ESP (https://esp.gs.washington.edu/drupal/). Sequencing the family revealed that the parents were heterozygous for the mutation (Fig. 5.1A), however the unaffected brother was homozygous for the defect, hence the variant did not segregate with the disease (Fig. 5.A).

Sequencing 100 FGD patients with unknown aetiology revealed one more patient with a homozygous mutation in *PRDX3*, which was a missense mutation R214C. No mutation in *GPX1*, *NNT* or *TXNRD2* was discovered in this patient on sequencing and unfortunately it was not possible to check whether the variant segregated with the disease as the DNA of the family members was not available. It is unlikely this variant on its own is the cause of FGD and further investigation of gene variants in this patient is underway by whole exome sequencing (WES).

The discovery of the *PRDX3* mutation in the unaffected sibling raised a few questions. It could suggest that mutations in *GPX1* alone are in fact capable of causing FGD. However, the previous chapter illustrated that loss of function in *GPX1* presents a subtle phenotype. We therefore hypothesised that mutation in *GPX1* or *PRDX3* alone is insufficient to cause FGD, but digenic inheritance of both mutations could tip the redox balance and present a similar phenotype to that of *NNT* mutations.

5.4 Generation of *GPX1*/*PRDX3* knockdown cell lines by RNAi

To investigate the possibility of digenic inheritance, single *PRDX3*, *GPX1* and double *PRDX3* and *GPX1* knockdown H295R cell lines were generated by RNAi using lentiviral transduction of shRNA targeting these genes, similarly to section 4.3.3.3. For *GPX1* knockdown, shRNA10 targeting exon 2 was used which previously generated an mRNA knockdown of 54% and protein knockdown of 91%.

For *PRDX3* knockdown, a selection of six shRNAs targeting exons 4-7 and the 3' UTR (section 2.1.7.2, Open Biosystems) were tested for optimal knockdown. HEK293 cells grown on 6 well plates were transiently transfected with a 1µg of individual shRNA constructs or a scrambled (SCR) negative control shRNA using lipofectamine 2000 reagent and incubated for 48 hours before protein extraction.

Western blot analysis of lysates using an antibody to PRDX3 and β-actin (section 2.5.7) as an loading control showed highest knockdown in cells transfected with either shRNA constructs 3 or 6 which both target exon 4, reducing PRDX3 protein abundance by 59% and 67% respectively (Fig. 5.2A-B). These shRNA constructs were selected to generate stable *PRDX3* knockdown (*PRDX3*-KD) in the H295R cells by lentiviral transduction (see section 2.1.7).

Briefly, HEK293T packaging cells were transiently transfected with lentiviral shRNA constructs in a 5:4:3 ratio with p8.74 (Gag/Pol) and pMDG (VSV-G) packaging vectors. After 48 h of expression, supernatant containing viral particles was concentrated by centrifugation overnight and transferred to H295R target cells, which were incubated over a 4 day period for transduction (section 2.1.7). Cells that had incorporated the shRNA were screened for presence of a fluorescent GFP marker flanking the shRNA, and were selected with 4µg/ml puromycin over a two week time course, however little cell death was observed (section 2.7.3). The dose was subsequently increased to 7.5µg/ml and cells were grown until all showed green fluorescence. Untransfected H295R cells were used as a negative control to check for autofluorescence.

Stable KD of *PRDX3* and *GPX1* was assessed by Western blotting for protein expression and qRT PCR for mRNA levels. Stable KD and SCR negative control cells were grown on 6 well plates for 48 hours then lysed for analysis.

Lysates were immunoblotted with antibody to PRDX3 or GPX1 and actin as an internal control. Western blot analysis demonstrated a significant reduction in PRDX3 protein abundance by 84% in PRDX3 KD (*PRDX3*-KD) cells and 84% in double KD (*double*-KD) cells (Fig. 5.2 C&D). Interestingly, a significant reduction in PRDX3 protein levels was also observed in *GPX1* KD (*GPX1*-KD) cells (38%) (Fig. 5.2 C&D). GPX1 protein levels were reduced significantly by 75% and 54% in *GPX1*-KD and *double*-KD cells respectively, but there was no alteration to GPX1 protein levels in *PRDX3*-KD cells (Fig. 5.2C&E).

qRT PCR analysis using primers for *PRDX3* or *GPX1* and GAPDH as a control, showed *PRDX3* mRNA levels were significantly reduced by 68% in *PRDX3*-KD cells and 42% in *double*-KD cells (Fig. 5.2F). Unlike protein expression levels, PRDX3 mRNA levels were not significantly lower in *GPX1*-KD cells compared to SCR cells.

GPX1 mRNA levels were significantly reduced by 61% in *GPX1*-KD, but did not reach statistical significance for *double*-KD cells (27%) (Fig. 5.2G). Therefore, the main output measure used for this project was protein levels.

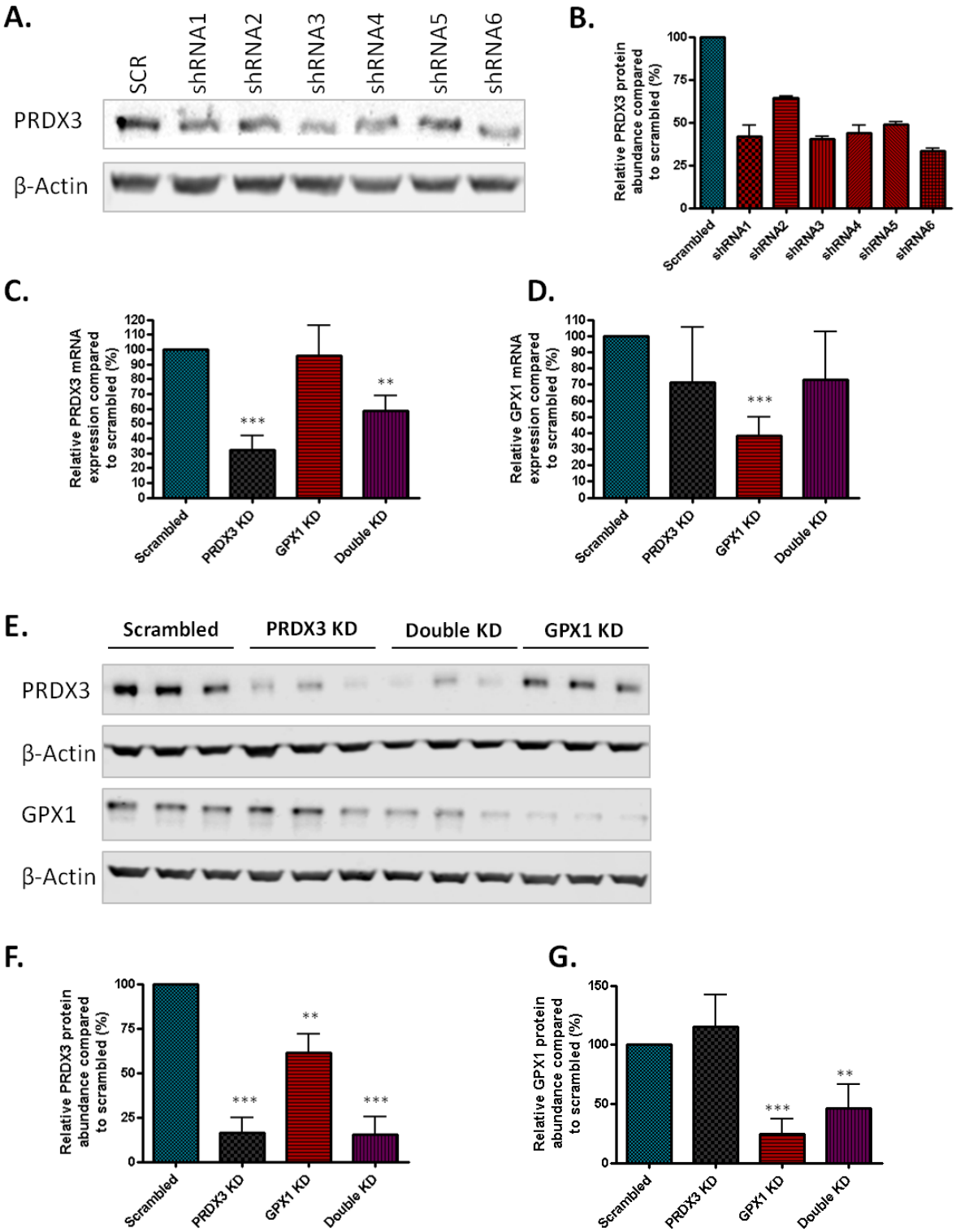

Figure 5. 2: Dual *GPX1* and *PRDX3* knockdown in H295R adrenocortical cells

A. Western blot analysis of HEK293 cells transiently transfected with shRNA for *PRDX3*. A. Cells grown in 6-well plates were transfected with shRNA targeting exons 3-7 and 3'UTR of *PRDX3* or a SCR control shRNA. 48 hours after transfection, lysates

were immunoblotted with anti-PRDX3 and anti-β-actin. B. Densitometric analysis quantifying PRDX3 protein levels relative to β-actin loading control, showing shRNAs 3 and 6 targeting exon 4 generate the highest knockdown (n=2). C-G. Validation of stable knockdown in H295R cells after transduction with lentiviral shRNA to *PRDX3, GPX1*, both, or a SCR negative control. Cells were grown in 6 well plates and harvested after 48h. C&D. mRNA knockdown validation by real time PCR analysis measuring *PRDX3* (C) or *GPX1* (D) expression relative to GADPH as a control (n=3±sd). E. Western blot analysis of PRDX3 and GPX1 protein levels in knockdown cells. F&G. Densitometric analysis of PRDX3 (F) and GPX1 (G) protein levels relative to β-actin as a loading control (n=3±sd). (p<0.05, **p<0.01***p<0.001*).**

5.5 Assessing GPX activity

In the previous chapter, I demonstrated that GPX1 accounted for 50% of total GPX activity in H295R adrenocortical cells (section 4.3.4**)**, suggesting other GPXs could not compensate for its loss. The effect of *PRDX3* KD or double KD on GPX activity was explored, to see whether loss of this additional antioxidant capacity invoked compensatory glutathione peroxidase activity. A similar experiment was performed as in section 4.3.4 with the addition of *PRDX3*-KD and *double*-KD cell lines, using a commercially available GPX assay kit.

Lysate from 3 x 10^6 stable KD and SCR H295R cells were collected in the assay buffer containing protein inhibitors and homogenised by sonication (section 2.7.3.2). The lysates were mixed with NADPH, GSH and GR and preincubated for 20 minutes at room temperature. Following addition of substrate cumene hydroperoxide, absorbance at 340nm (indicative of NADPH concentration) was measured for 10 minutes and then rates determined (section 2.7.3.2).

In agreement with findings from section 4.3.4, *GPX1*-KD cells had 50% less GPX activity compared to their SCR counterparts (Fig. 5.3). *PRDX3*- KD alone had no effect on GPX activity. *Double*-KD cells had a 40% decrease in GPX activity compared to SCR cells, with

no significant difference in activity compared to *GPX1*-KD cells. These data suggest the loss of both PRDX3 and GPX1 activity does not upregulate activity of the other glutathione peroxidases.

In order to determine whether *GPX1* KD influences PRDX function, a future direction would be to carry out a spectrophotometric assay measuring thioredoxin reductase activity, which would assess whether there is compensation by the thioredoxin/peroxidoxin antioxidant system.

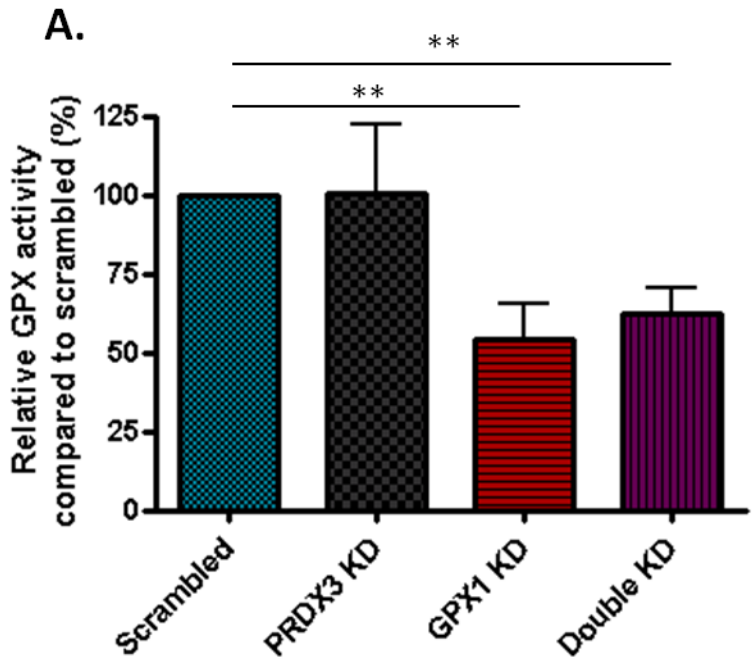

Figure 5. 3: NADPH coupled assay for total GPX activity in *PRDX*- KD, *GPX1*-KD and *double*-KD cells

Spectrophotometric enzymatic assay for total GPX activity following treatment with substrate H_2O_2. Cells harvested in an assay buffer (Abcam) were sonicated and protein extracts mixed with GSH, NADPH and glutathione reductase. Reactions were started with the addition of cumene hydroperoxide. Rate of absorbance of NADPH at 340nm over a 10 min period was determined and normalised to protein concentration using a Bradford assay. A. Total GPX activity of lysates taken from SCR and knockdown cells. GPX activity was significantly lower in the *GPX1*-KD and *double*-KD cell lines

compared to SCR, with no significant difference between *GPX1*-KD and *double*-KD cells (n=3 ± s.d. **$p<0.01$).

5.6 Assessing Cell viability

The previous chapter found untreated *GPX1*-KD cells had significantly higher levels of an apoptosis marker, cleaved-PARP, when compared to cells expressing SCR shRNA, and the MTS assay showed *GPX1*-KD cells had no changes to cell viability under physiological conditions but had increased susceptibility to cell death following H_2O_2 treatment.

PRDX3 has been similarly documented to influence cell death pathways, for example *PRDX3* KD by RNAi leaves Hela cells more susceptible to apoptosis induced by TNF-alpha or staurosporine (Chang *et al.*, 2004).

To investigate whether loss of function in both *PRDX3* and *GPX1* together presented a more severe phenotype than *GPX1* KD alone, the MTS assay was repeated using the same experimental conditions (sections 4.3.5) with the addition of *PRDX3*-KD and *double*-KD cell lines. Briefly, SCR and KD cells were seeded at a density of 5000 in triplicate, grown for 24h then either subjected to 100µM H_2O_2 or left untreated for 24h. The number of metabolically active, viable cells was determined by spectrophotometric MTS assay (section 2.7.4).

As demonstrated in the previous chapter, *GPX1* KD had no effect on viability under basal conditions, but led to a significant decrease in cell viability when treated with H_2O_2 (Fig. 5.4A). This effect was also seen for *PRDX3* KD, which did not affect cells under normal conditions but decreased viability after treatment. Crucially, double KD of *GPX1* and *PRDX3* significantly reduced the number of metabolically active cells under normal conditions compared to the SCR control. Hydrogen peroxide treatment significantly reduced cell viability in all three cell lines with the most dramatic effect seen in the *double*-KD cells,

however there was no significant difference between the single KD and the double KD cell line.

The ratio of reduced to oxidised glutathione (GSH/GSSG) is often used as an indicator of cell toxicity. Although GSH is used as a cosubstrate by GPXs, it is also a potent antioxidant itself, responsible for reducing protein thiols. The ratio of GSH/GSSG is significantly reduced in human *NNT* KD cells, showing the cells are generally less healthy with increased antioxidant consumption (Meimaridou *et al.*, 2012b). The GSH/GSSG ratio in *GPX1*-KD, *PRDX3*-KD and *double*-KD cells was assessed to see whether loss of the two antioxidants increased cell toxicity.

Cells were seeded in 96 well plates at a density of 10,000 and grown overnight. Cells were lysed and the ratio of reduced to oxidised glutathione was determined using a luciferase based assay (section 2.7.5). There was no significant difference in GSH/GSSG between cell lines, suggesting the cells were not under oxidative stress (Fig. 5.4B).

Together these results suggest that a significant decrease in viability is only seen under physiological conditions with double KD of *GPX1* and *PRDX3*. However, there was no significant difference in viability between double and single KD cells, suggesting double KD has no add-on effect. The GSH/GSSG ratio was unaltered by KD of either gene, suggesting the cells did not have high levels of toxicity.

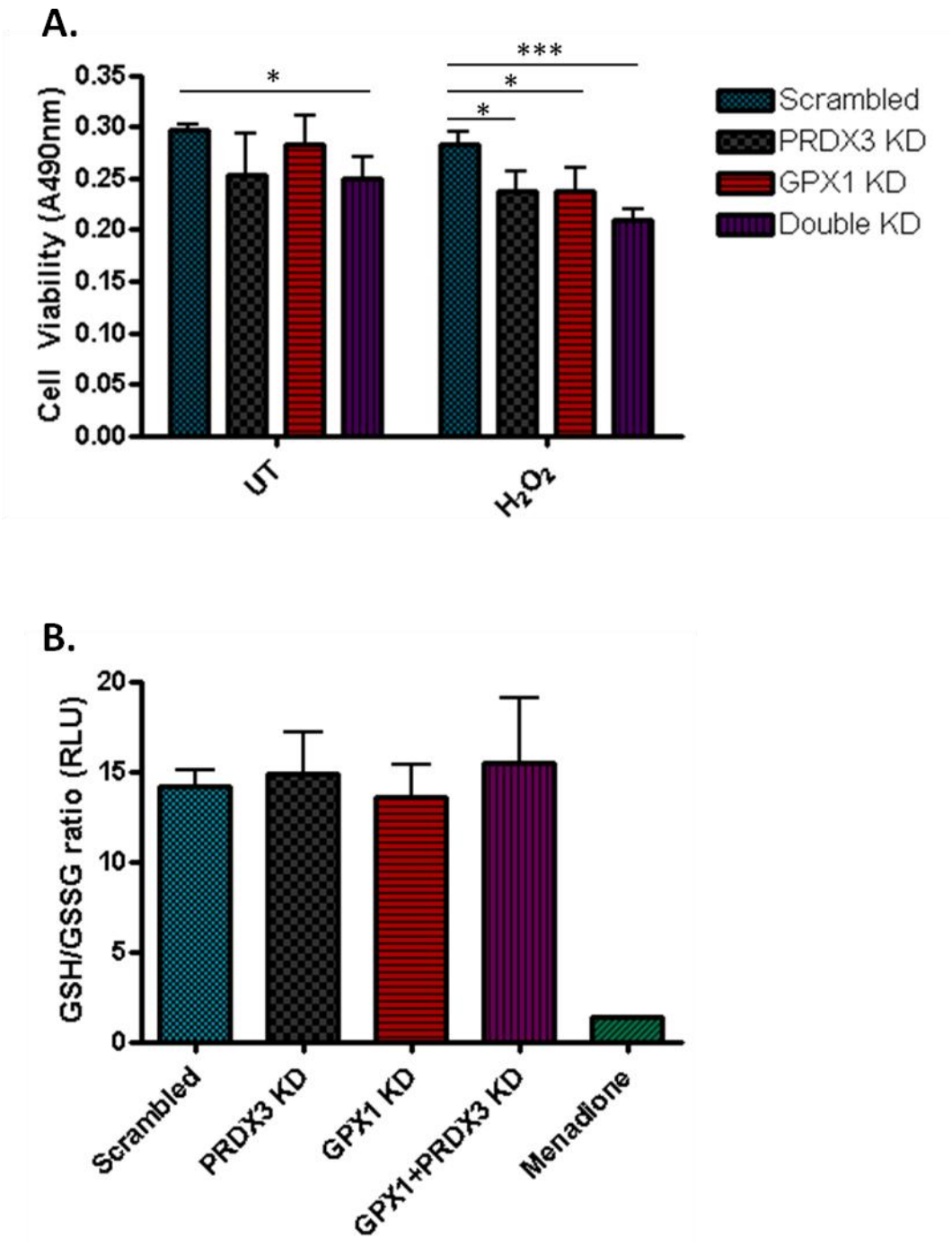

Figure 5. 4: Cell viability and toxicity in SCR and knockdown cells.

A. Cell viability was determined by MTS assay measuring absorbance at 490nm. SCR and knockdown cells were either left untreated or treated with 100µM H_2O_2 for 24 hours before assaying. A. At physiological levels only double knockdown of *PRDX3* and *GPX1* significantly reduced viability compared to SCR cells (*p<0.05*). 24h post treatment significantly less metabolically active cells were present for all three

knockdown cell lines compared to SCR (n=3 ±s.d **p<0.05, **p<0.01*p<0.001*). B. GSH/GSSG ratio in SCR and knockdown cells. Cells seeded at 10,000 and grown for 24h were harvested and subjected to luciferase based assay to determine the ratio of GSH to GSSG. Increased ROS levels induced by 40µM menadione to SCR cells reduced GSH/GSSG to 1.33 (n=1). There was no significant difference in GSH/GSSG between cell lines (n=3 ±s.d **p<0.05, **p<0.01***p<0.001*).**

5.7 Assessing the effects of *GPX1* and *PRDX3* knockdown on steroidogenesis

In the previous chapter I demonstrated that *GPX1* KD significantly reduced StAR protein levels. GPX1 has previously been implicated in the regulation of steroidogenesis through modulation of ROS levels. A study by Kil *et al.* (2012) also suggests a crucial role for PRDX3 in adrenal steroidogenesis. In brief, Kil *et al.* showed that PRDX3 is highly expressed in the mouse adrenal and is readily hyperoxidised and deactivated by high levels of H_2O_2 produced by steroidogenesis particularly CYP11B1. They demonstrate that inactivation of PRDX3 by H_2O_2 leads to the accumulation of H_2O_2, activation of p38MAPK, suppression of StAR and inhibition of steroidogenesis. The authors propose a model whereby PRDX3 inactivation acts as a feedback mechanism to inhibit further steroidogenesis following electron leakage from CYP11B1 activity.

GPX1 has also been reported to influence p38MAPK phosphorylation as overexpression of *GPX1* in mouse embryonic fibroblasts prevents phosphorylation under hypoxia (Emerling *et al.*, 2005). Although GPX1 is not inactivated in physiological conditions, it may inhibit steroidogenesis through a similar mechanism involving p38MAPK suppression of StAR synthesis.

To explore the effects of loss of PRDX3, GPX1 or both on steroidogenesis in human cells, *GPX1*-KD, *PRDX3*-KD and *double*-KD cell lines were grown in 6-well plates for 24h, then either treated with 100µM H_2O_2 for 24 h or left untreated. Lysates were immunoblotted with

antibodies to StAR relative to β-actin as an internal control and, in addition, with antibodies to phosphorylated p38MAPK (p-p38MAPK) relative to total p38MAPK.

A general trend was apparent whereby levels of StAR were highest in SCR cells, followed by *PRDX3*-KD cells, then *GPX1*-KD cells and lowest in the *double*-KD cells (Fig. 5.5 A&B). There was however, no significant difference between *GPX1*-KD and SCR cells, conflicting with our previous finding in chapter 4.3.6. There was also no statistical difference between SCR and *double*-KD cells however there was a significant difference between *PRDX3*-KD and SCR cells ($p<0.05$). More experimental repeats may be required in order to clarify whether the trend is real.

Similarly, levels of p-p38MAPK followed a trend being lowest in SCR cells, and highest in *GPX1*-KD and *double*-KD cell lines (Fig. 5.5.C-D). The only significant difference however was between SCR and *PRDX3*-KD cells. We also measured cortisol levels by immunoassay but found no significant difference between cell lines (Fig. 5.5.E).

To summarise, there was no significant difference in cortisol concentration between SCR and KD cell lines, but there was a trend towards decreased StAR and increased p-p38MAPK in the KD cells compared to SCR (Fig. 5.5). The only significant difference seen was between *PRDX3*-KD and SCR cells. More experimental repeats are required to clarify the trend.

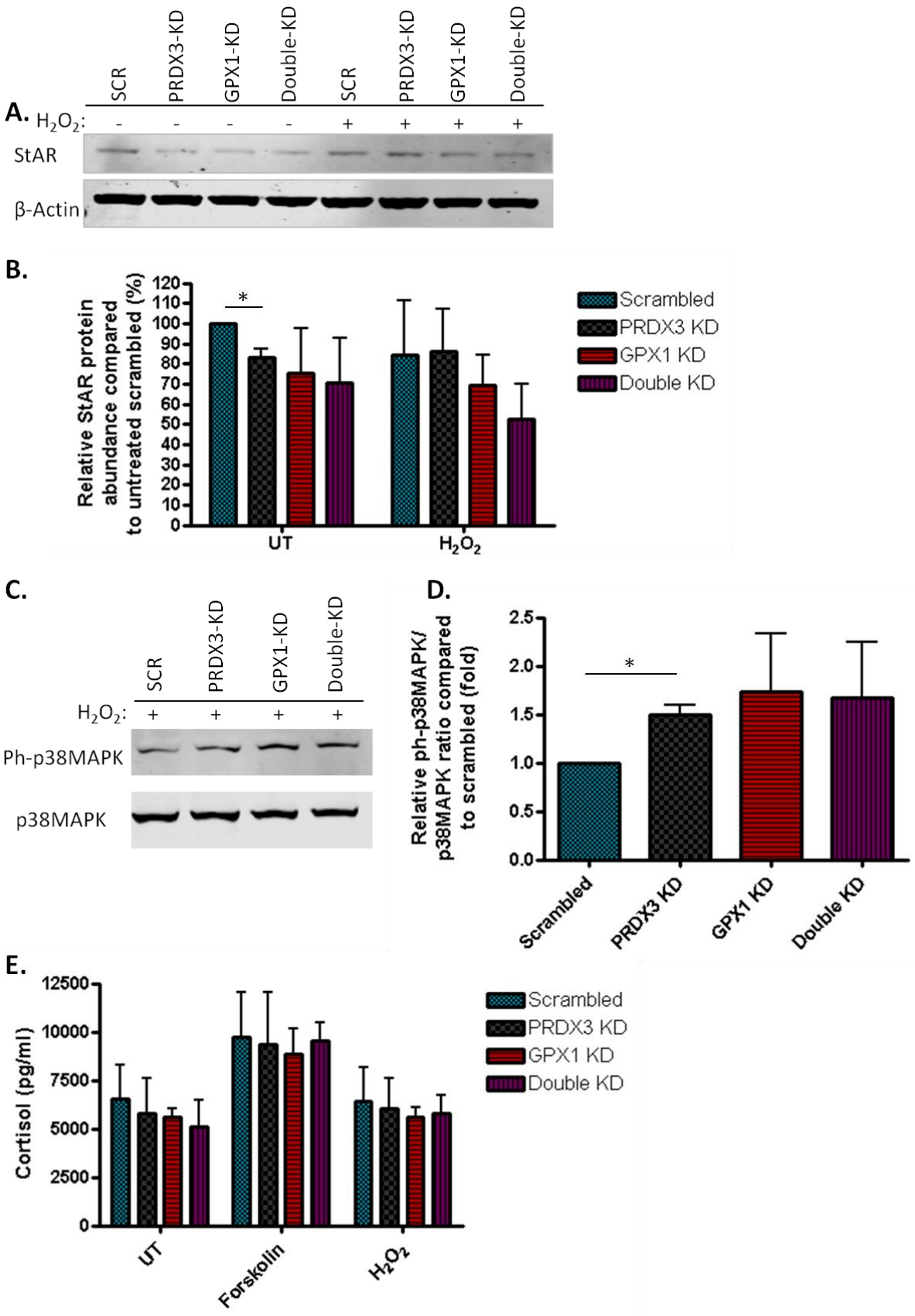

Figure 5. 5: Effects of *GPX1* and *PRDX3* knockdown on steroidogenesis. SCR and knockdown H295R cells were grown in 6 well plates for 24h and then either

subjected to 24h 100µM H_2O_2 or left untreated. A. Cell lysates immunoblotted with antibodies to StAR and also actin as a loading control. B. Densitometric analysis of the Western blots showing StAR protein levels significantly reduced in *PRDX3*-KD cells relative to SCR cells (untreated n=3±sd *$p<0.05$, H_2O_2 treated n=2). C. Cell lysates immunoblotted with antibodies to phospho-p38MAPK (p-p38MAPK) relative and total p38MAPK (D). Densitometric analysis of Western blot showing p-p38MAPK significantly increased (*$p<0.05$) in *PRDX3*-KD cells compared to SCR cells. (n=3 ±sd) E. Cortisol levels in SCR and knockdown cell lines detected by ELISA. Cells were either left untreated or subjected to 6h treatment with 10^{-5}M forskolin or 100µM H_2O_2 then lysed and assayed (n=5±sd).

5.8 Discussion

The pathogenesis of FGD has been recently associated with disease mechanisms involving ROS-induced suppression of steroidogenesis (Meimaridou et al., 2012b). The identification of a rare *GPX1* mutation in a FGD patient therefore provided a plausible candidate gene for investigation, however the effects of *GPX1* KD in cultured adrenocortical cells were mild compared to previously published data on *NNT* KD in analogous cells. *NNT* mutations account for 10% of the FGD cohort, but sequencing a further 100 FGD patients with unknown aetiology did not reveal any other *GPX1* homozygous or compound heterozygous mutations. To ascertain whether another gene defect, either alone or in combination with the *GPX* defect, was causative for disease in this proband, whole exome sequencing (WES) was carried out in the proband and his brother.

Using an Agilent V4 exome capture array and Illumina HiSeq2000 technology to sequence our samples, analysis of nucleotide level variation with a filtration strategy revealed a homozygous stop gain mutation in *PRDX3*, p.Q67X, with coverage of 20/20 reads.

Peroxiredoxin 3 (PRDX3) is part of the peroxiredoxin family of antioxidant enzymes with multiple isoforms that are capable of reducing hydrogen peroxide, organic hydroperoxides

and peroxinitrates (Bryk *et al.*, 2000), ultimately exhibiting the same function as the glutathione peroxidases. The enzymes are highly abundant antioxidants forming 1% of all soluble cellular protein in mammals and are ubiquitously expressed (Chae *et al.*, 1999). They are present in all organisms, all organelles (Hanschmann *et al.*, 2013) and are essential in the maintenance of a steady redox state.

PRDX3 was selected as a candidate gene on the grounds of its antioxidant function, fulfilling my hypothesis that a second causal gene could have a role in oxidative stress. The mutation was predicted to cause loss-of function as the truncation removed most of the protein including key residues for enzymatic activity. This gene defect would seem a highly plausible candidate for the phenotype on its own; however, Sanger sequencing of the kindred revealed the mutation did not segregate with the disease, as it was homozygous in the unaffected sibling. Hence *PRDX3* mutations alone were not capable of causing FGD. This raised the possibility that inheritance of both defects was necessary to cause FGD, or that the *GPX1* defect alone was responsible for disease progression.

Sanger sequencing a further 100 FGD patients of unknown aetiology revealed one further *PRDX3* mutation, a missense variant R214C previously documented as a somatic mutation, however it was not possible to check segregation of the variant because DNA samples from family members were unavailable. It seems unlikely that this missense mutation would be causative in isolation when a more severe, truncation mutation in *PRDX3* does not cause a phenotype in the unaffected brother, however the possibility of the variant affecting PRDX3 function cannot be ruled out.

Mammalian PRDXs can be grouped into 2-Cys (PRDX1-4), atypical 2-Cys (PRDX5) and 1-Cys PRDXs (PRDX6) which vary in subcellular expression patterns and catalytic mechanism.

Of the 2-Cys PRDXs, PRDX1 is predominantly cytosolic but also localised to the nucleus, peroxisomes and serum (Chang et al., 2005; Immenschuh et al., 2003); PRDX2 is present in the cytosol and the nucleus, but also associates with cell membranes (Cha *et al.*, 2000);

PRDX3 is entirely mitochondrial in localisation (Cao et al., 2007; Watabe et al., 1997); and PRDX4 is localised to cytosol and ER and contains a leader sequence required for its role as secretory protein (Matsumoto et al., 1999; Okado-Matsumoto et al., 2000). Atypical 2-Cys PRDX5 is the second mitochondrial PRDX and is also localised peroxisomes and the cytosol (Knoops *et al.*, 1999). Finally, 1-Cys PRDX6 is localised to the cytosol, vesicles and lysosomes (Sorokina *et al.*, 2009; Sorokina *et al.*, 2011).

All PRDXs have a conserved N-terminal redox active cysteine (Cys_P) which functions as the active site. At this cysteine the peroxide is reduced, oxidising the active site to a sulfenic acid, producing water/alcohol as a by-product. In 2-Cys PRDXs, the sulfenic acid moiety of the oxidised cysteine is 'resolved' by forming a disulfide bridge with a second conserved cysteine (Cys_R) at the C-terminus of an adjacent PRDX subunit, forming an anti-parallel homodimer. The oxidised dimer is recycled back to its reduced form by thioredoxin. Oxidised thioredoxin is subsequently recycled by thioredoxin reductase using NADPH as illustrated in figure 5.1.

Other conserved residues include an additional Arg residue 75 bp downstream of Cys_P which contributes to the active site which ensures stabilisation of the deprotonated thiol when the enzyme is in its fully folded (FF) state ready for peroxidation of the hydroperoxide (Hall *et al.*, 2010; Karplus and Hall, 2007; Nelson *et al.*, 2011).

For atypical 2-Cys PRDXs, an unconserved C-terminal Cys residue is used to reduce the oxidised Cys_P, forming an intramolecular disulfide within a monomer. With no resolving Cys, 1-Cys PRDX6 requires additional protein thiols such as GSH or ascorbic acid to complete catalysis (Hanschmann *et al.*, 2013).

PRDX3 is a 7 exon gene located on chromosome 10q25-q26 (Kim *et al.*, 1988), expressed as a 259aa protein, which is longer than PRDX1 and 2 (199 residues) due to a mitochondrial targetting leader sequence. In our proband, the stop gain mutation in *PRDX3*, p.Q67X, does not affect the N-terminal peroxidatic Cys_p residue at position 45. It does however ablate the

C-terminal resolving Cys_R and the Arg residue at p75 downstream of Cys_P, which we predict would result in a loss-of-function.

A loss-of-function mutation in *PRDX3* may compromise mitochondrial antioxidant defense. Mitochondria generate high levels of oxidants associated with energy metabolism and have therefore evolved competent antioxidant defenses to cope with the high demand, such as its own thioredoxin system and a strong reducing environment (see section 1.7.4 for overview) (Yin et al., 2012a). The mitochondrial peroxidases include peroxiredoxin 3 and 5 of the thioredoxin system, and GPX1 and the mitochondrial form of GPX4 (mtGPX4) of the glutathione system. Peroxiredoxin 5 is predominantly involved in peroxinitrate reduction and is less efficient in reducing H_2O_2 than PRDX3 (Trujillo et al., 2007; Yin et al., 2012a) and Glutathione peroxidase 1 (GPX1) is predominantly cytosolic and is present in mitochondria at levels of < 0.7 µg in mice (the relative levels in humans mitochondrial fractions has not been reported) (Kil *et al.*, 2012). PRDX3 is an exclusively mitochondrial protein that has been reported to consume 90% of H_2O_2 generated in mitochondria (Yin et al., 2012a), suggesting it contributes significantly to mitochondrial antioxidant defense. Therefore, the *PRDX3* mutation in the proband may impact strongly on mitochondrial redox homeostasis.

My findings from the previous chapter implied that loss of GPX1 alone did not present a severe phenotype, compared to that of *NNT* KD, suggesting *GPX1* may not be the causative gene in this proband. In this chapter, although the *PRDX3* mutation did not segregate with the disease, I hypothesised that GPX1 and PRDX3 had an additive and dual role in mitochondrial redox homeostasis in adrenocortical cells. I therefore investigated the concept of digenic inheritance by developing adrenocortical cells with targeted shRNA KD of either *GPX1* and *PRDX3* alone or in combination, to compare the effects of losing the function of either or both genes on steroidogenesis and viability, thereby aiming to clarify whether *GPX1* alone, or in combination with *PRDX3* could be the causative genes in our proband.

A marked loss of cell viability was seen in the *GPX1* and *PRDX3* double KD cells under physiological conditions. A significant loss of cell viability was not seen for either *GPX1* or *PRDX3* KD alone, unless cells were treated with hydrogen peroxide. When exposed to

increased ROS through hydrogen peroxide treatment, *double*-KD cells had the lowest viability with the highest statistical significance. This data suggest that in isolation loss of GPX1 and PRDX3 decrease cell viability but a notable effect is only evident under physiological conditions when both are compromised. This cumulative effect on cell viability could contribute to a potential disease mechanism in the proband.

A decrease in cell viability is most likely attributed to increased levels of mitochondrial and cytosolic H_2O_2. However, under physiological levels the ratio of GSH/GSSG was not altered in the *double*-KD cell line, which is a frequently used indicator of cell toxicity. My data also show that there was no compensatory GPX activity (all glutathione peroxidases) in the *PRDX3*-KD cells, nor was there an upregulation in *GPX1* mRNA or protein levels. The *double*-KD cells, had statistically similar total GPX activity to *GPX1*-KD cells, indicating no compensatory upregulation of the other glutathione peroxidases, again suggesting the cells were not under particularly high oxidative pressure. Interestingly, a reduction in PRDX3 protein levels was seen in *GPX1*-KD cells, however I did not complete the reciprocal experiment by measuring PRDX activity to investigate this result further, a direction that can be taken in future using a TXNRD assay.

Studies have demonstrated that cell viability is dependent on GSH/GSSG (Muyderman *et al.*, 2007), and even depletion of mitochondrial GSH alone, which accounts for 15% of total GSH, can induce cell death (Shan *et al.*, 1993). The above data indicate that under physiological conditions, the overall redox state of the cell is not changed significantly. However, these experiments do not consider the possibility of local redox changes that are mitochondria specific, which should be addressed in future experiments. Another consideration is the influence of GPX1 activity on GSH levels, as it oxidises GSH as a co-substrate. In this regard, KD of *GPX1* would mask decreases in GSH by alleviating the consumption of GSH. This effect has been seen in cells cultured from *GPX1*$^{-/-}$ mice, which have less/slower GSH depletion and lower GSSG levels than wildtype cells following treatment with diquat (Fu et al., 2001; Liddell et al., 2006b).

Both GPX1 and PRDX3 have been shown to modulate apoptosis through influencing cellular H_2O_2 levels. Cultured cells from *GPX1*$^{-/-}$mice are more susceptible to pro-apoptotic stimuli for example hydrogen peroxide and paraquat (Cheng et al., 2003; De Haan et al., 2003; Fu et al., 1999; Fu et al., 2001; Liddell et al., 2006b). Similarly, depletion of PRDX3 by RNA interference in cultured Hela cells rendered them more susceptible to apoptosis induced by TNF-alpha or staurosporine (Chang *et al.*, 2004), and SH-SY5Y cells with KD of *PRDX3* had higher levels of caspase-3 activity, protein carbonyls and apoptotic nuclei following MPP^+ exposure, a neurotoxic compound (De Simoni *et al.*, 2008). Overexpressing *PRDX3* protects cells from a number of apoptotic stimuli including TNFa (Chang *et al.*, 2004), cadmium, hydrogen peroxide, paraquat (Chen *et al.*, 2008) hypoxia, and anti-cancer drug Imexon (Nonn *et al.*, 2003).

To investigate the effects of *GPX1* and *PRDX3* combined KD on steroidogenesis, I employed similar methodology to Kil *et al.* (2012) who described an HPA-axis independent negative feedback loop whereby reversible inactivation of PRDX3 regulates adrenal steroidogenesis.

When engaged in catalysis PRDXs can undergo hyperoxidation, forming either sulfinic acid ($-SO_2$) or sulfonic acid ($-SO_3$) at the Cys_p, which are enzymatically inactive. The level of sensitivity to H_2O_2 induced inactivation is high considering it is the substrate of PRDXs (Poole *et al.*, 2011). In 2-Cys PRDXs, the sulfinic acid moiety can be actively reduced back by sulfiredoxin (SRX) consuming ATP, Mg^{2+} and electrons from a thiol donor (Rhee et al., 2005a).

It is becoming increasingly evident that this process has a biological role and has evolved over time. PRDX inactivation is rare in prokaryotes (Hall et al., 2009; Poole et al., 2011; Wood et al., 2003a) and eukaryotes PRDXs possess insertions of two conserved motifs (GGLG and YF) that are absent from more robust prokaryote isoforms (Wood et al., 2003a). The 'floodgate' hypothesis described by Wood *et al* 2003, implies that the abundance of PRDXs coupled with their sensitivity to hyperoxidation has evolved as a mechanism to keep basal H_2O_2 levels low, but allow localised peroxide production required for signal transduction (Poole et al., 2011; Wood et al., 2003a).

In the model described by Kil *et al.* (2012), the electron donor system supplying steroidogenic enzymes is leaky, leading to superoxide and subsequent H_2O_2 generation within the mitochondria. To compensate, high levels of PRDX3 are present in the mitochondria of the adrenal cortex. Inactivation of PRDX3 is a consequence of steroidogenesis, but is counteracted by SRX reversing this process. However, after long periods of steroidogenesis the level of excess H_2O_2 outweighs the capacity of SRX. An overspill of H_2O_2 into the cytosol occurs, leading to phosphorylation of p38MAPK, which through an unknown mechanism, is associated with the reduced synthesis of StAR protein. Reduced levels of StAR consequently downregulate steroidogenesis.

PRDX3 is only hyperoxidised when it is in the catalytic cycle, hence the level of PRDX3 inactivation is directly proportional to the level of H_2O_2 produced by steroidogenesis. The authors detected from mouse adrenal tissue 10% of total PRDX3 in its sulfinic form, suggesting that levels of H_2O_2 are high enough in the adrenal cortex for PRDX3 to be constantly engaged in its catalytic cycle.

In mice, the circadian oscillation of corticosterone production was accompanied by oscillations in H_2O_2, inactivated PRDX, SRX, phosphorylated p38 MAPK and StAR, which were all increased by ACTH stimulation. SRX^{SC} mice with reduced SRX expression had reduced corticosterone production and although oscillations remained, the amplitude was reduced.

Taken together, this study gave evidence of a critical role of PRDX3 reversible inactivation in an HPA axis independent negative feedback loop which can influence circadian rhythms of corticosteroid production (Kil *et al.*, 2012). On this basis, I investigated the effects of *GPX* and *PRDX* single or double KD on levels of StAR, corticosteroid production and the phosphorylation of p38-MAPK, to explore the effects on this proposed feedback system.

A general trend was seen where levels of StAR protein were highest in the SCR control cell line, following *PRDX3*-KD cells, then *GPX1*-KD cells and lowest in the *double*-KD cell line. However, only the change in *PRDX3*-KD cells reached statistical significance. This data was

not as convincing as the data for *GPX1*-KD cells in chapter 4, where statistical significance was reached. Levels of phosphorylated p38MAPK were highest in *GPX1*-KD cells, then *double*-KD cells, *PRDX3*-KD cells and lowest in SCR cells. Again, the only difference that reached statistical significance was between *PRDX3*-KD and SCR cells. The corresponding basal cortisol levels were highest in SCR cells, and lowest in the *double*-KD cell line however there was no significant difference in these changes.

The above data is preliminary, hence it is not possible to draw firm conclusions. A trend is seen whereby double KD has an additive effect in reducing both StAR and basal cortisol levels; however the changes were not significant. More experimental repeats would be required in order to clarify. Only PRDX3 KD resulted in a significant change in StAR and p-p38 MAPK levels, reflecting the pathway proposed by Kil *et al*, and that PRDX3 is the most significant antioxidant peroxidase for the adrenal cortex.

Different experimental approaches may also be necessary to clarify whether a trend is seen. For example, large concentrations of inactive StAR compared to newly synthesised active form may mask changes in StAR levels, as observed by Kil *et al.* (2012), who only noted an increase in StAR levels in mice following ACTH stimulation or p38MAPK inhibition after pre-treatment with DEX to deplete the inactive form. Similarly an increase in StAR levels was seen in mouse Y-1 cells, which contain low levels of the inactive form, after p38MAPK inhibition. Therefore, a future experiment could be to treat H295R cells with DEX to deplete pre-existing StAR and then stimulate with forskolin, before lysing cells. This may clarify whether there is a clear difference between cells lines.

Despite these considerations, a very recent study by Kil *et al.* (2013) suggested that H295R and Y1 cell lines are not suitable as *in vitro* models for redox signaling because expression levels of SRX and PRDX3 do not reflect *in vivo* levels, in either basal or ACTH stimulated states. Likewise, primary mouse adrenocortical cells are unsuitable because Srx levels increase, along with a decrease in levels of hyperoxidised PrxIII shortly after isolation. This report raises concerns for our immediate study of redox homeostasis in H295R cells and may require us to move to novel models such as zebrafish in the future (section 6.2 and 6.3)

Although the results were not conclusive, previous studies have implicated both GPX1 and PRDX3 in the regulation of steroidogenesis. Chanoine *et al.* (2001) implicated GPX1 in the regulation of steroidogenesis after demonstrating that Se deficient AN4Rppc7 adrenal cells with minimal GPX1 activity exhibited a marked decrease in corticosterone, aldosterone and progesterone after cAMP stimulation compared to Se adequate cells. Like PRDX3, GPX1 is also able to modulate p38MAPK activity by influencing hydrogen peroxide levels, as overexpression of *GPX1* in mouse embryonic fibroblasts prevents p38MAPK phosphorylation under hypoxia (Emerling *et al.,* 2005). My data also reveal that *GPX1* is highly expressed in the human adrenal cortex compared to other tissues (Section 4.3.2**)** in agreement with previous studies (Azhar *et al.,* 1995) suggesting it may have an important antioxidant role there.

In comparison to *GPX1*, *PRDX3* is more highly expressed in the adrenal cortex of mice (Kil *et al.,* 2012). In mitochondrial fractions taken from the adrenal cortex of mice, PRDX3 concentration was 10 times higher than GPX1, and 40 times higher than PRDX5, the only other mitochondrial PRDX. ACTH stimulation increases levels of hyperoxidised PRDX3, which are associated with the ROS induced negative feedback of adrenal steroidogenesis as described above. ACTH also induces translocation of SRX to the mitochondria which reverses PRDX3 inactivation, and SRX^{sc} mutant mice have reduced amplitude of the oscillations of corticosterone compared to WT (Kil *et al.*, 2012).

The mRNA and activity of mitochondrial antioxidant *SOD2,* which converts superoxide radicals to hydrogen peroxide, is also upregulated by ACTH stimulation (Goncharova et al., 2006; Raza and Vinson, 2000) and protein levels oscillate in correlation with the diurnal rhythm of cortisol, decreasing in parallel with cortisol with age. In keeping with the model proposed by Kil *et al.* (2012), this could be another factor allowing accumulation of H_2O_2 after cortisol production to halt further steroidogenesis.

In comparison to SOD2 and PRDX3, GPX1 is not upregulated by ACTH and does not have circadian rhythms. Glutathione peroxidases require millimolar concentrations of H_2O_2 to be

inactivated, and therefore would not be involved in negative feedback loop similar to that involving PRDX3 inactivation (Lubos *et al.*, 2011).

Based on the literature described and the preliminary data collected in this chapter, *PRDX3* presents a stronger candidate gene for FGD, however only the *GPX1* mutation segregated with the disease, as the unaffected brother was homozygous for the *PRDX3* mutation too. Data from the cell viability assay, suggest *GPX1* and *PRDX3* KD have an additive effect in reducing cell viability, presumably by increasing ROS levels, which impair steroidogenesis. Given that GSH-GPX1 and TXN2-PRDX3 antioxidant systems work synergistically to detoxify the same target (Zhang et al., 2007), it is likely that loss of GPX1 and PRDX3 in our proband cumulatively contribute to increased oxidative stress in the adrenal cortex.

Our group has recently described FGD cases with a loss of function *TXNRD2* mutation (Prasad *et al. unpublished*). As PRDX3 is reduced by thioredoxin 2 (TXN2) which is recycled by TXNRD2 (Fig. 5.35.3.2), it may be surprising that mutations in *PRDX3* do not cause FGD. However, TXNRD2 has multiple functions in addition to reducing PRDX3 for example it too has peroxidase activity (Björnstedt *et al.*, 1995), it can reduce cytochrome C (Nalvarte *et al.*, 2004) and reduce glutaredoxin 2 in the glutathione antioxidant system (Johansson *et al.*, 2004). Mutations in *NNT* and *TXNRD2* may cause FGD because these enzymes supply two antioxidant systems, whereas PRDX3 is involved in one, at the bottom of the electron chain.

Taken together, although GPX1 and PRDX3 have the same function in reducing hydrogen peroxide, the enzymes may have different roles in steroidogenesis. Evidence suggests that the inactivation of PRDX3 is critical to steroidogenesis under normal physiological conditions, allowing accumulation of hydrogen peroxide for negative feedback. *GPX1* is likely to be the second most highly expressed peroxidase in adrenal mitochondria as mt*GPX4* is mostly expressed in the testes with only low levels present in other tissues (Brigelius-Flohé and Maiorino, 2013). Hence it may be an advantage for GPX1 as the second most abundant

peroxidase to be independent of ACTH regulation, in order to allow the ACTH induced accumulation of H_2O_2 after PRDX3 inactivation. Its resistance to hyperoxidation may also play a part, ensuring some residual peroxidase activity remains within mitochondria to limit oxidative damage. Considering GPX1 is predominantly cytosolic, it may also minimise the extent of H_2O_2 overspill from the mitochondria to the cytosol, ensuring H_2O_2 signalling remains localised. Based on this speculative model, whereas PRDX3 has a regulatory role in steroidogenesis, GPX1 may have a protective role.

With this in mind, I propose a multiple hit model whereby, an inactivating mutation in *PRDX3* may reduce steroidogenic capacity by interfering with the internal feedback loop and increasing oxidative stress levels. Despite this, negative feedback from the HPA axis would remain. A mutation in *GPX1* would further increase oxidative stress in the cytosol and mitochondria which would exacerbate steroidogenesis impairment and mitochondrial oxidative damage.

In conclusion, multiple antioxidant systems exist to maintain a healthy redox balance. The glutathione peroxidases and peroxiredoxins work simultaneously to reduce hydrogen peroxide, preventing cellular damage. I identified a patient with two homozygous mutations in the redox pathway. My data show that loss of function in *PRDX3* alone is insufficient to cause adrenal failure and suggest that mutation in *GPX1*, either alone or in combination with *PRDX3* mutation, may tip the redox balance and cause FGD.

Chapter 6: Final Conclusions and Future Directions

6.1 Introduction

FGD is an autosomal recessive disorder characterised by the resistance of the adrenal cortex to ACTH and subsequent isolated glucocorticoid deficiency. FGD is a heterogeneous disease with 60% cases of known aetiology. Causal genes include *MC2R* (Clark *et al.*, 1993) and its accessory protein *MRAP* (Metherell *et al.*, 2005) and *STAR* (Metherell *et al.*, 2009) which constitute genes involved in ACTH signalling and steroidogenesis. More recently mutations in genes outside this pathway have been described, including the DNA helicase *MCM4* in the genetically isolated Irish traveller population (Hughes *et al.*, 2012) and *NNT*, the mitochondrial antioxidant dehydrogenase, which accounts for 10% of affected patients (Meimaridou *et al.*, 2012b).

The aim of this thesis was to discover genes that might be responsible for the disease in some or all of the remaining 40% of patients with unknown aetiology, using both proteomic and genomic approaches. After the discovery of *MRAP*, it was suggested that other causal genes may also be associated with MC2R trafficking (Clark and Metherell, 2006; Génin *et al.*, 2002; Metherell *et al.*, 2006). Therefore the proteomic side of this project aimed to find interacting partners of MC2R and/or MRAP in order to disclose FGD causal genes. This could reveal proteins that are embryonic lethal when defective and would therefore not be identified by the genetic approach. Such protein discovery might also broaden our understanding of MC2R regulation and MRAP function. This approach identified 5 putative interactors of MC2R/MRAP the most promising of which was clathrin heavy chain 1.

The genomic arm of this project aimed to investigate the cause of FGD in one affected individual with linkage to a region on chromosome 3. Following the discovery of *NNT* as a causal gene, the region was examined for genes in the same antioxidant pathway and *GPX1* was identified. GPX1 is an antioxidant enzyme that converts hydrogen peroxide to water. This arm of the project thereafter aimed to investigate *GPX1* as a putative candidate gene for FGD by sequencing further individuals with unknown aetiology for GPX1 mutations and examining its role in the adrenal cortex through *in vitro* and *in vivo* models. This revealed GPX1 ablation to cause a mild phenotype and subsequent finding of a ‘second hit’ in this

patient in *PRDX3* led to the investigation of gene knockdown for this enzyme too which revealed double knockdown of the two genes, but not single knockdowns, deleteriously affected human adrenocortical cell function.

6.2 Summary of findings

6.2.1 Proteomic Approach

A tandem affinity purification technique was employed to isolate interacting partners of MC2R and MRAP in human adrenocortical carcinoma (H295R) cells. Using the Interplay TAP mammalian system, N- and C-terminal MC2R and MRAP TAP-tag constructs were cloned, and MC2R-MRAP complexes possessing the double purification tag were capable of eliciting an ACTH response at the cell surface in HEK293 cells.

Lysates from H295R cells transfected with TAP-tag constructs were purified in two steps utilising the two purification tags, and analysed by mass spectrometry. The majority of proteins identified by mass spectrometry were highly abundant proteins such as cytoskeletal proteins. Although proteins such as β-tubulin might make good candidates for MC2R trafficking, the high occurrence of this type of protein as false positives in other studies meant these proteins could not be considered as candidates.

Following filtration of non-specific interactions five proteins remained, none of which were clear candidate proteins apart from clathrin which is involved in endocytosis of MC2R. It has previously been established that MC2R is internalised from the cell surface through a clathrin-dependent mechanism (Baig et al., 2001; Baig et al., 2002), however my data suggest that MC2R and clathrin interact directly. In order to confirm this result, reciprocal co-immunoprecipitation would be required.

Other proteins isolated using the TAP approach included a nuclear export protein, THO complex subunit 4, from MC2R-CTAP transfected cells. FGD and Triple A syndrome, another condition of adrenal insufficiency, are both associated with mutations in genes involved at the nuclear level. Mutations in *MCM4*, a DNA helicase, cause FGD in the Irish traveller community (Hughes *et al.*, 2012) and mutations in *AAAS*, a nuclear pore complex

protein are found in 90% of triple-A patients (Clark and Weber, 1998). However, as MC2R resides at the ER or cell surface, it is likely that these interactions were non- specific/non-physiological.

Similarly, mitochondrial proteins FDXR and MCCC2 were isolated from NTAP-MRAP and MRAP-CTAP transfected cells respectively, but according to current literature, MRAP also resides at the ER and the cell surface (Metherell *et al.*, 2005; Sebag and Hinkle, 2007; Webb *et al.*, 2009), and there is no data to suggest MRAP is mitochondrial or that MRAP has a mitochondrial leader sequence. It is therefore unclear whether these interactions are real.

Other proteomic techniques such as the yeast-2hybrid and bacterial-2-hybrid screens have been used by our laboratory to find interacting partners of MC2R, but have similarly failed to identify suitable candidate proteins. Although some studies have successfully isolated interacting partners of given proteins using the Interplay mammalian system (Griffin *et al.*, 2007; Xie *et al.*, 2009), others have failed to identify proteins that present clearly visible bands on a silver-stained SDS-PAGE (Ahlstrom and Yu, 2009), suggesting the problem is rooted in poor yield following purification preventing detection by MS. Studies that have succeeded in identifying interacting partners have carried out transfections on a larger scale (Griffin *et al.*, 2007; Xie *et al.*, 2009), which would increase the final yield after purification but may also increase the abundance of non-specific proteins. Other studies have taken further steps to reduce background noise from false positives, for example the use of high salt detergent washes (Ahlstrom and Yu, 2009). Furthermore, Interplay has developed a viral based delivery method for TAP-tagged genes to increase transfection efficiency, which would increase the recovery of target proteins and yield.

I therefore concluded from this section that despite the advantages of the TAP-tag technique over previous proteomic approaches, such as a natural environment for TMD proteins and the use of full length proteins, limitations remained in the high level of false positives and negatives. Namely, the affinity purification of TAP-tagged MC2R did not pull out endogenous MRAP and vice versus, which are known interacting partners. The technique would require further optimisation to increase yield and reduce background in order to find

interacting partners of MC2R and MRAP. It may be necessary to cotransfect TAP-tagged MC2R and MRAP to ensure cell surface expression of overexpressed MC2R, as correct subcellular localisation is key to the protein's function.

6.2.2 Genomic approach

In the genomic approach, a region of linkage in an FGD patient with unknown aetiology was screened for potential candidate genes, and *GPX1* was identified, based on the function and pathway of NNT (Fig.6.1). Sequencing the gene revealed a homozygous in-frame 12bp deletion in exon 2; c.del388-399; p.R130-L133del, this was heterozygous in the parents and the unaffected sibling. This is the first description of a human mutation in *GPX1*. Clinically the proband was in his 30s, with a mild phenotype and no other medical conditions.

The mutation was functionally characterised by overexpressing FLAG-tagged R130-L133del in mammalian HEK293 cells, and Western blotting with anti-FLAG antibody showed that R130-L133del was poorly expressed compared to the wild type. Treatment of transfected cells with cycloheximide revealed R130-L133del had a shorter half-life than the wild type protein, and that treating transfected cells with MG132 to inhibit the 26S proteasome significantly increased R130-L133del levels, suggesting the protein is degraded. Furthermore, CHX significantly reduced R130-L133del abundance compared to DMSO treatment, but had no significant effect on WT transfected cells. Despite this, there was no statistical difference between protein abundance of WT and R130-L133del proteins after 10h CHX treatment, suggesting other mechanisms such as poor translation are also involved.

R130-L133del is on alpha-helix 3 and the oligomerisation domain of GPX1 (Fig. 4.9), a region responsible for subunit interface, hence it was originally hypothesised that the mutation would affect oligomerisation of the tetrameric selenoprotein. However, Western blot analysis of lysates run in a non-reducing buffer showed R130-L133del presented a similar banding pattern to wild type, suggesting the protein is able to form a tetramer.

The mutation may have affected enzymatic activity as the 12 base pairs cross over a c-Abl/Arg tyrosine kinase phosphorylation site known to influence GPX1 activity (Cao *et al.*,

2003a; Cao *et al.*, 2003b), and the deletion would shorten the distance between key residues involved in the active site, potentially altering the tertiary structure. It would be interesting to assess activity of R130-L133del compared with wild-type by purifying the two enzymes *in vitro*. Low protein levels could also be due to poor translation efficiency if the mRNA was destabilised by the deletion, as selenocysteine incorporation is already an inefficient process that is sensitive to discrete changes in the transcript sequence (Kasaikina *et al.*, 2011). Poor expression levels could be investigated by substituting the selenocysteine for a cysteine, which may rescue the transcript from nonsense mediated decay.

Poor expression levels and degradation of GPX1 would reduce antioxidant defence and potentially increase cellular oxidative stress levels. A human model of *GPX1* knockdown was developed by lentiviral transduction of adrenal H295R cells with shRNA targeting GPX1, achieving 50% mRNA and 90% protein knockdown to investigate the role of GPX1 in the human adrenal cortex.

The effects of *GPX1* KD on steroidogenesis were investigated by immunoblotting lysates with an antibody to StAR, and found to be significantly lower in GPX-KD cells compared to wild type, with or without hydrogen peroxide treatment. The reduction in StAR protein levels posed a potential mechanism for FGD, as mutations in StAR that leave 20% of residual activity are a known cause of FGD (Metherell *et al.*, 2009). Furthermore, multiple studies have demonstrated that ROS impairs steroidogenesis through suppression of StAR protein levels in a mechanism that is not fully understood (Diemer *et al.*, 2003; Jin *et al.*, 2011; Kil *et al.*, 2012; Shi *et al.*, 2010).

Total GPX activity (all 8 GPX genes), measured by spectrophotometric assay, was 50% lower in GPX1 knockdown cells compared to wild type, suggesting GPX1 contributes 50% of total GPX activity and is therefore the predominant form of GPX in the adrenal cortex, and other GPXs do not compensate for its loss.

I anticipated loss of 50% GPX activity would have a significant impact on oxidative stress levels in the adrenal cortex. However, *GPX1* KD had no effect on SOD2 or NRF2 protein

levels, which are usually upregulated during oxidative stress (Purdom-Dickinson *et al.*, 2007; Warner *et al.*, 1996).

GPX1 KD cells did however, show increased basal levels of cleaved-PARP, a marker of apoptosis. But this finding was not recapitulated using an MTS assay to measure cell viability, which showed *GPX1* KD had no effect on viability under normal physiological conditions. The MTS assay did show that *GPX1* KD cells were more susceptible to H_2O_2 induced death than wild type cells. These experiments do reflect previously published *in vivo* studies on GPX1$^{-/-}$ mice showing mice are more susceptible to paraquat induced lethality than their wild type counterparts (Cheng *et al.*, 1998; de Haan *et al.*, 1998), and studies on cultured cells from *GPX1*$^{-/-}$ mice, which have higher levels of pro-apoptotic markers (Cheng *et al.*, 2003), following oxidative stress and in one study under low oxidative (6% oxygen) conditions (Lee *et al.*, 2006).

Post-mortem analysis of adrenals taken from FGD patients show disorganised cells of the ZG and loss of the ZF (Clark and Weber, 1998). Similarly, an autopsy of the 5-month old sibling of the proband revealed small adrenal with loss of the ZF. The DNA of this individual was not available for sequencing, however in light of this finding the adrenals of *GPX1*$^{-/-}$ mice were analysed by immunohistochemistry, staining with conventional H&E dyes and zonal specific markers IZA-1 (ZF and ZR marker) and CYP11A1 (ZG, ZF and ZR) to view morphology, and cleaved caspase-3, a marker of apoptosis.

GPX1$^{-/-}$ mice had normal adrenal morphology and zonation, and the expression of CYP11A1 also indicated the cells had steroidogenic capacity. Immunofluorescent staining with antibody to cleaved caspase-3 was pronounced in *GPX1*$^{-/-}$ adrenals in an unusual pattern resembling that of vascular endothelial cells which ran between cells of the ZG and the columnar structures of the ZF, suggesting increased apoptosis in the vasculature supplying the adrenal gland.

By comparison, mice harbouring a loss of function mutation in *NNT* have overcrowded, disorganised cells in the ZF with increased cleaved caspase-3 staining in the ZF, but do not

display the same vascular staining pattern (Meimaridou *et al.*, 2012b). There was no cleaved caspase-3 staining in steroidogenic cells of *GPX1*$^{-/-}$ mice suggesting steroidogenic cells were not apoptotic under physiological conditions, reflecting data gained in human H295R cells by MTS assay.

GPX1 has previously been implicated in the protection of vascular endothelial cells against ROS generated from NO during vasorelaxation, and *GPX1*$^{+/-}$ mice are more susceptible to vascular endothelial dysfunction following treatment with agonists of NO (Forgione *et al.*, 2002). Increased levels of oxidative stress in the adrenal vasculature may impact on adjacent steroidogenic cell function. However, although basal corticosterone levels of *GPX1*$^{-/-}$ mice were reduced, levels were not significantly different to wild type mice. By comparison, *NNT* mutant mice have 50% lower basal corticosterone levels than wild type.

The data gained from the *GPX1*$^{-/-}$ mouse model indicated that absence of a functional GPX1 did not significantly perturb steroidogenesis in the mouse adrenal cortex nor did it cause atrophy of the gland. There was a trend of reduced corticosterone in *GPX1*$^{-/-}$ mice compared to wild type, however the change was not significant. Similarly, despite 50% less GPX activity and a reduction in StAR protein levels in H295R *GPX1*-KD cells, levels of oxidative stress markers and cell viability showed variable degrees of change, suggesting no strong trend. Furthermore, sequencing of 100 individuals with FGD did not reveal another homozygous mutation in *GPX1*.

Taken together these data indicate GPX1 loss of function may not have a severe phenotype. This brought me to the conclusion that another gene defect may be present in the proband, which I hypothesised to be another protein involved in mitochondrial antioxidant defence like NNT.

Whole exome sequencing of the proband and analysis of nucleotide level variation with a filtration strategy revealed a homozygous stop gain mutation in *PRDX3*, p.Q67X, another antioxidant enzyme which catalyses the conversion of H_2O_2 to water. The mutation removed key residues for enzymatic activity which would cause a loss of function. *PRDX3* was a

good candidate gene because of its role in antioxidant defence as a mitochondrial peroxidase that contributes to a reported 90% of H_2O_2 removal in mouse adrenocortical cells (Cox *et al.*, 2010).

However, Sanger sequencing a further 100 FGD patients of unknown aetiology revealed only one missense mutation in *PRDX3*, and DNA from this individual's relatives was not available. Furthermore, Sanger sequencing of the kindred revealed the mutation did not segregate with the disease, as it was homozygous in the unaffected sibling, which indicated *PRDX3* mutations alone were not capable of causing FGD. This raised the possibility that digenic inheritance of both defects was necessary to cause FGD, or that mutation in *GPX1* alone was responsible for disease progression. We hypothesised that *PRDX3* and *GPX1* loss of function had a cumulative effect in mitochondrial redox homeostasis in adrenocortical cells which may lead to the progression of FGD in this patient.

Knockdown of both *PRDX3* and *GPX1* in H295R cells caused a significant reduction in cell viability at normal physiological conditions, which was not seen for *PRDX3* or *GPX1* knockdown alone unless cells were treated with hydrogen peroxide. This gave evidence to suggest that loss of *GPX1* or *PRDX3* function alone decrease viability, but a notable effect was only evident at physiological levels when both genes were silenced. Both genes have been shown to be individually implicated in modulation of apoptosis through influencing cellular ROS levels (Chang et al., 2004; Cheng et al., 2003; De Haan et al., 2003; De Simoni et al., 2008; Fu et al., 1999; Fu et al., 2001; Liddell et al., 2006a), however this is the first illustration of the effect of dual knockdown of these genes on cell viability in a human cell line.

The effects of dual knockdown on steroidogenesis were not conclusive. In previous experiments, knockdown of *GPX1* alone significantly decreased StAR protein levels compared to the SCR control. However, when investigating dual knockdown, only a general trend was observed where levels of StAR protein were highest in the SCR negative control cell line, followed by *PRDX3*-KD cells, then *GPX1*-KD cells and lowest in the *double*-KD

cell line. The only significant difference seen was between *PRDX3*-KD and SCR control cell lines.

Levels of ph-p38MAPK were measured because it has been reported that H_2O_2 impairs StAR function by activating p38MAPK, which through an unknown mechanism decreases synthesis of StAR protein (Kil *et al.*, 2012). p38MAPK levels followed a similar trend, and significance was only reached between *PRDX3*-KD and SCR control cell lines. Basal cortisol levels measured by immunoassay, were also lowest in the double knockdown cell line, but there was no significant difference to scrambled cells.

These preliminary data suggest that even when combined, loss of function in *GPX1* and *PRDX3* presents a mild phenotype. Knockdown of *NNT* in analogous cells causes a more severe phenotype (Meimaridou *et al.*, 2012b). For example, KD of *NNT* significantly reduced the GSH/GSSG ratio, which is associated with increased oxidative pressure and decreased viability. *GPX1* and *PRDX3* KD alone or in combination did not deplete GSH levels. NNT supplies NAPDH to mitochondria, which is the principle electron donor at the beginning of an electron transfer chain involving multiple mitochondrial antioxidants (Fig. 6.1). GPX1 and PRDX3 are placed at the end of this electron chain, with the least influence over other antioxidants, which may reduce the severity of a loss in function in these genes.

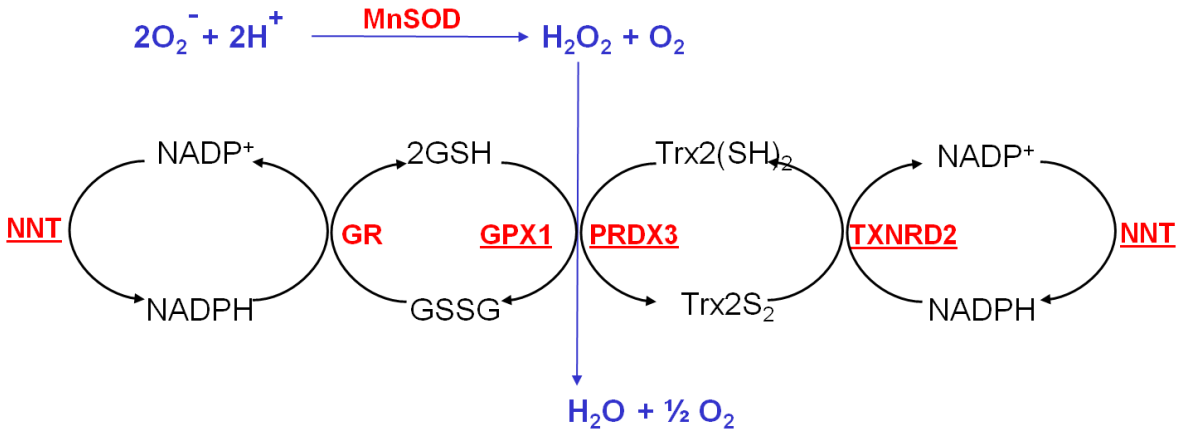

Figure 6. 1: Mitochondrial antioxidants.

Genes that have are causal or putative for FGD are underlined. Nicotinamide transhydrogenase (NNT) maintains high levels of NADPH which reduce glutathione

reductase (GR) and mitochondrial specific thioredoxin reductase 2 (TXNRD2). TXNRD2 reduces glutathione, maintaining a high reduced (GSH) to oxidised (GSSG) glutathione ratio, and TXNRD2 reduces thioredoxin 2 (Trx2) in parallel. GSH subsequently reduces glutathione peroxidase 1 (GPX1) and Trx2 reduces peroxiredoxin 3 (PRDX3). GPX1 and PRDX3 both reduce hydrogen peroxide (H_2O_2), which is the product of manganese superoxide dismutase (MnSOD).

Although GPX1 and PRDX3 are the predominant mitochondrial peroxidases, PRDX5 and mtGPX4 (predominantly in testes) are also a mitochondrial with the same function, and may delay an accumulation of H_2O_2. Furthermore, the proband of this study had a relatively mild phenotype with late presentation. Therefore, the effects of *GPX1* and *PRDX3* loss of function may be progressive, as are the effects of accumulated oxidative stress in conditions such as X-ALD where the AMN phenotype presents typically between ages 20 and 30 in hemizygous males (Chaudhry *et al.*, 1996).

However, I cannot rule out the possibility that neither *GPX1* nor *PRDX3* are causal genes in this proband. I do believe this thesis presents strong evidence to support *GPX1* and *PRDX3* as causal genes. Firstly, resequencing of the whole exome did not reveal any other potential candidate genes, and secondly I presented data showing the genes additively decrease viability of adrenal cells which could affect steroid secretion. There was also evidence that individual knockdown of *GPX1* or *PRDX3* significantly reduces StAR protein levels.

The identification of *PRDX3* and *GPX1* mutations in an individual with FGD, adds to the increasing number of oxidative stress genes that have been associated with the condition (Fig.6.1). As well as mutations in *NNT, TXNRD2* mutations have recently been described in one kindred (Prasad *et al. unpublished*). TXNRD2 is a mitochondrial antioxidant that reduces thioredoxin, and is reduced by NADPH supplied by NNT (Fig. 6.1). Mutations in *TXNRD2* cause a more severe phenotype of FGD than seen for my proband, and additional phenotypes of trivial tricuspid and mitral valve regurgitation were found in one patient.

Other conditions of adrenal insufficiency have also been associated with defects causing oxidative stress. For example, X-ALD is a condition of adrenal insufficiency and axonal degeneration, characterised by the accumulation of VLCFAs in the peroxisome leading to elevated oxidative stress (Galea *et al.*, 2012). Triple A syndrome, characterised by adrenal insufficiency and neurological impairment, is caused by mutations in *AAAS*, which encodes a nuclear pore complex protein (ALADIN) involved in nuclear import of the DNA-protective ferritin heavy chain. Knockdown of *AAAS* has been shown to reduce GSH levels in cultured adrenocortical and neuronal cells, but decrease cell viability only in adrenocortical cells (Prasad *et al.*, 2013).

The antioxidant genes associated with the above conditions all encode ubiquitous proteins, highlighting the sensitivity of the adrenal cortex to oxidative stress compared to other tissues. Indeed, steroidogenic cells are more likely to endure oxidative damage because of the additional source of ROS formed by steroidogenic enzymes. Multiple studies have illustrated the impact of ROS on impairing steroidogenesis (Diemer *et al.*, 2003; Shi *et al.*, 2010; Tsai *et al.*, 2003), and shown that StAR protein levels are reduced by oxidative stress (Diemer *et al.*, 2003; Jin *et al.*, 2011; Shi *et al.*, 2010). In this project, I showed knockdown of *GPX1* and *PRDX3* were individually capable of reducing StAR protein levels.

The electron donor system that supplies the steroidogenic enzymes is leaky, leading to superoxide radical formation. Steroidogenic CYP enzymes are expressed at ten times the concentration of mitochondrial respiratory enzymes, which constitute the main source of ROS in non-steroidogenic cells, hence the capacity for steroidogenic cells to produce ROS is far greater than other cell types (Hanukoglu and Hanukoglu, 1986). The predominant source of electron leakage is CYP11B1, which accounts for 40% leakage compared to 15% by CYP11A1 (Rapoport *et al.*, 1995). CYP11B1 is also more sensitive to ROS than other CYP enzymes undergoing degradation in the absence of antioxidants (Hanukoglu *et al.*, 1990; Hornsby, 1989; Hornsby *et al.*, 1985). This increased electron dispersal and sensitivity to ROS may explain why defects in oxidative stress genes are able to cause isolated glucocorticoid deficiency with no changes to mineralocorticoid levels.

Concentrations of antioxidants are particularly high in the adrenal cortex, presumably to compensate for excess ROS produced by steroidogenic CYP enzymes (Azhar *et al.*, 1995; Hanukoglu, 2006). Concentrations of vitamin C, vitamin E and glutathione are considerably higher in the adrenal than other tissues, and the expression and activity of antioxidant enzymes *SOD1*, *SOD2* and *GPX* and concentration of *PRDX3* are also higher particularly within the ZF and ZR (Azhar *et al.*, 1995; Hanukoglu, 2006; Watabe *et al.*, 1994). My data also reported high expression of *GPX1* and *GPX4* in the human adrenal cortex and it has previously been demonstrated that *PRDX3* is highly expressed in the adrenal cortex of mice and is the predominant antioxidant enzyme in adrenocortical mitochondria (Kil *et al.*, 2012). Recent work in our laboratory has also demonstrated *TXNRD2* is particularly highly expressed in the human adrenal cortex compared to other tissues.

Both GPX1 and TXNRD2 are selenoproteins, which generally appear to be important in the adrenal cortex, as Se is preferentially retained in the adrenal and testes following Se deprivation in rats (Behne and Höfer-Bosse, 1984). Other endocrine organs such as the thyroid also retain high levels of selenium (Beckett and Arthur, 2005). The majority of selenoproteins are involved in redox homeostasis, and Se deficiency can influence thyroid hormone metabolism, fertility and insulin signalling (Beckett and Arthur, 2005). Mutations in *SBP2*, part of the selenocysteine incorporation machinery, lead to a multisystem disorder in humans (Schoenmakers *et al.*, 2010). The discovery of mutations in individual selenoproteins causing isolated adrenal dysfunction stresses the importance of redox homeostasis in the adrenal cortex. Interestingly, several studies have demonstrated the benefit of Se supplementation in endocrine disorders such as autoimmune thyroid disorders (Drutel *et al.*, 2013). The effects of supplementation are attributed to the regulation of ROS and its effect on the immune system (Drutel *et al.*, 2013).

Likewise, in both models of X-ALD and triple A, antioxidant treatment can rescue the effects of oxidative stress. In the *AAAS* KD model, the reduction in cortisol could be partly rescued by treatment of cells with N-acetylcysteine (NAC). The mouse model of X-ALD (*ABCD1*$^{-/-}$ mice) is characterised by a neurodegenerative AMN-like phenotype and mice have oxidative

damage in the spinal cords prior to disease progression, which is thought to be due to build-up of VLCFAs. López-Erauskin *et al.* (2011) showed that a combination of antioxidants a-tocopherol, NAC, and a-lipoic acid (LA) reversed oxidative damage to proteins in spinal cords and halted histopathological signs of axonal degeneration, thus preventing clinical progression (López-Erauskin *et al.*, 2011). This study raised the implication that early intervention with antioxidant treatment could pose a potential therapeutic option for treating conditions of oxidative stress (López-Erauskin *et al.*, 2011).

The relationship between the adrenal cortex and antioxidant defence is evident by role of ACTH in influencing antioxidant expression and activity. Expression and activity of antioxidants *SOD2* and *SRX*, which recycles inactivated PRDX3, are both upregulated by ACTH (Belge *et al.*, 2004; Kil *et al.*, 2012; Raza and Vinson, 2000). Furthermore, in rhesus monkeys, levels of antioxidants SOD2 in blood correlates with cortisol in a diurnal rhythm which flattens in amplitude with age, suggesting cortisol regulates SOD expression (Goncharova *et al.*, 2006)**.** Similarly, PRDX3 has been recently reported to be involved in intra-adrenal negative feedback loop in which ROS regulates steroidogenesis through inactivation of PRDX3, making *PRDX3* a particularly strong candidate gene for FGD. In mice levels of H_2O_2, PRDX-SO_2, ph-p38MAPK and StAR correlate with corticosterone circadian rhythms and in mutant SRX mice the amplitude of oscillations and corticosterone levels are reduced. Interestingly, GPX and GR activities do not have diurnal rhythms and GPX is not upregulated by ACTH (Belge *et al.*, 2004; Goncharova *et al.*, 2006)**.** Although GPX1 does not follow circadian rhythms, Se deficient AN4Rppc7 adrenal cells with minimal GPX1 activity exhibit a marked decrease in corticosterone after cAMP stimulation compared to Se adequate cells. These studies suggest a strong link between antioxidant activity and the regulation of adrenal steroidogenesis.

My findings and the data reported in the above studies suggest *GPX1* and *PRDX3* are good candidate genes for FGD. It is therefore surprising that dual knockdown did not cause a significant reduction in cortisol production or steroidogenic capacity. The data presented is preliminary and may require more experimental repeats. The H295R KD model was chosen

in order to investigate a human model of the adrenal cortex. Although H295R cells have been widely used and have a similar steroidogenic gene expression profile to the human adrenal cortex (Oskarsson *et al.*, 2006), a very recent report by Kil *et al.* (2013), suggested that H295R and mouse Y-1 clonal cell lines are not suitable for *in vitro* models of redox signalling in the context or steroidogenesis, as levels of SRX are far higher and levels of PRDX3 are much lower than in mouse adrenals, and neither SRX or PRDX3 hyperoxidation are influenced by ACTH stimulation. The same characteristics are observed in mouse primary adrenocortical cells shortly after isolation (Kil *et al.*, 2013). This report raises concerns for our future studies of human adrenal steroidogenesis where *in vivo* studies are not possible.

In vivo mouse models of adrenal disorders have been explored, however many cases do not fully recapitulate the human model. For example, whereas post-mortem analysis of adrenals taken from triple A patients show atrophy of the ZF, *Aaas*$^{-/-}$ mouse model shows no histological abnormalities compared to wild type, and only mild neurological disturbances (Huebner *et al.*, 2006). Post mortem histological analyses of FGD patient adrenals show disorganised glomerulosa cells and absent ZF and ZR. However, *NNT* mutant mice display only a mild disorganisation of the ZF cells. Furthermore, although *NNT* mutant mice had 50% less basal corticosterone levels, patients are usually almost deplete of cortisol. If *GPX1* mutations cause a mild phenotype in the adrenal cortex, it may not be surprising that a significant decrease in corticosterone production was not seen in the knockout mouse.

Because of the limitations of mouse models and *in vitro* models, future work may need to apply other available *in vivo* models. Non-human primates such as the rhesus monkey have been used in studies to characterise expression and activity levels of antioxidant enzymes in the adrenal cortex and the correlation of antioxidants and cortisol during aging (Goncharova *et al.*, 2008; Goncharova *et al.*, 2006; Goncharova *et al.*, 2013). Unlike rodents, non-human primates express *CYP17* and therefore produce adrenal androgens, a better representation of human steroidogenesis.

Zebrafish are also emerging as a popular model to study steroidogenesis. Steroid synthesis occurs in the gonads, brain and interrenal, a region of steroidogenic cells homologous to the adrenal cortex in head kidney cells (Tokarz *et al.*, 2013). Synthesis of cortisol, the major glucocorticoid in zebrafish, is under the control of the hypothalamic-pituitary-interrenal axis (Liu *et al.*, 2011; Tokarz *et al.*, 2013)**.** Despite these anatomical differences the steroidogenic signalling pathway and steroid receptors are highly conserved between mammals and zebrafish (Tokarz *et al.*, 2013). However, a portion of the steroidogenesis pathway remains uncharacterised, for example steroidogenic enzymes *cyp21a* and *cyp11b,* and functional evidence is limited (Busby et al., 2010). In terms of practically zebrafish offer many benefits that make them an attractive model. Many endocrine genes are single copies making genetic manipulation such as CRISPR interference straightforward. The high numbers of progeny produced by single crosses are ideal for high throughput screens and the small size of fish makes for easy maintenance (Löhr and Hammerschmidt, 2011). The small size also allowed whole fish immunostaining or *in situ* hybridisation and the transparency of fish during embryogenesis also allows for use of transgene-encoded fluorochromes (Löhr and Hammerschmidt, 2011). Zebrafish have been used to study the toxic effects of endocrine disrupting chemicals (EDCs) such as oestrogens, gestagens or selenomethionine, which interfere with steroidogenesis (Tokarz *et al.*, 2013)**,** and therefore may present a useful model for future studies.

In conclusion, mutations in genes involved in antioxidant defence, or that lead to oxidative stress, are being increasingly associated with conditions involving adrenal insufficiency, emphasising the sensitivity of the adrenal cortex to oxidative changes. In this thesis, I have discovered an FGD patient with mutations in two antioxidant genes and provided data to suggest that loss of function in *GPX1* alone, or in combination with PRDX3 may cause FGD. Whole exome sequencing of the remaining 39% FGD patients with unknown aetiology may reveal further genes in the same antioxidant pathway.

6.3 Future directions

The future work after this project will confirm some of findings of this thesis. Firstly, the interaction of MC2R with clathrin will be checked by reciprocal co-immunoprecipitation. The subcellular localisation of TAP-tagged proteins should also be verified with compartmental markers, a step that was not taken. In addition, to further test the efficiency of the TAP system, an additional control experiment should be carried out, to coimmunoprecipitate MC2R and MRAP, using the TAP-tag technique, for example by pulling down with TAP-tagged MC2R and probing for FLAG tagged MRAP. The lysates would be subjected to Western blot analysis to confirm the proteins interact, and the gel would be stained and subjected to MS analysis to confirm whether MS was sensitive enough to detect the isolated proteins.

Although the TAP-tag technique could be further optimised, the genetic approach of whole exome sequencing is a more time and cost effective in identifying causes of FGD, hence the proteomic approach would not be continued further.

In this thesis I showed the R130-L133del protein had a shorter half-life than WT, and CHX treatment resulted in significantly less R130-L133del protein compared to vehicle by 10 hours, whereas the WT protein abundance did not significantly decrease. However there was no statistical difference between the percentage protein remaining for WT and R130-L133del. A more efficient technique to confirm degradation is the pulse-chase technique, which could be employed in future to confirm current data.

I also considered the possibility that low protein abundance of R130-L133del could be due to reduced mRNA transcript levels due to nonsense mediated decay. *GPX1* is a prime candidate for nonsense mediated decay because it has a UGA codon in the middle of an exon that is at least 50bp away from the intron (Lubos *et al.*, 2011; Silva and Romão, 2009). As a selenoprotein *GPX1* has a UGA stop codon that encodes the selenocysteine at its active site (Chambers *et al.*, 1986; Kraus *et al.*, 1983), and translation of the residue is dependent on selenium and the SECIS element in the 3'UTR (Berry et al., 1991; Shen et al., 1993; Shen et

al., 1995). In absence of these factors, evidence suggests the residue is read as a stop codon and the protein subsequently undergoes nonsense mediated decay (Shen *et al.*, 1993).

Variants and truncations that affect mRNA stability or selenocysteine incorporation may render the transcript more susceptible to nonsense mediated decay. Kasaikina *et al.* (2011) described a stop gain mutation in the naked mole rat GPX1 only five residues premature of the original stop codon. Functional characterisation of this protein showed that it had poor protein and mRNA expression, which was rescued by substituting the selenocysteine residue for a cysteine, suggesting the premature stop codon affected incorporation of the selenocysteine and mRNA stability. Using similar methodology, I plan to investigate whether R130-L133del affects mRNA stability by mutating the selenocysteine to cysteine using site directed mutagenesis in this transcript and checking whether protein levels are partially rescued.

The preliminary data collected from characterising *GPX1* and *PRDX3* double KD cell lines suggested a trend of reduced StAR and cortisol levels, however the data did not reach statistical significance. One of the most important future directions is to gain more experimental repeats for these experiments to clarify whether this trend is real. In addition to these experiments, the levels of StAR in SCR and KD cells would be measured following forskolin treatment, which may give a better indication to the effects of GPX1 and PRDX3 on steroidogenesis. The use of DEX to deplete pre-existing StAR could also be applied before forskolin treatment, to remove masking of changes in abundance of newly synthesised StAR. Furthermore, it would be necessary to measure the 37kDa form of StAR, which has been reported as the active form in several studies (Miller, 2013).

The *double*-KD cell line showed reduced cell viability at physiological conditions, however I did not measure cellular levels of ROS. As GPX1 and PRDX3 both reduce hydrogen peroxide, a spectrophotometric/fluorometric assay that measures H_2O_2 levels would be most appropriate. This data would confirm higher levels of oxidative stress in adrenocortical cells absent of *GPX1* and *PRDX3* expression. Previous studies have also shown that cells expressing a defective *PRDX3* have altered mitochondrial morphology (Mukhopadhyay *et*

al., 2006). It would therefore be interesting to explore the effects of double knockdown on the mitochondrial network in adrenocortical cells using mitochondrial markers such as MitoDSred.

It has been well documented that *GPX1*$^{-/-}$ mice are normal and viable and do not show abnormalities until 15 months (Esposito *et al.*, 2000). Our proband has a relatively mild phenotype and is in his 30's. Taking these factors into consideration, it would be desirable to study the adrenal morphology of older *GPX1*$^{-/-}$ mice. A progressive effect of decreased antioxidant defence may be apparent on staining with conventional dyes, and greater differences in basal and stimulated corticosterone levels may also be apparent. Similarly the *Prdx3*$^{-/-}$ mouse has been described to have increased susceptibility to oxidative stress but no adrenal phenotype is reported (Li et al., 2007). An investigation into possible adrenal dysfunction in these mice might yield positive results. Ultimately I would hope to generate a double knockout murine model for future studies.

My immunofluorent studies on *GPX1*$^{-/-}$ adrenals showed increased cleaved-caspase-3 staining suggesting increased apoptosis. To follow up this data, I would like to co-stain adrenal sections with Platelet endothelial cell adhesion molecule (PECAM-1), an endothelial and platelet cell marker, to confirm whether it is this type of cell that has increased apoptosis. It would also be interesting to further these experiments by quantifying apoptosis levels using a TUNEL assay to detect DNA fragmentation.

Given that mouse models do not always fully recapitulate human disease, it would also be interesting to use zebrafish models to explore the effects of antioxidant gene KD on steroidogenesis should the orthologs be identifiable.

Finally, since employing next generation sequencing, our research group has identified 3 causal genes and 2 putative candidate genes in the pathogenesis of FGD. The identification of novel causes of FGD has accelerated in recent years, because of the low time consumption and high quantity of data gained from the sequencing process. Whole exome sequencing is thus emerging as a useful diagnostic tool for monogenic disorders, which may allow more

targeted therapeutic treatment in future. It is therefore in the interest of our research group to continue to employ whole exome sequencing to unveil the remaining genetic causes of the 39% of FGD patients with unknown aetiology. Based on recent studies and the findings of this thesis, I anticipate a proportion of these genes will be involved in oxidative stress.

References

Agulleiro, M. J., S. Roy, E. Sánchez, S. Puchol, N. Gallo-Payet, and J. M. Cerdá-Reverter, 2010, Role of melanocortin receptor accessory proteins in the function of zebrafish melanocortin receptor type 2: Mol Cell Endocrinol, v. 320, p. 145-52.

Ahlstrom, R., and A. S. Yu, 2009, Characterization of the kinase activity of a WNK4 protein complex: Am J Physiol Renal Physiol, v. 297, p. F685-92.

Ahonen, P., S. Myllärniemi, I. Sipilä, and J. Perheentupa, 1990, Clinical variation of autoimmune polyendocrinopathy-candidiasis-ectodermal dystrophy (APECED) in a series of 68 patients: N Engl J Med, v. 322, p. 1829-36.

Akın, L., S. Kurtoğlu, M. Kendirici, and M. A. Akın, 2010, Familial glucocorticoid deficiency type 2: a case report: J Clin Res Pediatr Endocrinol, v. 2, p. 122-5.

Andersen, G. N., M. Hägglund, O. Nagaeva, L. Frängsmyr, R. Petrovska, L. Mincheva-Nilsson, and J. E. Wikberg, 2005, Quantitative measurement of the levels of melanocortin receptor subtype 1, 2, 3 and 5 and pro-opio-melanocortin peptide gene expression in subsets of human peripheral blood leucocytes: Scand J Immunol, v. 61, p. 279-84.

Arai, M., H. Imai, T. Koumura, M. Yoshida, K. Emoto, M. Umeda, N. Chiba, and Y. Nakagawa, 1999, Mitochondrial phospholipid hydroperoxide glutathione peroxidase plays a major role in preventing oxidative injury to cells: J Biol Chem, v. 274, p. 4924-33.

Arakane, F., S. R. King, Y. Du, C. B. Kallen, L. P. Walsh, H. Watari, D. M. Stocco, and J. F. Strauss, 1997, Phosphorylation of steroidogenic acute regulatory protein (StAR) modulates its steroidogenic activity: J Biol Chem, v. 272, p. 32656-62.

Arakane, F., T. Sugawara, H. Nishino, Z. Liu, J. A. Holt, D. Pain, D. M. Stocco, W. L. Miller, and J. F. Strauss, 1996, Steroidogenic acute regulatory protein (StAR) retains

activity in the absence of its mitochondrial import sequence: implications for the mechanism of StAR action: Proc Natl Acad Sci U S A, v. 93, p. 13731-6.

Arkblad, E. L., S. Tuck, N. B. Pestov, R. I. Dmitriev, M. B. Kostina, J. Stenvall, M. Tranberg, and J. Rydström, 2005, A Caenorhabditis elegans mutant lacking functional nicotinamide nucleotide transhydrogenase displays increased sensitivity to oxidative stress: Free Radic Biol Med, v. 38, p. 1518-25.

Arlt, W., and B. Allolio, 2003, Adrenal insufficiency: Lancet, v. 361, p. 1881-93.

Arlt, W., E. A. Walker, N. Draper, H. E. Ivison, J. P. Ride, F. Hammer, S. M. Chalder, M. Borucka-Mankiewicz, B. P. Hauffa, E. M. Malunowicz, P. M. Stewart, and C. H. Shackleton, 2004, Congenital adrenal hyperplasia caused by mutant P450 oxidoreductase and human androgen synthesis: analytical study: Lancet, v. 363, p. 2128-35.

Arvat, E., L. Di Vito, F. Lanfranco, M. Maccario, C. Baffoni, R. Rossetto, G. Aimaretti, F. Camanni, and E. Ghigo, 2000, Stimulatory effect of adrenocorticotropin on cortisol, aldosterone, and dehydroepiandrosterone secretion in normal humans: dose-response study: J Clin Endocrinol Metab, v. 85, p. 3141-6.

Asai, M., S. Ramachandrappa, M. Joachim, Y. Shen, R. Zhang, N. Nuthalapati, V. Ramanathan, D. E. Strochlic, P. Ferket, K. Linhart, C. Ho, T. V. Novoselova, S. Garg, M. Ridderstråle, C. Marcus, J. N. Hirschhorn, J. M. Keogh, S. O'Rahilly, L. F. Chan, A. J. Clark, I. S. Farooqi, and J. A. Majzoub, 2013, Loss of function of the melanocortin 2 receptor accessory protein 2 is associated with mammalian obesity: Science, v. 341, p. 275-8.

Asheuer, M., I. Bieche, I. Laurendeau, A. Moser, B. Hainque, M. Vidaud, and P. Aubourg, 2005, Decreased expression of ABCD4 and BG1 genes early in the pathogenesis of X-linked adrenoleukodystrophy: Hum Mol Genet, v. 14, p. 1293-303.

Atanasova, S., N. von Ahsen, C. Schlumbohm, E. Wieland, M. Oellerich, and V. Armstrong, 2006, Marmoset glutathione peroxidases: cDNA sequences, molecular evolution, and gene expression: J Med Primatol, v. 35, p. 155-64.

Avissar, N., D. B. Ornt, Y. Yagil, S. Horowitz, R. H. Watkins, E. A. Kerl, K. Takahashi, I. S. Palmer, and H. J. Cohen, 1994, Human kidney proximal tubules are the main source of plasma glutathione peroxidase: Am J Physiol, v. 266, p. C367-75.

Awasthi, Y. C., E. Beutler, and S. K. Srivastava, 1975, Purification and properties of human erythrocyte glutathione peroxidase: J Biol Chem, v. 250, p. 5144-9.

Ayres, P. J., J. Eichhorn, O. Hechter, N. Saba, J. F. Tait, and S. A. Tait, 1960, Some studies on the biosynthesis of aldosterone and other adrenal steroids: Acta Endocrinol (Copenh), v. 33, p. 27-58.

Azhar, S., L. Cao, and E. Reaven, 1995, Alteration of the adrenal antioxidant defense system during aging in rats: J Clin Invest, v. 96, p. 1414-24.

Baig, A. H., F. M. Swords, L. A. Noon, P. J. King, L. Hunyady, and A. J. Clark, 2001, Desensitization of the Y1 cell adrenocorticotropin receptor: evidence for a restricted heterologous mechanism implying a role for receptor-effector complexes: J Biol Chem, v. 276, p. 44792-7.

Baig, A. H., F. M. Swords, M. Szaszák, P. J. King, L. Hunyady, and A. J. Clark, 2002, Agonist activated adrenocorticotropin receptor internalizes via a clathrin-mediated G protein receptor kinase dependent mechanism: Endocr Res, v. 28, p. 281-9.

Baker, B. Y., L. Lin, C. J. Kim, J. Raza, C. P. Smith, W. L. Miller, and J. C. Achermann, 2006, Nonclassic congenital lipoid adrenal hyperplasia: a new disorder of the steroidogenic acute regulatory protein with very late presentation and normal male genitalia: J Clin Endocrinol Metab, v. 91, p. 4781-5.

Baker, B. Y., D. C. Yaworsky, and W. L. Miller, 2005, A pH-dependent molten globule transition is required for activity of the steroidogenic acute regulatory protein, StAR: J Biol Chem, v. 280, p. 41753-60.

Baker, R. D., S. S. Baker, K. LaRosa, C. Whitney, and P. E. Newburger, 1993, Selenium regulation of glutathione peroxidase in human hepatoma cell line Hep3B: Arch Biochem Biophys, v. 304, p. 53-7.

Banning, A., S. Deubel, D. Kluth, Z. Zhou, and R. Brigelius-Flohé, 2005, The GI-GPx gene is a target for Nrf2: Mol Cell Biol, v. 25, p. 4914-23.

Barnham, K. J., C. L. Masters, and A. I. Bush, 2004, Neurodegenerative diseases and oxidative stress: Nat Rev Drug Discov, v. 3, p. 205-14.

Beckett, G. J., and J. R. Arthur, 2005, Selenium and endocrine systems: J Endocrinol, v. 184, p. 455-65.

Behne, D., and T. Höfer-Bosse, 1984, Effects of a low selenium status on the distribution and retention of selenium in the rat: J Nutr, v. 114, p. 1289-96.

Belge, F., A. Cmar, and M. Selcuk, 2004, Effects of stress produced by adrenocorticotropin (ACTH) on lipid peroxidation and some antioxidants in vitamin C treated and nontreated chickens., *South African Journal of Animal Science*, p. 201-205.

Bermano, G., J. R. Arthur, and J. E. Hesketh, 1996, Selective control of cytosolic glutathione peroxidase and phospholipid hydroperoxide glutathione peroxidase mRNA stability by selenium supply: FEBS Lett, v. 387, p. 157-60.

Bermano, G., F. Nicol, J. A. Dyer, R. A. Sunde, G. J. Beckett, J. R. Arthur, and J. E. Hesketh, 1995, Tissue-specific regulation of selenoenzyme gene expression during selenium deficiency in rats: Biochem J, v. 311 (Pt 2), p. 425-30.

Berry, M. J., L. Banu, Y. Y. Chen, S. J. Mandel, J. D. Kieffer, J. W. Harney, and P. R. Larsen, 1991, Recognition of UGA as a selenocysteine codon in type I deiodinase requires sequences in the 3' untranslated region: Nature, v. 353, p. 273-6.

Betterle, C., C. Dal Pra, F. Mantero, and R. Zanchetta, 2002, Autoimmune adrenal insufficiency and autoimmune polyendocrine syndromes: autoantibodies, autoantigens, and their applicability in diagnosis and disease prediction: Endocr Rev, v. 23, p. 327-64.

Björnstedt, M., M. Hamberg, S. Kumar, J. Xue, and A. Holmgren, 1995, Human thioredoxin reductase directly reduces lipid hydroperoxides by NADPH and selenocystine strongly stimulates the reaction via catalytically generated selenols: J Biol Chem, v. 270, p. 11761-4.

Bose, H. S., V. R. Lingappa, and W. L. Miller, 2002, Rapid regulation of steroidogenesis by mitochondrial protein import: Nature, v. 417, p. 87-91.

Bose, H. S., O. H. Pescovitz, and W. L. Miller, 1997, Spontaneous feminization in a 46,XX female patient with congenital lipoid adrenal hyperplasia due to a homozygous frameshift mutation in the steroidogenic acute regulatory protein: J Clin Endocrinol Metab, v. 82, p. 1511-5.

Bose, H. S., T. Sugawara, J. F. Strauss, W. L. Miller, and I. C. L. A. H. Consortium, 1996, The pathophysiology and genetics of congenital lipoid adrenal hyperplasia: N Engl J Med, v. 335, p. 1870-8.

Bose, H. S., R. M. Whittal, M. A. Baldwin, and W. L. Miller, 1999, The active form of the steroidogenic acute regulatory protein, StAR, appears to be a molten globule: Proc Natl Acad Sci U S A, v. 96, p. 7250-5.

Bose, H. S., R. M. Whittal, Y. Ran, M. Bose, B. Y. Baker, and W. L. Miller, 2008, StAR-like activity and molten globule behavior of StARD6, a male germ-line protein: Biochemistry, v. 47, p. 2277-88.

Bosl, M. R., K. Takaku, M. Oshima, S. Nishimura, and M. M. Taketo, 1997, Early embryonic lethality caused by targeted disruption of the mouse selenocysteine tRNA gene (Trsp): Proc Natl Acad Sci U S A, v. 94, p. 5531-4.

Boston, B. A., 1999, The role of melanocortins in adipocyte function: Ann N Y Acad Sci, v. 885, p. 75-84.

Bradley, C. M., S. Jones, Y. Huang, Y. Suzuki, M. Kvaratskhelia, A. B. Hickman, R. Craigie, and F. Dyda, 2007, Structural basis for dimerization of LAP2alpha, a component of the nuclear lamina: Structure, v. 15, p. 643-53.

Brigelius-Flohé, R., K. D. Aumann, H. Blöcker, G. Gross, M. Kiess, K. D. Klöppel, M. Maiorino, A. Roveri, R. Schuckelt, and F. Usani, 1994, Phospholipid-hydroperoxide glutathione peroxidase. Genomic DNA, cDNA, and deduced amino acid sequence: J Biol Chem, v. 269, p. 7342-8.

Brigelius-Flohé, R., and M. Maiorino, 2013, Glutathione peroxidases: Biochim Biophys Acta, v. 1830, p. 3289-303.

Bryk, R., P. Griffin, and C. Nathan, 2000, Peroxynitrite reductase activity of bacterial peroxiredoxins: Nature, v. 407, p. 211-5.

Budiman, M. E., J. L. Bubenik, A. C. Miniard, L. M. Middleton, C. A. Gerber, A. Cash, and D. M. Driscoll, 2009, Eukaryotic initiation factor 4a3 is a selenium-regulated RNA-binding protein that selectively inhibits selenocysteine incorporation: Mol Cell, v. 35, p. 479-89.

Busby, E., G. J. Roch, and N. M. Sherwood, 2010, Endocrinology of zebrafish: a small fish with a large gene pool *in* S. Perry, F., A. P. Farrell, and C. J. Brauner, eds., Zebrafish: Fish Physiology, Academic Press Elsevier, p. 173–247.

Butler, A. A., R. A. Kesterson, K. Khong, M. J. Cullen, M. A. Pelleymounter, J. Dekoning, M. Baetscher, and R. D. Cone, 2000, A unique metabolic syndrome causes obesity in the melanocortin-3 receptor-deficient mouse: Endocrinology, v. 141, p. 3518-21.

Callewaert, L., and C. W. Michiels, 2010, Lysozymes in the animal kingdom: J Biosci, v. 35, p. 127-60.

Cao, C., Y. Leng, W. Huang, X. Liu, and D. Kufe, 2003a, Glutathione peroxidase 1 is regulated by the c-Abl and Arg tyrosine kinases: J Biol Chem, v. 278, p. 39609-14.

Cao, C., Y. Leng, C. Li, and D. Kufe, 2003b, Functional interaction between the c-Abl and Arg protein-tyrosine kinases in the oxidative stress response: J Biol Chem, v. 278, p. 12961-7.

Cao, Z., J. G. Lindsay, and N. W. Isaacs, 2007, Mitochondrial peroxiredoxins: Subcell Biochem, v. 44, p. 295-315.

Carazo, A., J. León, J. Casado, A. Gila, S. Delgado, A. Martín, L. Sanjuan, T. Caballero, J. A. Muñoz, R. Quiles, A. Ruiz-Extremera, L. M. Alcázar, and J. Salmerón, 2011, Hepatic expression of adiponectin receptors increases with non-alcoholic fatty liver disease progression in morbid obesity in correlation with glutathione peroxidase 1: Obes Surg, v. 21, p. 492-500.

Carlson, B. A., X. M. Xu, V. N. Gladyshev, and D. L. Hatfield, 2005, Selective rescue of selenoprotein expression in mice lacking a highly specialized methyl group in selenocysteine tRNA: J Biol Chem, v. 280, p. 5542-8.

Casey, J. P., M. Nobbs, P. McGettigan, S. Lynch, and S. Ennis, 2012, Recessive mutations in MCM4/PRKDC cause a novel syndrome involving a primary immunodeficiency and a disorder of DNA repair: J Med Genet, v. 49, p. 242-5.

Cha, M. K., C. H. Yun, and I. H. Kim, 2000, Interaction of human thiol-specific antioxidant protein 1 with erythrocyte plasma membrane: Biochemistry, v. 39, p. 6944-50.

Chabory, E., C. Damon, A. Lenoir, G. Kauselmann, H. Kern, B. Zevnik, C. Garrel, F. Saez, R. Cadet, J. Henry-Berger, M. Schoor, U. Gottwald, U. Habenicht, J. R. Drevet, and P. Vernet, 2009, Epididymis seleno-independent glutathione peroxidase 5 maintains sperm DNA integrity in mice: J Clin Invest, v. 119, p. 2074-85.

Chae, H. Z., H. J. Kim, S. W. Kang, and S. G. Rhee, 1999, Characterization of three isoforms of mammalian peroxiredoxin that reduce peroxides in the presence of thioredoxin: Diabetes Res Clin Pract, v. 45, p. 101-12.

Chagnon, Y. C., W. J. Chen, L. Pérusse, M. Chagnon, A. Nadeau, W. O. Wilkison, and C. Bouchard, 1997, Linkage and association studies between the melanocortin receptors 4 and 5 genes and obesity-related phenotypes in the Québec Family Study: Mol Med, v. 3, p. 663-73.

Chakravarthi, S., C. E. Jessop, and N. J. Bulleid, 2006, The role of glutathione in disulphide bond formation and endoplasmic-reticulum-generated oxidative stress: EMBO Rep, v. 7, p. 271-5.

Chambers, I., J. Frampton, P. Goldfarb, N. Affara, W. McBain, and P. R. Harrison, 1986, The structure of the mouse glutathione peroxidase gene: the selenocysteine in the active site is encoded by the 'termination' codon, TGA: EMBO J, v. 5, p. 1221-7.

Chan, L. F., A. J. Clark, and L. A. Metherell, 2008, Familial glucocorticoid deficiency: advances in the molecular understanding of ACTH action: Horm Res, v. 69, p. 75-82.

Chan, L. F., L. A. Metherell, and A. J. Clark, 2011, Effects of melanocortins on adrenal gland physiology: Eur J Pharmacol, v. 660, p. 171-80.

Chan, L. F., L. A. Metherell, H. Krude, C. Ball, S. M. O'Riordan, C. Costigan, S. A. Lynch, M. O. Savage, P. Cavarzere, and A. J. Clark, 2009a, Homozygous nonsense and frameshift mutations of the ACTH receptor in children with familial glucocorticoid deficiency (FGD) are not associated with long-term mineralocorticoid deficiency: Clin Endocrinol (Oxf), v. 71, p. 171-5.

Chan, L. F., T. R. Webb, T. T. Chung, E. Meimaridou, S. N. Cooray, L. Guasti, J. P. Chapple, M. Egertová, M. R. Elphick, M. E. Cheetham, L. A. Metherell, and A. J. Clark, 2009b, MRAP and MRAP2 are bidirectional regulators of the melanocortin receptor family: Proc Natl Acad Sci U S A, v. 106, p. 6146-51.

Chang, J. W., S. H. Lee, J. Y. Jeong, H. Z. Chae, Y. C. Kim, Z. Y. Park, and Y. J. Yoo, 2005, Peroxiredoxin-I is an autoimmunogenic tumor antigen in non-small cell lung cancer: FEBS Lett, v. 579, p. 2873-7.

Chang, T. S., C. S. Cho, S. Park, S. Yu, S. W. Kang, and S. G. Rhee, 2004, Peroxiredoxin III, a mitochondrion-specific peroxidase, regulates apoptotic signaling by mitochondria: J Biol Chem, v. 279, p. 41975-84.

Chanoine, J. P., N. A. Compagnone, A. C. Wong, and S. H. Mellon, 2001, Modulation of steroidogenesis by selenium in a novel adrenal cell line developed using targeted tumorigenesis: Biofactors, v. 14, p. 229-38.

Chaudhry, V., H. W. Moser, and D. R. Cornblath, 1996, Nerve conduction studies in adrenomyeloneuropathy: J Neurol Neurosurg Psychiatry, v. 61, p. 181-5.

Chavatte, L., B. A. Brown, and D. M. Driscoll, 2005, Ribosomal protein L30 is a component of the UGA-selenocysteine recoding machinery in eukaryotes: Nat Struct Mol Biol, v. 12, p. 408-16.

Chen, A. S., D. J. Marsh, M. E. Trumbauer, E. G. Frazier, X. M. Guan, H. Yu, C. I. Rosenblum, A. Vongs, Y. Feng, L. Cao, J. M. Metzger, A. M. Strack, R. E. Camacho, T. N. Mellin, C. N. Nunes, W. Min, J. Fisher, S. Gopal-Truter, D. E. MacIntyre, H. Y. Chen, and L. H. Van der Ploeg, 2000, Inactivation of the mouse melanocortin-3 receptor results in increased fat mass and reduced lean body mass: Nat Genet, v. 26, p. 97-102.

Chen, L., R. Na, M. Gu, A. B. Salmon, Y. Liu, H. Liang, W. Qi, H. Van Remmen, A. Richardson, and Q. Ran, 2008, Reduction of mitochondrial H2O2 by overexpressing peroxiredoxin 3 improves glucose tolerance in mice: Aging Cell, v. 7, p. 866-78.

Chen, M., C. J. Aprahamian, R. A. Kesterson, C. M. Harmon, and Y. Yang, 2007, Molecular identification of the human melanocortin-2 receptor responsible for ligand binding and signaling: Biochemistry, v. 46, p. 11389-97.

Chen, Q. M., D. Alexander, H. Sun, L. Xie, Y. Lin, J. Terrand, S. Morrissy, and S. Purdom, 2005, Corticosteroids inhibit cell death induced by doxorubicin in cardiomyocytes: induction of antiapoptosis, antioxidant, and detoxification genes: Mol Pharmacol, v. 67, p. 1861-73.

Cheng, W., Y. X. Fu, J. M. Porres, D. A. Ross, and X. G. Lei, 1999, Selenium-dependent cellular glutathione peroxidase protects mice against a pro-oxidant-induced oxidation of NADPH, NADH, lipids, and protein: FASEB J, v. 13, p. 1467-75.

Cheng, W. H., G. F. Combs, Jr., and X. G. Lei, 1998, Knockout of cellular glutathione peroxidase affects selenium-dependent parameters similarly in mice fed adequate and excessive dietary selenium: Biofactors, v. 7, p. 311-21.

Cheng, W. H., Y. S. Ho, D. A. Ross, Y. Han, G. F. Combs, Jr., and X. G. Lei, 1997a, Overexpression of cellular glutathione peroxidase does not affect expression of

plasma glutathione peroxidase or phospholipid hydroperoxide glutathione peroxidase in mice offered diets adequate or deficient in selenium: J Nutr, v. 127, p. 675-80.

Cheng, W. H., Y. S. Ho, D. A. Ross, B. A. Valentine, G. F. Combs, and X. G. Lei, 1997b, Cellular glutathione peroxidase knockout mice express normal levels of selenium-dependent plasma and phospholipid hydroperoxide glutathione peroxidases in various tissues: J Nutr, v. 127, p. 1445-50.

Cheng, W. H., X. Zheng, F. R. Quimby, C. A. Roneker, and X. G. Lei, 2003, Low levels of glutathione peroxidase 1 activity in selenium-deficient mouse liver affect c-Jun N-terminal kinase activation and p53 phosphorylation on Ser-15 in pro-oxidant-induced aponecrosis: Biochem J, v. 370, p. 927-34.

Chida, D., S. Nakagawa, S. Nagai, H. Sagara, H. Katsumata, T. Imaki, H. Suzuki, F. Mitani, T. Ogishima, C. Shimizu, H. Kotaki, S. Kakuta, K. Sudo, T. Koike, M. Kubo, and Y. Iwakura, 2007, Melanocortin 2 receptor is required for adrenal gland development, steroidogenesis, and neonatal gluconeogenesis: Proc Natl Acad Sci U S A, v. 104, p. 18205-10.

Chiu, Y. L., H. E. Witkowska, S. C. Hall, M. Santiago, V. B. Soros, C. Esnault, T. Heidmann, and W. C. Greene, 2006, High-molecular-mass APOBEC3G complexes restrict Alu retrotransposition: Proc Natl Acad Sci U S A, v. 103, p. 15588-93.

Cho, A. R., K. J. Yang, Y. Bae, Y. Y. Bahk, E. Kim, H. Lee, J. K. Kim, W. Park, H. Rhim, S. Y. Choi, T. Imanaka, S. Moon, J. Yoon, and S. K. Yoon, 2009, Tissue-specific expression and subcellular localization of ALADIN, the absence of which causes human triple A syndrome: Exp Mol Med, v. 41, p. 381-6.

Choi, M., U. I. Scholl, W. Ji, T. Liu, I. R. Tikhonova, P. Zumbo, A. Nayir, A. Bakkaloğlu, S. Ozen, S. Sanjad, C. Nelson-Williams, A. Farhi, S. Mane, and R. P. Lifton, 2009,

Genetic diagnosis by whole exome capture and massively parallel DNA sequencing: Proc Natl Acad Sci U S A, v. 106, p. 19096-101.

Chrissobolis, S., S. P. Didion, D. A. Kinzenbaw, L. I. Schrader, S. Dayal, S. R. Lentz, and F. M. Faraci, 2008, Glutathione peroxidase-1 plays a major role in protecting against angiotensin II-induced vascular dysfunction: Hypertension, v. 51, p. 872-7.

Chu, C. H., and D. Cheng, 2007, Expression, purification, characterization of human 3-methylcrotonyl-CoA carboxylase (MCCC): Protein Expr Purif, v. 53, p. 421-7.

Chu, F. F., R. S. Esworthy, Y. S. Ho, M. Bermeister, K. Swiderek, and R. W. Elliott, 1997, Expression and chromosomal mapping of mouse Gpx2 gene encoding the gastrointestinal form of glutathione peroxidase, GPX-GI: Biomed Environ Sci, v. 10, p. 156-62.

Chung, T. T., L. F. Chan, L. A. Metherell, and A. J. Clark, 2010, Phenotypic characteristics of familial glucocorticoid deficiency (FGD) type 1 and 2: Clin Endocrinol (Oxf), v. 72, p. 589-94.

Chung, T. T., T. R. Webb, L. F. Chan, S. N. Cooray, L. A. Metherell, P. J. King, J. P. Chapple, and A. J. Clark, 2008, The majority of adrenocorticotropin receptor (melanocortin 2 receptor) mutations found in familial glucocorticoid deficiency type 1 lead to defective trafficking of the receptor to the cell surface: J Clin Endocrinol Metab, v. 93, p. 4948-54.

Clark, A. J., A. H. Baig, L. Noon, F. M. Swords, L. Hunyady, and P. J. King, 2003, Expression, desensitization, and internalization of the ACTH receptor (MC2R): Ann N Y Acad Sci, v. 994, p. 111-7.

Clark, A. J., L. F. Chan, T. T. Chung, and L. A. Metherell, 2009, The genetics of familial glucocorticoid deficiency: Best Pract Res Clin Endocrinol Metab, v. 23, p. 159-65.

Clark, A. J., L. McLoughlin, and A. Grossman, 1993, Familial glucocorticoid deficiency associated with point mutation in the adrenocorticotropin receptor: Lancet, v. 341, p. 461-2.

Clark, A. J., L. Metherell, F. M. Swords, and L. L. Elias, 2001, The molecular pathogenesis of ACTH insensitivity syndromes: Ann Endocrinol (Paris), v. 62, p. 207-11.

Clark, A. J., and L. A. Metherell, 2006, Mechanisms of disease: the adrenocorticotropin receptor and disease: Nat Clin Pract Endocrinol Metab, v. 2, p. 282-90.

Clark, A. J., L. A. Metherell, M. E. Cheetham, and A. Huebner, 2005, Inherited ACTH insensitivity illuminates the mechanisms of ACTH action: Trends Endocrinol Metab, v. 16, p. 451-7.

Clark, A. J., and A. Weber, 1998, Adrenocorticotropin insensitivity syndromes: Endocr Rev, v. 19, p. 828-43.

Clark, L. C., G. F. Combs, Jr., B. W. Turnbull, E. H. Slate, D. K. Chalker, J. Chow, L. S. Davis, R. A. Glover, G. F. Graham, E. G. Gross, A. Krongrad, J. L. Lesher, Jr., H. K. Park, B. B. Sanders, Jr., C. L. Smith, and J. R. Taylor, 1996, Effects of selenium supplementation for cancer prevention in patients with carcinoma of the skin. A randomized controlled trial. Nutritional Prevention of Cancer Study Group: JAMA, v. 276, p. 1957-63.

Coll, A. P., M. Fassnacht, S. Klammer, S. Hahner, D. M. Schulte, S. Piper, Y. C. Tung, B. G. Challis, Y. Weinstein, B. Allolio, S. O'Rahilly, and F. Beuschlein, 2006, Peripheral administration of the N-terminal pro-opiomelanocortin fragment 1-28 to Pomc-/- mice reduces food intake and weight but does not affect adrenal growth or corticosterone production: J Endocrinol, v. 190, p. 515-25.

Colley, N. J., E. K. Baker, M. A. Stamnes, and C. S. Zuker, 1991, The cyclophilin homolog ninaA is required in the secretory pathway: Cell, v. 67, p. 255-63.

Collier, J. G., B. F. Robinson, and J. R. Vane, 1973, Reduction of pressor effects of angiotensin I in man by synthetic nonapeptide (B.P.P. 9a or SQ 20,881) which inhibits converting enzyme: Lancet, v. 1, p. 72-4.

Collins, S. R., P. Kemmeren, X. C. Zhao, J. F. Greenblatt, F. Spencer, F. C. Holstege, J. S. Weissman, and N. J. Krogan, 2007, Toward a comprehensive atlas of the physical interactome of Saccharomyces cerevisiae: Mol Cell Proteomics, v. 6, p. 439-50.

Cone, R. D., K. G. Mountjoy, L. S. Robbins, J. H. Nadeau, K. R. Johnson, L. Roselli-Rehfuss, and M. T. Mortrud, 1993, Cloning and functional characterization of a family of receptors for the melanotropic peptides: Ann N Y Acad Sci, v. 680, p. 342-63.

Cooray, S. N., I. Almiro Do Vale, K. Y. Leung, T. R. Webb, J. P. Chapple, M. Egertová, M. E. Cheetham, M. R. Elphick, and A. J. Clark, 2008, The melanocortin 2 receptor accessory protein exists as a homodimer and is essential for the function of the melanocortin 2 receptor in the mouse y1 cell line: Endocrinology, v. 149, p. 1935-41.

Cooray, S. N., L. Chan, T. R. Webb, L. Metherell, and A. J. Clark, 2009, Accessory proteins are vital for the functional expression of certain G protein-coupled receptors: Mol Cell Endocrinol, v. 300, p. 17-24.

Cooray, S. N., and A. J. Clark, 2011, Melanocortin receptors and their accessory proteins: Mol Cell Endocrinol, v. 331, p. 215-21.

Cowan, D. B., R. D. Weisel, W. G. Williams, and D. A. Mickle, 1993, Identification of oxygen responsive elements in the 5'-flanking region of the human glutathione peroxidase gene: J Biol Chem, v. 268, p. 26904-10.

Cox, A. G., C. C. Winterbourn, and M. B. Hampton, 2010, Mitochondrial peroxiredoxin involvement in antioxidant defence and redox signalling: Biochem J, v. 425, p. 313-25.

Crivello, J. F., and C. R. Jefcoate, 1978, Mechanisms of corticotropin action in rat adrenal cells. I. The effects of inhibitors of protein synthesis and of microfilament formation on corticosterone synthesis: Biochim Biophys Acta, v. 542, p. 315-29.

Cronshaw, J. M., and M. J. Matunis, 2003, The nuclear pore complex protein ALADIN is mislocalized in triple A syndrome: Proc Natl Acad Sci U S A, v. 100, p. 5823-7.

Curnow, K. M., M. T. Tusie-Luna, L. Pascoe, R. Natarajan, J. L. Gu, J. L. Nadler, and P. C. White, 1991, The product of the CYP11B2 gene is required for aldosterone biosynthesis in the human adrenal cortex: Mol Endocrinol, v. 5, p. 1513-22.

Dallman, M. F., N. Levin, C. S. Cascio, S. F. Akana, L. Jacobson, and R. W. Kuhn, 1989, Pharmacological evidence that the inhibition of diurnal adrenocorticotropin secretion by corticosteroids is mediated via type I corticosterone-preferring receptors: Endocrinology, v. 124, p. 2844-50.

Damier, P., E. C. Hirsch, P. Zhang, Y. Agid, and F. Javoy-Agid, 1993, Glutathione peroxidase, glial cells and Parkinson's disease: Neuroscience, v. 52, p. 1-6.

Daulat, A. M., P. Maurice, C. Froment, J. L. Guillaume, C. Broussard, B. Monsarrat, P. Delagrange, and R. Jockers, 2007, Purification and identification of G protein-coupled receptor protein complexes under native conditions: Mol Cell Proteomics, v. 6, p. 835-44.

Davidai, G., L. Kahana, and Z. Hochberg, 1984, Glomerulosa failure in congenital adrenocortical unresponsiveness to ACTH: Clin Endocrinol (Oxf), v. 20, p. 515-20.

de Haan, J. B., C. Bladier, P. Griffiths, M. Kelner, R. D. O'Shea, N. S. Cheung, R. T. Bronson, M. J. Silvestro, S. Wild, S. S. Zheng, P. M. Beart, P. J. Hertzog, and I. Kola, 1998, Mice with a homozygous null mutation for the most abundant glutathione peroxidase, Gpx1, show increased susceptibility to the oxidative stress-inducing agents paraquat and hydrogen peroxide: J Biol Chem, v. 273, p. 22528-36.

de Haan, J. B., C. Bladier, M. Lotfi-Miri, J. Taylor, P. Hutchinson, P. J. Crack, P. Hertzog, and I. Kola, 2004, Fibroblasts derived from Gpx1 knockout mice display senescent-like features and are susceptible to H2O2-mediated cell death: Free Radic Biol Med, v. 36, p. 53-64.

De Haan, J. B., P. J. Crack, N. Flentjar, R. C. Iannello, P. J. Hertzog, and I. Kola, 2003, An imbalance in antioxidant defense affects cellular function: the pathophysiological consequences of a reduction in antioxidant defense in the glutathione peroxidase-1 (Gpx1) knockout mouse: Redox Rep, v. 8, p. 69-79.

De Kloet, E. R., E. Vreugdenhil, M. S. Oitzl, and M. Joëls, 1998, Brain corticosteroid receptor balance in health and disease: Endocr Rev, v. 19, p. 269-301.

De Simoni, S., J. Goemaere, and B. Knoops, 2008, Silencing of peroxiredoxin 3 and peroxiredoxin 5 reveals the role of mitochondrial peroxiredoxins in the protection of human neuroblastoma SH-SY5Y cells toward MPP+: Neurosci Lett, v. 433, p. 219-24.

Deneke, S. M., and B. L. Fanburg, 1989, Regulation of cellular glutathione: Am J Physiol, v. 257, p. L163-73.

Dezso, Z., Y. Nikolsky, E. Sviridov, W. Shi, T. Serebriyskaya, D. Dosymbekov, A. Bugrim, E. Rakhmatulin, R. J. Brennan, A. Guryanov, K. Li, J. Blake, R. R. Samaha, and T. Nikolskaya, 2008, A comprehensive functional analysis of tissue specificity of human gene expression: BMC Biol, v. 6, p. 49.

Dias, R. P., L. F. Chan, L. A. Metherell, S. H. Pearce, and A. J. Clark, 2010, Isolated Addison's disease is unlikely to be caused by mutations in MC2R, MRAP or STAR, three genes responsible for familial glucocorticoid deficiency: Eur J Endocrinol, v. 162, p. 357-9.

Diemer, T., J. A. Allen, K. H. Hales, and D. B. Hales, 2003, Reactive oxygen disrupts mitochondria in MA-10 tumor Leydig cells and inhibits steroidogenic acute regulatory (StAR) protein and steroidogenesis: Endocrinology, v. 144, p. 2882-91.

DN, C., K. M, and A. SE., 1995, The nature and mechanisms of human gene mutation. , *in* C. Scriver, a. Beaudet, W. Sly, and D. Valle, eds., The Metabolic and Molecular Bases of Inherited Disease. , New York, McGraw-Hill, p. 259–291.

Domalik, L. J., D. D. Chaplin, M. S. Kirkman, R. C. Wu, W. W. Liu, T. A. Howard, M. F. Seldin, and K. L. Parker, 1991, Different isozymes of mouse 11 beta-hydroxylase produce mineralocorticoids and glucocorticoids: Mol Endocrinol, v. 5, p. 1853-61.

Dominguez, C., E. Ruiz, M. Gussinye, and A. Carrascosa, 1998, Oxidative stress at onset and in early stages of type 1 diabetes in children and adolescents: Diabetes Care, v. 21, p. 1736-42.

Donovan, J., K. Caban, R. Ranaweera, J. N. Gonzalez-Flores, and P. R. Copeland, 2008, A novel protein domain induces high affinity selenocysteine insertion sequence binding and elongation factor recruitment: J Biol Chem, v. 283, p. 35129-39.

Dorval, J., V. S. Leblond, and A. Hontela, 2003, Oxidative stress and loss of cortisol secretion in adrenocortical cells of rainbow trout (Oncorhynchus mykiss) exposed in vitro to endosulfan, an organochlorine pesticide: Aquat Toxicol, v. 63, p. 229-41.

Drutel, A., F. Archambeaud, and P. Caron, 2013, Selenium and the thyroid gland: more good news for clinicians: Clin Endocrinol (Oxf), v. 78, p. 155-64.

Elias, L. L., A. Huebner, L. A. Metherell, A. Canas, G. L. Warne, M. L. Bitti, S. Cianfarani, P. E. Clayton, M. O. Savage, and A. J. Clark, 2000, Tall stature in familial glucocorticoid deficiency: Clin Endocrinol (Oxf), v. 53, p. 423-30.

Elias, L. L., A. Huebner, G. D. Pullinger, A. Mirtella, and A. J. Clark, 1999, Functional characterization of naturally occurring mutations of the human adrenocorticotropin

receptor: poor correlation of phenotype and genotype: J Clin Endocrinol Metab, v. 84, p. 2766-70.

Emerling, B. M., L. C. Platanias, E. Black, A. R. Nebreda, R. J. Davis, and N. S. Chandel, 2005, Mitochondrial reactive oxygen species activation of p38 mitogen-activated protein kinase is required for hypoxia signaling: Mol Cell Biol, v. 25, p. 4853-62.

Epp, O., R. Ladenstein, and A. Wendel, 1983, The refined structure of the selenoenzyme glutathione peroxidase at 0.2-nm resolution: Eur J Biochem, v. 133, p. 51-69.

Esposito, L. A., J. E. Kokoszka, K. G. Waymire, B. Cottrell, G. R. MacGregor, and D. C. Wallace, 2000, Mitochondrial oxidative stress in mice lacking the glutathione peroxidase-1 gene: Free Radic Biol Med, v. 28, p. 754-66.

Esposito, L. A., S. Melov, A. Panov, B. A. Cottrell, and D. C. Wallace, 1999, Mitochondrial disease in mouse results in increased oxidative stress: Proc Natl Acad Sci U S A, v. 96, p. 4820-5.

Esworthy, R. S., M. A. Baker, and F. F. Chu, 1995, Expression of selenium-dependent glutathione peroxidase in human breast tumor cell lines: Cancer Res, v. 55, p. 957-62.

Esworthy, R. S., Y. S. Ho, and F. F. Chu, 1997, The Gpx1 gene encodes mitochondrial glutathione peroxidase in the mouse liver: Arch Biochem Biophys, v. 340, p. 59-63.

Evans, J. F., Q. T. Niu, J. A. Canas, C. L. Shen, J. F. Aloia, and J. K. Yeh, 2004, ACTH enhances chondrogenesis in multipotential progenitor cells and matrix production in chondrocytes: Bone, v. 35, p. 96-107.

Ewen, K. M., M. Ringle, and R. Bernhardt, 2012, Adrenodoxin--a versatile ferredoxin: IUBMB Life, v. 64, p. 506-12.

Faucher, K., H. Rabinovitch-Chable, J. Cook-Moreau, G. Barrière, F. Sturtz, and M. Rigaud, 2005, Overexpression of human GPX1 modifies Bax to Bcl-2 apoptotic ratio in human endothelial cells: Mol Cell Biochem, v. 277, p. 81-7.

Feng, N., S. F. Young, G. Aguilera, E. Puricelli, D. C. Adler-Wailes, N. G. Sebring, and J. A. Yanovski, 2005, Co-occurrence of two partially inactivating polymorphisms of MC3R is associated with pediatric-onset obesity: Diabetes, v. 54, p. 2663-7.

Ferrer, I., 2009, Altered mitochondria, energy metabolism, voltage-dependent anion channel, and lipid rafts converge to exhaust neurons in Alzheimer's disease: J Bioenerg Biomembr, v. 41, p. 425-31.

Flohe, L., W. A. Günzler, and H. H. Schock, 1973, Glutathione peroxidase: a selenoenzyme: FEBS Lett, v. 32, p. 132-4.

Flohé, L., B. Eisele, and A. Wendel, 1971, [Glutathion peroxidase. I. Isolation and determinations of molecular weight]: Hoppe Seylers Z Physiol Chem, v. 352, p. 151-8.

Flohé, L., S. Toppo, G. Cozza, and F. Ursini, 2011, A comparison of thiol peroxidase mechanisms: Antioxid Redox Signal, v. 15, p. 763-80.

Flück, C. E., and W. L. Miller, 2006, P450 oxidoreductase deficiency: a new form of congenital adrenal hyperplasia: Curr Opin Pediatr, v. 18, p. 435-41.

Flück, C. E., A. V. Pandey, N. Huang, V. Agrawal, and W. L. Miller, 2008, P450 oxidoreductase deficiency - a new form of congenital adrenal hyperplasia: Endocr Dev, v. 13, p. 67-81.

Forgione, M. A., A. Cap, R. Liao, N. I. Moldovan, R. T. Eberhardt, C. C. Lim, J. Jones, P. J. Goldschmidt-Clermont, and J. Loscalzo, 2002, Heterozygous cellular glutathione peroxidase deficiency in the mouse: abnormalities in vascular and cardiac function and structure: Circulation, v. 106, p. 1154-8.

Forss-Petter, S., H. Werner, J. Berger, H. Lassmann, B. Molzer, M. H. Schwab, H. Bernheimer, F. Zimmermann, and K. A. Nave, 1997, Targeted inactivation of the X-linked adrenoleukodystrophy gene in mice: J Neurosci Res, v. 50, p. 829-43.

Fourcade, S., J. López-Erauskin, J. Galino, C. Duval, A. Naudi, M. Jove, S. Kemp, F. Villarroya, I. Ferrer, R. Pamplona, M. Portero-Otin, and A. Pujol, 2008, Early oxidative damage underlying neurodegeneration in X-adrenoleukodystrophy: Hum Mol Genet, v. 17, p. 1762-73.

Fourcade, S., M. Ruiz, C. Guilera, E. Hahnen, L. Brichta, A. Naudi, M. Portero-Otín, G. Dacremont, N. Cartier, R. Wanders, S. Kemp, J. L. Mandel, B. Wirth, R. Pamplona, P. Aubourg, and A. Pujol, 2010, Valproic acid induces antioxidant effects in X-linked adrenoleukodystrophy: Hum Mol Genet, v. 19, p. 2005-14.

Fridmanis, D., R. Petrovska, I. Kalnina, M. Slaidina, R. Peculis, H. B. Schiöth, and J. Klovins, 2010, Identification of domains responsible for specific membrane transport and ligand specificity of the ACTH receptor (MC2R): Mol Cell Endocrinol, v. 321, p. 175-83.

Fu, Y., W. H. Cheng, J. M. Porres, D. A. Ross, and X. G. Lei, 1999, Knockout of cellular glutathione peroxidase gene renders mice susceptible to diquat-induced oxidative stress: Free Radic Biol Med, v. 27, p. 605-11.

Fu, Y., H. Sies, and X. G. Lei, 2001, Opposite roles of selenium-dependent glutathione peroxidase-1 in superoxide generator diquat- and peroxynitrite-induced apoptosis and signaling: J Biol Chem, v. 276, p. 43004-9.

Fujieda, K., T. Tajima, J. Nakae, S. Sageshima, K. Tachibana, S. Suwa, T. Sugawara, and J. F. Strauss, 1997, Spontaneous puberty in 46,XX subjects with congenital lipoid adrenal hyperplasia. Ovarian steroidogenesis is spared to some extent despite inactivating mutations in the steroidogenic acute regulatory protein (StAR) gene: J Clin Invest, v. 99, p. 1265-71.

Galasso, G., S. Schiekofer, K. Sato, R. Shibata, D. E. Handy, N. Ouchi, J. A. Leopold, J. Loscalzo, and K. Walsh, 2006, Impaired angiogenesis in glutathione peroxidase-1-

deficient mice is associated with endothelial progenitor cell dysfunction: Circ Res, v. 98, p. 254-61.

Galea, E., N. Launay, M. Portero-Otin, M. Ruiz, R. Pamplona, P. Aubourg, I. Ferrer, and A. Pujol, 2012, Oxidative stress underlying axonal degeneration in adrenoleukodystrophy: a paradigm for multifactorial neurodegenerative diseases?: Biochim Biophys Acta, v. 1822, p. 1475-88.

Galino, J., M. Ruiz, S. Fourcade, A. Schlüter, J. López-Erauskin, C. Guilera, M. Jove, A. Naudi, E. García-Arumí, A. L. Andreu, A. A. Starkov, R. Pamplona, I. Ferrer, M. Portero-Otin, and A. Pujol, 2011, Oxidative damage compromises energy metabolism in the axonal degeneration mouse model of X-adrenoleukodystrophy: Antioxid Redox Signal, v. 15, p. 2095-107.

Gallardo, M. E., L. R. Desviat, J. M. Rodríguez, J. Esparza-Gordillo, C. Pérez-Cerdá, B. Pérez, P. Rodríguez-Pombo, O. Criado, R. Sanz, D. H. Morton, K. M. Gibson, T. P. Le, A. Ribes, S. R. de Córdoba, M. Ugarte, and M. A. Peñalva, 2001, The molecular basis of 3-methylcrotonylglycinuria, a disorder of leucine catabolism: Am J Hum Genet, v. 68, p. 334-46.

Gallois-Montbrun, S., B. Kramer, C. M. Swanson, H. Byers, S. Lynham, M. Ward, and M. H. Malim, 2007, Antiviral protein APOBEC3G localizes to ribonucleoprotein complexes found in P bodies and stress granules: J Virol, v. 81, p. 2165-78.

Gavin, A. C., P. Aloy, P. Grandi, R. Krause, M. Boesche, M. Marzioch, C. Rau, L. J. Jensen, S. Bastuck, B. Dümpelfeld, A. Edelmann, M. A. Heurtier, V. Hoffman, C. Hoefert, K. Klein, M. Hudak, A. M. Michon, M. Schelder, M. Schirle, M. Remor, T. Rudi, S. Hooper, A. Bauer, T. Bouwmeester, G. Casari, G. Drewes, G. Neubauer, J. M. Rick, B. Kuster, P. Bork, R. B. Russell, and G. Superti-Furga, 2006, Proteome survey reveals modularity of the yeast cell machinery: Nature, v. 440, p. 631-6.

Gavin, A. C., M. Bösche, R. Krause, P. Grandi, M. Marzioch, A. Bauer, J. Schultz, J. M. Rick, A. M. Michon, C. M. Cruciat, M. Remor, C. Höfert, M. Schelder, M. Brajenovic, H. Ruffner, A. Merino, K. Klein, M. Hudak, D. Dickson, T. Rudi, V. Gnau, A. Bauch, S. Bastuck, B. Huhse, C. Leutwein, M. A. Heurtier, R. R. Copley, A. Edelmann, E. Querfurth, V. Rybin, G. Drewes, M. Raida, T. Bouwmeester, P. Bork, B. Seraphin, B. Kuster, G. Neubauer, and G. Superti-Furga, 2002, Functional organization of the yeast proteome by systematic analysis of protein complexes: Nature, v. 415, p. 141-7.

Ghyselinck, N. B., and J. P. Dufaure, 1990, A mouse cDNA sequence for epididymal androgen-regulated proteins related to glutathione peroxidase: Nucleic Acids Res, v. 18, p. 7144.

Gingras, A. C., M. Gstaiger, B. Raught, and R. Aebersold, 2007, Analysis of protein complexes using mass spectrometry: Nat Rev Mol Cell Biol, v. 8, p. 645-54.

Giroud, C. J., J. Stachenko, and E. H. Venning, 1956, Secretion of aldosterone by the zona glomerulosa of rat adrenal glands incubated in vitro: Proc Soc Exp Biol Med, v. 92, p. 154-8.

Gladyshev, V. N., V. M. Factor, F. Housseau, and D. L. Hatfield, 1998, Contrasting patterns of regulation of the antioxidant selenoproteins, thioredoxin reductase, and glutathione peroxidase, in cancer cells: Biochem Biophys Res Commun, v. 251, p. 488-93.

Goncharova, N. D., V. Y. Marenin, and T. N. Bogatyrenko, 2008, Stress, aging and reliability of antioxidant enzyme defense: Curr Aging Sci, v. 1, p. 22-9.

Goncharova, N. D., A. V. Shmaliy, T. N. Bogatyrenko, and V. K. Koltover, 2006, Correlation between activity of antioxidant enzymes and circadian rhythms of corticosteroids in Macaca mulatta monkeys of different age: Exp Gerontol, v. 41, p. 778-83.

Goncharova, N. D., V. Yu Marenin, and A. A. Vengerin, 2013, Age-related changes in the reliability of antioxidant enzyme defense in monkeys with different types of adaptive behavior: Curr Aging Sci, v. 6, p. 163-9.

Gorrigan, R. J., L. Guasti, P. King, A. J. Clark, and L. F. Chan, 2011, Localisation of the melanocortin-2-receptor and its accessory proteins in the developing and adult adrenal gland: J Mol Endocrinol, v. 46, p. 227-32.

Gouaze, V., M. E. Mirault, S. Carpentier, R. Salvayre, T. Levade, and N. Andrieu-Abadie, 2001, Glutathione peroxidase-1 overexpression prevents ceramide production and partially inhibits apoptosis in doxorubicin-treated human breast carcinoma cells: Mol Pharmacol, v. 60, p. 488-96.

Griffin, M. J., R. H. Wong, N. Pandya, and H. S. Sul, 2007, Direct interaction between USF and SREBP-1c mediates synergistic activation of the fatty-acid synthase promoter: J Biol Chem, v. 282, p. 5453-67.

Gucev, Z. S., M. K. Tee, D. Chitayat, D. K. Wherrett, and W. L. Miller, 2013, Distinguishing deficiencies in the steroidogenic acute regulatory protein and the cholesterol side chain cleavage enzyme causing neonatal adrenal failure: J Pediatr, v. 162, p. 819-22.

Génin, E., A. Huebner, C. Jaillard, A. Faure, G. Halaby, N. Saka, A. J. Clark, P. Durand, M. Bégeot, and D. Naville, 2002, Linkage of one gene for familial glucocorticoid deficiency type 2 (FGD2) to chromosome 8q and further evidence of heterogeneity: Hum Genet, v. 111, p. 428-34.

Haag Breese, E., V. N. Uversky, M. M. Georgiadis, and M. A. Harrington, 2006, The disordered amino-terminus of SIMPL interacts with members of the 70-kDa heat-shock protein family: DNA Cell Biol, v. 25, p. 704-14.

Habeb, A. M., C. R. Hughes, R. Al-Arabi, A. Al-Muhamadi, A. J. Clark, and L. A. Metherell, 2013, Familial glucocorticoid deficiency: a diagnostic challenge during acute illness: Eur J Pediatr.

Hall, A., P. A. Karplus, and L. B. Poole, 2009, Typical 2-Cys peroxiredoxins--structures, mechanisms and functions: FEBS J, v. 276, p. 2469-77.

Hall, A., D. Parsonage, L. B. Poole, and P. A. Karplus, 2010, Structural evidence that peroxiredoxin catalytic power is based on transition-state stabilization: J Mol Biol, v. 402, p. 194-209.

Hall, T. A., 1999, BioEdit: a user-friendly biological sequence alignment editor and analysis program for Windows 95/98/NT., *Nucleic acids symposium series* p. 95-98.

Hamanishi, T., H. Furuta, H. Kato, A. Doi, M. Tamai, H. Shimomura, S. Sakagashira, M. Nishi, H. Sasaki, T. Sanke, and K. Nanjo, 2004, Functional variants in the glutathione peroxidase-1 (GPx-1) gene are associated with increased intima-media thickness of carotid arteries and risk of macrovascular diseases in japanese type 2 diabetic patients: Diabetes, v. 53, p. 2455-60.

Han, J. D., and C. S. Rubin, 1996, Regulation of cytoskeleton organization and paxillin dephosphorylation by cAMP. Studies on murine Y1 adrenal cells: J Biol Chem, v. 271, p. 29211-5.

Hanschmann, E. M., J. R. Godoy, C. Berndt, C. Hudemann, and C. H. Lillig, 2013, Thioredoxins, Glutaredoxins, and Peroxiredoxins-Molecular Mechanisms and Health Significance: from Cofactors to Antioxidants to Redox Signaling: Antioxid Redox Signal.

Hanukoglu, I., 2006, Antioxidant protective mechanisms against reactive oxygen species (ROS) generated by mitochondrial P450 systems in steroidogenic cells: Drug Metab Rev, v. 38, p. 171-96.

Hanukoglu, I., R. Feuchtwanger, and A. Hanukoglu, 1990, Mechanism of corticotropin and cAMP induction of mitochondrial cytochrome P450 system enzymes in adrenal cortex cells: J Biol Chem, v. 265, p. 20602-8.

Hanukoglu, I., and Z. Hanukoglu, 1986, Stoichiometry of mitochondrial cytochromes P-450, adrenodoxin and adrenodoxin reductase in adrenal cortex and corpus luteum. Implications for membrane organization and gene regulation: Eur J Biochem, v. 157, p. 27-31.

Hauet, T., Z. X. Yao, H. S. Bose, C. T. Wall, Z. Han, W. Li, D. B. Hales, W. L. Miller, M. Culty, and V. Papadopoulos, 2005, Peripheral-type benzodiazepine receptor-mediated action of steroidogenic acute regulatory protein on cholesterol entry into leydig cell mitochondria: Mol Endocrinol, v. 19, p. 540-54.

Hay, D. L., D. R. Poyner, and P. M. Sexton, 2006, GPCR modulation by RAMPs: Pharmacol Ther, v. 109, p. 173-97.

Hentschke, M., L. Berneking, C. Belmar Campos, F. Buck, K. Ruckdeschel, and M. Aepfelbacher, 2010, Yersinia virulence factor YopM induces sustained RSK activation by interfering with dephosphorylation: PLoS One, v. 5.

Hillarp, N. A., and B. Nilson, 1954, The structure of the adrenaline and noradrenaline containing granules in the adrenal medullary cells with reference to the storage and release of the sympathomimetic amines: Acta Physiol Scand Suppl, v. 31, p. 79-107.

Hirano, M., Y. Furiya, H. Asai, A. Yasui, and S. Ueno, 2006, ALADINI482S causes selective failure of nuclear protein import and hypersensitivity to oxidative stress in triple A syndrome: Proc Natl Acad Sci U S A, v. 103, p. 2298-303.

Hofland, J., P. J. Delhanty, J. Steenbergen, L. J. Hofland, P. M. van Koetsveld, F. H. van Nederveen, W. W. de Herder, R. A. Feelders, and F. H. de Jong, 2012, Melanocortin 2 receptor-associated protein (MRAP) and MRAP2 in human adrenocortical tissues:

regulation of expression and association with ACTH responsiveness: J Clin Endocrinol Metab, v. 97, p. E747-54.

Holzinger, A., W. Röschinger, F. Lagler, P. U. Mayerhofer, P. Lichtner, T. Kattenfeld, L. P. Thuy, W. L. Nyhan, H. G. Koch, A. C. Muntau, and A. A. Roscher, 2001, Cloning of the human MCCA and MCCB genes and mutations therein reveal the molecular cause of 3-methylcrotonyl-CoA: carboxylase deficiency: Hum Mol Genet, v. 10, p. 1299-306.

Hornsby, P. J., 1980, Regulation of cytochrome P-450-supported 11 beta-hydroxylation of deoxycortisol by steroids, oxygen, and antioxidants in adrenocortical cell cultures: J Biol Chem, v. 255, p. 4020-7.

Hornsby, P. J., 1989, Steroid and xenobiotic effects on the adrenal cortex: mediation by oxidative and other mechanisms: Free Radic Biol Med, v. 6, p. 103-15.

Hornsby, P. J., S. E. Harris, and K. A. Aldern, 1985, The role of ascorbic acid in the function of the adrenal cortex: studies in adrenocortical cells in culture: Endocrinology, v. 117, p. 1264-71.

Hu, Y. J., and A. M. Diamond, 2003, Role of glutathione peroxidase 1 in breast cancer: loss of heterozygosity and allelic differences in the response to selenium: Cancer Res, v. 63, p. 3347-51.

Huebner, A., L. L. Elias, and A. J. Clark, 1999, ACTH resistance syndromes: J Pediatr Endocrinol Metab, v. 12 Suppl 1, p. 277-93.

Huebner, A., A. M. Kaindl, R. Braun, and K. Handschug, 2002, New insights into the molecular basis of the triple A syndrome: Endocr Res, v. 28, p. 733-9.

Huebner, A., P. Mann, E. Rohde, A. M. Kaindl, M. Witt, P. Verkade, S. Jakubiczka, M. Menschikowski, G. Stoltenburg-Didinger, and K. Koehler, 2006, Mice lacking the

nuclear pore complex protein ALADIN show female infertility but fail to develop a phenotype resembling human triple A syndrome: Mol Cell Biol, v. 26, p. 1879-87.

Hughes, C. R., T. T. Chung, A. M. Habeb, F. Kelestimur, A. J. Clark, and L. A. Metherell, 2010, Missense mutations in the melanocortin 2 receptor accessory protein that lead to late onset familial glucocorticoid deficiency type 2: J Clin Endocrinol Metab, v. 95, p. 3497-501.

Hughes, C. R., L. Guasti, E. Meimaridou, C. H. Chuang, J. C. Schimenti, P. J. King, C. Costigan, A. J. Clark, and L. A. Metherell, 2012, MCM4 mutation causes adrenal failure, short stature, and natural killer cell deficiency in humans: J Clin Invest, v. 122, p. 814-20.

Höftberger, R., M. Kunze, I. Weinhofer, F. Aboul-Enein, T. Voigtländer, I. Oezen, G. Amann, H. Bernheimer, H. Budka, and J. Berger, 2007, Distribution and cellular localization of adrenoleukodystrophy protein in human tissues: implications for X-linked adrenoleukodystrophy: Neurobiol Dis, v. 28, p. 165-74.

Ichimura, Y., T. Habuchi, N. Tsuchiya, L. Wang, C. Oyama, K. Sato, H. Nishiyama, O. Ogawa, and T. Kato, 2004, Increased risk of bladder cancer associated with a glutathione peroxidase 1 codon 198 variant: J Urol, v. 172, p. 728-32.

Imai, H., and Y. Nakagawa, 2003, Biological significance of phospholipid hydroperoxide glutathione peroxidase (PHGPx, GPx4) in mammalian cells: Free Radic Biol Med, v. 34, p. 145-69.

Imamine, H., H. Mizuno, Y. Sugiyama, Y. Ohro, T. Sugiura, and H. Togari, 2005, Possible relationship between elevated plasma ACTH and tall stature in familial glucocorticoid deficiency: Tohoku J Exp Med, v. 205, p. 123-31.

Immenschuh, S., E. Baumgart-Vogt, M. Tan, S. Iwahara, G. Ramadori, and H. D. Fahimi, 2003, Differential cellular and subcellular localization of heme-binding protein

23/peroxiredoxin I and heme oxygenase-1 in rat liver: J Histochem Cytochem, v. 51, p. 1621-31.

Ishii, T., T. Ogata, G. Sasaki, S. Sato, E. I. Kinoshita, and N. Matsuo, 2000, Novel mutations of the ACTH receptor gene in a female adult patient with adrenal unresponsiveness to ACTH: Clin Endocrinol (Oxf), v. 53, p. 389-92.

Ivashchenko, O., P. P. Van Veldhoven, C. Brees, Y. S. Ho, S. R. Terlecky, and M. Fransen, 2011, Intraperoxisomal redox balance in mammalian cells: oxidative stress and interorganellar cross-talk: Mol Biol Cell, v. 22, p. 1440-51.

Jain, V., L. A. Metherell, A. David, R. Sharma, P. K. Sharma, A. J. Clark, and L. F. Chan, 2011, Neonatal presentation of familial glucocorticoid deficiency resulting from a novel splice mutation in the melanocortin 2 receptor accessory protein: Eur J Endocrinol, v. 165, p. 987-91.

Jin, Y., L. Wang, M. Ruan, J. Liu, Y. Yang, C. Zhou, B. Xu, and Z. Fu, 2011, Cypermethrin exposure during puberty induces oxidative stress and endocrine disruption in male mice: Chemosphere, v. 84, p. 124-30.

Johansson, C., C. H. Lillig, and A. Holmgren, 2004, Human mitochondrial glutaredoxin reduces S-glutathionylated proteins with high affinity accepting electrons from either glutathione or thioredoxin reductase: J Biol Chem, v. 279, p. 7537-43.

Johnson, J. A., and J. O. Davis, 1973, Angiotensin. II. Important role in the maintenance of arterial blood pressure: Science, v. 179, p. 906-7.

Johnsson, N., and A. Varshavsky, 1994, Split ubiquitin as a sensor of protein interactions in vivo: Proc Natl Acad Sci U S A, v. 91, p. 10340-4.

Joseph-Liauzun, E., P. Delmas, D. Shire, and P. Ferrara, 1998, Topological analysis of the peripheral benzodiazepine receptor in yeast mitochondrial membranes supports a five-transmembrane structure: J Biol Chem, v. 273, p. 2146-52.

Juillard, F., E. Hiriart, N. Sergeant, V. Vingtdeux-Didier, H. Drobecq, A. Sergeant, E. Manet, and H. Gruffat, 2009, Epstein-Barr virus protein EB2 contains an N-terminal transferable nuclear export signal that promotes nucleocytoplasmic export by directly binding TAP/NXF1: J Virol, v. 83, p. 12759-68.

Kaneto, H., D. Kawamori, T. A. Matsuoka, Y. Kajimoto, and Y. Yamasaki, 2005, Oxidative stress and pancreatic beta-cell dysfunction: Am J Ther, v. 12, p. 529-33.

Karpac, J., D. Ostwald, S. Bui, P. Hunnewell, M. Shankar, and U. Hochgeschwender, 2005, Development, maintenance, and function of the adrenal gland in early postnatal proopiomelanocortin-null mutant mice: Endocrinology, v. 146, p. 2555-62.

Karplus, P. A., and A. Hall, 2007, Structural survey of the peroxiredoxins: Subcell Biochem, v. 44, p. 41-60.

Kasaikina, M. V., A. V. Lobanov, M. Y. Malinouski, B. C. Lee, J. Seravalli, D. E. Fomenko, A. A. Turanov, L. Finney, S. Vogt, T. J. Park, R. A. Miller, D. L. Hatfield, and V. N. Gladyshev, 2011, Reduced utilization of selenium by naked mole rats due to a specific defect in GPx1 expression: J Biol Chem, v. 286, p. 17005-14.

Kavanagh, K. L., C. Johansson, C. Smee, O. Gileadi, F. von Delft, and U. Oppermann, Crystal structure of the selenocysteine to glycine mutant of human glutathione peroxidase 1.

Kayanoki, Y., J. Fujii, K. N. Islam, K. Suzuki, S. Kawata, Y. Matsuzawa, and N. Taniguchi, 1996, The protective role of glutathione peroxidase in apoptosis induced by reactive oxygen species: J Biochem, v. 119, p. 817-22.

Kelberman, D., K. Rizzoti, R. Lovell-Badge, I. C. Robinson, and M. T. Dattani, 2009, Genetic regulation of pituitary gland development in human and mouse: Endocr Rev, v. 30, p. 790-829.

Kelner, M. J., R. D. Bagnell, S. F. Uglik, M. A. Montoya, and G. T. Mullenbach, 1995, Heterologous expression of selenium-dependent glutathione peroxidase affords cellular resistance to paraquat: Arch Biochem Biophys, v. 323, p. 40-6.

Kemp, S., J. Berger, and P. Aubourg, 2012, X-linked adrenoleukodystrophy: clinical, metabolic, genetic and pathophysiological aspects: Biochim Biophys Acta, v. 1822, p. 1465-74.

Kemp, S., and R. Wanders, 2010, Biochemical aspects of X-linked adrenoleukodystrophy: Brain Pathol, v. 20, p. 831-7.

Kensler, T. W., G. S. Qian, J. G. Chen, and J. D. Groopman, 2003, Translational strategies for cancer prevention in liver: Nat Rev Cancer, v. 3, p. 321-9.

Kil, I. S., S. H. Bae, and S. G. Rhee, 2013, Study of the Signaling Function of Sulfiredoxin and Peroxiredoxin III in Isolated Adrenal Gland: Unsuitability of Clonal and Primary Adrenocortical Cells: Methods Enzymol, v. 527, p. 169-81.

Kil, I. S., S. K. Lee, K. W. Ryu, H. A. Woo, M. C. Hu, S. H. Bae, and S. G. Rhee, 2012, Feedback control of adrenal steroidogenesis via H2O2-dependent, reversible inactivation of peroxiredoxin III in mitochondria: Mol Cell, v. 46, p. 584-94.

Kilianova, Z., N. Basora, P. Kilian, M. D. Payet, and N. Gallo-Payet, 2006, Human melanocortin receptor 2 expression and functionality: effects of protein kinase A and protein kinase C on desensitization and internalization: Endocrinology, v. 147, p. 2325-37.

Kim, H. J., and N. D. Vaziri, 2010, Contribution of impaired Nrf2-Keap1 pathway to oxidative stress and inflammation in chronic renal failure: Am J Physiol Renal Physiol, v. 298, p. F662-71.

Kim, K., I. H. Kim, K. Y. Lee, S. G. Rhee, and E. R. Stadtman, 1988, The isolation and purification of a specific "protector" protein which inhibits enzyme inactivation by a thiol/Fe(III)/O2 mixed-function oxidation system: J Biol Chem, v. 263, p. 4704-11.

Kind, B., K. Koehler, M. Krumbholz, D. Landgraf, and A. Huebner, 2010, Intracellular ROS level is increased in fibroblasts of triple A syndrome patients: J Mol Med (Berl), v. 88, p. 1233-42.

Kiriyama, T., M. Hirano, H. Asai, M. Ikeda, Y. Furiya, and S. Ueno, 2008, Restoration of nuclear-import failure caused by triple A syndrome and oxidative stress: Biochem Biophys Res Commun, v. 374, p. 631-4.

Klovins, J., T. Haitina, D. Fridmanis, Z. Kilianova, I. Kapa, R. Fredriksson, N. Gallo-Payet, and H. B. Schiöth, 2004, The melanocortin system in Fugu: determination of POMC/AGRP/MCR gene repertoire and synteny, as well as pharmacology and anatomical distribution of the MCRs: Mol Biol Evol, v. 21, p. 563-79.

Knoops, B., A. Clippe, C. Bogard, K. Arsalane, R. Wattiez, C. Hermans, E. Duconseille, P. Falmagne, and A. Bernard, 1999, Cloning and characterization of AOEB166, a novel mammalian antioxidant enzyme of the peroxiredoxin family: J Biol Chem, v. 274, p. 30451-8.

Kobayashi, T., N. Shinnoh, A. Kondo, and T. Yamada, 1997, Adrenoleukodystrophy protein-deficient mice represent abnormality of very long chain fatty acid metabolism: Biochem Biophys Res Commun, v. 232, p. 631-6.

Kong, M. F., and W. Jeffcoate, 1994, Eighty-six cases of Addison's disease: Clin Endocrinol (Oxf), v. 41, p. 757-61.

Korkhov, V. M., C. Sachse, J. M. Short, and C. G. Tate, 2010, Three-dimensional structure of TspO by electron cryomicroscopy of helical crystals: Structure, v. 18, p. 677-87.

Korytowski, W., A. Pilat, J. C. Schmitt, and A. W. Girotti, 2013, Deleterious cholesterol hydroperoxide trafficking in steroidogenic acute regulatory (StAR) protein-expressing MA-10 Leydig cells: implications for oxidative stress-impaired steroidogenesis: J Biol Chem, v. 288, p. 11509-19.

Korytowski, W., D. Rodriguez-Agudo, A. Pilat, and A. W. Girotti, 2010, StarD4-mediated translocation of 7-hydroperoxycholesterol to isolated mitochondria: deleterious effects and implications for steroidogenesis under oxidative stress conditions: Biochem Biophys Res Commun, v. 392, p. 58-62.

Kraus, R. J., S. J. Foster, and H. E. Ganther, 1983, Identification of selenocysteine in glutathione peroxidase by mass spectroscopy: Biochemistry, v. 22, p. 5853-8.

Kretz-Remy, C., and A. P. Arrigo, 2001, Selenium: a key element that controls NF-kappa B activation and I kappa B alpha half life: Biofactors, v. 14, p. 117-25.

Krogan, N. J., G. Cagney, H. Yu, G. Zhong, X. Guo, A. Ignatchenko, J. Li, S. Pu, N. Datta, A. P. Tikuisis, T. Punna, J. M. Peregrín-Alvarez, M. Shales, X. Zhang, M. Davey, M. D. Robinson, A. Paccanaro, J. E. Bray, A. Sheung, B. Beattie, D. P. Richards, V. Canadien, A. Lalev, F. Mena, P. Wong, A. Starostine, M. M. Canete, J. Vlasblom, S. Wu, C. Orsi, S. R. Collins, S. Chandran, R. Haw, J. J. Rilstone, K. Gandi, N. J. Thompson, G. Musso, P. St Onge, S. Ghanny, M. H. Lam, G. Butland, A. M. Altaf-Ul, S. Kanaya, A. Shilatifard, E. O'Shea, J. S. Weissman, C. J. Ingles, T. R. Hughes, J. Parkinson, M. Gerstein, S. J. Wodak, A. Emili, and J. F. Greenblatt, 2006, Global landscape of protein complexes in the yeast Saccharomyces cerevisiae: Nature, v. 440, p. 637-43.

Krone, N., V. Dhir, H. E. Ivison, and W. Arlt, 2007, Congenital adrenal hyperplasia and P450 oxidoreductase deficiency: Clin Endocrinol (Oxf), v. 66, p. 162-72.

Krumbholz, M., K. Koehler, and A. Huebner, 2006, Cellular localization of 17 natural mutant variants of ALADIN protein in triple A syndrome - shedding light on an unexpected splice mutation: Biochem Cell Biol, v. 84, p. 243-9.

Kryukov, G. V., S. Castellano, S. V. Novoselov, A. V. Lobanov, O. Zehtab, R. Guigo, and V. N. Gladyshev, 2003, Characterization of mammalian selenoproteomes: Science, v. 300, p. 1439-43.

Labbé, O., F. Desarnaud, D. Eggerickx, G. Vassart, and M. Parmentier, 1994, Molecular cloning of a mouse melanocortin 5 receptor gene widely expressed in peripheral tissues: Biochemistry, v. 33, p. 4543-9.

Latreche, L., O. Jean-Jean, D. M. Driscoll, and L. Chavatte, 2009, Novel structural determinants in human SECIS elements modulate the translational recoding of UGA as selenocysteine: Nucleic Acids Res, v. 37, p. 5868-80.

Lee, H. T., and C. W. Emala, 2002, Adenosine attenuates oxidant injury in human proximal tubular cells via A(1) and A(2a) adenosine receptors: Am J Physiol Renal Physiol, v. 282, p. F844-52.

Lee, S., H. S. Shin, P. K. Shireman, A. Vasilaki, H. Van Remmen, and M. E. Csete, 2006, Glutathione-peroxidase-1 null muscle progenitor cells are globally defective: Free Radic Biol Med, v. 41, p. 1174-84.

Lee, Y. S., L. K. Poh, B. L. Kek, and K. Y. Loke, 2008, Novel melanocortin 4 receptor gene mutations in severely obese children: Clin Endocrinol (Oxf), v. 68, p. 529-35.

Lei, C., X. Niu, J. Wei, J. Zhu, and Y. Zhu, 2009, Interaction of glutathione peroxidase-1 and selenium in endemic dilated cardiomyopathy: Clin Chim Acta, v. 399, p. 102-8.

Lei, X. G., W. H. Cheng, and J. P. McClung, 2007, Metabolic regulation and function of glutathione peroxidase-1: Annu Rev Nutr, v. 27, p. 41-61.

Lei, X. G., J. K. Evenson, K. M. Thompson, and R. A. Sunde, 1995, Glutathione peroxidase and phospholipid hydroperoxide glutathione peroxidase are differentially regulated in rats by dietary selenium: J Nutr, v. 125, p. 1438-46.

Li, L., W. Shoji, H. Takano, N. Nishimura, Y. Aoki, R. Takahashi, S. Goto, T. Kaifu, T. Takai, and M. Obinata, 2007, Increased susceptibility of MER5 (peroxiredoxin III) knockout mice to LPS-induced oxidative stress: Biochem Biophys Res Commun, v. 355, p. 715-21.

Li, P., F. Sun, H. M. Cao, Q. Y. Ma, C. M. Pan, J. H. Ma, X. N. Zhang, H. Jiang, H. D. Song, and M. D. Chen, 2009, Expression of adiponectin receptors in mouse adrenal glands and the adrenocortical Y-1 cell line: adiponectin regulates steroidogenesis: Biochem Biophys Res Commun, v. 390, p. 1208-13.

Li, Q., S. Sanlioglu, S. Li, T. Ritchie, L. Oberley, and J. F. Engelhardt, 2001, GPx-1 gene delivery modulates NFkappaB activation following diverse environmental injuries through a specific subunit of the IKK complex: Antioxid Redox Signal, v. 3, p. 415-32.

Li, Y., 2011, The tandem affinity purification technology: an overview: Biotechnol Lett, v. 33, p. 1487-99.

Li, Y., S. Franklin, M. J. Zhang, and T. M. Vondriska, 2011, Highly efficient purification of protein complexes from mammalian cells using a novel streptavidin-binding peptide and hexahistidine tandem tag system: application to Bruton's tyrosine kinase: Protein Sci, v. 20, p. 140-9.

Liddell, J. R., R. Dringen, P. J. Crack, and S. R. Robinson, 2006a, Glutathione peroxidase 1 and a high cellular glutathione concentration are essential for effective organic hydroperoxide detoxification in astrocytes: Glia, v. 54, p. 873-9.

Liddell, J. R., H. H. Hoepken, P. J. Crack, S. R. Robinson, and R. Dringen, 2006b, Glutathione peroxidase 1 and glutathione are required to protect mouse astrocytes from iron-mediated hydrogen peroxide toxicity: J Neurosci Res, v. 84, p. 578-86.

Lin, L., P. C. Hindmarsh, L. A. Metherell, M. Alzyoud, M. Al-Ali, C. E. Brain, A. J. Clark, M. T. Dattani, and J. C. Achermann, 2007, Severe loss-of-function mutations in the adrenocorticotropin receptor (ACTHR, MC2R) can be found in patients diagnosed with salt-losing adrenal hypoplasia: Clin Endocrinol (Oxf), v. 66, p. 205-10.

Lippman, S. M., E. A. Klein, P. J. Goodman, M. S. Lucia, I. M. Thompson, L. G. Ford, H. L. Parnes, L. M. Minasian, J. M. Gaziano, J. A. Hartline, J. K. Parsons, J. D. Bearden, 3rd, E. D. Crawford, G. E. Goodman, J. Claudio, E. Winquist, E. D. Cook, D. D. Karp, P. Walther, M. M. Lieber, A. R. Kristal, A. K. Darke, K. B. Arnold, P. A. Ganz, R. M. Santella, D. Albanes, P. R. Taylor, J. L. Probstfield, T. J. Jagpal, J. J. Crowley, F. L. Meyskens, Jr., L. H. Baker, and C. A. Coltman, Jr., 2009, Effect of selenium and vitamin E on risk of prostate cancer and other cancers: the Selenium and Vitamin E Cancer Prevention Trial (SELECT): JAMA, v. 301, p. 39-51.

Liu, C., X. Zhang, J. Deng, M. Hecker, A. Al-Khedhairy, J. P. Giesy, and B. Zhou, 2011, Effects of prochloraz or propylthiouracil on the cross-talk between the HPG, HPA, and HPT axes in zebrafish: Environ Sci Technol, v. 45, p. 769-75.

Liu, J., M. B. Rone, and V. Papadopoulos, 2006, Protein-protein interactions mediate mitochondrial cholesterol transport and steroid biosynthesis: J Biol Chem, v. 281, p. 38879-93.

Loh, K., H. Deng, A. Fukushima, X. Cai, B. Boivin, S. Galic, C. Bruce, B. J. Shields, B. Skiba, L. M. Ooms, N. Stepto, B. Wu, C. A. Mitchell, N. K. Tonks, M. J. Watt, M. A. Febbraio, P. J. Crack, S. Andrikopoulos, and T. Tiganis, 2009, Reactive oxygen species enhance insulin sensitivity: Cell Metab, v. 10, p. 260-72.

Low, S. C., E. Grundner-Culemann, J. W. Harney, and M. J. Berry, 2000, SECIS-SBP2 interactions dictate selenocysteine incorporation efficiency and selenoprotein hierarchy: EMBO J, v. 19, p. 6882-90.

Lu, J. F., E. Barron-Casella, R. Deering, A. K. Heinzer, A. B. Moser, K. L. deMesy Bentley, G. S. Wand, M. C McGuinness, Z. Pei, P. A. Watkins, A. Pujol, K. D. Smith, and J. M. Powers, 2007, The role of peroxisomal ABC transporters in the mouse adrenal gland: the loss of Abcd2 (ALDR), Not Abcd1 (ALD), causes oxidative damage: Lab Invest, v. 87, p. 261-72.

Lu, J. F., A. M. Lawler, P. A. Watkins, J. M. Powers, A. B. Moser, H. W. Moser, and K. D. Smith, 1997, A mouse model for X-linked adrenoleukodystrophy: Proc Natl Acad Sci U S A, v. 94, p. 9366-71.

Lubos, E., J. Loscalzo, and D. E. Handy, 2011, Glutathione peroxidase-1 in health and disease: from molecular mechanisms to therapeutic opportunities: Antioxid Redox Signal, v. 15, p. 1957-97.

López-Erauskin, J., S. Fourcade, J. Galino, M. Ruiz, A. Schlüter, A. Naudi, M. Jove, M. Portero-Otin, R. Pamplona, I. Ferrer, and A. Pujol, 2011, Antioxidants halt axonal degeneration in a mouse model of X-adrenoleukodystrophy: Ann Neurol, v. 70, p. 84-92.

Löhr, H., and M. Hammerschmidt, 2011, Zebrafish in endocrine systems: recent advances and implications for human disease: Annu Rev Physiol, v. 73, p. 183-211.

Maffei, M., H. Fei, G. H. Lee, C. Dani, P. Leroy, Y. Zhang, R. Proenca, R. Negrel, G. Ailhaud, and J. M. Friedman, 1995, Increased expression in adipocytes of ob RNA in mice with lesions of the hypothalamus and with mutations at the db locus: Proc Natl Acad Sci U S A, v. 92, p. 6957-60.

Maiorino, M., K. D. Aumann, R. Brigelius-Flohé, D. Doria, J. van den Heuvel, J. McCarthy, A. Roveri, F. Ursini, and L. Flohé, 1998, Probing the presumed catalytic triad of a selenium-containing peroxidase by mutational analysis: Z Ernahrungswiss, v. 37 Suppl 1, p. 118-21.

Maiorino, M., M. Scapin, F. Ursini, M. Biasolo, V. Bosello, and L. Flohé, 2003, Distinct promoters determine alternative transcription of gpx-4 into phospholipid-hydroperoxide glutathione peroxidase variants: J Biol Chem, v. 278, p. 34286-90.

Mariotti, M., P. G. Ridge, Y. Zhang, A. V. Lobanov, T. H. Pringle, R. Guigo, D. L. Hatfield, and V. N. Gladyshev, 2012, Composition and evolution of the vertebrate and mammalian selenoproteomes: PLoS One, v. 7, p. e33066.

Marsh, D. J., G. Hollopeter, D. Huszar, R. Laufer, K. A. Yagaloff, S. L. Fisher, P. Burn, and R. D. Palmiter, 1999, Response of melanocortin-4 receptor-deficient mice to anorectic and orexigenic peptides: Nat Genet, v. 21, p. 119-22.

Marí, M., A. Morales, A. Colell, C. García-Ruiz, and J. C. Fernández-Checa, 2009, Mitochondrial glutathione, a key survival antioxidant: Antioxid Redox Signal, v. 11, p. 2685-700.

Masuda, S., R. Das, H. Cheng, E. Hurt, N. Dorman, and R. Reed, 2005, Recruitment of the human TREX complex to mRNA during splicing: Genes Dev, v. 19, p. 1512-7.

Matsumoto, A., A. Okado, T. Fujii, J. Fujii, M. Egashira, N. Niikawa, and N. Taniguchi, 1999, Cloning of the peroxiredoxin gene family in rats and characterization of the fourth member: FEBS Lett, v. 443, p. 246-50.

Mattson, M. P., and T. Magnus, 2006, Ageing and neuronal vulnerability: Nat Rev Neurosci, v. 7, p. 278-94.

McCann, J. C., and B. N. Ames, 2011, Adaptive dysfunction of selenoproteins from the perspective of the triage theory: why modest selenium deficiency may increase risk of diseases of aging: FASEB J, v. 25, p. 1793-814.

McClung, J. P., C. A. Roneker, W. Mu, D. J. Lisk, P. Langlais, F. Liu, and X. G. Lei, 2004, Development of insulin resistance and obesity in mice overexpressing cellular glutathione peroxidase: Proc Natl Acad Sci U S A, v. 101, p. 8852-7.

McLatchie, L. M., N. J. Fraser, M. J. Main, A. Wise, J. Brown, N. Thompson, R. Solari, M. G. Lee, and S. M. Foord, 1998, RAMPs regulate the transport and ligand specificity of the calcitonin-receptor-like receptor: Nature, v. 393, p. 333-9.

Medina-Palazon, C., H. Gruffat, F. Mure, O. Filhol, V. Vingtdeux-Didier, H. Drobecq, C. Cochet, N. Sergeant, A. Sergeant, and E. Manet, 2007, Protein kinase CK2 phosphorylation of EB2 regulates its function in the production of Epstein-Barr virus infectious viral particles: J Virol, v. 81, p. 11850-60.

Meimaridou, E., C. R. Hughes, J. Kowalczyk, L. Guasti, J. P. Chapple, P. J. King, L. F. Chan, A. J. Clark, and L. A. Metherell, 2012a, Familial glucocorticoid deficiency: New genes and mechanisms: Mol Cell Endocrinol.

Meimaridou, E., J. Kowalczyk, L. Guasti, C. R. Hughes, F. Wagner, P. Frommolt, P. Nürnberg, N. P. Mann, R. Banerjee, H. N. Saka, J. P. Chapple, P. J. King, A. J. Clark, and L. A. Metherell, 2012b, Mutations in NNT encoding nicotinamide nucleotide transhydrogenase cause familial glucocorticoid deficiency: Nat Genet, v. 44, p. 740-2.

Metherell, L. A., L. F. Chan, and A. J. Clark, 2006, The genetics of ACTH resistance syndromes: Best Pract Res Clin Endocrinol Metab, v. 20, p. 547-60.

Metherell, L. A., J. P. Chapple, S. Cooray, A. David, C. Becker, F. Rüschendorf, D. Naville, M. Begeot, B. Khoo, P. Nürnberg, A. Huebner, M. E. Cheetham, and A. J. Clark,

2005, Mutations in MRAP, encoding a new interacting partner of the ACTH receptor, cause familial glucocorticoid deficiency type 2: Nat Genet, v. 37, p. 166-70.

Metherell, L. A., D. Naville, G. Halaby, M. Begeot, A. Huebner, G. Nürnberg, P. Nürnberg, J. Green, J. W. Tomlinson, N. P. Krone, L. Lin, M. Racine, D. M. Berney, J. C. Achermann, W. Arlt, and A. J. Clark, 2009, Nonclassic lipoid congenital adrenal hyperplasia masquerading as familial glucocorticoid deficiency: J Clin Endocrinol Metab, v. 94, p. 3865-71.

Miller, E. D., 1981, The role of the renin-angiotensin-aldosterone system in circulatory control and hypertension: Br J Anaesth, v. 53, p. 711-8.

Miller, W. L., 1991, Congenital adrenal hyperplasias: Endocrinol Metab Clin North Am, v. 20, p. 721-49.

Miller, W. L., 1995, Mitochondrial specificity of the early steps in steroidogenesis: J Steroid Biochem Mol Biol, v. 55, p. 607-16.

Miller, W. L., 1997, Congenital lipoid adrenal hyperplasia: the human gene knockout for the steroidogenic acute regulatory protein: J Mol Endocrinol, v. 19, p. 227-40.

Miller, W. L., 2005, Minireview: regulation of steroidogenesis by electron transfer: Endocrinology, v. 146, p. 2544-50.

Miller, W. L., 2013, Steroid hormone synthesis in mitochondria: Mol Cell Endocrinol.

Miller, W. L., and R. J. Auchus, 2011, The molecular biology, biochemistry, and physiology of human steroidogenesis and its disorders: Endocr Rev, v. 32, p. 81-151.

Miniard, A. C., L. M. Middleton, M. E. Budiman, C. A. Gerber, and D. M. Driscoll, 2010, Nucleolin binds to a subset of selenoprotein mRNAs and regulates their expression: Nucleic Acids Res, v. 38, p. 4807-20.

Mitani, F., K. Mukai, H. Miyamoto, M. Suematsu, and Y. Ishimura, 2003, The undifferentiated cell zone is a stem cell zone in adult rat adrenal cortex: Biochim Biophys Acta, v. 1619, p. 317-24.

Mitani, F., H. Suzuki, J. Hata, T. Ogishima, H. Shimada, and Y. Ishimura, 1994, A novel cell layer without corticosteroid-synthesizing enzymes in rat adrenal cortex: histochemical detection and possible physiological role: Endocrinology, v. 135, p. 431-8.

Mlakar, S. J., J. Osredkar, J. Prezelj, and J. Marc, 2010, The antioxidant enzyme GPX1 gene polymorphisms are associated with low BMD and increased bone turnover markers: Dis Markers, v. 29, p. 71-80.

Modan-Moses, D., B. Ben-Zeev, C. Hoffmann, T. C. Falik-Zaccai, Y. A. Bental, O. Pinhas-Hamiel, and Y. Anikster, 2006, Unusual presentation of familial glucocorticoid deficiency with a novel MRAP mutation: J Clin Endocrinol Metab, v. 91, p. 3713-7.

Moriarty, P. M., C. C. Reddy, and L. E. Maquat, 1998, Selenium deficiency reduces the abundance of mRNA for Se-dependent glutathione peroxidase 1 by a UGA-dependent mechanism likely to be nonsense codon-mediated decay of cytoplasmic mRNA: Mol Cell Biol, v. 18, p. 2932-9.

Moscow, J. A., L. Schmidt, D. T. Ingram, J. Gnarra, B. Johnson, and K. H. Cowan, 1994, Loss of heterozygosity of the human cytosolic glutathione peroxidase I gene in lung cancer: Carcinogenesis, v. 15, p. 2769-73.

Moser, H. W., 1997, Adrenoleukodystrophy: phenotype, genetics, pathogenesis and therapy: Brain, v. 120 (Pt 8), p. 1485-508.

Mountjoy, K. G., L. S. Robbins, M. T. Mortrud, and R. D. Cone, 1992, The cloning of a family of genes that encode the melanocortin receptors: Science, v. 257, p. 1248-51.

Mukhopadhyay, S. S., K. S. Leung, M. J. Hicks, P. J. Hastings, H. Youssoufian, and S. E. Plon, 2006, Defective mitochondrial peroxiredoxin-3 results in sensitivity to oxidative stress in Fanconi anemia: J Cell Biol, v. 175, p. 225-35.

Muyderman, H., A. L. Wadey, M. Nilsson, and N. R. Sims, 2007, Mitochondrial glutathione protects against cell death induced by oxidative and nitrative stress in astrocytes: J Neurochem, v. 102, p. 1369-82.

Nalvarte, I., A. E. Damdimopoulos, and G. Spyrou, 2004, Human mitochondrial thioredoxin reductase reduces cytochrome c and confers resistance to complex III inhibition: Free Radic Biol Med, v. 36, p. 1270-8.

Navarro, A., and A. Boveris, 2007, The mitochondrial energy transduction system and the aging process: Am J Physiol Cell Physiol, v. 292, p. C670-86.

Nelson, K. J., S. T. Knutson, L. Soito, C. Klomsiri, L. B. Poole, and J. S. Fetrow, 2011, Analysis of the peroxiredoxin family: using active-site structure and sequence information for global classification and residue analysis: Proteins, v. 79, p. 947-64.

Nerup, J., 1974, Addison's disease--clinical studies. A report fo 108 cases: Acta Endocrinol (Copenh), v. 76, p. 127-41.

Neufeld, M., N. K. Maclaren, and R. M. Blizzard, 1981, Two types of autoimmune Addison's disease associated with different polyglandular autoimmune (PGA) syndromes: Medicine (Baltimore), v. 60, p. 355-62.

Ng, S. B., K. J. Buckingham, C. Lee, A. W. Bigham, H. K. Tabor, K. M. Dent, C. D. Huff, P. T. Shannon, E. W. Jabs, D. A. Nickerson, J. Shendure, and M. J. Bamshad, 2010, Exome sequencing identifies the cause of a mendelian disorder: Nat Genet, v. 42, p. 30-5.

Ng, S. B., E. H. Turner, P. D. Robertson, S. D. Flygare, A. W. Bigham, C. Lee, T. Shaffer, M. Wong, A. Bhattacharjee, E. E. Eichler, M. Bamshad, D. A. Nickerson, and J.

Shendure, 2009, Targeted capture and massively parallel sequencing of 12 human exomes: Nature, v. 461, p. 272-6.

Nguyen, V. D., M. J. Saaranen, A. R. Karala, A. K. Lappi, L. Wang, I. B. Raykhel, H. I. Alanen, K. E. Salo, C. C. Wang, and L. W. Ruddock, 2011, Two endoplasmic reticulum PDI peroxidases increase the efficiency of the use of peroxide during disulfide bond formation: J Mol Biol, v. 406, p. 503-15.

Nishimoto, K., K. Nakagawa, D. Li, T. Kosaka, M. Oya, S. Mikami, H. Shibata, H. Itoh, F. Mitani, T. Yamazaki, T. Ogishima, M. Suematsu, and K. Mukai, 2010, Adrenocortical zonation in humans under normal and pathological conditions: J Clin Endocrinol Metab, v. 95, p. 2296-305.

Nomura, K., H. Imai, T. Koumura, M. Arai, and Y. Nakagawa, 1999, Mitochondrial phospholipid hydroperoxide glutathione peroxidase suppresses apoptosis mediated by a mitochondrial death pathway: J Biol Chem, v. 274, p. 29294-302.

Nonn, L., M. Berggren, and G. Powis, 2003, Increased expression of mitochondrial peroxiredoxin-3 (thioredoxin peroxidase-2) protects cancer cells against hypoxia and drug-induced hydrogen peroxide-dependent apoptosis: Mol Cancer Res, v. 1, p. 682-9.

Noon, L. A., J. M. Franklin, P. J. King, N. J. Goulding, L. Hunyady, and A. J. Clark, 2002, Failed export of the adrenocorticotrophin receptor from the endoplasmic reticulum in non-adrenal cells: evidence in support of a requirement for a specific adrenal accessory factor: J Endocrinol, v. 174, p. 17-25.

Norman, D., A. M. Isidori, V. Frajese, M. Caprio, S. L. Chew, A. B. Grossman, A. J. Clark, G. Michael Besser, and A. Fabbri, 2003, ACTH and alpha-MSH inhibit leptin expression and secretion in 3T3-L1 adipocytes: model for a central-peripheral melanocortin-leptin pathway: Mol Cell Endocrinol, v. 200, p. 99-109.

Novoselova, T. V., D. Jackson, D. C. Campbell, A. J. Clark, and L. F. Chan, 2013, Melanocortin receptor accessory proteins in adrenal gland physiology and beyond: J Endocrinol, v. 217, p. R1-11.

Nussey, S. S., S. C. Soo, S. Gibson, I. Gout, A. White, M. Bain, and A. P. Johnstone, 1993, Isolated congenital ACTH deficiency: a cleavage enzyme defect?: Clin Endocrinol (Oxf), v. 39, p. 381-5.

O'Shaughnessy, P. J., L. M. Fleming, G. Jackson, U. Hochgeschwender, P. Reed, and P. J. Baker, 2003, Adrenocorticotropic hormone directly stimulates testosterone production by the fetal and neonatal mouse testis: Endocrinology, v. 144, p. 3279-84.

Ogawa, K., H. Matsui, S. Ohtsuka, and H. Niwa, 2004, A novel mechanism for regulating clonal propagation of mouse ES cells: Genes Cells, v. 9, p. 471-7.

Ogishima, T., H. Suzuki, J. Hata, F. Mitani, and Y. Ishimura, 1992, Zone-specific expression of aldosterone synthase cytochrome P-450 and cytochrome P-45011 beta in rat adrenal cortex: histochemical basis for the functional zonation: Endocrinology, v. 130, p. 2971-7.

Okado-Matsumoto, A., A. Matsumoto, J. Fujii, and N. Taniguchi, 2000, Peroxiredoxin IV is a secretable protein with heparin-binding properties under reduced conditions: J Biochem, v. 127, p. 493-501.

Oparil, S., C. A. Sanders, and E. Haber, 1970, In-vivo and in-vitro conversion of angiotensin I to angiotensin II in dog blood: Circ Res, v. 26, p. 591-9.

Oskarsson, A., E. Ullerås, K. E. Plant, J. P. Hinson, and P. S. Goldfarb, 2006, Steroidogenic gene expression in H295R cells and the human adrenal gland: adrenotoxic effects of lindane in vitro: J Appl Toxicol, v. 26, p. 484-92.

Paglia, D. E., and W. N. Valentine, 1967, Studies on the quantitative and qualitative characterization of erythrocyte glutathione peroxidase: J Lab Clin Med, v. 70, p. 158-69.

Papadopoulos, V., H. Amri, H. Li, N. Boujrad, B. Vidic, and M. Garnier, 1997, Targeted disruption of the peripheral-type benzodiazepine receptor gene inhibits steroidogenesis in the R2C Leydig tumor cell line: J Biol Chem, v. 272, p. 32129-35.

Papp, L. V., J. Lu, F. Striebel, D. Kennedy, A. Holmgren, and K. K. Khanna, 2006, The redox state of SECIS binding protein 2 controls its localization and selenocysteine incorporation function: Mol Cell Biol, v. 26, p. 4895-910.

Parajes, S., C. Kamrath, I. T. Rose, A. E. Taylor, C. F. Mooij, V. Dhir, J. Grötzinger, W. Arlt, and N. Krone, 2011, A novel entity of clinically isolated adrenal insufficiency caused by a partially inactivating mutation of the gene encoding for P450 side chain cleavage enzyme (CYP11A1): J Clin Endocrinol Metab, v. 96, p. E1798-806.

Park, M. S., F. Chu, J. Xie, Y. Wang, P. Bhattacharya, and W. K. Chan, 2011, Identification of cyclophilin-40-interacting proteins reveals potential cellular function of cyclophilin-40: Anal Biochem, v. 410, p. 257-65.

Parrish, J. R., K. D. Gulyas, and R. L. Finley, 2006, Yeast two-hybrid contributions to interactome mapping: Curr Opin Biotechnol, v. 17, p. 387-93.

Participants, N. R. D. D. G. Q., 2004, The state of GPCR research in 2004: Nat Rev Drug Discov, v. 3, p. 575, 577-626.

Paz-y-Mino, C., C. Carrera, A. Lopez-Cortes, M. J. Munoz, N. Cumbal, B. Castro, A. Cabrera, and M. E. Sanchez, 2010, Genetic polymorphisms in apolipoprotein E and glutathione peroxidase 1 genes in the Ecuadorian population affected with Alzheimer's disease: Am J Med Sci, v. 340, p. 373-7.

Peng, D., A. Belkhiri, T. Hu, R. Chaturvedi, M. Asim, K. T. Wilson, A. Zaika, and W. El-Rifai, 2012, Glutathione peroxidase 7 protects against oxidative DNA damage in oesophageal cells: Gut, v. 61, p. 1250-60.

Poole, L. B., A. Hall, and K. J. Nelson, 2011, Overview of peroxiredoxins in oxidant defense and redox regulation: Curr Protoc Toxicol, v. Chapter 7, p. Unit7.9.

Powers, J. M., Z. Pei, A. K. Heinzer, R. Deering, A. B. Moser, H. W. Moser, P. A. Watkins, and K. D. Smith, 2005, Adreno-leukodystrophy: oxidative stress of mice and men: J Neuropathol Exp Neurol, v. 64, p. 1067-79.

Prasad, R., L. A. Metherell, A. J. Clark, and H. L. Storr, 2013, Deficiency of ALADIN impairs redox homeostasis in human adrenal cells and inhibits steroidogenesis: Endocrinology.

Prpic, I., A. Huebner, M. Persic, K. Handschug, and M. Pavletic, 2003, Triple A syndrome: genotype-phenotype assessment: Clin Genet, v. 63, p. 415-7.

Puglisi, R., I. Maccari, S. Pipolo, M. Conrad, F. Mangia, and C. Boitani, 2012, The nuclear form of glutathione peroxidase 4 is associated with sperm nuclear matrix and is required for proper paternal chromatin decondensation at fertilization: J Cell Physiol, v. 227, p. 1420-7.

Puig, O., F. Caspary, G. Rigaut, B. Rutz, E. Bouveret, E. Bragado-Nilsson, M. Wilm, and B. Séraphin, 2001, The tandem affinity purification (TAP) method: a general procedure of protein complex purification: Methods, v. 24, p. 218-29.

Pujol, A., I. Ferrer, C. Camps, E. Metzger, C. Hindelang, N. Callizot, M. Ruiz, T. Pàmpols, M. Giròs, and J. L. Mandel, 2004, Functional overlap between ABCD1 (ALD) and ABCD2 (ALDR) transporters: a therapeutic target for X-adrenoleukodystrophy: Hum Mol Genet, v. 13, p. 2997-3006.

Pujol, A., C. Hindelang, N. Callizot, U. Bartsch, M. Schachner, and J. L. Mandel, 2002, Late onset neurological phenotype of the X-ALD gene inactivation in mice: a mouse model for adrenomyeloneuropathy: Hum Mol Genet, v. 11, p. 499-505.

Purdom-Dickinson, S. E., E. V. Sheveleva, H. Sun, and Q. M. Chen, 2007, Translational control of nrf2 protein in activation of antioxidant response by oxidants: Mol Pharmacol, v. 72, p. 1074-81.

Rached, M., H. El Mourabit, A. Buronfosse, A. Blondet, D. Naville, M. Begeot, and A. Penhoat, 2005, Expression of the human melanocortin-2 receptor in different eukaryotic cells: Peptides, v. 26, p. 1842-7.

Raffin-Sanson, M. L., Y. de Keyzer, and X. Bertagna, 2003, Proopiomelanocortin, a polypeptide precursor with multiple functions: from physiology to pathological conditions: Eur J Endocrinol, v. 149, p. 79-90.

Rapoport, R., D. Sklan, and I. Hanukoglu, 1995, Electron leakage from the adrenal cortex mitochondrial P450scc and P450c11 systems: NADPH and steroid dependence: Arch Biochem Biophys, v. 317, p. 412-6.

Ratka, A., W. Sutanto, M. Bloemers, and E. R. de Kloet, 1989, On the role of brain mineralocorticoid (type I) and glucocorticoid (type II) receptors in neuroendocrine regulation: Neuroendocrinology, v. 50, p. 117-23.

Raza, F. S., and G. P. Vinson, 2000, Adrenocortical expression of MnSOD: Endocr Res, v. 26, p. 959-63.

Reddy, P., 2011, Clinical approach to adrenal insufficiency in hospitalised patients: Int J Clin Pract, v. 65, p. 1059-66.

Reeves, W. C., S. P. Marcuard, S. E. Willis, and A. Movahed, 1989, Reversible cardiomyopathy due to selenium deficiency: JPEN J Parenter Enteral Nutr, v. 13, p. 663-5.

Reincke, M., F. Beuschlein, G. Menig, G. Hofmockel, W. Arlt, R. Lehmann, M. Karl, and B. Allolio, 1998, Localization and expression of adrenocorticotropic hormone receptor mRNA in normal and neoplastic human adrenal cortex: J Endocrinol, v. 156, p. 415-23.

Reul, J. M., and E. R. de Kloet, 1985, Two receptor systems for corticosterone in rat brain: microdistribution and differential occupation: Endocrinology, v. 117, p. 2505-11.

Reul, J. M., and E. R. de Kloet, 1986, Anatomical resolution of two types of corticosterone receptor sites in rat brain with in vitro autoradiography and computerized image analysis: J Steroid Biochem, v. 24, p. 269-72.

Rhee, S. G., H. Z. Chae, and K. Kim, 2005a, Peroxiredoxins: a historical overview and speculative preview of novel mechanisms and emerging concepts in cell signaling: Free Radic Biol Med, v. 38, p. 1543-52.

Rhee, S. G., S. W. Kang, T. S. Chang, W. Jeong, and K. Kim, 2001, Peroxiredoxin, a novel family of peroxidases: IUBMB Life, v. 52, p. 35-41.

Rhee, S. G., and H. A. Woo, 2011, Multiple functions of peroxiredoxins: peroxidases, sensors and regulators of the intracellular messenger H_2O_2, and protein chaperones: Antioxid Redox Signal, v. 15, p. 781-94.

Rhee, S. G., H. A. Woo, I. S. Kil, and S. H. Bae, 2012, Peroxiredoxin functions as a peroxidase and a regulator and sensor of local peroxides: J Biol Chem, v. 287, p. 4403-10.

Rhee, S. G., K. S. Yang, S. W. Kang, H. A. Woo, and T. S. Chang, 2005b, Controlled elimination of intracellular H(2)O(2): regulation of peroxiredoxin, catalase, and glutathione peroxidase via post-translational modification: Antioxid Redox Signal, v. 7, p. 619-26.

Rigaut, G., A. Shevchenko, B. Rutz, M. Wilm, M. Mann, and B. Séraphin, 1999, A generic protein purification method for protein complex characterization and proteome exploration: Nat Biotechnol, v. 17, p. 1030-2.

Ritter, S. L., and R. A. Hall, 2009, Fine-tuning of GPCR activity by receptor-interacting proteins: Nat Rev Mol Cell Biol, v. 10, p. 819-30.

Rocher, C., J. L. Lalanne, and J. Chaudière, 1992, Purification and properties of a recombinant sulfur analog of murine selenium-glutathione peroxidase: Eur J Biochem, v. 205, p. 955-60.

Rodriguez-Agudo, D., S. Ren, E. Wong, D. Marques, K. Redford, G. Gil, P. Hylemon, and W. M. Pandak, 2008, Intracellular cholesterol transporter StarD4 binds free cholesterol and increases cholesteryl ester formation: J Lipid Res, v. 49, p. 1409-19.

Roy, S., B. Perron, and N. Gallo-Payet, 2010, Role of asparagine-linked glycosylation in cell surface expression and function of the human adrenocorticotropin receptor (melanocortin 2 receptor) in 293/FRT cells: Endocrinology, v. 151, p. 660-70.

Roy, S., M. Rached, and N. Gallo-Payet, 2007, Differential regulation of the human adrenocorticotropin receptor [melanocortin-2 receptor (MC2R)] by human MC2R accessory protein isoforms alpha and beta in isogenic human embryonic kidney 293 cells: Mol Endocrinol, v. 21, p. 1656-69.

Rumie, H., L. A. Metherell, A. J. Clark, V. Beauloye, and M. Maes, 2007, Clinical and biological phenotype of a patient with familial glucocorticoid deficiency type 2 caused by a mutation of melanocortin 2 receptor accessory protein: Eur J Endocrinol, v. 157, p. 539-42.

Rydström, J., 2006, Mitochondrial NADPH, transhydrogenase and disease: Biochim Biophys Acta, v. 1757, p. 721-6.

Saito, H., M. Kubota, R. W. Roberts, Q. Chi, and H. Matsunami, 2004, RTP family members induce functional expression of mammalian odorant receptors: Cell, v. 119, p. 679-91.

Sandhu, N., and M. M. Vijayan, 2011, Cadmium-mediated disruption of cortisol biosynthesis involves suppression of corticosteroidogenic genes in rainbow trout: Aquat Toxicol, v. 103, p. 92-100.

Sandström, B. E., J. Carlsson, and S. L. Marklund, 1987, Variations among cultured cells in glutathione peroxidase activity in response to selenite supplementation: Biochim Biophys Acta, v. 929, p. 148-53.

Sanger, F., S. Nicklen, and A. R. Coulson, 1977, DNA sequencing with chain-terminating inhibitors: Proc Natl Acad Sci U S A, v. 74, p. 5463-7.

Sapolsky, R. M., L. M. Romero, and A. U. Munck, 2000, How do glucocorticoids influence stress responses? Integrating permissive, suppressive, stimulatory, and preparative actions: Endocr Rev, v. 21, p. 55-89.

Sasano, H., J. I. Mason, and N. Sasano, 1989, Immunohistochemical study of cytochrome P-45017 alpha in human adrenocortical disorders: Hum Pathol, v. 20, p. 113-7.

Sawchenko, P. E., and L. W. Swanson, 1985, Localization, colocalization, and plasticity of corticotropin-releasing factor immunoreactivity in rat brain: Fed Proc, v. 44, p. 221-7.

Schimmer, B. P., W. K. Kwan, J. Tsao, and R. Qiu, 1995, Adrenocorticotropin-resistant mutants of the Y1 adrenal cell line fail to express the adrenocorticotropin receptor: J Cell Physiol, v. 163, p. 164-71.

Schneider, M., H. Förster, A. Boersma, A. Seiler, H. Wehnes, F. Sinowatz, C. Neumüller, M. J. Deutsch, A. Walch, M. Hrabé de Angelis, W. Wurst, F. Ursini, A. Roveri, M. Maleszewski, M. Maiorino, and M. Conrad, 2009, Mitochondrial glutathione peroxidase 4 disruption causes male infertility: FASEB J, v. 23, p. 3233-42.

Schoenmakers, E., M. Agostini, C. Mitchell, N. Schoenmakers, L. Papp, O. Rajanayagam, R. Padidela, L. Ceron-Gutierrez, R. Doffinger, C. Prevosto, J. Luan, S. Montano, J. Lu, M. Castanet, N. Clemons, M. Groeneveld, P. Castets, M. Karbaschi, S. Aitken, A. Dixon, J. Williams, I. Campi, M. Blount, H. Burton, F. Muntoni, D. O'Donovan, A. Dean, A. Warren, C. Brierley, D. Baguley, P. Guicheney, R. Fitzgerald, A. Coles, H. Gaston, P. Todd, A. Holmgren, K. K. Khanna, M. Cooke, R. Semple, D. Halsall, N. Wareham, J. Schwabe, L. Grasso, P. Beck-Peccoz, A. Ogunko, M. Dattani, M. Gurnell, and K. Chatterjee, 2010, Mutations in the selenocysteine insertion sequence-binding protein 2 gene lead to a multisystem selenoprotein deficiency disorder in humans: J Clin Invest, v. 120, p. 4220-35.

Scornik, O. A., and A. C. Paladini, 1964, Angiotensin Blood Levels in Hemorrhagic Hypotension and other Related Conditions: Am J Physiol, v. 206, p. 553-6.

Sebag, J. A., and P. M. Hinkle, 2007, Melanocortin-2 receptor accessory protein MRAP forms antiparallel homodimers: Proc Natl Acad Sci U S A, v. 104, p. 20244-9.

Sebag, J. A., and P. M. Hinkle, 2009a, Opposite effects of the melanocortin-2 (MC2) receptor accessory protein MRAP on MC2 and MC5 receptor dimerization and trafficking: J Biol Chem, v. 284, p. 22641-8.

Sebag, J. A., and P. M. Hinkle, 2009b, Regions of melanocortin 2 (MC2) receptor accessory protein necessary for dual topology and MC2 receptor trafficking and signaling: J Biol Chem, v. 284, p. 610-8.

Sebag, J. A., and P. M. Hinkle, 2010, Regulation of G protein-coupled receptor signaling: specific dominant-negative effects of melanocortin 2 receptor accessory protein 2: Sci Signal, v. 3, p. ra28.

Sewer, M. B., and D. Li, 2008, Regulation of steroid hormone biosynthesis by the cytoskeleton: Lipids, v. 43, p. 1109-15.

Shan, X., D. P. Jones, M. Hashmi, and M. W. Anders, 1993, Selective depletion of mitochondrial glutathione concentrations by (R,S)-3-hydroxy-4-pentenoate potentiates oxidative cell death: Chem Res Toxicol, v. 6, p. 75-81.

Sheeran, F. L., J. Rydström, M. I. Shakhparonov, N. B. Pestov, and S. Pepe, 2010, Diminished NADPH transhydrogenase activity and mitochondrial redox regulation in human failing myocardium: Biochim Biophys Acta, v. 1797, p. 1138-48.

Shen, Q., F. F. Chu, and P. E. Newburger, 1993, Sequences in the 3'-untranslated region of the human cellular glutathione peroxidase gene are necessary and sufficient for selenocysteine incorporation at the UGA codon: J Biol Chem, v. 268, p. 11463-9.

Shen, Q., L. Fan, and P. E. Newburger, 2006, Nuclease sensitive element binding protein 1 associates with the selenocysteine insertion sequence and functions in mammalian selenoprotein translation: J Cell Physiol, v. 207, p. 775-83.

Shen, Q., J. L. Leonard, and P. E. Newburger, 1995, Structure and function of the selenium translation element in the 3'-untranslated region of human cellular glutathione peroxidase mRNA: RNA, v. 1, p. 519-25.

Shen, Q., P. L. Townes, C. Padden, and P. E. Newburger, 1994, An in-frame trinucleotide repeat in the coding region of the human cellular glutathione peroxidase (GPX1) gene: in vivo polymorphism and in vitro instability: Genomics, v. 23, p. 292-4.

Shendure, J., 2011, Next-generation human genetics: Genome Biol, v. 12, p. 408.

Shendure, J., and E. Lieberman Aiden, 2012, The expanding scope of DNA sequencing: Nat Biotechnol, v. 30, p. 1084-94.

Shepard, T. H., B. H. Landing, and D. G. Mason, 1959, Familial Addison's disease; case reports of two sisters with corticoid deficiency unassociated with hypoaldosteronism: AMA J Dis Child, v. 97, p. 154-62.

Sheu, Y. J., and B. Stillman, 2010, The Dbf4-Cdc7 kinase promotes S phase by alleviating an inhibitory activity in Mcm4: Nature, v. 463, p. 113-7.

Shi, Z., Y. Feng, J. Wang, H. Zhang, L. Ding, and J. Dai, 2010, Perfluorododecanoic acid-induced steroidogenic inhibition is associated with steroidogenic acute regulatory protein and reactive oxygen species in cAMP-stimulated Leydig cells: Toxicol Sci, v. 114, p. 285-94.

Sies, H., W. Stahl, and A. R. Sundquist, 1992, Antioxidant functions of vitamins. Vitamins E and C, beta-carotene, and other carotenoids: Ann N Y Acad Sci, v. 669, p. 7-20.

Silva, A. L., and L. Romão, 2009, The mammalian nonsense-mediated mRNA decay pathway: to decay or not to decay! Which players make the decision?: FEBS Lett, v. 583, p. 499-505.

Silva, J. M., M. Z. Li, K. Chang, W. Ge, M. C. Golding, R. J. Rickles, D. Siolas, G. Hu, P. J. Paddison, M. R. Schlabach, N. Sheth, J. Bradshaw, J. Burchard, A. Kulkarni, G. Cavet, R. Sachidanandam, W. R. McCombie, M. A. Cleary, S. J. Elledge, and G. J. Hannon, 2005, Second-generation shRNA libraries covering the mouse and human genomes: Nat Genet, v. 37, p. 1281-8.

Simard, M., M. Côté, P. R. Provost, and Y. Tremblay, 2010, Expression of genes related to the hypothalamic-pituitary-adrenal axis in murine fetal lungs in late gestation: Reprod Biol Endocrinol, v. 8, p. 134.

Slominski, A., G. Ermak, and M. Mihm, 1996, ACTH receptor, CYP11A1, CYP17 and CYP21A2 genes are expressed in skin: J Clin Endocrinol Metab, v. 81, p. 2746-9.

Smith, S. M., and W. W. Vale, 2006, The role of the hypothalamic-pituitary-adrenal axis in neuroendocrine responses to stress: Dialogues Clin Neurosci, v. 8, p. 383-95.

Sorokina, E. M., S. I. Feinstein, T. N. Milovanova, and A. B. Fisher, 2009, Identification of the amino acid sequence that targets peroxiredoxin 6 to lysosome-like structures of lung epithelial cells: Am J Physiol Lung Cell Mol Physiol, v. 297, p. L871-80.

Sorokina, E. M., S. I. Feinstein, S. Zhou, and A. B. Fisher, 2011, Intracellular targeting of peroxiredoxin 6 to lysosomal organelles requires MAPK activity and binding to 14-3-3ε: Am J Physiol Cell Physiol, v. 300, p. C1430-41.

Soule, S., 1999, Addison's disease in Africa--a teaching hospital experience: Clin Endocrinol (Oxf), v. 50, p. 115-20.

Spark, R. F., and J. R. Etzkorn, 1977, Absent aldosterone response to ACTH in familial glucocorticoid deficiency: N Engl J Med, v. 297, p. 917-20.

Sparkes, R. S., I. Klisak, and W. L. Miller, 1991, Regional mapping of genes encoding human steroidogenic enzymes: P450scc to 15q23-q24, adrenodoxin to 11q22; adrenodoxin reductase to 17q24-q25; and P450c17 to 10q24-q25: DNA Cell Biol, v. 10, p. 359-65.

Spiga, F., E. J. Waite, Y. Liu, Y. M. Kershaw, G. Aguilera, and S. L. Lightman, 2011, ACTH-dependent ultradian rhythm of corticosterone secretion: Endocrinology, v. 152, p. 1448-57.

Squires, J. E., I. Stoytchev, E. P. Forry, and M. J. Berry, 2007, SBP2 binding affinity is a major determinant in differential selenoprotein mRNA translation and sensitivity to nonsense-mediated decay: Mol Cell Biol, v. 27, p. 7848-55.

Stocco, D. M., X. Wang, Y. Jo, and P. R. Manna, 2005, Multiple signaling pathways regulating steroidogenesis and steroidogenic acute regulatory protein expression: more complicated than we thought: Mol Endocrinol, v. 19, p. 2647-59.

Storr, H. L., A. J. Clark, J. V. Priestley, and G. J. Michael, 2005, Identification of the sites of expression of triple A syndrome mRNA in the rat using in situ hybridisation: Neuroscience, v. 131, p. 113-23.

Storr, H. L., B. Kind, D. A. Parfitt, J. P. Chapple, M. Lorenz, K. Koehler, A. Huebner, and A. J. Clark, 2009, Deficiency of ferritin heavy-chain nuclear import in triple a syndrome implies nuclear oxidative damage as the primary disease mechanism: Mol Endocrinol, v. 23, p. 2086-94.

Su, A. I., M. P. Cooke, K. A. Ching, Y. Hakak, J. R. Walker, T. Wiltshire, A. P. Orth, R. G. Vega, L. M. Sapinoso, A. Moqrich, A. Patapoutian, G. M. Hampton, P. G. Schultz, and J. B. Hogenesch, 2002, Large-scale analysis of the human and mouse transcriptomes: Proc Natl Acad Sci U S A, v. 99, p. 4465-70.

Sun, J. S., Y. H. Tsuang, W. C. Huang, L. T. Chen, Y. S. Hang, and F. J. Lu, 1997, Menadione-induced cytotoxicity to rat osteoblasts: Cell Mol Life Sci, v. 53, p. 967-76.

Sun, X., P. M. Moriarty, and L. E. Maquat, 2000, Nonsense-mediated decay of glutathione peroxidase 1 mRNA in the cytoplasm depends on intron position: EMBO J, v. 19, p. 4734-44.

Sunde, R. A., A. M. Raines, K. M. Barnes, and J. K. Evenson, 2009, Selenium status highly regulates selenoprotein mRNA levels for only a subset of the selenoproteins in the selenoproteome: Biosci Rep, v. 29, p. 329-38.

Suwa, T., T. Mune, H. Morita, H. Daido, M. Saio, and K. Yasuda, 2000, Role of rat adrenal antioxidant defense systems in the aldosterone turn-off phenomenon: J Steroid Biochem Mol Biol, v. 73, p. 71-8.

Swords, F. M., A. Baig, D. M. Malchoff, C. D. Malchoff, M. O. Thorner, P. J. King, L. Hunyady, and A. J. Clark, 2002, Impaired desensitization of a mutant

adrenocorticotropin receptor associated with apparent constitutive activity: Mol Endocrinol, v. 16, p. 2746-53.

Takahashi, K., N. Avissar, J. Whitin, and H. Cohen, 1987, Purification and characterization of human plasma glutathione peroxidase: a selenoglycoprotein distinct from the known cellular enzyme: Arch Biochem Biophys, v. 256, p. 677-86.

Tan, M., S. Li, M. Swaroop, K. Guan, L. W. Oberley, and Y. Sun, 1999, Transcriptional activation of the human glutathione peroxidase promoter by p53: J Biol Chem, v. 274, p. 12061-6.

Taylor, J. M., P. J. Crack, J. A. Gould, U. Ali, P. J. Hertzog, and R. C. Iannello, 2004, Akt phosphorylation and NFkappaB activation are counterregulated under conditions of oxidative stress: Exp Cell Res, v. 300, p. 463-75.

Thaminy, S., D. Auerbach, A. Arnoldo, and I. Stagljar, 2003, Identification of novel ErbB3-interacting factors using the split-ubiquitin membrane yeast two-hybrid system: Genome Res, v. 13, p. 1744-53.

Theda, C., A. B. Moser, J. M. Powers, and H. W. Moser, 1992, Phospholipids in X-linked adrenoleukodystrophy white matter: fatty acid abnormalities before the onset of demyelination: J Neurol Sci, v. 110, p. 195-204.

Thistlethwaite, D., J. A. Darling, R. Fraser, P. A. Mason, L. H. Rees, and R. A. Harkness, 1975, Familial glucocorticoid deficiency. Studies of diagnosis and pathogenesis: Arch Dis Child, v. 50, p. 291-7.

Thistlethwaite, D., J. A. Darling, R. Fraser, L. H. Rees, and R. A. Harkness, 1974, Proceedings: Familial glucocorticoid deficiency: J Endocrinol, v. 63, p. 48P-49P.

Tobian, L., A. Tomboulian, and J. Janecek, 1959, The effect of high perfusion pressures on the granulation of juxtaglomerular cells in an isolated kidney: J Clin Invest, v. 38, p. 605-10.

Tokarz, J., G. Möller, M. Hrabě de Angelis, and J. Adamski, 2013, Zebrafish and steroids: What do we know and what do we need to know?: J Steroid Biochem Mol Biol.

Toppo, S., L. Flohé, F. Ursini, S. Vanin, and M. Maiorino, 2009, Catalytic mechanisms and specificities of glutathione peroxidases: variations of a basic scheme: Biochim Biophys Acta, v. 1790, p. 1486-500.

Tosatto, S. C., V. Bosello, F. Fogolari, P. Mauri, A. Roveri, S. Toppo, L. Flohé, F. Ursini, and M. Maiorino, 2008, The catalytic site of glutathione peroxidases: Antioxid Redox Signal, v. 10, p. 1515-26.

Toye, A. A., J. D. Lippiat, P. Proks, K. Shimomura, L. Bentley, A. Hugill, V. Mijat, M. Goldsworthy, L. Moir, A. Haynes, J. Quarterman, H. C. Freeman, F. M. Ashcroft, and R. D. Cox, 2005, A genetic and physiological study of impaired glucose homeostasis control in C57BL/6J mice: Diabetologia, v. 48, p. 675-86.

Trujillo, M., A. Clippe, B. Manta, G. Ferrer-Sueta, A. Smeets, J. P. Declercq, B. Knoops, and R. Radi, 2007, Pre-steady state kinetic characterization of human peroxiredoxin 5: taking advantage of Trp84 fluorescence increase upon oxidation: Arch Biochem Biophys, v. 467, p. 95-106.

Tsai, S. C., C. C. Lu, C. S. Lin, and P. S. Wang, 2003, Antisteroidogenic actions of hydrogen peroxide on rat Leydig cells: J Cell Biochem, v. 90, p. 1276-86.

Turan, S., C. Hughes, Z. Atay, T. Guran, B. Haliloglu, A. J. Clark, A. Bereket, and L. A. Metherell, 2012, An atypical case of familial glucocorticoid deficiency without pigmentation caused by coexistent homozygous mutations in MC2R (T152K) and MC1R (R160W): J Clin Endocrinol Metab, v. 97, p. E771-4.

Umlauf, D., J. Bonnet, F. Waharte, M. Fournier, M. Stierle, B. Fischer, L. Brino, D. Devys, and L. Tora, 2013, The human TREX-2 complex is stably associated with the nuclear pore basket: J Cell Sci, v. 126, p. 2656-67.

Ursini, F., S. Heim, M. Kiess, M. Maiorino, A. Roveri, J. Wissing, and L. Flohé, 1999, Dual function of the selenoprotein PHGPx during sperm maturation: Science, v. 285, p. 1393-6.

Vaisse, C., K. Clement, B. Guy-Grand, and P. Froguel, 1998, A frameshift mutation in human MC4R is associated with a dominant form of obesity: Nat Genet, v. 20, p. 113-4.

Valverde, P., E. Healy, I. Jackson, J. L. Rees, and A. J. Thody, 1995, Variants of the melanocyte-stimulating hormone receptor gene are associated with red hair and fair skin in humans: Nat Genet, v. 11, p. 328-30.

van Geel, B. M., L. Bezman, D. J. Loes, H. W. Moser, and G. V. Raymond, 2001, Evolution of phenotypes in adult male patients with X-linked adrenoleukodystrophy: Ann Neurol, v. 49, p. 186-94.

Vilgrain, I., A. Chinn, I. Gaillard, E. M. Chambaz, and J. J. Feige, 1998, Hormonal regulation of focal adhesions in bovine adrenocortical cells: induction of paxillin dephosphorylation by adrenocorticotropic hormone: Biochem J, v. 332 (Pt 2), p. 533-40.

Vinson, G. P., 2003, Adrenocortical zonation and ACTH: Microsc Res Tech, v. 61, p. 227-39.

Walker, J. R., A. I. Su, D. W. Self, J. B. Hogenesch, H. Lapp, R. Maier, D. Hoyer, and G. Bilbe, 2004, Applications of a rat multiple tissue gene expression data set: Genome Res, v. 14, p. 742-9.

Wang, B., M. Nguyen, D. G. Breckenridge, M. Stojanovic, P. A. Clemons, S. Kuppig, and G. C. Shore, 2003, Uncleaved BAP31 in association with A4 protein at the endoplasmic reticulum is an inhibitor of Fas-initiated release of cytochrome c from mitochondria: J Biol Chem, v. 278, p. 14461-8.

Wang, B., J. Pelletier, M. J. Massaad, A. Herscovics, and G. C. Shore, 2004, The yeast split-ubiquitin membrane protein two-hybrid screen identifies BAP31 as a regulator of the turnover of endoplasmic reticulum-associated protein tyrosine phosphatase-like B: Mol Cell Biol, v. 24, p. 2767-78.

Wang, T., and W. E. Rainey, 2012, Human adrenocortical carcinoma cell lines: Mol Cell Endocrinol, v. 351, p. 58-65.

Wang, X. J., Z. Sun, N. F. Villeneuve, S. Zhang, F. Zhao, Y. Li, W. Chen, X. Yi, W. Zheng, G. T. Wondrak, P. K. Wong, and D. D. Zhang, 2008, Nrf2 enhances resistance of cancer cells to chemotherapeutic drugs, the dark side of Nrf2: Carcinogenesis, v. 29, p. 1235-43.

Warner, B. B., L. Stuart, S. Gebb, and J. R. Wispé, 1996, Redox regulation of manganese superoxide dismutase: Am J Physiol, v. 271, p. L150-8.

Watabe, S., T. Hiroi, Y. Yamamoto, Y. Fujioka, H. Hasegawa, N. Yago, and S. Y. Takahashi, 1997, SP-22 is a thioredoxin-dependent peroxide reductase in mitochondria: Eur J Biochem, v. 249, p. 52-60.

Watabe, S., H. Kohno, H. Kouyama, T. Hiroi, N. Yago, and T. Nakazawa, 1994, Purification and characterization of a substrate protein for mitochondrial ATP-dependent protease in bovine adrenal cortex: J Biochem, v. 115, p. 648-54.

Webb, T. R., L. Chan, S. N. Cooray, M. E. Cheetham, J. P. Chapple, and A. J. Clark, 2009, Distinct melanocortin 2 receptor accessory protein domains are required for melanocortin 2 receptor interaction and promotion of receptor trafficking: Endocrinology, v. 150, p. 720-6.

Webb, T. R., and A. J. Clark, 2010, Minireview: the melanocortin 2 receptor accessory proteins: Mol Endocrinol, v. 24, p. 475-84.

Weber, A., and A. J. Clark, 1994, Mutations of the ACTH receptor gene are only one cause of familial glucocorticoid deficiency: Hum Mol Genet, v. 3, p. 585-8.

Weber, A., A. J. Clark, L. A. Perry, J. W. Honour, and M. O. Savage, 1997, Diminished adrenal androgen secretion in familial glucocorticoid deficiency implicates a significant role for ACTH in the induction of adrenarche: Clin Endocrinol (Oxf), v. 46, p. 431-7.

Weber, A., T. F. Wienker, M. Jung, D. Easton, H. J. Dean, C. Heinrichs, A. Reis, and A. J. Clark, 1996, Linkage of the gene for the triple A syndrome to chromosome 12q13 near the type II keratin gene cluster: Hum Mol Genet, v. 5, p. 2061-6.

Wei, X., T. Shimizu, and Z. C. Lai, 2007, Mob as tumor suppressor is activated by Hippo kinase for growth inhibition in Drosophila: EMBO J, v. 26, p. 1772-81.

Weiss Sachdev, S., and R. A. Sunde, 2001, Selenium regulation of transcript abundance and translational efficiency of glutathione peroxidase-1 and -4 in rat liver: Biochem J, v. 357, p. 851-8.

Weiss, S. L., and R. A. Sunde, 1998, Cis-acting elements are required for selenium regulation of glutathione peroxidase-1 mRNA levels: RNA, v. 4, p. 816-27.

Weitzman, E. D., D. Fukushima, C. Nogeire, H. Roffwarg, T. F. Gallagher, and L. Hellman, 1971, Twenty-four hour pattern of the episodic secretion of cortisol in normal subjects: J Clin Endocrinol Metab, v. 33, p. 14-22.

Westphal, N. J., and A. F. Seasholtz, 2006, CRH-BP: the regulation and function of a phylogenetically conserved binding protein: Front Biosci, v. 11, p. 1878-91.

White, P. C., and P. W. Speiser, 2000, Congenital adrenal hyperplasia due to 21-hydroxylase deficiency: Endocr Rev, v. 21, p. 245-91.

Wiederschain, D., L. Chen, B. Johnson, K. Bettano, D. Jackson, J. Taraszka, Y. K. Wang, M. D. Jones, M. Morrissey, J. Deeds, R. Mosher, P. Fordjour, C. Lengauer, and J. D.

Benson, 2007, Contribution of polycomb homologues Bmi-1 and Mel-18 to medulloblastoma pathogenesis: Mol Cell Biol, v. 27, p. 4968-79.

Wingler, K., M. Böcher, L. Flohé, H. Kollmus, and R. Brigelius-Flohé, 1999, mRNA stability and selenocysteine insertion sequence efficiency rank gastrointestinal glutathione peroxidase high in the hierarchy of selenoproteins: Eur J Biochem, v. 259, p. 149-57.

Wiseman, S., J. K. Thomas, L. McPhee, O. Hursky, J. C. Raine, M. Pietrock, J. P. Giesy, M. Hecker, and D. M. Janz, 2011, Attenuation of the cortisol response to stress in female rainbow trout chronically exposed to dietary selenomethionine: Aquat Toxicol, v. 105, p. 643-51.

Wood, Z. A., L. B. Poole, and P. A. Karplus, 2003a, Peroxiredoxin evolution and the regulation of hydrogen peroxide signaling: Science, v. 300, p. 650-3.

Wood, Z. A., E. Schröder, J. Robin Harris, and L. B. Poole, 2003b, Structure, mechanism and regulation of peroxiredoxins: Trends Biochem Sci, v. 28, p. 32-40.

Wright, N., and D. Voncina, 1977, Studies on the postnatal growth of the rat adrenal cortex: J Anat, v. 123, p. 147-56.

Wu, J., and G. L. Xu, 1987, Plasma selenium content, platelet glutathione peroxidase and superoxide dismutase activity of residents in Kashin-Beck disease affected area in China: J Trace Elem Electrolytes Health Dis, v. 1, p. 39-43.

Wu, R., Q. Shen, and P. E. Newburger, 2000, Recognition and binding of the human selenocysteine insertion sequence by nucleolin: J Cell Biochem, v. 77, p. 507-16.

Xia, Y., and J. E. Wikberg, 1996, Localization of ACTH receptor mRNA by in situ hybridization in mouse adrenal gland: Cell Tissue Res, v. 286, p. 63-8.

Xie, X., Y. Chen, P. Xue, Y. Fan, Y. Deng, G. Peng, F. Yang, and T. Xu, 2009, RUVBL2, a novel AS160-binding protein, regulates insulin-stimulated GLUT4 translocation: Cell Res, v. 19, p. 1090-7.

Xing, Y., C. R. Parker, M. Edwards, and W. E. Rainey, 2010, ACTH is a potent regulator of gene expression in human adrenal cells: J Mol Endocrinol, v. 45, p. 59-68.

Xu, A., K. L. Choi, Y. Wang, P. A. Permana, L. Y. Xu, C. Bogardus, and G. J. Cooper, 2002, Identification of novel putative membrane proteins selectively expressed during adipose conversion of 3T3-L1 cells: Biochem Biophys Res Commun, v. 293, p. 1161-7.

Xu, X., Y. Song, Y. Li, J. Chang, H. Zhang, and L. An, 2010, The tandem affinity purification method: an efficient system for protein complex purification and protein interaction identification: Protein Expr Purif, v. 72, p. 149-56.

Yamada, Y., G. V. Limmon, D. Zheng, N. Li, L. Li, L. Yin, V. T. Chow, J. Chen, and B. P. Engelward, 2012, Major shifts in the spatio-temporal distribution of lung antioxidant enzymes during influenza pneumonia: PLoS One, v. 7, p. e31494.

Yasumura, Y., V. Buonassisi, and G. Sato, 1966, Clonal analysis of differentiated function in animal cell cultures. I. Possible correlated maintenance of differentiated function and the diploid karyotype: Cancer Res, v. 26, p. 529-35.

Yates, R., H. Katugampola, D. Cavlan, K. Cogger, E. Meimaridou, C. Hughes, L. Metherell, L. Guasti, and P. King, 2013, Adrenocortical development, maintenance, and disease: Curr Top Dev Biol, v. 106, p. 239-312.

Yeo, G. S., I. S. Farooqi, S. Aminian, D. J. Halsall, R. G. Stanhope, and S. O'Rahilly, 1998, A frameshift mutation in MC4R associated with dominantly inherited human obesity: Nat Genet, v. 20, p. 111-2.

Yin, F., H. Sancheti, and E. Cadenas, 2012a, Mitochondrial thiols in the regulation of cell death pathways: Antioxid Redox Signal, v. 17, p. 1714-27.

Yin, F., H. Sancheti, and E. Cadenas, 2012b, Silencing of nicotinamide nucleotide transhydrogenase impairs cellular redox homeostasis and energy metabolism in PC12 cells: Biochim Biophys Acta, v. 1817, p. 401-9.

Yoshimura, S., K. Watanabe, H. Suemizu, T. Onozawa, J. Mizoguchi, K. Tsuda, H. Hatta, and T. Moriuchi, 1991, Tissue specific expression of the plasma glutathione peroxidase gene in rat kidney: J Biochem, v. 109, p. 918-23.

Zhang, H., Y. M. Go, and D. P. Jones, 2007, Mitochondrial thioredoxin-2/peroxiredoxin-3 system functions in parallel with mitochondrial GSH system in protection against oxidative stress: Arch Biochem Biophys, v. 465, p. 119-26.

Zhang, Y., D. E. Handy, and J. Loscalzo, 2005, Adenosine-dependent induction of glutathione peroxidase 1 in human primary endothelial cells and protection against oxidative stress: Circ Res, v. 96, p. 831-7.

Zhang, Y., R. Proenca, M. Maffei, M. Barone, L. Leopold, and J. M. Friedman, 1994, Positional cloning of the mouse obese gene and its human homologue: Nature, v. 372, p. 425-32.

Zhou, L. Z., A. P. Johnson, and T. A. Rando, 2001, NF kappa B and AP-1 mediate transcriptional responses to oxidative stress in skeletal muscle cells: Free Radic Biol Med, v. 31, p. 1405-16.

Zhuo, P., M. Goldberg, L. Herman, B. S. Lee, H. Wang, R. L. Brown, C. B. Foster, U. Peters, and A. M. Diamond, 2009, Molecular consequences of genetic variations in the glutathione peroxidase 1 selenoenzyme: Cancer Res, v. 69, p. 8183-90.

Appendices

Appendix 1: Whole Exome Sequencing Data

1. 1: Non-synonymous missense mutations identified by whole exome sequencing of the proband.

Details include: chromosome number (Chrom), genomic location (left position), reference nucleotide (Ref Nuc), variant nucleotide (Var nuc), total number of reads for the variant locus (Read depth), number of reads for the variant allele (Var freq) gene name, reference peptide (Ref pep) at this position and variant peptide (Var pep) introduced as a consequence of the variant allele (*=stop). All variants had a read depth> 20 .

Chrom	Left position	Ref Nuc	Var Nuc	Read Depth	Var Freq	Gene Name	Ref peptide	Var peptide
chr1	892284	t	g	45	44	NOC2L	Q	P
chr1	153941536	c	t	33	32	CREB3L4	P	L
chr1	155002628	c	t	32	30	DCST2	R	H
chr1	228412227	tg	ca	30	28	OBSCN	SA	ST
chr2	98128194	ggt	cac	40	36	ANKRD36B	YR	CG
chr2	232087474	at	ga	34	33	ARMC9	I	E
chr3	19961330	ct	tc	26	26	EFHB	SV	SI
chr3	37050392	g	a	46	46	MLH1	G	S
chr3	52556127	a	g	24	24	STAB1	T	A
chr3	148897356	a	g	40	40	CP	V	A
chr3	194373832	tg	ca	22	21	LSG1	TK	TE
chr3	195451880	ag	ga	53	52	MUC20	R	E
chr3	195506530	c	a	31	28	MUC4	R	L
chr3	195507226	a	g	159	158	MUC4	V	A
chr3	195507372	c	g	47	47	MUC4	Q	H
chr3	195508336	c	t	23	21	MUC4	G	D
chr3	195509423	g	a	25	20	MUC4	P	S
chr3	195509954	g	c	106	101	MUC4	L	V

chr3	195509974	a	g	84	83	MUC4	F	S
chr3	195510943	g	t	66	63	MUC4	S	Y
chr3	195511336	g	c	174	153	MUC4	T	S
chr3	195511690	g	c	167	156	MUC4	T	S
chr3	195511740	c	g	88	86	MUC4	Q	H
chr3	195512003	tt	tg	45	38	MUC4	ET	DT
chr3	195512107	t	a	93	91	MUC4	D	V
chr3	195512117	c	g	88	85	MUC4	A	P
chr3	195512186	t	c	60	60	MUC4	I	V
chr3	195512206	a	g	45	41	MUC4	L	P
chr3	195512767	tt	ga	95	90	MUC4	N	S
chr3	195514956	c	g	46	44	MUC4	Q	H
chr3	195514969	g	a	57	55	MUC4	A	V
chr4	88536692	a	g	53	52	DSPP	S	G
chr4	88537035	a	g	21	21	DSPP	D	G
chr5	1225687	ct	tc	38	38	SLC6A18	T	I
chr6	3264526	ct	tc	44	43	PSMG4	L	S
chr6	31324525	cc	tg	20	19	HLA-B	QA	HT
chr6	31324602	tct	gtc	22	17	HLA-B	RE	RT
chr6	47649573	ca	tg	27	27	GPR111	SK	SE
chr6	56918867	c	g	21	21	KIAA1586	Q	E
chr6	143092151	t	c	35	35	HIVEP2	Y	C
chr7	72738762	ca	tg	45	45	TRIM50	L	P
chr7	74303828	c	t	44	43	STAG3L2	R	Q
chr7	100636722	g	c	30	30	MUC12	V	L
chr8	17796382	ac	gt	35	35	PCM1	N	S
chr8	142446139	c	t	26	25	FLJ43860	M	I
chr10	119774577	g	a	54	53	RAB11FIP2	P	L
chr10	135491030	g	c	23	21	LOC653544	G	A
chr10	135491030	g	c	23	21	LOC653545	G	A

chr10	135491030	g	c	23	21	LOC653548	G	A
chr10	135491030	g	c	23	21	LOC728410	G	A
chr11	280816	at	tc	27	27	NLRP6	Y	F
chr11	57147016	at	gt	30	26	PRG3	I	T
chr11	58207203	ca	tg	56	54	OR5B12	C	H
chr11	63999929	c	t	25	23	DNAJC4	P	S
chr12	11244230	c	a	30	30	TAS2R43	C	F
chr13	46108853	tg	ca	36	36	COG3	L	S
chr17	39619093	gt	ac	53	51	KRT32	N	S
chr17	39742898	gc	at	21	20	KRT14	C	Y
chr17	44144993	c	g	35	35	KIAA1267	R	P
chr18	52265307	aa	ac	21	18	C18orf26	TT	TP
chr19	39308104	t	c	29	29	ECH1	N	S
chr19	40368498	aa	cc	56	55	FCGBP	LS	LA
chr19	41382560	a	t	52	52	CYP2A7	F	Y
chr20	44038574	at	gt	24	21	DBNDD2	M	V
chr21	31869285	gt	gc	48	42	KRTAP19-4	Y	C
chrX	35821055	at	ga	31	31	MAGEB16	M	E
chrX	54263878	t	c	22	21	WNK3	K	R
chrX	70524052	c	t	30	29	ITGB1BP2	R	C
chrX	114426193	g	a	29	29	RBMXL3	R	Q
chrX	152482522	g	c	39	39	MAGEA1	D	E
chrX	153458965	g	t	52	51	OPN1MW	V	L
chrX	153458965	g	t	52	51	OPN1MW2	V	L

1. 2: Non-synonymous in-frame deletions identified by whole exome sequencing of the proband.

Details include: chromosome number (Chrom), genomic location (left position), reference nucleotide (Ref Nuc), variant nucleotide (Var nuc), total number of reads for the variant locus (Read depth), number of reads for the variant allele (Var freq) gene

name, reference peptide (Ref pep) at this position and variant peptide (Var pep) introduced as a consequence of the variant allele (*=stop). All variants had a read depth> 20 .

Chrom	Left position	Ref Nuc	Var Nuc	Read Depth	Var Freq	Gene Name	Ref peptide	Var peptide
chr5	98192167	gag	-	31	28	CHD1	SP	S
chr9	97080947	aag	-	40	34	FAM22F	PS	P
chr20	238439	tcttgg	-	28	23	DEFB132	VLA	A
chr20	1896052	cga	-	36	30	SIRPA	PD	P
chrX	135474448	gat	-	22	21	GPR112	D	

1. 3: Frame-shift mutation identified by whole exome sequencing of the proband.

Details include: Details include: chromosome number (Chrom), genomic location (left position), reference nucleotide (Ref Nuc), variant nucleotide (Var nuc), total number of reads for the variant locus (Read depth), number of reads for the variant allele (Var freq) gene name, reference peptide (Ref pep) at this position and variant peptide (Var pep) introduced as a consequence of the variant allele (*=stop). All variants had a read depth> 20 .

Chrom	Left position	Ref Nuc	Var Nuc	Read Coverage	Var Freq	Gene Name	Ref peptide	Var peptide
chr19	52004796	INS	t	43	36	SIGLEC12		

1. 4: Stop-gain mutations identified by whole exome sequencing of the proband.

Details include: variant ID number, chromosome number (Chrom), genomic location (left position), reference nucleotide (Ref Nuc), variant nucleotide (Var nuc), total number of reads for loci (Read coverage), number of reads for variant allele at loci (Var freq) (heterozygous variants would be 50%), gene name, reference peptide (Ref pep)

and variant peptide (Var pep) (*=stop). All variants had coverage of at least 20 reads. Grey shading highlights the variant in PRDX3 which is our 'second hit' candidate gene.

Chrom	Left position	Ref Nuc	Var Nuc	Read Coverage	Var Freq	Gene Name	Ref peptide	Var peptide
chr10	120934075	G	a	20	20	PRDX3	Q	*
chr11	58893362	C	t	41	40	FAM111B	R	*

Appendix 2: Vector maps

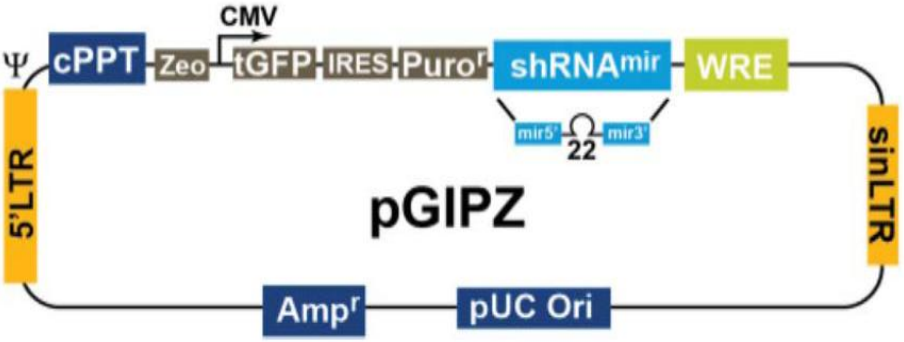

CMV promoter 1–602
c-myc tag 679–708
multiple cloning site 710–783
SV40 polyA 860–1243
f1 origin 1381–1687
***bla* promoter** 1712–1836
SV40 promoter 1856–2194
neomycin/kanamycin resistance ORF 2229–3020
HSV-TK polyA 3021–3479
pUC origin 3608–4275

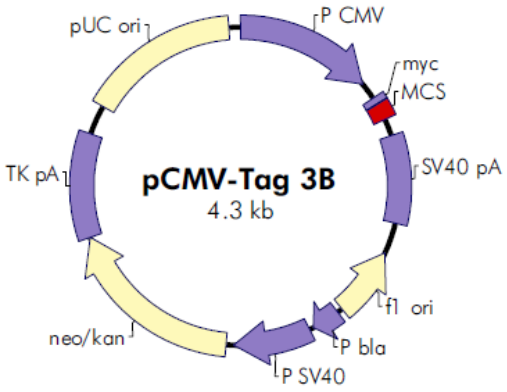

pCMV-Tag 3B Multiple Cloning Site Region
(sequence shown 620–847)

T3 promoter
AA TTA ACC CTC ACT AAA GGG AAC AAA AGC TGG AGC TCC ACC GCG GTG GCG GCC GCC ATG...
M
KOZAK

myc tag
E Q K L I S E E D L
Srf I
BamH I
Pst I
...GAG CAG AAA CTC ATC TCT GAA GAG GAT CTG AGC CCG GGC GGA TCC CCC GGG CTG CAG...

EcoR I
EcoR V
Hind III
Acc I/Sal I
Xho I
Apa I
...GAA TTC GAT ATC AAG CTT ATC GAT ACC GTC GAC CTC GAG GGG GGG CCC GGT ACC T...

T7 promoter
...TAATTAATTAAGGTACCAGGTAAGTGTACCCAATTCGCCCTATAGTGAGTCGTATTA
MULTIPLE STOP CODONS

pNTAP Vector Map

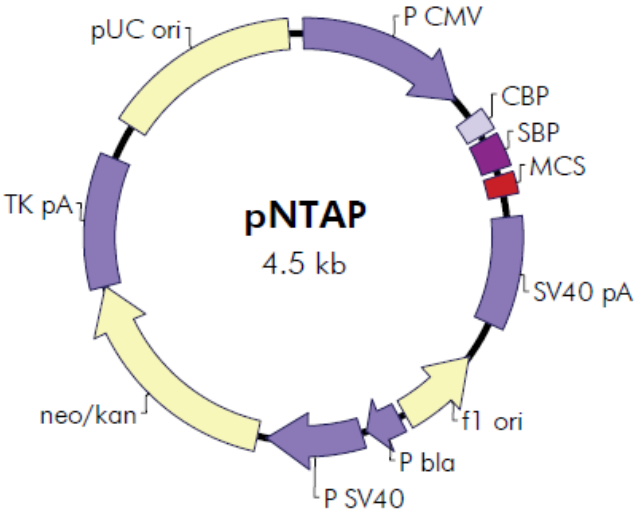

pNTAP Multiple Cloning Site Region
(sequence shown 889–1051)

```
                SBP tag (3′ end)
                P   S   G   G   C   K   L   G
                                    Srf I                BamH I                Pst I       EcoR I
CCC TCC GGC GGC TGC AAG CTG GGC * GCC CGG GCG GAT CCC CCG GGC TGC AGG AAT TC...

    EcoR V      Hind III                Acc I/Sal I  Xho I          Apa I
...G ATA TCA AGC TTA TCG ATA CCG TCG ACC TCG AGG GGG GCC CCG GTA CCT...

                                                                T7 promoter
...TAATTAATTAAGGTACCAGGTAAGTGTACCCAATTCGCCCTATAGTGAGTCGTATTAC
   MULTIPLE STOP CODONS
```

pCTAP Vector Map

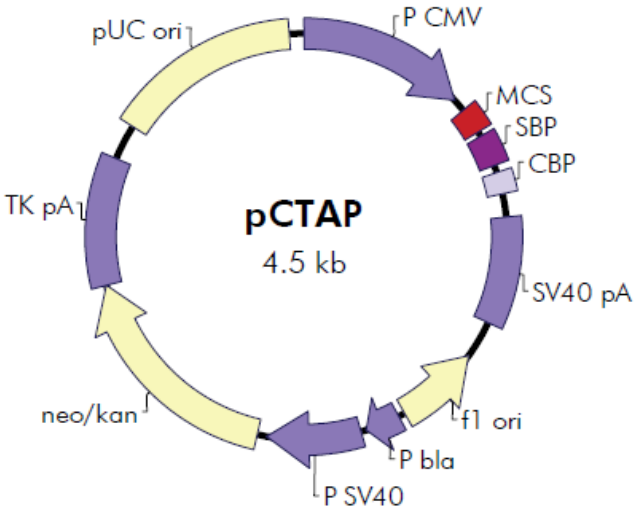

pCTAP Multiple Cloning Site Region
(sequence shown 620–797)

```
                T3 promoter                                                  Sac I  BstX I  Sac II        Not I                Srf I
A ATT AAC CCT CAC TAA AGG GAA CAA AAG CTG GAG CTC CAC CGC GGT GGC GGC CGC TCT AGC...
                                                                                                        STOP

                BamH I                Pst I  EcoR I  EcoR V  Hind III                Acc I/Sal I
...CCG GGC GGA TCC CCC GGG CTG CAG GAA TTC GAT ATC AAG CTT ATC GAT ACC GTC GAC *...

                                                                SBP tag (5′ end)
    Xho I
                                                M   D   E   K   T   T   G   W   R   G   G   H
...CTC GAG GGA AGC GGT AGC GGT ACC ATG GAC GAG AAG ACC ACC GGC TGG CGG GGC GGC CAC
```

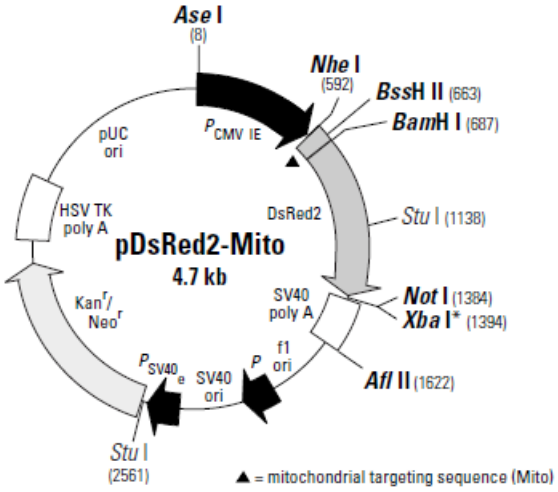

Restriction Map of pDsRed2-Mito. Unique restriction sites are shown in bold. The *Xba* I site (*) is methylated in the DNA provided by Clontech. If you wish to digest the vector with this enzyme, you will need to transform the vector into a *dam*⁻ host and isolate fresh DNA.

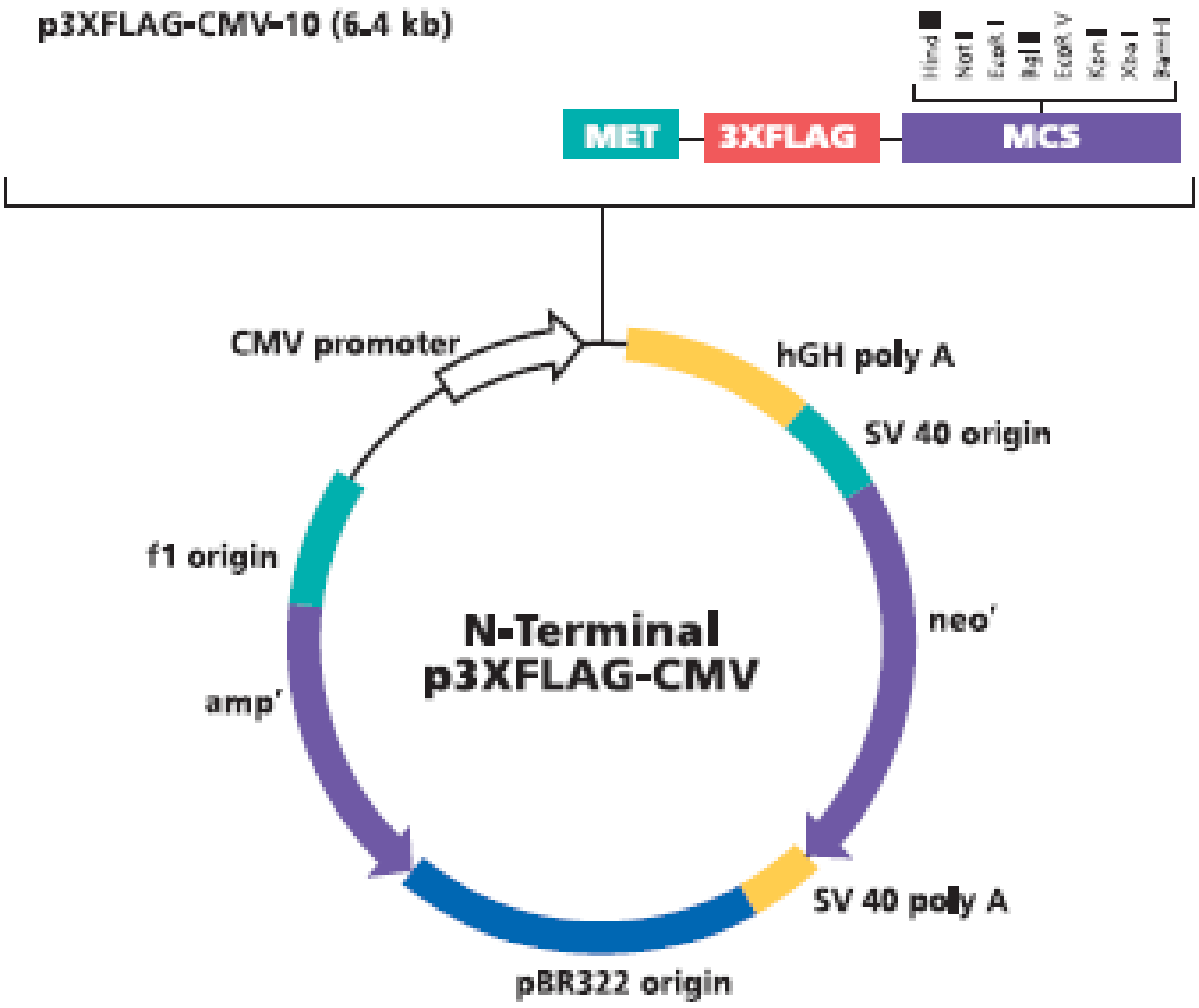

Multiple Cloning Site

(p3XFLAG-CMV-9* and p3XFLAG-CMV-10)

3XFLAG Peptide Sequence

Met*	Asp	Tyr	Lys	Asp	His	Asp	Gly	Asp	Tyr	Lys	Asp	His	Asp	Ile
ATG	GAC	TAC	AAA	GAC	CAT	GAC	GGT	GAT	TAT	AAA	GAT	CAT	GAC	ATC
TAC	CTG	ATG	TTT	CTG	GTA	CTG	CCA	CTA	ATA	TTT	CTA	GTA	CTG	TAG

3XFLAG Peptide Sequence

Asp	Tyr	Lys	Asp	Asp	Asp	Asp	Lys							
GAT	TAC	AAG	GAT	GAC	GAT	GAC	AAG	CTT	GCG	GCC	GCA	GAA	TTC	GAT
CTA	ATG	TTC	CTA	CTG	CTA	CTG	TTC	GAA	CGC	CGG	CGT	CTT	AAG	CTA

Not I EcoR I Hind III

Bgl II		EcoR V		Kpn I			Xba I		Bam HI					
GAT	CTG	ATA	TCG	GTA	CCA	GTC	GAC	TCT	AGA	GGA	TCC	CGG	GTG	
CTA	GAC	TAT	AGC	CAT	GGT	CAG	CTG	AGA	TCT	CCT	AGG	GCC	CAC	

Appendix 3: *GPX1* and *PRDX3* cDNA sequences

GPX1 cDNA (transcript 1):

GAGCCCTCGAGGGCCCCAGCCCTTGGAAGGGTAACCTGGACCGCTGCCGCCTGGTTGCCT
GGGCCAGACCAGACATGCCTGCTGCTCCTTCCGGCTTAGGAGGAGCACGCGTCCCGCTCG
GGCGCACTCTCCAGCCTTTTCCTGGCTGAGGAGGGGCCGAGCCCTCCGGGTAGGGCGGG
GGCCGGATGAGGCGGGACCCTCAGGCCCGGAAAACTGCCTGTGCCACGTGACCCGCCGC
CGGCCAGTTAAAAGGAGGCGCCTGCTGGCCTCCCCTTACAGTGCTTGTTCGGGGCGCTCC
GCTGGCTTCTTGGACAATTGCGCCATGTGTGCTGCTCGGCTAGCGGCGGCGGCGGCGGCG
GCCCAGTCGGTGTATGCCTTCTCGGCGCGCCCGCTGGCCGGCGGGGAGCCTGTGAGCCTG
GGCTCCCTGCGGGGCAAGGTACTACTTATCGAGAATGTGGCGTCCCTCTGAGGCACCACG
GTCCGGGACTACACCCAGATGAACGAGCTGCAGCGGCGCCTCGGACCCCGGGGCCTGGT
GGTGCTCGGCTTCCCGTGCAACCAGTTTGGGCATCAGGAGAACGCCAAGAACGAAGAGA
TTCTGAATTCCCTCAAGTACGTCCGGCCTGGTGGTGGGTTCGAGCCCAACTTCATGCTCTT
CGAGAAGTGCGAGGTGAACGGTGCGGGGGCGCACCCTCTCTTCGCCTTCCTGCGGGAGG
CCCTGCCAGCTCCCAGCGACGACGCCACCGCGCTTATGACCGACCCCAAGCTCATCACCT
GGTCTCCGGTGTGTCGCAACGATGTTGCCTGGAACTTTGAGAAGTTCCTGGTGGGCCCTG
ACGGTGTGCCCCTACGCAGGTACAGCCGCCGCTTCCAGACCATTGACATCGAGCCTGACA
TCGAAGCCCTGCTGTCTCAAGGGCCCAGCTGTGCCTAGGGCGCCCCTCCTACCCCGGCTG
CTTGGCAGTTGCAGTGCTGCTGTCTCGGGGGGGTTTTCATCTATGAGGGTGTTTCCTCTAA
ACCTACGAGGGAGGAACACCTGATCTTACAGAAAATACCACCTCGAGATGGGTGCTGGT
CCTGTTGATCCCAGTCTCTGCCAGACCAAGGCGAGTTTCCCCACTAATAAAGTGCCGGGT
GTCAGCAGAA

Grey depicts utr. *Red*

PRDX3 cDNA:

CCCTGCGTCTCTGCCCGCCCCGTGGCGCCCGAGTGCACTGAAGATGGCGGCTGCTGTAGG
ACGGTTGCTCCGAGCGTCGGTTGCCCGACATGTGAGTGCCATTCCTTGGGGCATTTCTGC
CACTGCAGCCCTCAGGCCTGCTGCATGTGGAAGAACGAGCTTGACAAATTTATTGTGTTC
TGGTTCCAGTCAAGCAAAATTATTCAGCACCAGTTCCTCATGCCATGCACCTGCTGTCAC
CCAGCATGCACCCTATTTTAAGGGTACAGCCGTTGTCAATGGAGAGTTCAAAGACCTAAG
CCTTGATGACTTTAAGGGGAAATATTTGGTGCTTTTCTTCTATCCTTTGGATTTCACCTTT
GTGTGTCCTACAGAAATTGTTGCTTTTAGTGACAAAGCTAACGAATTTCACGACGTGAAC
TGTGAAGTTGTCGCAGTCTCAGTGGATTCCCACTTTAGCCATCTTGCCTGGATAAATACA
CCAAGAAAGAATGGTGGTTTGGGCCACATGAACATCGCACTCTTGTCAGACTTAACTAA
GCAGATTTCCCGAGACTACGGTGTGCTGTTAGAAGGTTCTGGTCTTGCACTAAGAGGTCT
CTTCATAATTGACCCCAATGGAGTCATCAAGCATTTGAGCGTCAACGATCTCCCAGTGGG
CCGAAGCGTGGAAGAAACCCTCCGCTTGGTGAAGGCGTTCCAGTATGTAGAAACACATG
GAGAAGTCTGCCCAGCGAACTGGACACCGGATTCTCCTACGATCAAGCCAAGTCCAGCT
GCTTCCAAAGAGTACTTTCAGAAGGTAAATCAGTAGATCACCCATGTGTATCTGCACCTT
CTCAACTGAGAGAAGAACCACAGTTGAAACCTGCTTTTATCATTTTCAAGATGGTTATTT
GTAGAAGGCAAGGAACCAATTATGCTTGTATTCATAAGTATTACTCTAAATGTTTTGTTTT

TGTAATTCTGGCTAAGACCTTTTAAACATGGTTAGTTGCTAGTACAAGGAATCCTTTATTG
GTAACATCTTGGTGGCTGGCTAGCTAGTTTCTACAGAACATAATTTGCCTCTATAGAAGG
CTATTCTTAGATCATGTCTCAATGGAAACACTCTTCTTTCTTAGCCTTACTTGAATCTTGC
CTATAATAAAGTAGAGCAACACACATTGAAAGCTTCTGATCAACGGTCCTGAAATTTTCA
TCTTGAATGTCTTTGTATTAAACTGAATTTTCTTTTAAGCTAACAAAGATCATAATTTTCA
ATGATTAGCCGTGTAACTCCTGCAATGAATGTTTATGTGATTGAAGCAAATGTGAATCGT
ATTATTTTAAAAAGTGGCAGAGTGACTTAACTGATCATGCATGATCCCTCATCCCTGAAA
TTGAGTTTATGTAGTCATTTTACTTATTTTATTCATTAGCTAACTTTGTCTATGTATATTTC
TAGATATTGATTAGTGTAATCGATTATAAAGGATATTTATCAAATCCAGGGATTGCATTT
TGAAATTATAATTATTTTCTTTGCTGAAGTATTCATTGTAAAACATACAAAATAAACATA
TTTTAAAACATTTGCATTTT

Grey depicts UTR.

Appendix 4: Presentations and prizes relating to this thesis

Oral communications

British Society for Endocrinology annual meeting: A homozygous glutathione peroxidase 1 mutation p.Arg130-Leu133del, in a patient with familial glucocorticoid deficiency.

QMUL WHRI day 'Digenic inheritance of mutations in antioxidant pathway genes in Familial Glucocorticoid Deficiency'

European Society for Paediatric Endocrinologists 'Digenic inheritance of mutations in antioxidant pathway genes in Familial Glucocorticoid Deficiency'

Posters

British Society of Paediatric Endocrinology and Diabetes annual meeting: A homozygous glutathione peroxidase 1 mutation p.Arg130-Leu133del, in a patient with familial glucocorticoid deficiency.

Society for Free Radical Research International annual meeting: A homozygous glutathione peroxidase 1 mutation p.Arg130-Leu133del, in a patient with familial glucocorticoid deficiency.

Prizes

BES conference: Highly commended for oral communication

BSPED conference: Poster Prize